



**The Studies of Genipin-Crosslinked Chitosan-poly(vinyl pyrrolidone) Hydrogels as Smart pH Responsive Materials**

**Glenn Adam Hurst**

School of Chemical Engineering and Advanced Materials  
Newcastle University, United Kingdom

A Thesis Submitted to Newcastle University for the Degree of Doctor of  
Philosophy in Chemical Engineering

Newcastle Upon Tyne, May 2016

## Abstract

Smart hydrogels are macromolecular networks that can exhibit significant and reversible changes in volume upon application of an external stimulus such as pH or temperature. These polymers are well suited for use in delivery systems, tissue engineering and actuation, although currently volume changes must be externally initiated and release is often uncontrolled. Gels able to self-oscillate and distribute absorbed moieties in a controlled regime can be realised by coupling such smart materials to oscillatory chemical reactions that oscillate in the relevant stimuli to induce a volume change within a polymer gel. This work comprises of the synthesis and characterisation of a pH-sensitive hydrogel that has shown to be a good candidate for combination with appropriate oscillatory reactions.

Genipin-crosslinked chitosan-poly(vinyl pyrrolidone) hydrogels were synthesised and investigated for their potential to be coupled to chemical oscillators. This semi-interpenetrating network combines biocompatibility, low toxicity, biodegradability and haemocompatibility attributes using genipin, a natural crosslinking agent with low cytotoxicity that autofluoresces upon crosslink formation. Effects of gel composition, gelation time and post synthetic manipulation on the structure, swelling, responsiveness and the mechanical properties are evaluated. Particular emphasis is placed upon improving network stability via freezing and thawing hydrogels for various timescales and cycles. Mechanical properties of the hydrogels were determined via uniaxial compression tests in multiple environments where they may find application. These results are related to the morphology and swelling potential of the networks. Further to determining volume variations gravimetrically, the hydrogels are also characterised optically, examining the change in surface area and height of the specimens. The force response upon swelling and collapse is investigated under an oscillatory regime and subsequently applied with the bromate-sulfite-ferrocyanide oscillatory reaction. In view of prospective applications, the potential of the hydrogel to release absorbed constituents from within the matrix is also determined.

This thesis aids the development towards applications in controlled, pulsatile and sustained actuation and release.

## Presentations and Publications

### Publications

A facile in situ morphological characterisation of smart genipin-crosslinked chitosan-poly(vinyl pyrrolidone) hydrogels.

**G.A. Hurst\*** and K. Novakovic. Journal of Materials Research, 2013; 28 (17): 2401-2408.

### Oral Presentations

1. *Using Oscillatory Reactions to Control Smart Gels.*

2014 IUPAC Macro Group Young Researchers Meeting, Durham University, United Kingdom, 2014.

2. *Enhancing Control in Smart Hydrogels. (1<sup>st</sup> Prize)*

CEAM Postgraduate Research Conference, Newcastle University, United Kingdom, 2014.

3. *Understanding and enhancing stability of pH responsive genipin crosslinked chitosan-poly(vinyl pyrrolidone) hydrogels.*

Functional Polymeric Materials, Mexico, 2014.

4. *A relation of the swelling and viscoelastic behaviours of smart hydrogels for combination with oscillatory reactions.*

Physical Aspects of Polymer Science 2013, University of Sheffield, United Kingdom, 2013.

5. *Smart Genipin-crosslinked Chitosan-poly(vinyl pyrrolidone) as a Self-oscillatory Hydrogel*

International Conference on Materials for Advanced Technologies, Suntec Singapore, 2013.

6. *Smart hydrogel development for combination with pH oscillators. (Travel Grants Awarded include €250 from European Colloid and Interface Society plus £250 RSC/SCI Sir Eric Rideal Bursary)*

14<sup>th</sup> European Student Colloid Conference, Max Planck Institute of Colloids and Interfaces, Potsdam, Germany, 2013.

7. *Design and characterisation of smart hydrogels for combination with pH oscillators. (1<sup>st</sup> Prize)*

CEAM Postgraduate Research Conference, Newcastle University, United Kingdom, 2013.

8. *Smart hydrogels for biomedical use with oscillatory reactions.*

7th Annual Royal Society of Chemistry (RSC) Biomaterials Chemistry Meeting, Sheffield Hallam University, United Kingdom, 2013.

9. *Engineering smart hydrogels for combination with oscillatory reactions.*

1<sup>st</sup> Northern Chemistry Postgraduate Research Conference, Newcastle University, United Kingdom, 2012.

10. *Smart Hydrogels Meet Oscillatory Reactions: Potential as Biomedical Materials.*

Faculty of Science, Agriculture and Engineering Seminar Series, Newcastle University, United Kingdom, 2012.

#### Poster Presentations

1. *Tailoring pH responsive genipin crosslinked chitosan-poly(vinyl pyrrolidone) hydrogels for medical applications.*

2014 IUPAC World Polymer Congress / Macro 2014, Chiang Mai, Thailand, 2014.

2. *Tailoring pH responsive genipin crosslinked chitosan-poly(vinyl pyrrolidone) hydrogels for medical applications.*

2014 IUPAC Macro Group Young Researchers Meeting, Durham University, United Kingdom, 2014.

3. *Towards self oscillating organogels via palladium-catalysed oxidative carbonylation.*

IUPAC 10<sup>th</sup> International Conference on Advanced Polymers via Macromolecular Engineering, Durham, United Kingdom, 2013.

4. *Characterisation of the structural properties of genipin-crosslinked chitosan-poly(vinyl pyrrolidone) smart hydrogels. (Travel Grant Awarded £50 Macro Group UK / SCI Joint Colloids Group)*

Polymeric and Self-Assembled Hydrogels: From Fundamental Understanding To Applications, King's College, London, United Kingdom, 2012.

5. *Genipin-crosslinked chitosan-poly(vinyl pyrrolidone) hydrogel for coupling with pH oscillators.*

Oscillations & Dynamic Instabilities in Chemical Systems Gordon Research Conference, Waterville, Maine, USA 2012.

6. *Smart Polymer Gels: The Quest for Control.*

CEAM Postgraduate Research Conference, Newcastle University, United Kingdom, 2012.

7. *Smart Polymer Gels: Past, Present and Future.*

Industrial Advisory Board Conference Newcastle University, United Kingdom, 2011.

# Dedication

For my Mam and Dad

## **Acknowledgements**

I would like to thank my main supervisor Dr Katarina Novakovic for her fantastic supervision, guidance and support throughout my studies. I would also like to acknowledge Dr Kamelia Boodhoo and Professor Allen Wright who were my other supervisors for useful discussions throughout the project. Many thanks to Julie Parker and Dr Lynn Donlon for their fantastic technical advice throughout. Thanks to Professor Patrick Bunton for his advice with regards to optics. I would like to acknowledge the students who have participated in the Novakovic lab between 2011 and 2014 especially Lim Kai En, Chinyelumdu Jennifer Nwosu, Spryridon Diakakis and Maryam Madzi. I would like to acknowledge all staff, students and employers of the School of Chemical Engineering at Newcastle University.

I would like to thank the School of Chemical Engineering and Advanced Materials at Newcastle University together with the Engineering and Physical Sciences Research Council (EP/H003908/1) for funding my studies.

I am very grateful to the eternal support and guidance from my mam, dad and the rest of my family (especially Mika, Kyle and Fabio).

# Table of Contents

Abstract	i
Presentations and Publications	ii
Dedication	v
Acknowledgements	vi
Table of Contents	vii
List of Tables	xi
List of Figures	xiii
Abbreviations	xxiv
Symbols	xxvi
<b>Chapter 1 – Introduction</b>	<b>1</b>
<b>Chapter 2 – Literature Review</b>	<b>5</b>
2.1 Overview of polymer gels and their responsive nature	5
2.2 Types of polymer gel	9
2.3 Hydrogels	10
2.3.1 Variables affecting hydrogel swelling	11
2.3.2 Stimuli	12
2.3.3 pH	12
2.3.4 Temperature sensitive hydrogels	25
2.3.5 pH-sensitive hydrogels	26
2.3.6 Other stimuli able to induce a volume change in smart polymer gels	28
2.4 Applications	31
2.4.1 Targeted drug delivery	31
2.4.2 Antibacterial properties	38
2.4.3 Tissue engineering	38
2.4.4 Other applications	39
2.5 Synthesis of smart hydrogels	39
2.6 Characterisation techniques of smart hydrogels	46
2.6.1 Swelling behaviour of smart hydrogels	46
2.6.2 Force response testing	48
2.6.3 Thermal behaviour	49
2.6.4 Structural characterisation	49
2.6.5 Mechanical characterisation	55
2.6.6 Release of biomaterials	61
2.7 Oscillatory chemical reactions	62
2.7.1 Belousov-Zhabotinsky reaction	62
2.7.2 Other oscillatory reactions	64
2.8 Some applications of oscillatory chemical reactions	67
2.8.1 Polymer gels and oscillatory reactions: experimental studies	67
2.8.2 Polymer gels and oscillatory reactions – modelling studies	76
2.9 Selecting and engineering a hydrogel to be combined with an oscillatory chemical reaction	78

<b>Chapter 3 – Methodology</b>	<b>84</b>
3.1 Preparation of genipin-crosslinked chitosan-poly(vinyl pyrrolidone) hydrogels	84
3.1.1 Control reactions of genipin with n-butylamine and chitosan with ethylacetate	86
3.2 Gel permeation chromatography	86
3.3 Fourier-Transform Infrared spectroscopy	87
3.4 Ultraviolet-visible spectroscopy of genipin-crosslinked chitosan-poly(vinyl pyrrolidone) hydrogels	87
3.5 Fluorescence spectroscopy of genipin-crosslinked chitosan-poly(vinyl pyrrolidone) hydrogels	87
3.6 Morphological evaluation of genipin-crosslinked chitosan poly(vinyl pyrrolidone) hydrogels via scanning electron microscopy	88
3.6.1 Critical point drying sample preparation	88
3.6.2 Freeze drying sample preparation	88
3.6.3 Scanning electron microscopy analysis	88
3.7 Environmental scanning electron microscopy	89
3.8 Optical microscopy	89
3.9 Confocal laser scanning microscopy utilising bright-field and fluorescence illumination	89
3.9.1 Crosslinking analysis	89
3.9.2 Pore structure analysis	90
3.10 Swelling measurements of genipin-crosslinked chitosan-poly(vinyl pyrrolidone) hydrogels	90
3.10.1 Hand-held microscope	93
3.10.2 Digital cameras	94
3.10.3 Macroscale swelling analysis via fluorescence	95
3.10.4 Microscale swelling analysis via confocal laser scanning microscopy	96
3.10.5 Gravimetric swelling analysis	97
3.11 Oscillatory swelling measurements of genipin-crosslinked chitosan-poly(vinyl pyrrolidone) hydrogels	98
3.12 Oscillatory force response measurements of genipin-crosslinked chitosan-poly(vinyl pyrrolidone) hydrogels	99
3.13 Compression testing	101
3.14 Release of chemical moieties from hydrogels	103
3.14.1 Macroscale visualisation of fluorescein isothiocyanate-dextran release	104
3.14.2 Microscale visualisation of fluorescein isothiocyanate-dextran release	105
3.14.3 Ultraviolet-visible spectroscopy for characterisation of amoxicillin release	105
3.15 The bromate-sulfite-ferrocyanide reaction as a pH oscillator for cationic hydrogels	106
3.16 Force response in real-time of a hydrogel immersed in a bromate-sulfite-ferrocyanide oscillatory reaction	108

<b>Chapter 4 – Results and Discussion: Synthesis and Characterisation of Genipin-Crosslinked Chitosan-Poly(vinyl pyrrolidone) Hydrogels</b>	<b>110</b>
4.1 Chitosan molecular weight determination	110
4.2 Hydrogel preparation	110
4.3 Visual observations and UV-vis spectroscopy of hydrogels	111
4.4 Utilising confocal laser scanning microscopy with fluorescence to investigate crosslinking	115
4.5 Scanning electron microscopy analysis of the effects gelation time has on network porosity	118
4.5.1 Effect of freeze drying	118
4.5.2 Effect of critical point drying	120
4.6 Swelling measurements	123
4.7 Gravimetric swelling measurements	125
4.8 Utilising Fourier-Transform Infrared spectroscopy to study the protonation and deprotonation of network moieties	129
4.9 Utilising optical microscopy to study gel morphology as a function of pH	133
4.10 Study to determine the dependence of pH on fluorescence	136
4.11 Combination of chitosan and genipin with simple compounds to determine the behaviour of individual gel components	139
4.12 Further swelling studies to understand gel behaviour	142
4.13 Mechanical characterisation	161
4.14 Conclusions	162
<b>Chapter 5 – Results and Discussion: Improving the Stability of Genipin-Crosslinked Chitosan-Poly(vinyl pyrrolidone) Hydrogels</b>	<b>165</b>
5.1 Visual and morphological characterisation of freeze-thawed hydrogels	165
5.2 Smart behaviour of freeze-thawed hydrogels	170
5.3 Washing genipin-crosslinked chitosan-poly (vinyl pyrrolidone) hydrogels in distilled water to determine the presence of residuals	180
5.4 A study to determine the effects of freezing and thawing on the mechanical properties of genipin-crosslinked chitosan-poly (vinyl pyrrolidone) hydrogels	181
5.4.1 Uniaxial compression of genipin-crosslinked chitosan-poly (vinyl pyrrolidone) hydrogels evaluated in a dry environment	182
5.4.2 Uniaxial compression of genipin-crosslinked chitosan-poly (vinyl pyrrolidone) hydrogels evaluated in a wet environment	187
5.5 Swelling potential of freeze-thawed genipin-crosslinked chitosan-poly (vinyl pyrrolidone) hydrogels	194
5.6 Effect of constituents of genipin-crosslinked chitosan-poly (vinyl pyrrolidone) hydrogels on the swelling response	204
5.7 Further investigations of how varying the amount of chemical constituents in genipin-crosslinked chitosan-poly (vinyl pyrrolidone) hydrogels affects network properties	207
5.8 Conclusions	223

<b>Chapter 6 – Results and Discussion: Potential Applications of Genipin-Crosslinked Chitosan-Poly(vinyl pyrrolidone) Hydrogels</b>	<b>226</b>
6.1 Genipin-crosslinked chitosan-poly (vinyl pyrrolidone) hydrogels responding to oscillations in pH	226
6.2 Bromate-sulfite-ferrocyanide oscillatory chemical reaction	227
6.3 Combining freeze-thawed genipin-crosslinked chitosan-poly (vinyl pyrrolidone) hydrogels with the bromate-sulfite-ferrocyanide reaction	229
6.4 The ability of genipin-crosslinked chitosan-poly (vinyl pyrrolidone) hydrogels to release absorbed constituents	233
6.5 The potential of freeze-dried genipin-crosslinked chitosan-poly (vinyl pyrrolidone) hydrogels to release a therapeutic moiety	237
6.6 Conclusions	240
<b>Chapter 7 – Conclusions and Recommendations for Future Work</b>	<b>242</b>
<b>References</b>	<b>247</b>
<b>Appendix</b>	<b>276</b>

## List of Tables

<b>Table 2.1</b> Origins and examples of stimuli-responsive polymer gels.	18
<b>Table 2.2</b> The code and composition of G-Ch-PVP hydrogels synthesised from following a full factorial method of experimental design (Nwosu, 2013).	80
<b>Table 2.3</b> Process parameters used to study the effects of varying gelation temperature and various post-synthetic treatments on the responsiveness of G-Ch-PVP hydrogels synthesised according to the LHL composition (Nwosu, 2013).	82
<b>Table 3.1</b> Composition of glycine buffered solution.	91
<b>Table 3.2</b> Composition of phthalate buffered solution.	91
<b>Table 3.3</b> Composition of phosphate buffered solution.	91
<b>Table 3.4</b> Composition of borate buffered solution.	92
<b>Table 3.5</b> Buffer solutions synthesised upon titrating 5 M phosphoric acid against 1 M sodium hydroxide and adding sodium chloride to tailor the ionic strength.	93
<b>Table 3.6</b> Buffer solutions synthesised upon titrating 5 M citric acid against 1 M sodium hydroxide and adding sodium chloride to tailor the ionic strength.	93
<b>Table 4.1</b> Effects of gelation time and temperature on the colour of G-C-PVP hydrogels.	111
<b>Table 4.2</b> Surface porosities of freeze-dried G-Ch-PVP hydrogels determined via the analysis of SEM images using ImageJ software.	119
<b>Table 4.3</b> Internal porosities of freeze-dried G-Ch-PVP hydrogels determined via the analysis of SEM images using ImageJ software.	120
<b>Table 4.4</b> Surface porosities of critically-point dried G-Ch-PVP hydrogels determined via the analysis of SEM images using ImageJ software.	122
<b>Table 4.5</b> Internal porosities of critically-point dried G-Ch-PVP hydrogels determined via the analysis of SEM images using ImageJ software.	122
<b>Table 4.6</b> Surface porosities of G-Ch-PVP hydrogels immersed in either citric acid or phosphoric acid-based solutions in combination with sodium hydroxide. Values were determined using ImageJ.	134
<b>Table 4.7</b> Maximum excitation and emission wavelengths collected according to the method in Section 3.5 when G-Ch-PVP hydrogels immersed in citric acid or phosphoric acid-based solutions in combination with sodium hydroxide.	138
<b>Table 4.8</b> Average gravimetric swelling ratio of G-Ch-PVP hydrogels after being placed in glycine, phthalate, phosphate and borate buffers for 15 min.	144
<b>Table 5.1</b> Elastic modulus between 0-20% strain of G-Ch-PVP hydrogels that were freeze-thawed for 5 min for a varying number of cycles.	183
<b>Table 5.2</b> Elastic modulus between 0-20% strain of G-Ch-PVP hydrogels that were freeze-thawed for 15 min for a varying number of cycles.	184
<b>Table 5.3</b> Elastic modulus between 0-20% strain of G-Ch-PVP hydrogels that were freeze-thawed for 30 min for a varying number of cycles.	185
<b>Table 5.4</b> Elastic modulus between 0-20% strain of G-Ch-PVP hydrogels that were freeze-thawed for 1 h for a varying number of cycles.	186
<b>Table 5.5</b> Elastic modulus between 0-20% strain of G-Ch-PVP hydrogels that were freeze-thawed for 15 min for a varying number of cycles and immersed in a pH 2 glycine buffered solution.	188
<b>Table 5.6</b> Elastic modulus between 0-20% strain of G-Ch-PVP hydrogels that were freeze-thawed for 30 min for a varying number of cycles and immersed in a pH 2 glycine buffered solution.	189
<b>Table 5.7</b> Elastic modulus between 0-20% strain of G-Ch-PVP hydrogels that were freeze-thawed for 1 h for a varying number of cycles and immersed in a pH 2 glycine buffered solution.	191
<b>Table 5.8</b> Volume of chitosan, PVP and genipin used when alterations to the default composition were made. Specimens were placed in an oven at 37 °C for 24 h.	205
<b>Table 5.9</b> The code and composition of G-Ch-PVP hydrogels synthesised from	208

following a full factorial method of experimental design (Nwosu, 2013).	
<b>Table 5.10</b> Absorbance at 610 nm of G-Ch-PVP hydrogels synthesised according to Table 5.9 as determined by UV-Vis spectroscopy.	208
<b>Table 5.11</b> Fluorescence intensity of G-Ch-PVP hydrogels synthesised according to Table 5.9 as determined via CLSM in fluorescence mode.	209
<b>Table 5.12</b> Values of pKa of G-Ch-PVP hydrogels synthesised according to Table 5.9 as determined from Figure 5.60.	213
<b>Table 5.13</b> Process parameters used to study the effects of varying gelation temperature and various post-synthetic treatments on the responsiveness of G-Ch-PVP hydrogels synthesised according to the LHL composition (Nwosu, 2013).	214
<b>Table 5.14</b> Absorbance at 610 nm and fluorescence intensity of G-Ch-PVP hydrogels synthesised according to Table 5.13 as determined by UV-Vis spectroscopy and CLSM in fluorescence mode respectively.	214
<b>Table 5.15</b> Initial gradient during the first 30 min of swelling in Figure 5.60 where G-Ch-PVP hydrogels prepared according to Table 5.13 were swollen in a pH 2 glycine buffered solution.	216
<b>Table 5.16</b> Surface porosities of freeze-dried G-Ch-PVP hydrogels synthesised according to the LHL composition determined via the analysis of SEM images using ImageJ software.	216
<b>Table 5.17</b> Elastic modulus between 0-20% strain of LHL G-Ch-PVP hydrogels that were subject to continuous freezing or freeze-thaw treatment.	222

## List of Figures

<b>Figure 2.1</b> Polymer gels can undergo reversible volume changes in response to application of appropriate stimuli.	5
<b>Figure 2.2</b> Chemical structure of polyacrylamide.	6
<b>Figure 2.3</b> The swelling ratio ( $\phi/\phi^*$ where $\phi^*$ and $\phi$ are the volume fractions of the gel before and after the change, respectively) of a polyacrylamide gel as a function of acetone concentration in the acetone-water gel fluid mixtures at 23 °C. Gel I (solid circles) exemplifies a discrete phase transition where gelation was left to occur for 30 days and gel II (open circles) depicts a continuous phase transition where gelation was halted after 3 days (Tanaka, 1978).	7
<b>Figure 2.4</b> Chemical structure of 4-acrylamidosalicylic acid polymers exemplifying intermolecular interactions (Annaka et al., 2000).	9
<b>Figure 2.5</b> Chemical structure of poly(2-hydroxyethyl methacrylate).	10
<b>Figure 2.6</b> Diagram of stimuli responsive swelling of hydrogels (Gupta et al., 2002).	17
<b>Figure 2.7</b> Chemical structures of (a) poly(N-isopropylacrylamide) and (b) poly(acrylic acid).	26
<b>Figure 2.8</b> Diagram displaying pH dependent behaviour of (a) anionic and (b) cationic hydrogels (Gupta et al., 2002).	27
<b>Figure 2.9</b> Effect on the chemical structure of pH-sensitive anionic poly(acrylic acid) (a) and cationic chitosan (b) hydrogels on immersion in acidic and basic media.	27
<b>Figure 2.10</b> Chemical structures of the phase transition of bis(4-(dimethylamino)phenyl)(4-vinylphenyl)methyl leucocyanide which is sensitive to UV (Mamada et al., 1990).	29
<b>Figure 2.11</b> Chemical structures of poly(N-isopropylacrylamide) (a) and the trisodium salt of copper chlorophyllin (b).	30
<b>Figure 2.12</b> Conversion of spherical micelles to rod-like structures on increasing sodium chloride concentration in water.	31
<b>Figure 2.13</b> Some applications of smart polymer gels.	31
<b>Figure 2.14</b> Smart polymer gels in targeted drug delivery.	32
<b>Figure 2.15</b> Image displaying the therapeutic band showing the effects of burst release, controlled release and pulsatile release in relation to effective concentration and toxic concentration (Liechty et al., 2010).	33
<b>Figure 2.16</b> Deacetylation of chitin to form chitosan.	34
<b>Figure 2.17</b> Chemical structure of amoxicillin.	34
<b>Figure 2.18</b> Chemical structures of (a) formaldehyde, (b) glutaraldehyde, (c) ethylene glycol diglycidyl ether (an epoxy compound) and (d) genipin.	35
<b>Figure 2.19</b> Enzymatic hydrolysis of geniposide to genipin using $\beta$ -glucosidase.	36
<b>Figure 2.20</b> Proposed reaction mechanism between chitosan and genipin (Chen et al., 2005).	36
<b>Figure 2.21</b> Proposed reaction mechanism between chitosan and genipin to form a conjugated genipin derivative (Chen et al., 2005).	37
<b>Figure 2.22</b> Schematic representation of: (a) full IPN and (b) semi-IPN (Bajpai et al., 2008).	41
<b>Figure 2.23</b> Schematic of a DN gel displaying the opposite physical natures of polymer components in the structure (Gong, 2010).	42
<b>Figure 2.24</b> Optical micrographs of freeze-thawed PVA hydrogels showing the increase in polymer densification and porosity with increasing freeze thaw cycles and polymer concentration. The scale bars represent 80 $\mu$ m (Holloway et al., 2013).	44
<b>Figure 2.25</b> Schematic of the probable freeze-thawing mechanism of PVA.	45
<b>Figure 2.26</b> A typical hydrogel SEM image of a freeze dried chitosan-alginate hydrogel (Levengood and Zhang, 2014).	49
<b>Figure 2.27</b> Phase diagram illustrating how FD (outline arrow) brings the system	50

around the triple point and how CPD (solid arrow) brings the system through the supercritical region.	
<b>Figure 2.28</b> A typical hydrogel ESEM image of a hydrogel (Bai et al., 2012).	51
<b>Figure 2.29</b> Confocal microscopy image of a PVA-PEG hydrogel (Bodugoz-Senturk et al., 2009).	52
<b>Figure 2.30</b> A Jablonski diagram illustrating the transitions between electronic states.	53
<b>Figure 2.31</b> X-ray microtomography image of a poly (epsilon-caprolactone fumarate) hydrogel (Kim et al., 2009).	54
<b>Figure 2.32</b> A stress-strain graph depicting the elastic and plastic regions.	56
<b>Figure 2.33</b> A materials selection chart in order to compare the mechanical properties of various materials based on the Young's modulus and density (Ashby et al., 2009).	57
<b>Figure 2.34</b> Stress strain curves of (a) cellulose gels and (b) cellulose foams where the numbers next to each curve are density values ( $\text{kg m}^{-3}$ ). Magnified sections show strain hardening (a) and elastic behaviour followed by densification (b) (Sehaqui et al., 2011).	58
<b>Figure 2.35</b> Schematics of (a) tensile testing (Johnson et al., 2004) and (b) compression testing of hydrogels (Webber et al., 2007).	60
<b>Figure 2.36</b> Image showing chemical waves in the BZ reaction. Target patterns and spiral waves are displayed in the top and bottom rows respectively (Epstein and Showalter, 1996).	63
<b>Figure 2.37</b> Oscillations in pH recorded from the bromate-sulfite-ferrocyanide reaction (Edblom et al., 1989).	66
<b>Figure 2.38</b> Reaction scheme of PCPOC reaction (Novakovic et al., 2008).	67
<b>Figure 2.39</b> A tris (2,2'-bipyridyl) ruthenium (II) BZ reaction catalyst grafted onto a thermosensitive PNIPAAm backbone.	68
<b>Figure 2.40</b> A scheme to compare a "smart" gel and a "self-oscillating" gel (Yoshida, 2011).	69
<b>Figure 2.41</b> Time course of peristaltic motion of thermosensitive PNIPAAm hydrogel immersed in the BZ reaction where the green and orange regions correspond to the oxidised and reduced states of the ruthenium catalyst in the network, respectively (Yoshida et al., 2009).	70
<b>Figure 2.42</b> The self-walking motion of a hydrogel in the BZ reaction. Owing to the ratchet surface base, during stretching, the front edge can move forwards on the base but the back edge is prevented from sliding backwards. The opposite is the case during bending, promoting forward motion (Maeda et al., 2007).	71
<b>Figure 2.43</b> Schematic illustration and experimental observation of the mass transport of a cylindrical PAAm gel on a poly(NIPAAm-co-Ru(bpy) <sub>3</sub> -co-AMPS) gel surface (Yoshida et al., 2009).	72
<b>Figure 2.44</b> Chemical structure of poly(methacrylic acid) (PMAA).	73
<b>Figure 2.45</b> A polyacid triblock copolymer composed of poly(methyl methacrylate)- <i>block</i> -poly(methacrylic acid)- <i>block</i> -poly(methyl methacrylate) under (a) acidic and (b) neutral/basic conditions (Topham et al., 2007a).	74
<b>Figure 2.46</b> A polybase triblock copolymer composed of poly(methyl methacrylate)- <i>block</i> -poly(2-(diethyl-amino)ethyl methacrylate)- <i>block</i> -poly(methyl methacrylate) under (a) acidic and (b) neutral/basic conditions (Topham et al., 2007a).	75
<b>Figure 2.47</b> Poly(2-vinyl pyridine)	76
<b>Figure 2.48</b> Images of BZ gel morphology during one period of oscillation at simulation times: (a) 1761, (b) 1767, (c) 1773, (d) 1779, (e) 1788 and (f) 1794 seconds. The concentration of the oxidised catalyst, $v$ , is represented in colour (Yashin et al., 2010).	77
<b>Figure 2.49</b> Chemical structures of the constituents of a chitosan-PVP hydrogel crosslinked with genipin.	78
<b>Figure 2.50</b> Schematic of the probable structure of a G-Ch-PVP hydrogel where chitosan is shown in black, PVP in blue and genipin in green. Note: some bonds	79

have been stretched in order to show the hydrogen bonding between chitosan and PVP moieties.	
<b>Figure 2.51</b> Ionic forms of glycine.	80
<b>Figure 2.52</b> Optical measurement of the change in diameter and thickness to calculate the variation in volume when G-Ch-PVP hydrogels were swollen in a pH 2 glycine buffered solution (Nwosu, 2013).	81
<b>Figure 2.53</b> Optical measurement of the change in diameter and thickness to calculate the variation in volume when G-Ch-PVP hydrogels synthesised according to the LHL gel code were swollen in a pH 2 glycine buffered solution (Nwosu, 2013).	83
<b>Figure 3.1</b> Schematic depicting how the blue hydrogel is cut into discs using a sharp blade that is shown to be slicing the specimen from right to left (top view as shown in (a)) in order to produce a consistent thickness of 3 mm (side view as shown in (b)).	85
<b>Figure 3.2</b> Screenshot of the process of measuring the diameter of a hydrogel sample using ImageJ.	95
<b>Figure 3.3</b> Experimental setup to study microscale swelling via CLSM.	96
<b>Figure 3.4</b> Optical sectioning within a thick sample (green refers to the signal generated from the sample).	97
<b>Figure 3.5</b> Net and photograph of cubic PTFE cage.	98
<b>Figure 3.6</b> Experimental setup for detecting the force response of a hydrogel.	99
<b>Figure 3.7</b> Schematic of how to study the force variation of a hydrogel upon changing pH of the surrounding solution.	101
<b>Figure 3.8</b> Chemical structure of FITC-dextran.	103
<b>Figure 3.9</b> Experimental setup for the macroscale visualisation of FITC-dextran release from a polymeric hydrogel.	104
<b>Figure 3.10</b> Experimental setup for measuring the force oscillations of hydrogels during the bromate-sulfite-ferrocyanide reaction.	106
<b>Figure 3.11</b> Experimental setup for recording the temperature and pH changes due to the bromate-sulfite-ferrocyanide reaction.	107
<b>Figure 4.1</b> Time-resolved UV-Visible spectra of G-Ch-PVP hydrogels placed in an oven at 37 °C.	112
<b>Figure 4.2</b> Time-resolved UV-Visible spectra of G-Ch-PVP hydrogels placed in an oven at 37 °C focusing on the band at 610 nm.	113
<b>Figure 4.3</b> Time-resolved UV-Visible spectra of G-Ch-PVP hydrogels placed in an oven at 50 °C focusing on the band at 610 nm.	114
<b>Figure 4.4</b> Comparative plot of the absorbance maxima at 610 nm for G-Ch-PVP hydrogels placed in an oven at 37 and 50 °C.	115
<b>Figure 4.5</b> Fluorescence intensity profile of G-C-PVP hydrogels synthesised as a function of time at 37 °C.	116
<b>Figure 4.6</b> Proposed reaction mechanism between chitosan and genipin to form a conjugated genipin derivative (Chen et al., 2005).	117
<b>Figure 4.7</b> Electron micrographs of freeze-dried G-C-PVP hydrogels synthesised for (a) 6 h, (b) 12 h, (c) 48 h, (d) 72 h and (e) 96 h at 37 °C.	119
<b>Figure 4.8</b> Electron micrographs of freeze-dried G-C-PVP hydrogels depicting (a) the channels and (b) the interior structures present.	120
<b>Figure 4.9</b> Electron micrographs of G-C-PVP hydrogels that have been critically point dried following incubation at 37 °C for 24 h (a,d), 48 h (b,e) and 72 h (c,f).	121
<b>Figure 4.10</b> Electron micrographs of G-Ch-PVP hydrogels subjected to critical point drying illustrating (a) the boundary between the surface layer and the inner sphere of hydrogels, (b) the channels formed as part of the skin and (c) the honeycomb morphology.	123
<b>Figure 4.11</b> Swelling of G-Ch-PVP hydrogels placed in an oven for 24 hours and immersed in a pH 2 glycine buffered solution in a temperature-controlled water bath at 37 °C. Images were collected using a USB microscope adjusted to a constant height away from the sample.	123
<b>Figure 4.12</b> Gravimetric swelling measurements of G-Ch-PVP hydrogels	126

synthesised at 37 °C. Gels were immersed in various mixtures of phosphoric acid and sodium hydroxide solutions that were either unmodified or adjusted with sodium chloride to a higher ionic strength (25%, 50% and 75%) and monitored at 37 °C.	
<b>Figure 4.13</b> The effect of ionic strength of the surrounding buffer solution during gravimetric swelling measurements of G-Ch-PVP hydrogels synthesised at 37 °C. Gels were immersed in various mixtures of phosphoric acid and sodium hydroxide solutions that were either unmodified or adjusted with sodium chloride to a higher ionic strength (25%, 50% and 75%) and monitored at 37 °C.	127
<b>Figure 4.14</b> Gravimetric swelling measurements of G-Ch-PVP hydrogels synthesised at 37 °C. Gels were immersed in various mixtures of citric acid and sodium hydroxide solutions that were either unmodified or adjusted with sodium chloride to a higher ionic strength (25%, 50% and 75%) and monitored at 37 °C.	128
<b>Figure 4.15</b> The effect of ionic strength of the surrounding buffer solution during gravimetric swelling measurements of G-Ch-PVP hydrogels synthesised at 37 °C. Gels were immersed in various mixtures of citric acid and sodium hydroxide solutions that were either unmodified or adjusted with sodium chloride to a higher ionic strength (25%, 50% and 75%) and monitored at 37 °C.	129
<b>Figure 4.16</b> FTIR spectrum of G-Ch-PVP hydrogels immersed in various mixtures of citric acid and sodium hydroxide solutions with an unmodified ionic strength (0%).	130
<b>Figure 4.17</b> Normalised transmittance at 3300 cm <sup>-1</sup> of G-Ch-PVP hydrogels immersed in various mixtures of citric acid and sodium hydroxide solutions that were either unmodified or adjusted with sodium chloride to a higher ionic strength (25%, 50% and 75%).	131
<b>Figure 4.18</b> Variation in the wavenumber recorded of the band between 3450-3300 cm <sup>-1</sup> of G-Ch-PVP hydrogels immersed in various mixtures of citric acid and sodium hydroxide solutions that were either unmodified or adjusted with sodium chloride to a higher ionic strength (25%, 50% and 75%).	131
<b>Figure 4.19</b> Normalised transmittance at 3300 cm <sup>-1</sup> of G-Ch-PVP hydrogels immersed in various mixtures of phosphoric acid and sodium hydroxide solutions that were either unmodified or adjusted with sodium chloride to a higher ionic strength (25%, 50% and 75%).	132
<b>Figure 4.20</b> Variation in the wavenumber recorded of the band between 3450-3100 cm <sup>-1</sup> of G-Ch-PVP hydrogels immersed in various mixtures of phosphoric acid and sodium hydroxide solutions that were either unmodified or adjusted with sodium chloride to a higher ionic strength (25%, 50% and 75%).	133
<b>Figure 4.21</b> Representative optical microscopy images of G-Ch-PVP hydrogels immersed in solutions of varying pH consisting of citric acid and sodium hydroxide mixtures.	134
<b>Figure 4.22</b> Surface porosity of G-Ch-PVP hydrogels as a function of pH immersed in citric acid and phosphoric acid-based solutions in combination with sodium hydroxide.	136
<b>Figure 4.23</b> Excitation and emission spectra of a G-Ch-PVP hydrogel.	136
<b>Figure 4.24</b> Excitation spectra at 380 nm of G-Ch-PVP hydrogels as a function of pH immersed in citric acid solutions in combination with sodium hydroxide.	137
<b>Figure 4.25</b> Emission spectra at 440 nm of G-Ch-PVP hydrogels as a function of pH immersed in citric acid solutions in combination with sodium hydroxide.	138
<b>Figure 4.26</b> FTIR spectra of chitosan immersed in a pH 2 and a pH 13 solution of mixtures of hydrochloric acid and sodium hydroxide.	139
<b>Figure 4.27</b> FTIR spectra of chitosan in combination with ethyl acetate followed by immersion in various hydrochloric acid and sodium hydroxide-based buffer solutions.	140
<b>Figure 4.28</b> FTIR spectra of genipin in combination with n-butylamine followed by immersion in various hydrochloric acid and sodium hydroxide-based buffer solutions.	141
<b>Figure 4.29</b> Excitation and emission spectra of a genipin in combination with	141

n-butylamine.

- Figure 4.30** Gravimetric swelling measurements of G-Ch-PVP hydrogels synthesised at 37 °C contained in steel mesh cages immersed in various buffers at 37 °C. 142
- Figure 4.31** Gravimetric swelling measurements of G-Ch-PVP hydrogels synthesised at 37 °C contained in steel mesh cages immersed in various buffers at 10 °C. 143
- Figure 4.32** Simulated oscillatory swelling of G-Ch-PVP hydrogel (blue line) alternately immersed in pH 2 glycine buffer and pH 10 borate buffer (green line) with a time period of 15 min. 145
- Figure 4.33** Swelling of G-Ch-PVP hydrogels placed in an oven at 37 °C for various time periods and subsequently washed for 24 h in methanol before being immersed in a pH 2 glycine buffered solution. 146
- Figure 4.34** Comparative plot of porosity determined via SEM following CPD with swelling rate during the first 15 min of G-Ch-PVP hydrogels placed in an oven at 37 °C for various time periods and subsequently washed for 24 h in methanol before being immersed in a pH 2 glycine buffered solution. 147
- Figure 4.35** Swelling of G-Ch-PVP hydrogels placed in an oven at 37 °C for various time periods and subsequently washed for 24 h in methanol before being immersed in a pH 4 phthalate buffered solution. 148
- Figure 4.36** Swelling of G-Ch-PVP hydrogels placed in an oven at 37 °C for various time periods and subsequently washed for 24 h in methanol before being immersed in a pH 7 phosphate buffered solution. 149
- Figure 4.37** Swelling of G-Ch-PVP hydrogels placed in an oven at 37 °C for various time periods and subsequently washed for 24 h in methanol before being immersed in a pH 10 borate buffered solution. 149
- Figure 4.38** Swelling of G-Ch-PVP hydrogels placed in an oven at 37 °C for 24 h and subsequently washed for 24 h in methanol before being immersed in various buffered solutions. 150
- Figure 4.39** Swelling of G-Ch-PVP hydrogels placed in an oven at 37 °C for 48 h and subsequently washed for 24 h in methanol before being immersed in various buffered solutions. 151
- Figure 4.40** Swelling of G-Ch-PVP hydrogels placed in an oven at 37 °C for 72 h and subsequently washed for 24 h in methanol before being immersed in various buffered solutions. 151
- Figure 4.41** Oscillatory swelling of hydrogels placed in an oven for 24 h at 37 °C, washed in methanol and immersed in a pH 2 glycine buffer first in an alternate fashion with a time period of 15 min at 20 °C. 152
- Figure 4.42** Oscillatory swelling of hydrogels placed in an oven for 24 h at 37 °C, washed in methanol and immersed in a pH 4 phthalate buffer first in an alternate fashion with a time period of 15 min at 20 °C. 153
- Figure 4.43** Oscillatory swelling of hydrogels placed in an oven for 24 h at 37 °C, washed in methanol and immersed in a pH 2 glycine buffer first in an alternate fashion with a time period of 150 min at 20 °C. 154
- Figure 4.44** Oscillatory swelling of hydrogels placed in an oven for 24 h at 37 °C, washed in methanol and immersed in a pH 4 phthalate buffer first in an alternate fashion with a time period of 150 min at 20 °C. 154
- Figure 4.45** Oscillatory swelling of hydrogels placed in an oven for 24 h at 37 °C, washed in methanol, pre-swollen in a pH 4 phthalate buffer then immersed in a pH 2 glycine buffer first in an alternate fashion with a time period of 15 min at 20 °C. 155
- Figure 4.46** Oscillatory swelling of hydrogels placed in an oven for 24 h at 37 °C, washed in methanol pre-swollen in a pH 2 buffer then immersed in a pH 4 buffer first in an alternate fashion with a time period of 15 min at 20 °C. 156
- Figure 4.47** Oscillatory swelling of hydrogels placed in an oven for 24 h at 37 °C, washed in methanol, pre-swollen in a pH 4 phthalate buffer then immersed in a pH 2 glycine buffer in an alternate fashion with a time period of 157

150 min at 20 °C.	
<b>Figure 4.48</b> Oscillatory swelling of hydrogels placed in an oven for 24 h at 37 °C, washed in methanol pre-swollen in a pH 2 buffer then immersed in a pH 4 buffer first in an alternate fashion with a time period of 150 min at 20 °C.	157
<b>Figure 4.49</b> Swelling of G-Ch-PVP hydrogels of varying thicknesses placed in an oven at 37 °C and washed for 24 h in methanol before being immersed in a pH 2 glycine buffered solution.	158
<b>Figure 4.50</b> Swelling of G-Ch-PVP hydrogels of varying thicknesses placed in an oven at 37 °C and washed for 24 h in methanol before being immersed in a pH 4 phthalate buffered solution.	159
<b>Figure 4.51</b> Swelling of G-Ch-PVP hydrogels of varying thicknesses placed in an oven at 37 °C and washed for 24 h in methanol before being immersed in a pH 7 phosphate buffered solution.	159
<b>Figure 4.52</b> Swelling of G-Ch-PVP hydrogels of varying thicknesses placed in an oven at 37 °C and washed for 24 h in methanol before being immersed in a pH 10 borate buffered solution.	160
<b>Figure 4.53</b> Oscillatory swelling of hydrogels of varying thicknesses placed in an oven for 24 h at 37 °C, washed in methanol, pre-swollen in a pH 2 buffer then immersed in a pH 4 buffer first in an alternate fashion with a time period of 15 min at 20 °C.	161
<b>Figure 4.54</b> Oscillatory swelling of hydrogels of varying thicknesses placed in an oven for 24 h at 37 °C, washed in methanol, pre-swollen in a pH 2 buffer then immersed in a pH 4 buffer first in an alternate fashion with a time period of 150 min at 20 °C.	161
<b>Figure 4.55</b> A stress-strain graph depicting a uniaxial compression test of G-Ch-PVP hydrogels where samples were compressed to 50% of their thickness.	162
<b>Figure 5.1</b> An image of a G-Ch-PVP hydrogel placed in an oven for 24 h at 37 °C, frozen for 30 min at -10 °C, thawed for 24 h at 2 °C and swollen in distilled water for 24 h at room temperature taken with a digital camera.	166
<b>Figure 5.2</b> G-C-PVP hydrogel microstructure analysed by optical microscopy.	167
<b>Figure 5.3</b> G-C-PVP hydrogel microstructure analysed by SEM following CPD (Hurst and Novakovic, 2013).	167
<b>Figure 5.4</b> G-C-PVP hydrogel microstructure analysed by SEM following FD (Hurst and Novakovic, 2013).	168
<b>Figure 5.5</b> G-C-PVP hydrogel microstructure analysed by ESEM (Hurst and Novakovic, 2013).	168
<b>Figure 5.6</b> G-C-PVP hydrogel microstructure analysed by CLSM in reflectance mode.	169
<b>Figure 5.7</b> G-C-PVP hydrogel microstructure analysed by CLSM in fluorescence mode.	170
<b>Figure 5.8</b> Swelling of freeze-thawed G-Ch-PVP hydrogels in a pH 2 glycine buffer studied via gravimetric and optical techniques (Hurst and Novakovic, 2013).	171
<b>Figure 5.9</b> Swelling of freeze-thawed G-Ch-PVP hydrogels in a pH 2 glycine buffer studied by determining the change in macro-fluorescence intensity over time (Hurst and Novakovic, 2013).	172
<b>Figure 5.10</b> Swelling of freeze-thawed G-Ch-PVP hydrogels in a pH 2 glycine buffer studied by determining the change in macro-fluorescence intensity over time (normalised values).	173
<b>Figure 5.11</b> Normalised values of a freeze-thawed G-Ch-PVP hydrogel pre-swollen in a pH 2 glycine buffer where the change in macro-fluorescence intensity was measured over time.	173
<b>Figure 5.12</b> A plot of the swelling ratio of freeze-thawed G-Ch-PVP hydrogels in a pH 2 glycine buffer determined gravimetrically and optically against the macro-fluorescence intensity.	174
<b>Figure 5.13</b> CLSM images of freeze-thawed G-Ch-PVP swelling in a pH 2	175

glycine buffer at 0 min collected in reflectance mode (Hurst and Novakovic, 2013).	
<b>Figure 5.14</b> CLSM images of freeze-thawed G-Ch-PVP swelling in a pH 2 glycine buffer at 15 min collected in reflectance mode (Hurst and Novakovic, 2013).	176
<b>Figure 5.15</b> CLSM images of freeze-thawed G-Ch-PVP swelling in a pH 2 glycine buffer at 30 min collected in reflectance mode (Hurst and Novakovic, 2013).	176
<b>Figure 5.16</b> Change in porosity of freeze-thawed G-Ch-PVP hydrogels as a function of time during swelling in a pH 2 glycine buffer (Hurst and Novakovic, 2013).	177
<b>Figure 5.17</b> The relationship between the porosity and gravimetric measurements of freeze-thawed G-Ch-PVP hydrogels swelling in a pH 2 glycine buffer (Hurst and Novakovic, 2013).	177
<b>Figure 5.18</b> Image collected using CLSM with fluorescence of a freeze-thawed G-Ch-PVP hydrogel swelling in a pH 2 glycine buffered solution at 0 min (Hurst and Novakovic, 2013).	178
<b>Figure 5.19</b> Images collected using CLSM with fluorescence of a freeze-thawed G-Ch-PVP hydrogel swelling in a pH 2 glycine buffered solution at 15 min (Hurst and Novakovic, 2013).	178
<b>Figure 5.20</b> Images collected using CLSM with fluorescence of a freeze-thawed G-Ch-PVP hydrogel swelling in a pH 2 glycine buffered solution at 30 min (Hurst and Novakovic, 2013).	179
<b>Figure 5.21</b> Change in micro-fluorescence intensity of freeze-thawed G-Ch-PVP hydrogels during swelling in a pH 2 glycine buffered solution (Hurst and Novakovic, 2013).	179
<b>Figure 5.22</b> A plot of the swelling ratio of freeze-thawed G-Ch-PVP hydrogels in a pH 2 glycine buffer determined gravimetrically and optically against the micro-fluorescence intensity.	180
<b>Figure 5.23</b> Absorbance data to analyse for PVP (213 nm) and genipin (240 nm) from UV-Vis spectroscopy of distilled water wash solutions following immersions with a G-Ch-PVP hydrogel after 30 min (Wash 1), 1 h (Wash 2), 2 h (Wash 3), 3 h (Wash 4) and 48 h (Wash 5) to include a purely distilled water reference following no washes.	181
<b>Figure 5.24</b> Stress-strain graph depicting uniaxial compression tests for G-Ch-PVP hydrogels that were freeze-thawed for 5 min for a varying number of cycles.	183
<b>Figure 5.25</b> Stress-strain graph depicting uniaxial compression tests for G-Ch-PVP hydrogels that were freeze-thawed for 15 min for a varying number of cycles.	184
<b>Figure 5.26</b> Stress-strain graph depicting uniaxial compression tests for G-Ch-PVP hydrogels that were freeze-thawed for 30 min for a varying number of cycles.	185
<b>Figure 5.27</b> Stress-strain graph depicting uniaxial compression tests for G-Ch-PVP hydrogels that were freeze-thawed for 1 h for a varying number of cycles.	186
<b>Figure 5.28</b> Comparison of the effects of freeze-thaw time and the number of freeze-thaw cycles on the average variation in the elastic modulus of G-Ch-PVP hydrogels.	187
<b>Figure 5.29</b> Stress-strain graph depicting uniaxial compression tests for G-Ch-PVP hydrogels that were freeze-thawed for 15 min for a varying number of cycles and immersed in a pH 2 buffered solution during testing.	188
<b>Figure 5.30</b> Stress-strain graph depicting uniaxial compression tests for G-Ch-PVP hydrogels that were freeze-thawed for 30 min for a varying number of cycles and immersed in a pH 2 glycine buffered solution during testing.	189
<b>Figure 5.31</b> Stress-strain graph depicting uniaxial compression tests for G-Ch-PVP hydrogels that were freeze-thawed for 1 h for a varying number of	190

cycles and immersed in a pH 2 glycine buffered solution during testing.	
<b>Figure 5.32</b> Comparison of the effects of freeze-thaw time and the number of freeze-thaw cycles on the average variation in the elastic modulus of G-Ch-PVP hydrogels immersed in a pH 2 glycine buffered solution.	191
<b>Figure 5.33</b> Comparison between the elastic modulus of G-Ch-PVP hydrogels that were freeze-thawed for 15 min for various cycles and compressed in either a dry environment or via immersion in a pH 2 glycine buffer.	192
<b>Figure 5.34</b> Comparison between the elastic modulus of G-Ch-PVP hydrogels that were freeze-thawed for 30 min for various cycles and compressed in either a dry environment or via immersion in a pH 2 glycine buffer.	192
<b>Figure 5.35</b> Comparison between the elastic modulus of G-Ch-PVP hydrogels that were freeze-thawed for 1 h for various cycles and compressed in either a dry environment or via immersion in a pH 2 glycine buffer.	193
<b>Figure 5.36</b> Comparison between the elastic modulus of G-Ch-PVP hydrogels that were freeze-thawed once for various time periods and compressed in either a dry environment or via immersion in a pH 2 glycine buffer.	193
<b>Figure 5.37</b> Gravimetric swelling of G-Ch-PVP hydrogels swollen in distilled water.	194
<b>Figure 5.38</b> Gravimetric swelling of G-Ch-PVP hydrogels swollen in distilled water showing the initial response.	195
<b>Figure 5.39</b> Gravimetric swelling of G-Ch-PVP hydrogels freeze-thawed for 5 min and swollen in distilled water.	196
<b>Figure 5.40</b> Gravimetric swelling of G-Ch-PVP hydrogels freeze-thawed for 5 min and swollen in distilled water showing the initial response.	196
<b>Figure 5.41</b> Gravimetric swelling of G-Ch-PVP hydrogels freeze-thawed for 15 min and swollen in distilled water.	197
<b>Figure 5.42</b> Gravimetric swelling of G-Ch-PVP hydrogels freeze-thawed for 15 min and swollen in distilled water showing the initial response.	197
<b>Figure 5.43</b> Gravimetric swelling of G-Ch-PVP hydrogels freeze-thawed for 30 min and swollen in distilled water.	198
<b>Figure 5.44</b> Gravimetric swelling of G-Ch-PVP hydrogels freeze-thawed for 30 min and swollen in distilled water showing the initial response.	198
<b>Figure 5.45</b> Gravimetric swelling of G-Ch-PVP hydrogels freeze-thawed for 1 h and swollen in distilled water.	199
<b>Figure 5.46</b> Gravimetric swelling of G-Ch-PVP hydrogels freeze-thawed for 1 h and swollen in distilled water showing the initial response.	199
<b>Figure 5.47</b> Comparison of the swelling ratio of G-Ch-PVP hydrogels in distilled water that were freeze-thawed for various cycles and time scales with the elastic modulus.	200
<b>Figure 5.48</b> Comparison of the elastic modulus of freeze-thawed G-Ch-PVP hydrogels as a function of pH in citric acid and sodium hydroxide-based buffer solutions.	201
<b>Figure 5.49</b> Comparison of the elastic modulus of G-Ch-PVP hydrogels freeze-thawed for 15 min with the overall swelling ratio after 24 h in citric acid and sodium hydroxide-based buffer solutions at varying pH.	201
<b>Figure 5.50</b> Variation in the surface porosity of G-Ch-PVP hydrogels immersed in various mixtures of citric acid and sodium hydroxide solutions as a function of their elastic modulus.	202
<b>Figure 5.51</b> Representation of hydrogen bonding between chitosan and PVP moieties prior to freeze-thawing. Genipin moieties have been omitted for clarity.	203
<b>Figure 5.52</b> Representation of hydrogen bonding between chitosan and PVP moieties upon freeze-thawing. Genipin moieties have been omitted for clarity.	203
<b>Figure 5.53</b> Representation of hydrogen bonding between chitosan and PVP moieties upon continued freeze-thawing. Genipin moieties have been omitted for clarity.	204
<b>Figure 5.54</b> Gravimetric swelling measurements in a pH 2 buffered solution of high (2000 $\mu$ L) and low (500 $\mu$ L) chitosan combined with PVP (200 $\mu$ L) and	205

genipin (100 $\mu$ L) to form a hydrogel.	
<b>Figure 5.55</b> Gravimetric swelling measurements in a pH 2 buffered solution of high (400 $\mu$ L) and low (100 $\mu$ L) PVP combined with chitosan (1000 $\mu$ L) and genipin (100 $\mu$ L) to form a hydrogel.	206
<b>Figure 5.56</b> Gravimetric swelling measurements in a pH 2 buffered solution of high (200 $\mu$ L) and low (50 $\mu$ L) genipin combined with chitosan (1000 $\mu$ L) and PVP (200 $\mu$ L) to form a hydrogel.	207
<b>Figure 5.57</b> A comparison between the average pixel intensity of 0.25 mm <sup>2</sup> samples of G-Ch-PVP hydrogels determined via CLSM in fluorescence mode and their absorbance at 610 nm as measured by UV-Vis spectroscopy.	209
<b>Figure 5.58</b> Gravimetric swelling of G-Ch-PVP hydrogels prepared according to Table 5.9 in a pH 2 glycine buffered solution.	210
<b>Figure 5.59</b> Pareto chart displaying the importance of chitosan (A), PVP (B) and genipin (C) with respect to the swelling ratio of hydrogels in Figure 5.58.	212
<b>Figure 5.60</b> Gravimetric swelling of G-Ch-PVP hydrogels prepared according to Table 5.9 during a potentiometric titration of sodium hydroxide and phosphoric acid. The ionic strength of all solutions was adjusted to 0.1 mol kg <sup>-1</sup> using sodium chloride. Samples were left for 3 h to equilibrate.	213
<b>Figure 5.61</b> Gravimetric swelling of G-Ch-PVP hydrogels prepared according to Table 5.13 in a pH 2 glycine buffered solution.	215
<b>Figure 5.62</b> SEM images of G-Ch-PVP hydrogels synthesised according to the LHL gel code composition and placed in an oven at 30 (LHLa), 40 (LHLb) and 50 °C (LHLc) with no post-synthetic treatment.	217
<b>Figure 5.63</b> SEM images of G-Ch-PVP hydrogels synthesised according to the LHL gel code composition and placed in an oven at 30 (LHL1), 40 (LHL3) and 50 °C (LHL5) continuously frozen for 72 h.	218
<b>Figure 5.64</b> SEM images of G-Ch-PVP hydrogels synthesised according to the LHL gel code composition and placed in an oven at 30 (LHL2), 40 (LHL4) and 50 °C (LHL6) subjected to 3 freeze-thaw cycles of 24 h freezing and 3 h thawing.	219
<b>Figure 5.65</b> Photograph of LHL hydrogels placed in an oven at 30, 40 and 50 °C and stored in a fridge (5 °C) without subsequent manipulation.	220
<b>Figure 5.66</b> Uniaxial compression tests of LHL G-Ch-PVP hydrogels that were subject to post-synthesis continuous freezing.	221
<b>Figure 5.67</b> Uniaxial compression tests of LHL G-Ch-PVP hydrogels that were subject to post-synthesis freeze-thaw treatment.	221
<b>Figure 5.68</b> Comparison between the elastic modulus of LHL G-Ch-PVP hydrogels that were subject to continuous freezing or freeze-thaw treatment.	223
<b>Figure 6.1</b> Oscillatory swelling of freeze-thawed G-Ch-PVP hydrogels (30 min, 1 cycle) determined by measuring the change in force exerted on a compression plate during immersion in pH 2 glycine and pH 4 phthalate buffered solutions.	227
<b>Figure 6.2</b> Variation in pH as a function of time during the BSF oscillatory reaction.	228
<b>Figure 6.3</b> Oscillatory swelling of freeze-thawed G-Ch-PVP hydrogels (30 min, 1 cycle) determined by measuring the change in force exerted on a compression plate during immersion in pH 4 phthalate and pH 7 phosphate buffered solutions.	228
<b>Figure 6.4</b> Variation in pH as a function of time during the BSF reaction (blue curve) and the force response of a G-Ch-PVP hydrogel freeze-thawed for 30 min (red curve). Hydrogel is composed of 1 mL chitosan (1.5% w/v), 200 $\mu$ L PVP (5% w/v) and 100 $\mu$ L genipin (0.5% w/v).	230
<b>Figure 6.5</b> Gravimetric swelling measurements of G-Ch-PVP hydrogels synthesised at 37 °C. Gels were immersed in various mixtures of citric acid/phosphoric acid and sodium hydroxide solutions. The hydrogel is composed of 1.5 mL chitosan (1.5% w/v), 50 $\mu$ L PVP (5% w/v) and 100 $\mu$ L genipin (0.5% w/v).	231
<b>Figure 6.6</b> Variation in pH as a function of time during the BSF reaction (blue	232

curve) and the force response of a G-Ch-PVP hydrogel freeze-thawed for 30 min (red curve). The hydrogel is composed of 1.5 mL chitosan (1.5% w/v), 50 $\mu$ L PVP (5% w/v) and 100 $\mu$ L genipin (0.5% w/v).	
<b>Figure 6.7</b> The relationship between variation in pH during the BSF reaction and the force response of a G-Ch-PVP hydrogel freeze-thawed for 30 min. The hydrogel is composed of 1.5 mL chitosan (1.5% w/v), 50 $\mu$ L PVP (5% w/v) and 100 $\mu$ L genipin (0.5% w/v).	233
<b>Figure 6.8</b> Fluorescence excitation and emission spectra for a FITC-dextran solution (10 mg mL <sup>-1</sup> ). Parameters utilised to acquire the spectra are detailed in Section 3.14.	234
<b>Figure 6.9</b> Photographs of a 30 min freeze-thawed G-Ch-PVP hydrogel equilibrated in a pH 7 buffered solution; transferred to a FITC-dextran solution (10 mg mL <sup>-1</sup> ) and collapsed in a pH 10 borate solution. Images were taken at (a) 0 min, (b) 1 h (c) 2 h and (d) 3 h. All scale bars are 20 mm.	235
<b>Figure 6.10</b> Variation in fluorescence intensity as a function of pixels (blue curve) as a dextran-loaded G-Ch-PVP hydrogel is forced to collapse (red curve).	236
<b>Figure 6.11</b> CLSM images of (a) autofluorescence from the hydrogel matrix, (b) fluorescence from FITC-dextran and (c) an overlay of the fluorescence from the FITC-dextran on the autofluorescent gel surface. All scale bars are 150 $\mu$ m.	236
<b>Figure 6.12</b> Variation of fluorescence intensity as a function of pixel intensity on the microscale during collapse of G-Ch-PVP hydrogels, resulting in the expulsion of FITC-dextran.	237
<b>Figure 6.13</b> Amoxicillin released from freeze-dried G-Ch-PVP hydrogels in simulated GI fluid (blue curve) and the simultaneous swelling of samples recorded optically (red curve).	238
<b>Figure 6.14</b> Comparison between cumulative amoxicillin released from freeze-dried G-Ch-PVP hydrogels in simulated GI fluid and the simultaneous swelling of samples recorded optically.	239

## Abbreviations

3-D: Three-Dimensional  
AFM: Atomic Force Microscopy  
AMPS: 2-acrylamido-2-methylpropanesulfonic acid  
ATR: Attenuated Total Reflectance  
BL: Bray-Liebhafsky  
BR: Briggs-Rauscher  
BSF: Bromate-Sulfite-Ferrocyanide  
BZ: Belousov-Zhabotinsky  
CCD: Charge-Coupled Device  
CLSM: Confocal Laser Scanning Microscopy  
CPD: Critical Point Drying  
CSTR: Continuous-flow, Stirred Tank Reactor  
DOE: Design of Experiment  
DN: Double-Network  
DSC: Differential Scanning Calorimetry  
EMAAM: N-Ethylmethacrylamide  
ESEM: Environmental Scanning Electron Microscopy  
EVAc: Ethylene-vinyl acetate  
FD: Freeze-Drying  
FITC: Fluorescein Isothiocyanate  
FTIR: Fourier Transform Infrared Spectroscopy  
G-Ch-PVP: Genipin-crosslinked chitosan-poly(vinyl pyrrolidone)  
GI: Gastrointestinal  
GPC: Gel Permeation Chromatography  
HPLC: High Performance Liquid Chromatography  
IPN: Interpenetrating Networks  
IR: Infrared  
LCST: Lower Critical Solution Temperature

MCT: Mercury Cadmium Telluride  
MTC: Minimum Toxic Concentration  
NIH: National Institutes of Health  
PAAc: Poly(acrylic acid)  
PAAm: Polyacrylamide  
PAMPS: Poly (2-acrylamido, 2-methyl, 1-propanesulfonic acid)  
PCPOC: Palladium Catalysed Phenylacetylene Oxidative Carbonylation  
PEG: Poly(ethylene glycol)  
PMAA: Poly(methacrylic acid)  
PNIPAAm: Poly(N-isopropylacrylamide)  
PVP: Poly(vinyl pyrrolidone)  
PTFE: Poly(tetrafluoroethylene)  
PVA: Poly(vinyl alcohol)  
P2VP: Poly(2-vinyl pyridine)  
QCM: Quartz Crystal Microbalance  
SAOS: Small-Amplitude Oscillatory Shear  
SAXS: Small-Angle X-Ray Scattering  
SEM: Scanning Electron Microscopy  
UCST: Upper Critical Solution Temperature  
UV: Ultra-Violet

## Symbols

$(\phi/\phi^*)$ : Swelling ratio	%
$\sigma$ : Stress	Pa
$\epsilon$ : Engineering strain	Dimensionless
$\lambda$ : Elastic modulus	Pa
$a$ : Final gel area	$\text{mm}^2$
$a^*$ : Initial gel area	$\text{mm}^2$
$a_{\text{H}^+}$ : Hydrogel ion activity	Dimensionless
$a_i$ : Activity of a species	Dimensionless
$\underline{a}$ : Exponent of Mark-Houwink equation	Dimensionless
$A$ : Deformation area	$\text{m}^2$
$A$ : Empirical parameter defined as 0.509	$\text{mol}^{-1/2} \text{kg}^{1/2}$
$\underline{A}$ : Pre-exponential factor	$\text{s}^{-1}$ (if first order)
$A(\text{aq})$ : Conjugate base	-
$c_i$ : Molar concentration	$\text{mol dm}^{-3}$
$d$ : Final gel diameter	mm
$d^*$ : Initial gel diameter	mm
$D$ : Distance	nm
$e$ : Elementary charge	C
$E$ : Recorded potential	$\text{J C}^{-1}$
$E^0$ : Standard electrode potential	$\text{J C}^{-1}$
$E_a$ : Activation energy	$\text{kJ mol}^{-1}$
$F$ : Force	N
$F$ : Faraday constant	$\text{C mol}^{-1}$
$\underline{F}$ : Coulomb Force	N
$\Delta G$ : Gibbs free energy change	$\text{J mol}^{-1}$
$h$ : Final gel height	mm
$h^*$ : Initial gel height	Mm
$\Delta H$ : Enthalpy change	$\text{J mol}^{-1}$
$\text{HA}(\text{aq})$ : Weak acid	-
$I$ : Ionic strength	$\text{mol kg}^{-1}$
$K$ : Spring constant	$\text{N m}^{-1}$
$\underline{K}$ : Exponent of Mark-Houwink equation	Dimensionless
$K$ : Rate constant for a reaction	$\text{s}^{-1}$ (if first order)
$\kappa$ : Debye screening length	nm
$K_a$ : Acid dissociation constant	$\text{mol dm}^{-3}$
$K_b$ : Base dissociation constant	$\text{mol dm}^{-3}$
$K_w$ : Ionic product of water	$\text{mol}^2 \text{dm}^{-6}$
$L^*$ : Initial gel length	mm
$L$ : Final gel length	mm
$M_i$ : Molar mass of polymer species	$\text{g mol}^{-1}$
$M_n$ : Number average molar mass	$\text{g mol}^{-1}$
$M_v$ : Viscosity average molar mass	$\text{g mol}^{-1}$
$M_w$ : Weight average molar mass	$\text{g mol}^{-1}$
$M_z$ : Z-average molar mass	$\text{g mol}^{-1}$
$N_i$ : Number of moles of polymer species	mol
$Q_1$ and $Q_2$ : Charge 1 and Charge 2	Dimensionless
$R$ : Universal gas constant	$\text{J K}^{-1} \text{mol}^{-1}$
$\Delta S$ : Entropy change	$\text{J K}^{-1} \text{mol}^{-1}$
$T$ : Temperature	K

V: Final gel volume	mm <sup>3</sup>
V*: Initial gel volume	mm <sup>3</sup>
W <sub>s</sub> : Weight of a swollen hydrogel	g
W <sub>d</sub> : Weight of a dry hydrogel	g
w(r): Free energy of the Coulombic interaction	J
x: Extension	m
z: Ionic valency	Dimensionless
ε: Relative permittivity of a medium	J <sup>-1</sup> C <sup>2</sup> m <sup>-1</sup>
ε <sub>0</sub> : Permittivity of a vacuum	J <sup>-1</sup> C <sup>2</sup> m <sup>-1</sup>
μ <sub>i</sub> : Chemical potential of a species under specified conditions	J mol <sup>-1</sup>
μ <sup>⊖</sup> <sub>i</sub> : Chemical potential of a species in the selected standard state	J mol <sup>-1</sup>
[η]: Intrinsic viscosity	Dimensionless

## Chapter 1 – Introduction

Smart materials are able to detect a change in their surrounding environment and respond by varying some of their properties in a controlled fashion. In particular, smart polymer gels are able to undergo a conformational rearrangement upon variation in a stimulus such as pH/temperature/magnetic field/electric field. Such intelligent materials can be applied in a range of scenarios. For example, the associated structural change may be used to force host molecules out of the gel matrix during network collapse or into the porous architecture during swelling. This mechanism is very useful in developing systems for separation and drug delivery (Vashist et al., 2014, Kim and Park, 1998). In the release of therapeutics, this allows for drugs to be delivered only where and when required. For example, in the treatment of diabetes, insulin can be loaded into a glucose-sensitive hydrogel (Traitel et al., 2000). Upon an increase in the blood glucose level, smart networks can detect this change and respond by releasing insulin. Release will then be automatically halted when the glucose level drops and stabilises. By carefully selecting the stimulus that the gel responds to, release can occur in a targeted manner. Alternatively, antibacterial compounds can be contained within the hydrogel matrix and only released when desired according to the an appropriate stimulus such as pH (Pavlukhina et al., 2010). Owing to the major problem of bacterial resistance in the modern world, partially originating from the accumulation of antibiotics in the environment (Silver and Bostian, 1993, Khan et al., 2012), novel approaches to tackle this problem are in high demand. Such a smart antibiotic carrier may prevent the accumulation of antimicrobial materials in the environment. Another application of smart polymer gels is as chemo-mechanical valves for microfluidic systems whereby the gel can restrict fluid flow when swollen and allow fluid to pass upon network collapse (Park et al., 2006). Every year millions of patients suffer the loss or failure of an organ or tissue due to accidents or disease (Song and Ott, 2011), transplantation is a popular solution, but extremely limited by donor shortage (Yusen et al., 2013). Smart hydrogels that can selectively respond to cells to initiate tissue growth and regeneration may be a viable alternative to transplantation (Nichol et al., 2010). As polymer gels mimic the natural extracellular matrices found in tissues, such materials make for highly desirable candidates.

However, all of these applications require an external variation in an appropriate stimulus for the hydrogel to respond. Additionally, the release of therapeutic moieties is often uncontrolled and limited by diffusion. This results in a burst release regime, which is far from optimal as it requires frequent administration (Fu and Kao, 2010). Release of a therapeutic in a controlled and sustained manner so that intervention is needed on a less frequent basis (e.g. at least over one month) is far more desirable. One way to gain control is to couple intelligent polymer gels with oscillatory chemical reactions that generate pronounced changes in a stimulus to which the smart network can respond. This allows for the development of autonomous, self-oscillatory gels (Yoshida, 2010). In theory, an oscillatory reaction may occur inside a smart gel, forcing the network to swell and collapse, and in doing so release absorbed therapeutics in pulses where the time period can be tuned according to the nature of the reaction.

The combination of smart polymer gels and oscillatory reactions also has potential in developing new modes of actuation in terms of the generation of force, physical movement or transportation of loads. These systems can also be applied in biomimetics in order to artificially copy how critical functions in the body such as respiration or digestion may occur (Yoshida et al., 2009, Maeda et al., 2008, Shiraki and Yoshida, 2012, Tabata et al., 2002).

Current challenges include the low stability and mechanical strength of polymer gels. This severely limits the development of applications. For example, if the drug carrier were to allow the leakage of therapeutics before reaching the target site, the drug delivery system will ultimately fail. It is currently very difficult to engineer hydrogels with good bio-properties whilst retaining a fast swelling response and being sufficiently stable to be applied in multiple harsh environments (Imran et al., 2010). For example, increasing the crosslinking density may enhance the stability of the network, but the degree of swelling may diminish (Abdeen, 2011). Furthermore, accurate characterisation of smart hydrogels in terms of swelling response, morphology and mechanical properties is not very well developed, making it difficult to engineer these networks with a prospective application in mind.

This thesis uses genipin-crosslinked chitosan-poly(vinyl pyrrolidone) hydrogels as a core material. Chitosan is a cationic natural polymer with exceptional bio-related properties; it is biocompatible, biodegradable, mucoadhesive and has been used as the major component of several smart delivery systems (Munjeri et al., 1997, Sogias et al., 2008, Khurma et al., 2005, Muzzarelli, 2009, Jayakumar et al., 2010, Kean and Thanou, 2010, Risbud et al., 2000). Poly(vinyl pyrrolidone) is a synthetic polymer used to enhance the mechanical stability of the network whilst retaining haemocompatibility of the system. Genipin is a natural crosslinking agent with low cytotoxicity that autofluoresces upon the formation of crosslinks (Hwang et al., 2011). The combination of smart attributes, bio-related properties and potential stability made this system a strong candidate for coupling to reactions that can oscillate in pH. This investigation employs a multitude of hydrogel characterisation techniques in order to understand more about this smart network, whilst improving the swelling response and stability. Further to this, potential applications of the material are explored. As such, the aims of this study are to characterise a pH-responsive hydrogel and investigate the feasibility of coupling the smart material to a reaction that oscillates in pH. From this, the key objectives are to:

- Synthesise a pH-responsive hydrogel and determine the pH-dependent swelling behaviour.
- Characterise the hydrogel by determining the morphology and mechanical properties
- Couple the gel to a reaction that oscillates in pH.

Chapter 2 outlines what smart polymer gels are and will discuss their synthesis and current characterisation methods. Emphasis is placed on where these smart materials are currently being engineered to find application. An introduction to oscillatory chemical reactions is provided together with published literature of the combination of smart polymer gels with such non-equilibrium systems. Chapter 3 discusses the methods used in subsequent studies, which can be briefly summarised as synthesis, characterisation of swelling response (e.g. gravimetrically or optically), mechanical stability and structural morphology.

Finally, development towards prospective applications such as combination with an oscillatory reaction and release of absorbed chemical moieties are evaluated.

The results and discussion chapters (4, 5 and 6) detail the synthesis of genipin-crosslinked chitosan-poly(vinyl pyrrolidone) hydrogels together with characterisation of the swelling response, morphology, ability to respond to an oscillatory pH regime and mechanical stability. These studies are built upon by exploring methods to increase the stability of the network via freezing and thawing for various timescales and cycles. Following this, an experimental design is constructed where the gel constituents are varied and the effects on structure, swelling and morphology are investigated. Links between each of these network properties are subsequently made. This knowledge is subsequently consolidated in order to explore applications of these materials. Studies include the combination of these hydrogels with an oscillatory reaction and monitoring release of absorbed constituents qualitatively and quantitatively. Finally, conclusions are drawn and directions for potential future work are outlined in chapter 7.

## Chapter 2 – Literature Review

This chapter details the published literature in the field of smart polymeric hydrogels from synthesis, characterisation to application development. Oscillatory chemical reactions are discussed and investigations where such non-equilibrium systems have successfully been coupled to polymers are reviewed.

### 2.1 Overview of polymer gels and their responsive nature

Polymer gels are defined as extensively crosslinked macromolecular networks (Flory, 1941) that are able to swell to many times their original size (Free, 1917). By carefully selecting gel constituents, it is possible to engineer these materials to be “smart”. This work was pioneered by Toyochi Tanaka who discovered that gels can exhibit significant and reversible conformational rearrangements upon variable changes in the local environment (Figure 2.1) (Tanaka, 1978).

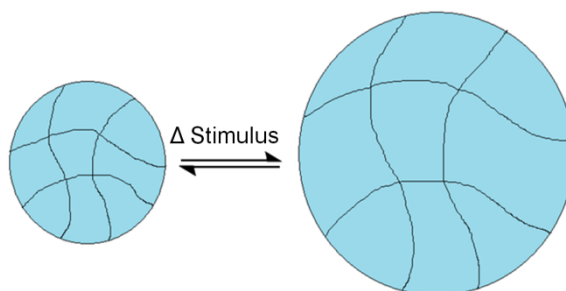


**Figure 2.1** Polymer gels can undergo reversible volume changes in response to application of appropriate stimuli.

Owing to their high water-absorbency, polyacrylamide (Figure 2.2) gels were used in initial studies where reversible phase transitions upon changing temperature or solvent conditions were reported (Tanaka, 1978, Tanaka, 1979). This transition between collapsed and swollen states was previously thought to be smooth and continuous, although under certain conditions, a discrete, coil-globule transition between polymer chains has been reported (Domb, 1974). Opinion at the time was divided as to which explanation was correct.

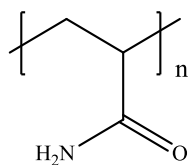


**Figure 2.2** Chemical structure of polyacrylamide.

The difference between discrete and continuous phase transitions in polymer gels is depicted in Figure 2.3 where gel I indicates a discrete phase transition where gelation was left to occur for 30 days and gel II indicates a continuous phase transition where gelation was halted after 3 days. Further evidence for a discrete transition was collated during an investigation demonstrating ionisation within gel networks plays a critical role in phase transitions (Tanaka et al., 1980). It was also realised that by varying the pH of the surrounding solvent (water or a 50% acetone-water mixture in this case), large volume changes would be induced. This paper was the first to suggest that a volume change within a polymer gel could be instigated by altering the pH of the immediate environment, leading to a concomitant variation in the degree of network ionisation and eventual phase transition. This was taken further when a non-ionic N-isopropylacrylamide gel was shown to go through a discontinuous phase transition, demonstrating the universality of phase transitions in polymer gels (Hirokawa and Tanaka, 1984). The authors concluded that the number of ionisable groups contained within the gel network and the stiffness of the polymer chains within the gel determined whether a continuous or discontinuous transition would be observed. If both these variables are sufficiently large, the osmotic pressure acting to swell the gel will be high, resulting in a discontinuous transition and vice versa.

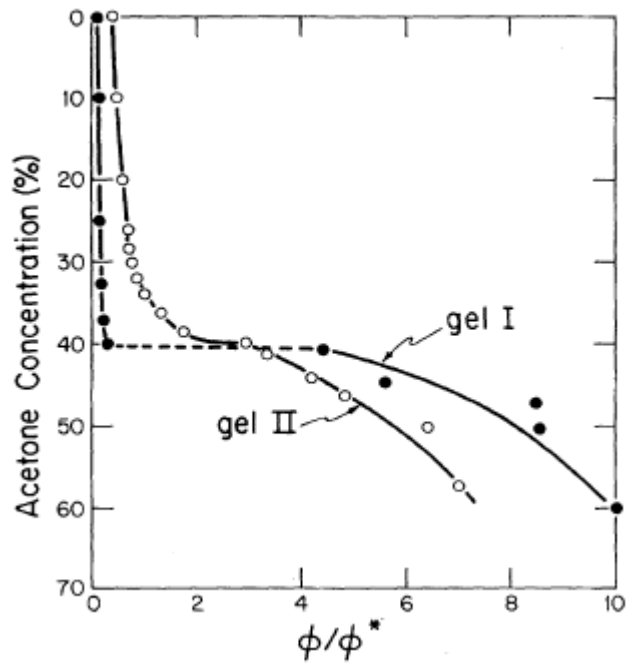


**Figure 2.3** The swelling ratio ( $\phi/\phi^*$  where  $\phi^*$  and  $\phi$  are the volume fractions of the gel before and after the change, respectively) of a polyacrylamide gel as a function of acetone concentration in the acetone-water gel fluid mixtures at 23 °C. Gel I (solid circles) exemplifies a discrete phase transition where gelation was left to occur for 30 days and gel II (open circles) depicts a continuous phase transition where gelation was halted after 3 days (Tanaka, 1978).

The swelling and shrinking process of a gel was initially thought to be due to the diffusion of individual solvent molecules into the polymer network (Tanaka and Fillmore, 1979). However, it was later demonstrated that this process is controlled by the collective diffusion of the network in the solvent associated with a bulk counterflow of solvent through the gel network (Matsuo and Tanaka, 1988). Upon substantial network swelling, regular patterns appear on the gel surface due to mechanical and thermodynamical instabilities. This pattern formation is crucial in determining the kinetic processes occurring. In general, the collapsing process is faster than the swelling one. This is because the aggregated state is more thermodynamically stable than the elongated state, resulting in a long recovery time for the gel to achieve a swollen conformation following collapse (Nakamaru et al., 2009). It is important to note that the swelling process is isotropic and that swelling is proportional in both radial and axial directions. This indicates that volume changes are not solely governed by diffusion but instead, the existence of the shear modulus of the network also acts to minimise non-isotropic deformation (Li and Tanaka, 1990). The lack of

relative motion (and therefore absence of friction) between a gel network and solvent during a shear relaxation process allows the system to adjust its conformation to diminish the total shear energy. This means that a change in one direction is coupled with an equivalent change in the opposite direction to ensure an overall uniform swelling or collapse. Therefore, the total energy of a gel is composed of a bulk component (diffusion-controlled and related to volume change) and a shear component (which can be minimised by altering the shape of the gel). Phase transitions are highly geometry dependent and therefore this must be controlled throughout swelling studies (Shibayama et al., 1992, Yashin et al., 2010).

The phase transitions that actually induce swelling or collapse originate from competition between repulsive intermolecular interactions and attractive forces. Repulsive interactions include ionic or hydrophobic, leading to network swelling. Hydrophobic interactions are attractive between two hydrophobes (but repulsive to water). Attractive forces include van der Waals and hydrogen bonding (leading to cooperative “zipping” interactions) that result in network collapse (Ilmain et al., 1991, Li and Tanaka, 1992). Hydrophobic interactions may also lead to gel collapse. It can therefore be concluded that these intermolecular forces are collectively responsible for discontinuous volume transitions in polymer gels. Gels composed of copolymers of randomly distributed positively and negatively charged groups have been shown to exhibit multiple phases (apart from just swollen and collapsed) (Annaka and Tanaka, 1992). Combination of the aforementioned intermolecular forces can lead to the appearance of several phases. The specific number of observable phases can be increased by varying the proportions of positively and negatively charged monomers. Further work was subsequently conducted to prove that multiple phases can exist in homopolymers (poly(4-acrylamidosalicylic acid)) where monomer units interact via intermolecular interactions (Figure 2.4) (Annaka et al., 2000). Hydrogen bonding and hydrophobic interactions were found to be dependent on temperature whereas electrostatic interactions were influenced by pH and shown to be the most significant. The monomer can be ionised both at the carboxyl and hydroxyl groups. These interactions also provide this gel with a degree of memory. The observed phase behaviour depends on whether the network has experienced a swollen or shrunken phase in the immediate

past. This is an extension of the shape-memory behaviour exhibited by polymer gels that allow volume changes to be fully reversible (Gupta et al., 2002).

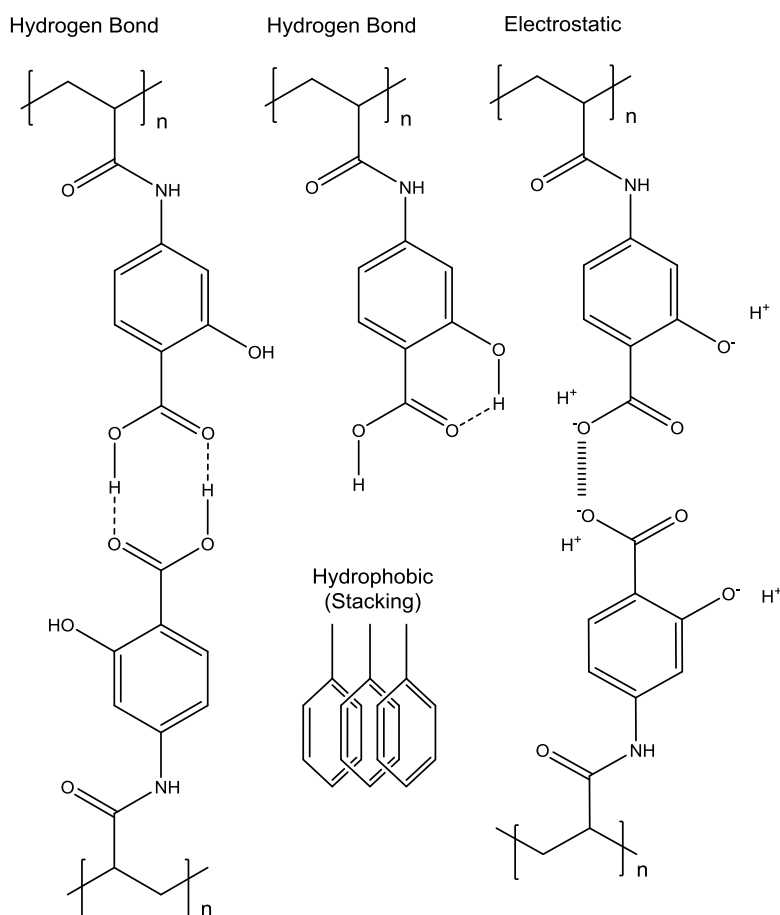


**Figure 2.4** Chemical structure of 4-acrylamidosalicylic acid polymers exemplifying intermolecular interactions (Annaka et al., 2000).

## 2.2 Types of polymer gel

Polymer gels can be synthesised via two crosslinking methods. Chemical crosslinking results in strong covalent bonds between polymer chains that cannot be re-dissolved whereas physical crosslinks are reversible owing to the formation of weak noncovalent interactions, leading to inferior mechanical strength (Maity, 2007). During synthesis if an organic solvent is used in preparation, an organogel is made whilst if water is employed, a hydrogel is formed. Gels can be further subdivided according to the drying technique applied. Aerogels are formed when the pore fluid is replaced with air and consequently they have a high porosity with very low densities. Such properties make aerogels particularly useful thermal insulators (Bi et al., 2014). Upon freeze-drying, cryogels can be obtained. A xerogel is formed by conventional

drying at elevated temperature, which induces large shrinkage and production of networks with very small pores (1-10 nm). This account will particularly focus on hydrogels, although there are some excellent reviews on organogels (Vintiloiu and Leroux, 2008), aerogels (Hüsing and Schubert, 1998), cryogels (Plieva et al., 2008) and xerogels (Quintanar-Guerrero et al., 2009) available.

### 2.3 Hydrogels

Hydrogels are three-dimensional, hydrophilic, high-molecular weight polymeric networks capable of absorbing large amounts of water or biological fluids leading to swelling (Peppas et al., 2000). Owing to their large water content and soft texture, hydrogels bear a close resemblance to natural tissue and possess good biocompatibility properties especially upon integration of natural polymers into the hydrogel matrix (Ratner and Hoffman, 1976). Functional groups such as -OH, -CO<sub>2</sub>H, -CONH<sub>2</sub> and -SO<sub>3</sub>H contribute to the hydrophilicity of the hydrogel, imparting water-attracting properties to the system (Bajpai et al., 2008). Owing to the presence of chemical (e.g. tie-points) and physical crosslinks (e.g. entanglements), these networks are insoluble. Since a poly(2-hydroxyethyl methacrylate) (Figure 2.5) hydrogel was first proposed for use in contact lenses (Wichterle and Lím, 1960), hydrogels have received considerable attention in developing both medicinal (Peppas et al., 2000, Lee and Mooney, 2001) and non-medicinal (Sidorenko et al., 2007, Wang et al., 1993) applications.

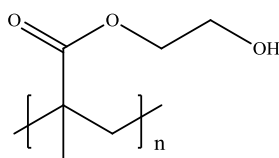


**Figure 2.5** Chemical structure of poly(2-hydroxyethyl methacrylate).

Hydrogels can be synthesised from natural (e.g. agarose, alginate and chitosan) or synthetic (poly(ethylene glycol) (PEG) and poly(vinylpyrrolidone) (PVP)) polymers (Lee and Mooney, 2001). Natural polymers tend to suffer from low mechanical strength although do possess inherent biocompatibility and biodegradability properties whereas synthetic polymers can be tailored to have well-defined structures but lack bioactive attributes. As a consequence, it is highly desirable to synthesise hydrogels to combine both natural and synthetic polymers in the network.

### 2.3.1 Variables affecting hydrogel swelling

The crosslinking ratio is defined as the ratio of moles of crosslinking agent compared to moles of polymer repeating units (Peppas et al., 2000). Consequently a high ratio means that there is a large amount of crosslinking agent incorporated into the polymer network. If this is the case, this will lead to a tighter structure with high mechanical strength. This is exemplified by elastin-mimetic protein polymers capable of physical and chemical crosslinking. It was demonstrated that physically crosslinked networks displayed an elastic modulus of 0.49 MPa, an ultimate tensile strength of 2.88 MPa and a strain at failure of 43% compared to the chemically crosslinked counterparts exhibiting a two- to three-fold increase in Young's modulus and a 50% decrease in strain at failure with a modest increase in ultimate tensile strength (3.62 MPa) (Sallach et al., 2009). However, as the pores will be smaller and polymer chains will not be very mobile, the hydrogel will not swell as much had the crosslinking ratio been lower (Ranjha et al., 2010). Therefore it is important to achieve a balance between the ability of a gel to swell and the mechanical strength of the network.

The degree of swelling can also be tuned by varying the number of hydrophilic moieties within the gel network. For example polymers incorporated that are more hydrophobic will collapse in the presence of water, minimising exposure and hence swelling will be minimal. However, due to collapse, the hydrogel will have improved mechanical properties (Xue and Hamley, 2002).

Swelling of environmentally-sensitive (smart) hydrogels can be controlled by applying an appropriate stimulus (or stimuli). This will be discussed in more detail in the following section. One method to increase the response dynamics of a gel during an environmental change is to increase the porosity to aid the diffusion of the surrounding fluid into the polymer network (Kabiri et al., 2003). Response rates can also be increased by decreasing the size of the hydrogels as the swelling rate is inversely proportional to the square of the smallest dimension of the gel (Chaterji et al., 2007). In contrast, a more elegant approach by tailoring the gel at the molecular level to create hydrophobic regions increases the expulsion rate of water from the polymer network, aiding gel collapse (Yoshida et al., 1995).

### 2.3.2 Stimuli

Smart hydrogels are able to swell or collapse in aqueous solutions upon application of an external stimulus. This thesis will specifically examine the effects of varying pH on the ability of a hydrogel to change in volume. A fundamental understanding of pH and associated parameters is therefore crucial.

### 2.3.3 pH

pH is commonly defined via Equation 2.1 (Housecroft and Constable, 2006, Burrows et al., 2013), although it is also given in terms of hydrogen ion activity ( $a_{H^+}$ ) in solution (Equation 2.2) (Bates, 1948). Activity is a measure of the “effective concentration” of a species in a mixture and can be written in terms of chemical potential (Equation 2.3) where  $a_i$  is the activity of a species (dimensionless),  $\mu_i$  is the chemical potential of the species under selected conditions,  $\mu_i^\ominus$  is the chemical potential of that species in the standard state (both given in Joules per mol ( $J\ mol^{-1}$ ),  $R$  is the universal gas constant given in Joules per Kelvin per mol ( $J\ K^{-1}\ mol^{-1}$ ) and  $T$  is the temperature in Kelvin (K). Therefore from Equations 2.2 and 2.3, it is clear that activity, and consequently pH, is dependent upon factors that can vary the chemical potential such as temperature or the chemical environment for instance.

$$pH = -\log_{10}[H_3O^+] \quad (2.1)$$

$$pH = -\log_{10}[a_{H^+}] \quad (2.2)$$

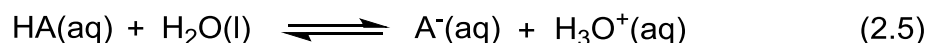
$$\mu_i = \mu_i^\ominus + RT \ln(a_i) \quad (2.3)$$

The latter definition of pH in Equation 2.2 will be discussed here because pH can be measured using ion-selective electrodes. The sensing functionality of the device is achieved by setting up a galvanic cell in order to record the electromotive force between a reference electrode (such as silver chloride) and an electrode that is sensitive to hydrogen ion activity when they are both immersed in the same aqueous solution (Housecroft and Constable, 2006). It is able to sense and specifically respond to activity by converting the activity of an ion dissolved in a solution into an electrical potential, which follows the Nernst

equation according to Equation 2.4 where  $E$  is the potential recorded,  $E^0$  is the standard electrode potential (both in volts (v) or Joules per Coulomb ( $\text{J C}^{-1}$ )),  $R$  and  $T$  are as previously defined and  $F$  is the Faraday constant in Coulombs per mol ( $\text{C mol}^{-1}$ ) (Atkins and de Paula, 2006). Hence from Equations 2.2 and 2.4, the electrode potential is proportional to pH when pH is measured as a function of activity.

$$E = E^0 + (RT/F) \ln(a_{\text{H}^+}) \quad (2.4)$$

In practice, a glass electrode is used to measure pH as opposed to a hydrogen electrode. It contains an integrated reference electrode and is calibrated against buffer solutions of known hydrogen ion activity (Bates, 1948). A buffer solution resists changes of pH so that the pH stays approximately constant upon addition of small amounts of acids and alkalis (Burrows et al., 2013). A buffer solution is commonly made up from a weak acid and its conjugate base or a weak base and its conjugate acid (Housecroft and Constable, 2006). The effect of a buffer solution composed of a weak acid,  $\text{HA}(\text{aq})$ , and its conjugate base,  $\text{A}^-(\text{aq})$  ions depends on the equilibrium in Equation 2.5.



Upon addition of a small amount of acid to the buffer solution, the additional  $\text{H}_3\text{O}^+(\text{aq})$  ions perturb the equilibrium and by Le Chatelier's principle,  $\text{A}^-(\text{aq})$  ions react with the surplus  $\text{H}_3\text{O}^+(\text{aq})$  ions and the position of the equilibrium is moved to the left. This minimises the effect of the perturbation and prevents a significant change in pH (Burrows et al., 2013). Equation 2.5 represents the process of dissociation. The strength of an acid (how well it dissociates) can be represented by the acid dissociation constant ( $K_a$  in  $\text{mol dm}^{-3}$ ) given in Equation 2.6. As the reaction occurs in dilute solution,  $[\text{H}_2\text{O}(\text{l})]$  is essentially constant. Since  $K_a$  values can be very small or large numbers, they are more commonly quoted as  $\text{p}K_a$  values according to Equation 2.7 (Burrows et al., 2013). These values can be determined via potentiometric acid-base titration where a sample is titrated with acid or base and monitored with a pH electrode. The  $\text{p}K_a$  value is calculated from the change in slope of titration curve compared to that without a

sample present (Babić et al., 2007). A Gran plot can be subsequently used to derive pKa values from a titration curves (Andrasi et al., 2007).

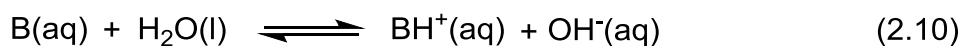
$$K_a = ([A^-(aq)][H_3O^+(aq)]/[HA(aq)]) \quad (2.6)$$

$$pK_a = -\log_{10}K_a \quad (2.7)$$

Acids such as hydrochloric acid or hydrogen cyanide are monobasic as one proton is lost per molecule of acid. However some acids may lose multiple protons such as sulphuric acid. The two dissociation steps are shown in Equations 2.8 and 2.9 where the first step goes to completion as H<sub>2</sub>SO<sub>4</sub> is a strong acid and HSO<sub>4</sub><sup>-</sup> is a relatively weak acid. As such, the dissociation of HSO<sub>4</sub><sup>-</sup> is represented by a comparatively higher acid dissociation constant and hence a lower pKa.



The proton transfer equilibrium for a base in water (Equation 2.10) can also be assigned a corresponding base dissociation constant, K<sub>b</sub> (Equation 2.11) and associated pK<sub>b</sub> (Equation 2.12) (Atkins et al., 2006).



$$K_b = ([BH^+(aq)][OH^-(aq)]/[B(aq)]) \quad (2.11)$$

$$pK_b = -\log_{10}K_b \quad (2.12)$$

In order to estimate the pH of a buffer solution, the Henderson-Hasselbalch equation can be used (Equation 2.13). This shows that the pH of a buffer solution depends on the value of K<sub>a</sub> where the selected weak acid or base determines the region of the pH range of the buffer and the ratio of [A<sup>-</sup>(aq)]/[HA], which provides “fine tuning” of the buffer pH (Burrows et al., 2013). This also illustrates why buffers are unaffected by dilution as upon addition of water, the

concentrations of the acid and conjugate base are reduced equally, hence the ratio remains unchanged.

$$\text{pH} = \text{pK}_a + \log_{10} ([\text{A}^-(\text{aq})]/[\text{HA}(\text{aq})]) \quad (2.13)$$

In summary, a range of charged moieties are present in buffered environments and if a pH-sensitive hydrogel is placed in such an environment, formation and removal of charges is likely to occur. Therefore it is important to understand the basis of the intermolecular forces present between charges in aqueous solutions. Generally, there are three types of intermolecular forces; electrostatic, polarisation and quantum mechanical forces. This discussion will focus on the electrostatic interactions between charges arising from the associated Coulomb forces.

The free energy of the Coulombic interaction,  $w(r)$  in Joules (J), between two charges  $Q_1$  and  $Q_2$  is defined in Equation 2.14 where  $r$  is the distance between the two charges in metres (m) and  $\epsilon$  is the relative permittivity of the medium ( $\text{J}^{-1}\text{C}^2\text{m}^{-1}$ ) and  $\epsilon_0$  is the permittivity of a vacuum ( $8.854 \times 10^{-12} \text{ J}^{-1}\text{C}^2\text{m}^{-1}$ ). The relative permittivity of a medium is large if its molecules are polar or highly polarisable (Atkins and de Paula, 2006). Equation 2.14 can be amended for ionic interactions according to Equation 2.15 where the size and the sign of individual ionic charges is provided in terms of the elementary charge ( $e = 1.602 \times 10^{-19} \text{ C}$ ) multiplied by the ionic valency,  $z$ . The Coulomb force,  $\underline{F}$  in Newtons (N), is shown in Equation 2.16 whereby for like charges,  $\underline{F}$  is positive, indicating a repulsive force and for unlike charges,  $\underline{F}$  is negative, representing an attractive force (Israelachvili, 1991).

$$w(r) = (Q_1Q_2)/(4\pi\epsilon_0\epsilon r) \quad (2.14)$$

$$w(r) = (z_1z_2e^2)/(4\pi\epsilon_0\epsilon r) \quad (2.15)$$

$$\underline{F} = - dw(r) / dr = (Q_1Q_2)/(4\pi\epsilon_0\epsilon r^2) = (z_1z_2e^2)/(4\pi\epsilon_0\epsilon r^2) \quad (2.16)$$

As Coulombic interactions between ions are both long range (the inverse-square distance dependence) and high strength, such electrostatic forces are likely to form the dominant contribution of nonideality in ionic solutions (Atkins

and de Paula, 2006). This is the basis of Debye-Hückel theory of ionic solutions. As previously mentioned, activity is a measure of the “effective concentration” and as such can be represented using an activity coefficient,  $\gamma$ , as in Equation 2.17 where as previously defined,  $a_i$  is the activity of a species,  $[C^\ominus]$  is the concentration of the chosen standard state and  $[C]$  is the measure of concentration. This factor specifically takes into account the interaction energy of ions in solution. Since cations and anions are always in close proximity because oppositely charged ions attract each other, ionic atmospheres are formed. This polarisation leads to the electric field becoming screened, reducing the Coulomb potential of the ion. The electric field subsequently decays away from the ionic atmosphere faster than from an isolated ion. This screened electric field decays approximately exponentially with distance according to  $\exp^{-\kappa D}$  where  $\kappa^{-1}$  is the Debye screening length and  $D$  is distance (both in nanometres (nm)) (Israelachvili, 1991). This model leads to the result that at low concentrations, the activity coefficient can be determined from the Debye-Hückel limiting law (Equation 2.18) where  $A$  is an empirical parameter defined as 0.509 and  $I$  is the dimensionless ionic strength of the solution (Atkins and de Paula, 2006). Ionic strength is given in Equation 2.19 as a function of molality ( $b_i$  in mol kg<sup>-1</sup> (Field and Försterling)) to account for non-ideal behaviour as volumes are no longer additive. For ideal solutions, the ionic strength is a function of concentration of all ions present in that solution as in Equation 2.20 where  $c_i$  is the molar concentration in mol dm<sup>-3</sup>.

$$a_i = \gamma ([C]/[C^\ominus]) \quad (2.17)$$

$$\log_{10}\gamma_{\pm} = - |z_+z_-|A(I)^{0.5} \quad (2.18)$$

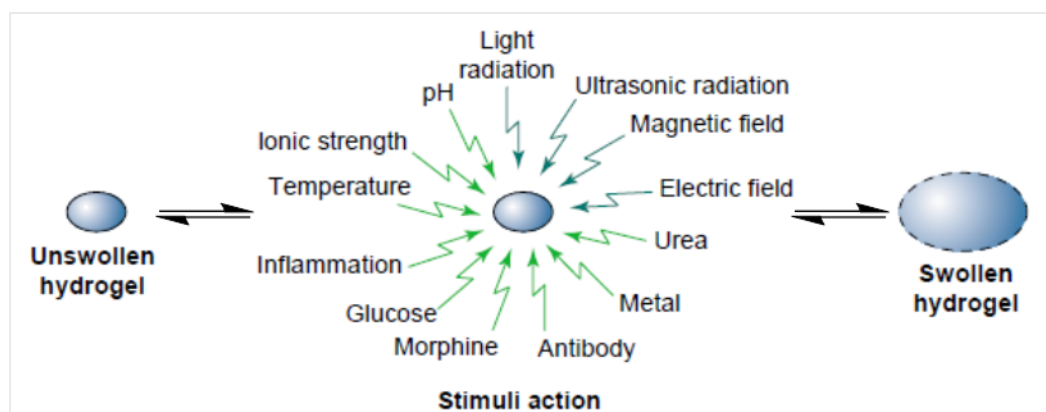
$$I = 0.5 \sum z_i^2 b_i \quad (2.19)$$

$$I = 0.5 \sum z_i^2 c_i \quad (2.20)$$

Taking into account the electrostatic interaction between ions in solution, these concepts can be translated to aid understanding as to how a pH-sensitive hydrogel is able to swell. The ion swelling pressure can be thought to arise from differences between the osmotic pressure of freely mobile ions in the hydrogel

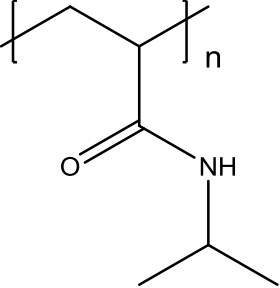
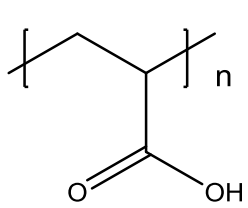
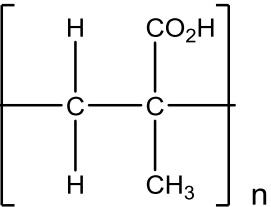
and in the surrounding solution (Procter and Wilson, 1916). The distribution of the ions between the gel and the outer solution is acquired via the Donnan equilibrium (Rička and Tanaka, 1984). The Donnan equilibrium illustrates the behaviour of charged particles near a semi-permeable membrane that leads to an uneven distribution of ions across the two sides of the membrane. Indeed, the boundary between a hydrogel and the outer solution can act as a selective barrier. The uneven distribution of charge may result from some species being unable to pass through the membrane, leading to an electrical potential arising between the gel and surrounding solution. This is called the Donnan potential and the Donnan effect creates extra osmotic pressure, hence changing the ion swelling pressure and overall swelling degree of the network. Consequently, by utilising this theory, the ionic forces depend solely on the ionic composition of the solvent and on the composition of fixed ionisable functional groups in the gel but not on the properties of the neutral network (Rička and Tanaka, 1984). Therefore, this can be related to understanding how the ionic strength of the solvent in which a hydrogel is immersed can affect the degree of swelling. Upon an increase in ionic strength, more ionic atmospheres are formed, leading to a greater degree of charge screening, reducing the Coulomb potential of the ions, hence the charge distribution will be less, lowering the Donnan potential and hence decreasing the amount of osmotic pressure exerted, resulting in weaker swelling (Rička and Tanaka, 1984, Israelachvili, 1991).

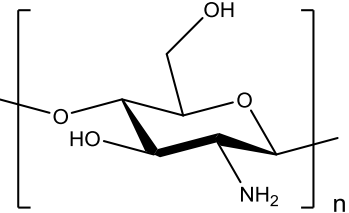
Some examples of other stimuli which can impact on hydrogels (including pH) are depicted in Figure 2.6 and subsequently discussed in more detail in Table 2.1.

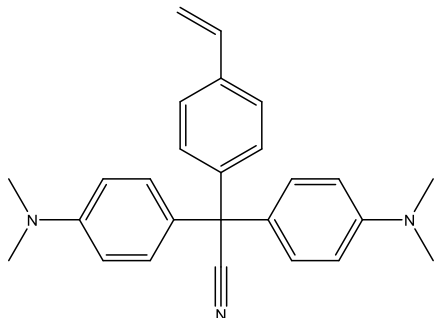
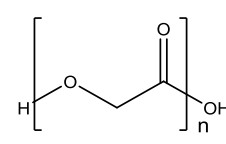
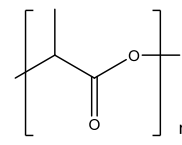


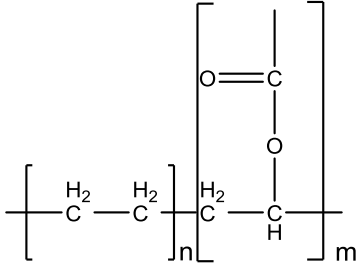
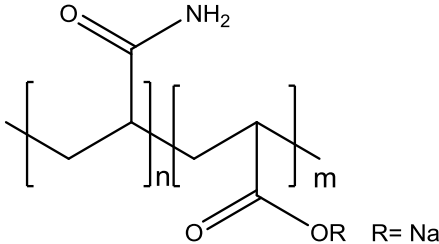
**Figure 2.6** Diagram of stimuli responsive swelling of hydrogels (Gupta et al., 2002).

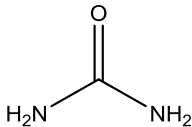
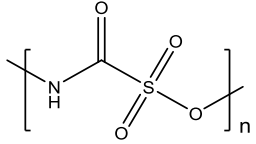
**Table 2.1** Origins and examples of stimuli-responsive polymer gels.

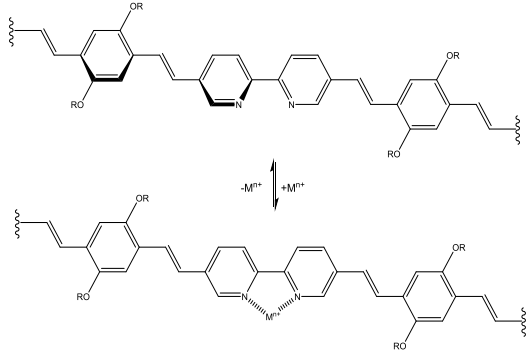
Stimulus	Origin of the Response	Examples	Chemical Structure
Temperature	<p>Polymer-polymer and polymer-solvent interactions can be strongly influenced by temperature (Gutowska et al., 1992). Negative and positive temperature-sensitive hydrogels exist. These will be discussed in more detail in Section 2.3.4.</p>	<p>Poly(N-isopropylacrylamide) (PNIPAAm)-based hydrogels (a) exhibit negative thermosensitivity where they are swollen at low temperatures and collapse with increasing temperature. An abrupt change in swelling is observed at 32 °C corresponding to the lower critical solution temperature where the entropy-driven release of water molecules structured around the hydrophobic side chains results in network collapse. Poly(acrylic acid) (b) is an example of a positive thermosensitive hydrogel. Both are discussed in more detail in Section 2.3.4.</p>	<p>(a) </p> <p>(b) </p>
pH	<p>pH-sensitive hydrogels can be swollen to form ionic networks. Such networks contain either acidic or basic pendant groups, which can be ionised to develop a fixed charge in the gel. Ionisation occurs when the pH of the environment is above the pK<sub>a</sub> of the ionisable group</p>	<p>Poly (methacrylic acid) (PMAA) (c) was initially used to prove that by varying the pH of the surrounding fluid, swelling and collapse of a gel network can occur (Kuhn et al., 1950). This is an example of an anionic hydrogel whereby the carboxyl group is ionised in a basic solution. Chitosan (d) is a cationic hydrogel</p>	<p>(c) </p>

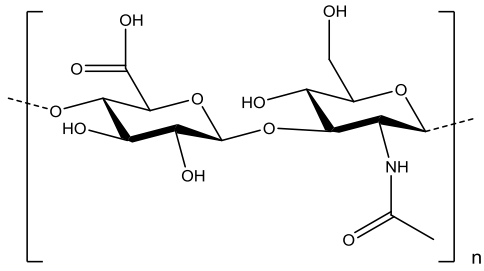
	<p>for anionic polymers or below the <math>pK_b</math> of cationic materials (Rička and Tanaka, 1984, Skouri et al., 1995). As the degree of ionisation increases, the number of fixed charges increases leading to more electrostatic repulsions within the network, increasing hydrophilicity and hence promoting gel swelling (Brannon-Peppas and Peppas, 1991). This will be discussed in more detail in Section 2.3.5.</p>	<p>whereby the pendant amine groups are protonated in acidic media. Hydrogels have also been developed to exhibit dual sensitivities to temperature and pH (combination of PNIPAAm and poly(propylacrylic acid) (Yin et al., 2006).</p>	<p>(d)</p> 
<p>Ionic Strength</p>	<p>The degree of swelling has also been shown to be highly dependent on ionic strength (Ohmine and Tanaka, 1982). As the ionic strength of the surrounding fluid increases, the concentration of ions within the network also increases to satisfy the Donnan equilibrium. Following this, the swelling force is reduced due to a stronger interaction between the gel and the counterion and a decrease in the osmotic swelling forces (Peppas et al., 2000).</p>	<p>When an acrylic acid-based hydrogel (such as (b) or (c) is at pH 7 in a sodium chloride solution and the salt concentration is increased, <math>H^+</math> ions in the gel are exchanged for <math>Na^+</math> cations. This leads to a higher ion swelling pressure because of a greater number of free counterions produced as a consequence of dissociation of acrylic acid. Upon complete dissociation, increasing the salt concentration further will actually reduce the ion swelling pressure (Rička and Tanaka, 1984). As a consequence, the hydrogel conformation</p>	

		changes from a swollen to a collapsed state upon further increasing salt concentration (Zhang et al., 2005).	
Light Radiation	Light as a stimulus is advantageous as it can be imposed instantly and delivered in specific amounts with high accuracy. Detail on the mechanisms of UV-sensitive and visible light-sensitive hydrogels are provided in Section 2.3.6.	UV-sensitive hydrogels have been prepared based upon a bis-(4-dimethylamino)phenylmethy leucocyanide network whereby upon irradiation of UV-light, cyanide ions were formed, leading to an increase in osmotic pressure and concomitant swelling (Mamada et al., 1990). This is further discussed in Section 2.3.6.	(e) 
Ultrasonic Radiation	Upon exposure to ultrasound, certain polymers are able to degrade, hence selectively releasing the contained therapeutic.	During treatment with ultrasonic radiation, bioerodible polymers such as polyglycolide (f) or polylactide (g) were shown to respond promptly and reversibly. It is believed that the ultrasound causes an increase in temperature within the system, facilitating diffusion (Bawa et al., 2009).	(f)  (g) 

<p>Magnetic Field</p>	<p>An oscillating magnetic field can be used to modulate the release of macromolecules from polymer matrices. This has been accomplished by embedding magnetic steel beads in an ethylene-vinyl acetate (EVAc) (h) copolymer matrix (Hsieh et al., 1981). Upon exposure to the magnetic field, the steel beads oscillated within the matrix, creating compressive and tensile forces, which contribute to pushing an increased amount of the absorbed constituents out of the polymer network (Sershen and West, 2002).</p>	<p>The rate of release of bovine serum albumin from the EVAc polymer matrix could be modulated by varying the position, orientation and magnetic strength of the embedded steel beads as well as by changing the amplitude and frequency of the applied magnetic field (Kost et al., 1985). The extent of modulated release can be tuned by varying the Young's modulus of the copolymer matrix whereby a stiffer polymer is less able to contribute to pushing out absorbed constituents compared to a flexible network (Kost et al., 1985).</p>	<p>(h)</p> 
<p>Electric Field</p>	<p>Electro-sensitive hydrogels undergo swelling or collapse in the presence of an electric field. Upon application of an electric potential to the gel surface, hydrated H<sup>+</sup> ions move towards the cathode, resulting in a deficit of water at the anode. Simultaneously, electrostatic attraction of a negatively charged anionic</p>	<p>The volume change of a sodium acrylic acid-acrylamide copolymer (i) in an aqueous solution and subjected to an electric field depends on the concentration of the electrolytes. In the presence of no/a low concentration of electrolytes, the gel collapses due to the migration of Na<sup>+</sup> ions to the cathode resulting in the carboxyl group changing from</p>	<p>(i)</p> 

	<p>polymer (such as acrylic acid for instance) towards the surface of the anode creates a uniaxial stress along the gel axis, resulting in network collapse near the anode (Qiu and Park, 2001, Tanaka et al., 1982).</p>	<p>-COO<sup>-</sup>Na<sup>+</sup> to -COOH. Conversely, a high electrolyte concentration leads to more Na<sup>+</sup> ions entering the hydrogel than migrating the hydrogel to the cathode, leading to network swelling (Shiga et al., 1992).</p>	
Urea	<p>Hydrogels have also been used for sensing applications. For example, an ammonium sensitive transducer has been used to detect urea (j) in the bloodstream (Eggenstein et al., 1999). Urea is hydrolysed by urease according to:</p> $(NH_2)_2CO + 2 H_2O + H^+ \longrightarrow 2NH_4^+ + HCO_3^-$ <p>Therefore by casting a layer of urease on the surface of an NH<sub>4</sub><sup>+</sup> sensitive membrane and combination with an Ag/AgCl reference electrode, a urea biosensor can be fabricated (Eggenstein et al., 1999).</p>	<p>A hydrophilic poly(carbamoylsulfonate) hydrogel was used as the immobilisation material to cast a layer of urease onto (Eggenstein et al., 1999).</p>	<p>(j)</p>  <p>(k)</p> 

<p><b>Metal</b></p>	<p>Metal ions may be used to modify polymers from an initial partially conjugated state to a fully conjugated state upon exposure. Such an ion-induced conjugation enhancement can be transduced into a measurable signal (Wang and Wasielewski, 1997). This could be one method to produce metal ion sensory materials.</p>	<p>An enhancement in the conjugation of ligand-containing polymers (such as (I)), along with the simultaneous variation in electron density caused by incorporation of a metal ion generates corresponding changes in the electronic properties of the material (Wang and Wasielewski, 1997). As well as the ability of 2,2'-bipyridine to coordinate to a range of metal ions, as there is an approximate 20° dihedral angle between the two pyridine planes in a transoid-like conformation (Cumper et al., 1962), these polymers are not fully conjugated. However, coordination of the bipyridine with a metal ion forces the twisted conformation into a planar one, hence making the polymer fully conjugated (Wang and Wasielewski, 1997).</p>	<p>(I)</p> 
<p><b>Antigen</b></p>	<p>Hydrogels can also be engineered to be responsive to a specific antigen. An antibody can be grafted onto a polymer network so that binding with an antigen introduces crosslinks into the material. Competitive binding of the free antigen</p>	<p>Rabbit immunoglobulin G and goat anti-rabbit IgG acted as the antigen and antibody respectively and were combined to form a polyacrylamide hydrogel. The hydrogel swells in the presence of a free antigen because the intra-chain antigen-antibody binding can be</p>	

	stimulates a change in gel volume due to the breaking of such crosslinks (Miyata et al., 1999b).	dissociated via exchange of the grafted antigen for the mobile antigen. Without a free antigen, the hydrogel collapses (Miyata et al., 1999a, Miyata et al., 1999b).	
Glucose	Glucose-sensitive hydrogels have found application as insulin-delivery systems whereby in general, glucose oxidase is grafted onto a polymer and in the presence of glucose, gluconic acid is produced, lowering the pH in the microenvironment of the matrix and resulting in release of entrapped insulin (Brown et al., 1996).	Glucose oxidase has been immobilised onto Sepharose beads and combined with insulin within a EVAc (h) matrix. The beads could not diffuse out of the matrix (only the insulin). As described, glucose oxidase converts glucose to gluconic acid, lowering the pH within the matrix and resulting in insulin release.	
Inflammation	Inflammation-responsive polymers have been utilised in drug delivery and are based on biodegradable hydrogels that are degraded by hydroxyl radicals or enzymes produced at inflammatory sites. Upon degradation, release of the bioactive agent ensues, making this system relevant for the treatment of osteoarthritis (Traitel et al., 2008).	Hyaluronic acid (m) is an example of such a polymer that can be degraded by hydroxyl radicals produced by the reaction of hydrogen peroxide with iron(II) sulfate. In vivo implantation experiments revealed the degradability of the hyaluronic acid gel in response to inflammation (Nobuhiko et al., 1992).	(m) 

### 2.3.4 Temperature sensitive hydrogels

Temperature sensitive hydrogels are able to undergo a phase transition as a result of a change in temperature of the surrounding fluid (Tanaka, 1978). Two types of thermosensitive hydrogels exist; negative and positive. Classification depends on whether the gel exhibits a discontinuous phase transition above or below a certain temperature.

A lower critical solution temperature (LCST) exists for negative thermosensitive hydrogels (such as PNIPAAm) at 32 °C in water (Figure 2.7 (a)). This is defined as the critical temperature below which the polymer swells in the solution while above it, the polymer collapses (Bajpai et al., 2008). The hydrophobic effect (defined as the observed tendency of non-polar substances to aggregate in solution and exclude water (Atkins and de Paula, 2006)) is extremely sensitive to temperature whereby above the LCST, there is a domination of hydrophobic interactions forming aggregations between polymer backbones leading to gel collapse (Van Der Linden et al., 2003). This is because the hydrophobic effect is entropically driven (positive entropy) according to Equation 2.21 where  $\Delta G$  is defined as the Gibbs free energy change in J mol<sup>-1</sup>,  $\Delta H$  is the enthalpy change in J mol<sup>-1</sup>, T is temperature in Kelvin and  $\Delta S$  is the entropy change in J K<sup>-1</sup> mol<sup>-1</sup>. Therefore the hydrophobic effect increases with temperature and the network collapses above a certain temperature (the LCST)

$$\Delta G = \Delta H - T\Delta S \quad (2.21)$$

Below the LCST, hydrogen bonding dominates, preventing the formation of aggregates, leading to swelling. It is possible to modulate the value of the LCST by tuning the hydrophobicity of the constituents of the gel network. This is because more hydrophobic polymers possess stronger hydrophobic interaction forces, allowing the gel to collapse at lower temperatures. However, increasing the hydrophilicity will serve to increase the LCST (Inomata et al., 1990). Further to the ability to manipulate the volume change of thermosensitive gels, materials may also undergo a transition between solution and a gel (referred to as a sol-gel transition). Predictably, below the LCST, the polymers are soluble and above the LCST, they become increasingly hydrophobic and insoluble, resulting in gel formation (Klouda and Mikos, 2008). Consequently, a

temperature change may be used to trigger gelation. The sol-gel transition can be investigated experimentally via spectroscopy, differential scanning calorimetry or rheology (Li et al., 2002, Liu et al., 2006).

A positive thermosensitive hydrogel such as poly(acrylic acid) (PAAc) shown in Figure 2.7 (b) has an upper critical solution temperature (UCST) where the gel collapses upon cooling below the UCST, hence exhibiting directly opposite behaviour than aforementioned gels possessing an LCST. This is because collapse is driven by acid-acid interactions, which are favoured at lower temperature.

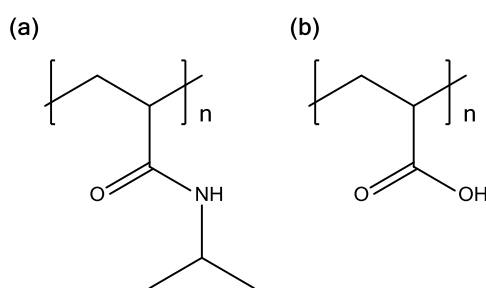


**Figure 2.7** Chemical structures of (a) poly(N-isopropylacrylamide) and (b) poly(acrylic acid).

### 2.3.5 pH-sensitive hydrogels

Hydrogels containing suitable ionic pendant groups that are immersed in aqueous solutions of appropriate pH and ionic strength can be ionised to induce electrostatic repulsion and an increase in osmotic pressure within the polymer network leading to swelling (or as a trigger for gelation akin to temperature) (Tanaka et al., 1980, Gupta et al., 2002). Depending on the nature of the pendant groups, pH-sensitive hydrogels can be classified as being either anionic or cationic (Figure 2.8).

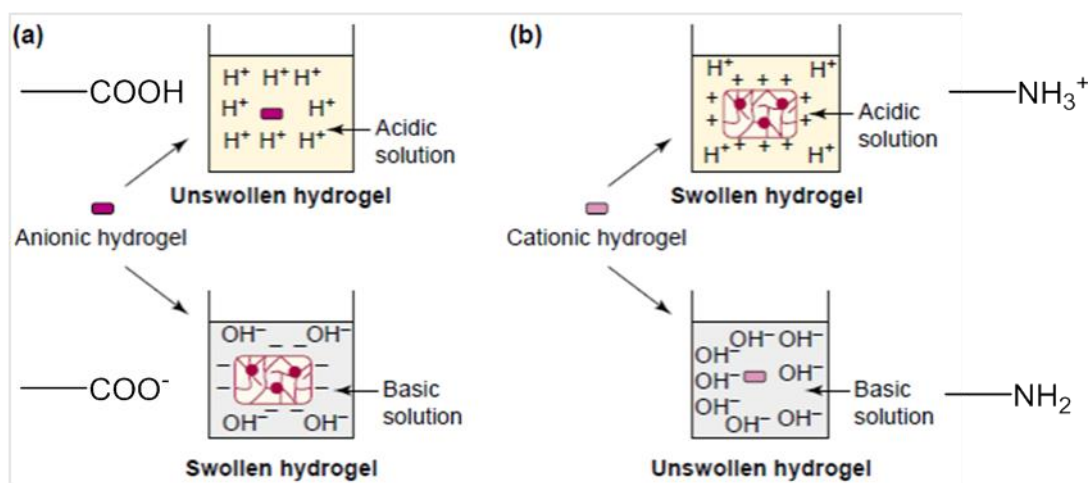


**Figure 2.8** Diagram displaying pH dependent behaviour of (a) anionic and (b) cationic hydrogels (Gupta et al., 2002).

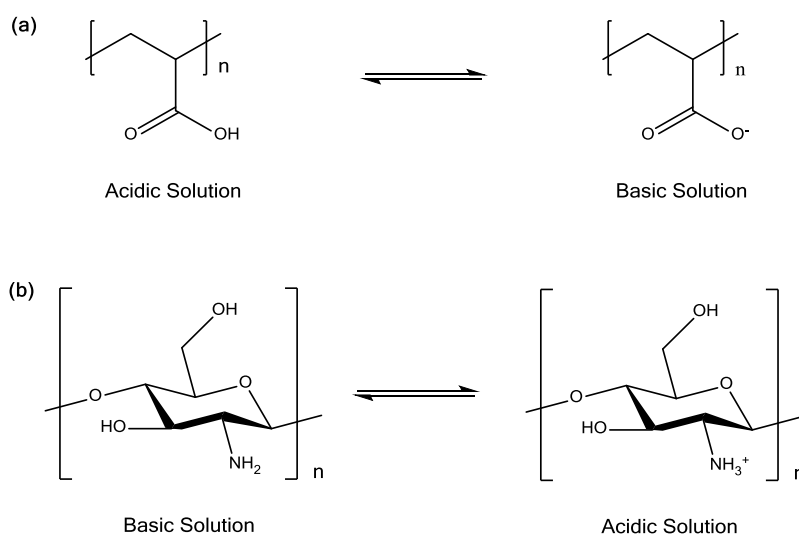


**Figure 2.9** Effect on the chemical structure of pH-sensitive anionic poly(acrylic acid) (a) and cationic chitosan (b) hydrogels on immersion in acidic and basic media.

Anionic hydrogels such as PAAc are ionised above the  $pK_a$  of the polymeric network, leading to swelling at pH values above the polymer  $pK_a$  (Figures 2.8 (a) and 2.9 (a)). In the case of PAAc, ionisation of the carboxyl groups from  $CO_2H$  to  $CO_2^-$  generates electrostatic repulsion between the negatively charged groups, resulting in an increase in internal osmotic pressure with a concomitant increase in swelling. Taking this further to consider how the charges are interacting within the gel and in the outer solution, as the pH is increased, the concentration of base cations in the surrounding solution will increase. These ions will be attracted into the gel and replace mobile  $H^+$  ions whereby the gel acts as an ion exchanger. Upon dissociation of the acrylic acid moiety, new  $H^+$

ions will be provided, resulting in more rapid increase of the concentration of mobile ions in the gel than in the outer solution, leading to a concomitant increase in ion swelling pressure and hence network swelling. However upon increasing the pH further, following complete dissociation the ion swelling pressure will drop, resulting in a slight collapse (Rička and Tanaka, 1984). The opposite is the case for cationic hydrogels such as chitosan that swell in acidic pH due to the electrostatic repulsion between positively charged chemical moieties, which in the case of chitosan are amine functional groups (Figures 2.8 (b) and 2.9 (b)) (Qu et al., 1999). The amino group on chitosan has a pKa in the range of 6.3-6.6 (Claesson and Ninham, 1992, Müzzarelli, 1971). This accounts for the ability of chitosan to bind to negatively charged surfaces such as mucosal membranes, making the polymer bioadhesive (Suknuntha et al., 2011).

### **2.3.6 Other stimuli able to induce a volume change in smart polymer gels**

As depicted in Figure 2.6, a variety of stimuli can be used to trigger a response within a smart network. A phase transition in a polymer gel can be induced via application of an electric field for instance (Tanaka et al., 1982). A stress gradient along the electric field lines in the network is produced owing to generation of electric forces on charged sites within the gel. Depending on gel constituents a critical stress is in place below which the gel swells and above which shrinkage is observed (Irie, 1986). This stimulus could be used to develop switches or mechanochemical transducers.

Thermosensitive PNIPAAm gels seeded with ferromagnetic materials can exhibit magnetic-field-sensitive swelling behaviour. Owing to the heat released from the magnets contained in a magnetic field, a phase transition around the LCST can be induced (Zrínyi, 2000). As such gels can undergo fast and controllable shape changes, this system can be used to mimic muscular contraction.

Equilibrium swelling upon irradiation of ultraviolet (UV) light on a PNIPAAm gel copolymerised with a photosensitive bis(4-(dimethylamino)phenyl) (4-vinylphenyl)methyl leucocyanide moiety can be induced (Mamada et al., 1990). Prior to irradiation, the copolymer is neutral but upon application of UV light, an ionic gel is formed owing to the generation of cyanide ions which lead to increased internal osmotic pressure, resulting in gel swelling (Figure 2.10). In

the absence of UV light, the equilibrium moves towards the neutral complex and the network collapses. This could be useful in the development of optical switches and display units.

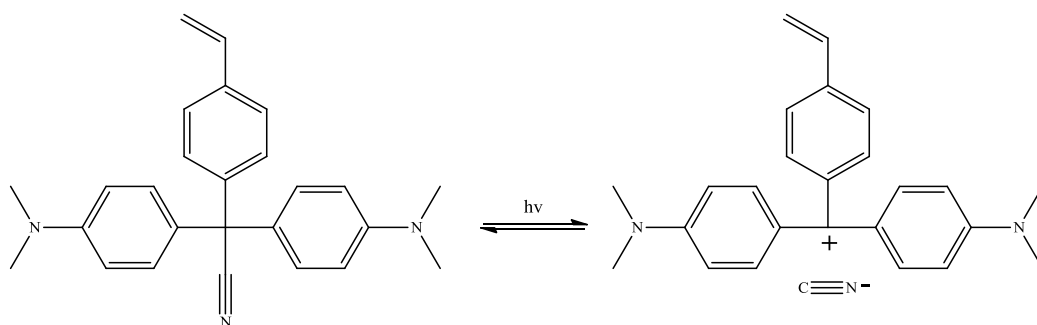


**Figure 2.10** Chemical structures of the phase transition of bis(4-(dimethylamino)phenyl)(4-vinylphenyl)methyl leucocyanide which is sensitive to UV (Mamada et al., 1990).

In relation to gel stimulation with UV light, the transition to return to the neutral complex is very slow as it depends on photochemical ionisation and recombination of ions. However, a good alternative is to irradiate with less harmful and more abundant visible light. Upon irradiation of NIPAAm gels copolymerised with a trisodium salt of copper chlorophyllin chromophore (Figure 2.11), light is absorbed and dissipated as heat by radiationless transitions, increasing the local temperature of the thermosensitive polymer, leading to a phase transition. As thermal diffusion is much faster than collective diffusion, the processes of swelling and collapse are relatively fast (Suzuki and Tanaka, 1990).

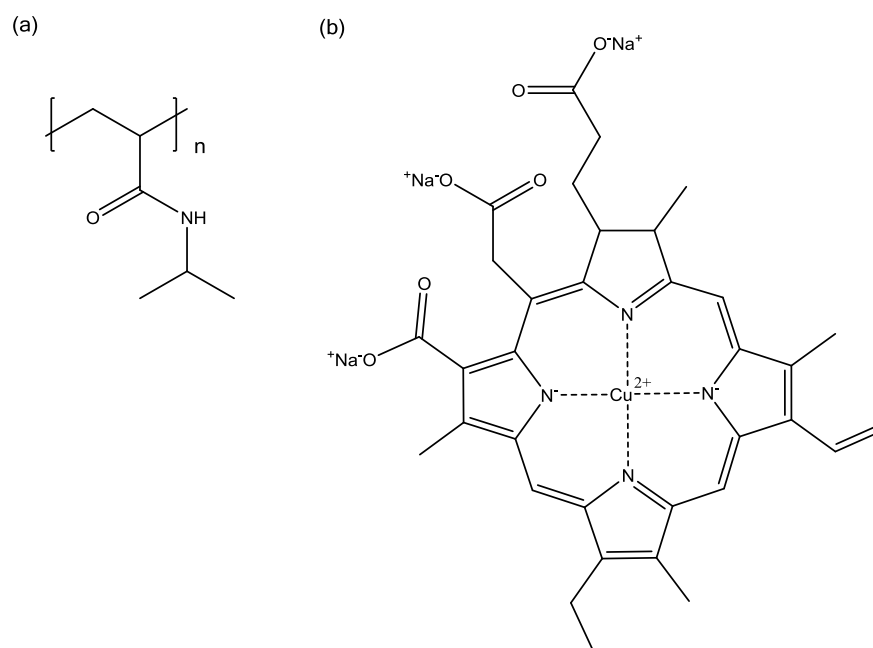


**Figure 2.11** Chemical structures of poly(N-isopropylacrylamide) (a) and the trisodium salt of copper chlorophyllin (b).

Salt concentration of the fluid in which a polymer gel is immersed, can be used to bring about a phase transition (Ohmine and Tanaka, 1982). The critical salt concentration is strongly dependent on the valency of the positive ions of the salt. For example NaCl concentration has to be at least double that of  $\text{MgCl}_2$  concentration at the transition because less divalent ions are needed to neutralise the polymer network than monovalent ions. Accumulation of these cations causes an increase in internal osmotic pressure due to the enhanced electrostatic repulsion, leading to network swelling. However in some cases, salt solutions actually screen native charges on polymers, eliminating the osmotic imbalance and converting the network to a non-ionic gel, reducing the swelling ability. To tackle this, ionised sodium dodecyl sulphate surfactants were combined with a non-ionic gel to yield a network with superabsorbent behaviour in the presence of salt (Zhang et al., 1992). Formation of spherical surfactant micelles within the network occurs when it is immersed in water. These micelles act as a good structural mimic to charged sites in an ionic gel. Upon increasing salt concentration, micelles become more rod-like (Figure 2.12), maintaining internal electrostatic repulsion and thus swelling ability is sustained.

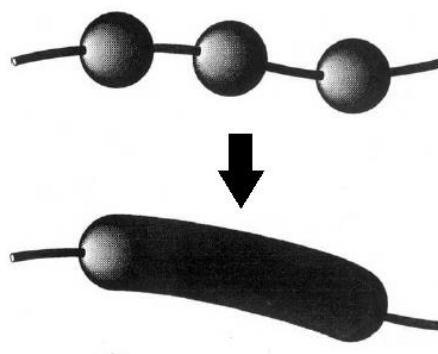


**Figure 2.12** Conversion of spherical micelles to rod-like structures on increasing sodium chloride concentration in water.

Gels have also been engineered to swell or collapse in response to specific environmental changes for the design of molecule-specific systems. Examples of such stimuli include antigens for interaction with antibodies (Miyata et al., 1999b), glucose for applications in diabetes (Matsumoto et al., 2010) and saccharides for lectin binding (Kokufata et al., 1991).

## 2.4 Applications

Smart polymer gels are very promising materials as the structural change caused by a change in the environment can lead to a wide variety of applications (Figure 2.13). This section describes some of these applications in more detail.

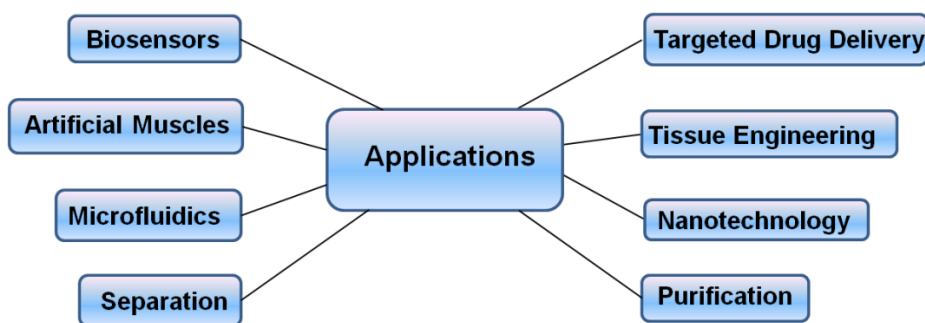


**Figure 2.13** Some applications of smart polymer gels.

### 2.4.1 Targeted drug delivery

Host molecules can be introduced (e.g. via loading) and selectively expelled (e.g. via swelling) from a gel in a controlled manner (Figure 2.14). This can be capitalised on for use in targeted drug delivery. Figure 2.14 depicts a pre-loaded gel (light blue) containing an entrapped therapeutic moiety (yellow circles) at an

intermediate site such as a healthy cell (green circles). Following an appropriate variation in a stimulus towards which the network is responsive (such as pH) gel swelling will be initiated (orange shapes) and release the absorbed constituents selectively at this location. From a biomedical perspective, one of the most important stimuli is pH. For example, there are large variations in pH along the gastrointestinal (GI) tract and at tumour cells (Bajpai et al., 2008). The GI tract forms the digestive system responsible for consuming and digesting foodstuffs, absorbing nutrients and expelling waste.

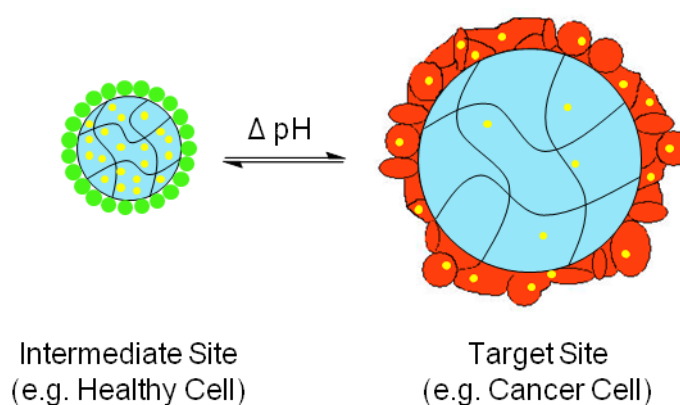


**Figure 2.14** Smart polymer gels in targeted drug delivery.

It is highly advantageous that delivery systems can release therapeutics only at specifically desired sites in the body and to maintain release of a drug at the required concentration for a sustained period of time until treatment is successful (Liechty et al., 2010). Uncontrolled burst release limited by diffusion is highly undesirable as following initial expulsion, the drug concentration in the plasma may exceed the minimum toxic concentration (MTC), potentially inducing adverse effects. Additionally, owing to the diffusive nature of the release regime, the drug delivery duration is typically short (hours), which is undesirable for treating long term illness. A controlled and sustained regime whereby the drug concentration in the plasma is above the median effective concentration (permitting the drug to deliver the desired effect) but below the MTC so no unwanted side effects occur is highly desirable. Such delivery is said to be within the “therapeutic band”. Furthermore, the symptoms of many disease states correspond to a rhythmic pattern and hence pulsatile drug delivery within the therapeutic band is highly sought after so that drugs can be dispersed in bursts that can go on for a precise time period that can be tailored (Figure 2.15) (Gupta et al., 2002). Different shapes of hydrogels are also

required depending upon the route of administration. For example, disc shapes are preferred for oral routes whilst cylinders are favoured for rectal administration. This must be carefully considered as hydrogel shape has a profound effect on swelling ability (Li and Tanaka, 1990, Shibayama et al., 1992).

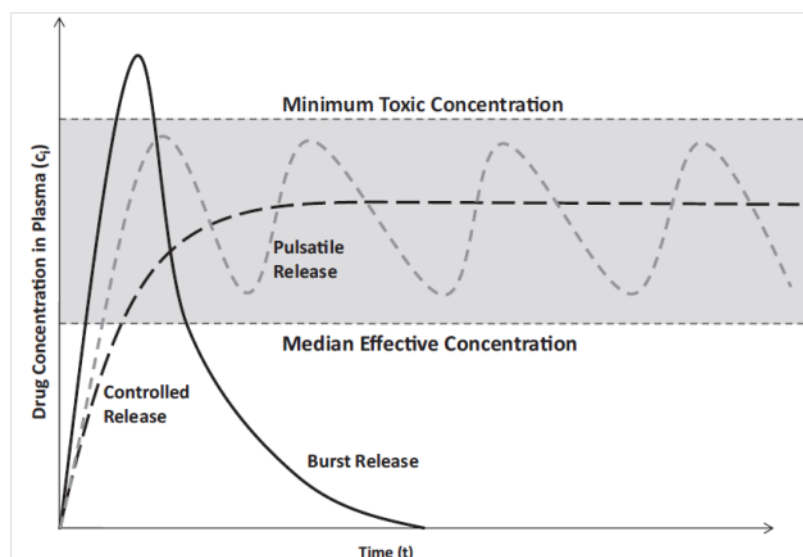


**Figure 2.15** Image displaying the therapeutic band showing the effects of burst release, controlled release and pulsatile release in relation to effective concentration and toxic concentration (Liecchy et al., 2010).

Hydrogels with both temperature (Zhang et al., 2004) and pH sensitive (Bhattarai et al., 2010) swelling abilities show the most promise for application in targeted drug delivery. Cationic hydrogels that are able to swell in acidic pH are particularly useful for modulating the release of antibiotics in the stomach (Patel and Amiji, 1996) and the delivery of cancer therapeutics (Zhang et al., 2006, Lee et al., 2008) to tumour cells owing to the low pH of the target sites. Chitosan is produced from thermochemical deacetylation of chitin (Figure 2.16), a natural and abundant polymer found in the exoskeletons of many invertebrates (Tolaimate et al., 2000). This natural polymer is a strong candidate to be incorporated into a hydrogel for targeted drug delivery as it is receptive to pH and temperature stimuli, biocompatible, non-toxic, biodegradable, antimicrobial and mucoadhesive (Khurma and Nand, 2008, Munjeri et al., 1997, Muzzarelli, 2009, Sogias et al., 2008, Jayakumar et al., 2010, Rabea et al., 2003, Kean and Thanou, 2010).

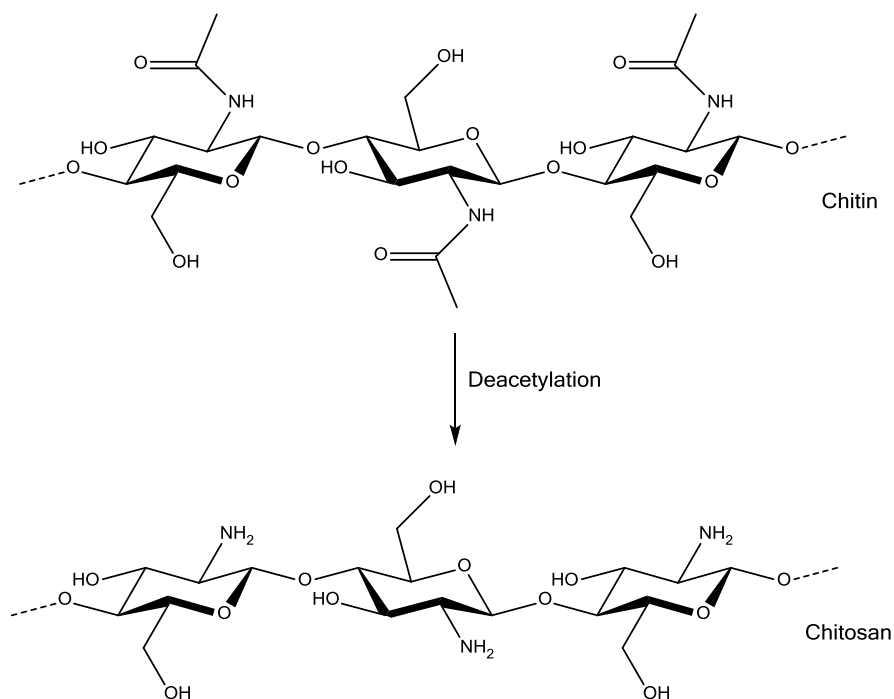


**Figure 2.16** Deacetylation of chitin to form chitosan.

The mucoadhesive properties of chitosan make it very desirable to use as a delivery vehicle to the GI tract. The stomach is located in the upper GI tract and owing to its low pH, (between 1 and 4), has evolved to be fatal for many microorganisms that enter it. This also poses significant problems as many drugs are also broken down in the stomach before they can be absorbed. This can make it difficult to treat infections in the GI tract and indeed makes it hard to deliver any oral therapeutics even if they are not going to operate in the GI tract. These infections can cause gastritis, gastric or peptic ulcer diseases or gastric carcinoma (Patel and Amiji, 1996, Risbud et al., 2000, Altinisik and Yurdakoc, 2014). An antibiotic such as amoxicillin (Figure 2.17), by itself, is not an effective treatment of these infections due to the low pH of the stomach affecting the stability of the antibiotic. A chitosan-based carrier system could increase the effectiveness of current GI infection treatments.

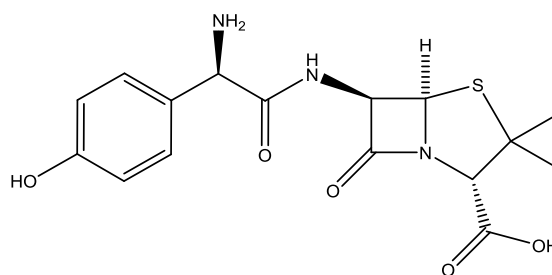


**Figure 2.17** Chemical structure of amoxicillin.

By themselves, chitosan matrices exhibit uncontrollable porosity and suffer from poor mechanical properties (Risbud et al., 2000). To enhance stability, chitosan can be crosslinked with agents such as formaldehyde (Singh et al., 2006), glutaraldehyde (Monteiro and Airoidi, 1999) or epoxy compounds (Wan Ngah et al., 2002) (Figure 2.18 (a-c) respectively), although all are cytotoxic prior to reaction and therefore not suitable for biomedical applications. Genipin is an alternative natural crosslinking agent that is 10,000 times less cytotoxic than glutaraldehyde (Sung et al., 1999) and has a slower degradation rate (Mi et al., 2001) (Figure 2.18 (d)).

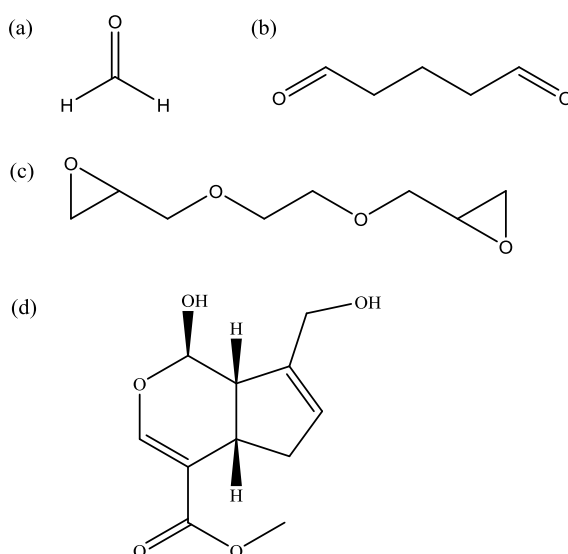


**Figure 2.18** Chemical structures of (a) formaldehyde, (b) glutaraldehyde, (c) ethylene glycol diglycidyl ether (an epoxy compound) and (d) genipin.

Genipin is isolated from the fruits of the plant *Gardenia jasminoides* and obtained from its parent compound, geniposide, via enzymatic hydrolysis with  $\beta$ -glucosidase (Butler et al., 2003, Chen et al., 2005) (Figure 2.19) and reacts with primary amines (Figure 2.20) to form a conjugated, fluorescent structure (Figure 2.21) (Hwang et al., 2011) with a blue pigmentation (Chen et al., 2004). Such genipin-chitosan matrices show promise to encapsulate bioactive molecules where the mechanical performance can be tailored for the system to be used in specific applications (Moura et al., 2007). Coupled with the attractive autofluorescent nature of such matrices as well as the favourable bio-related properties, despite the greater cost of purchasing a natural product such as genipin, it is an excellent alternative to other common crosslinking agents.

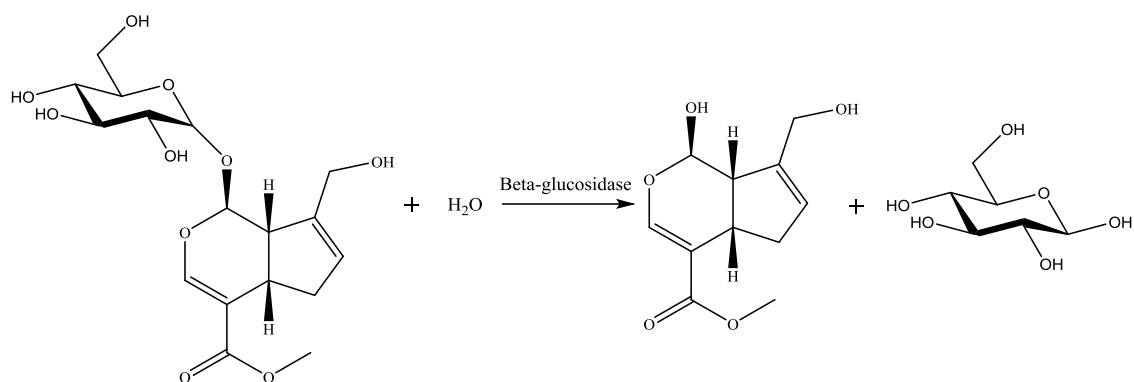


**Figure 2.19** Enzymatic hydrolysis of geniposide to genipin using  $\beta$ -glucosidase.

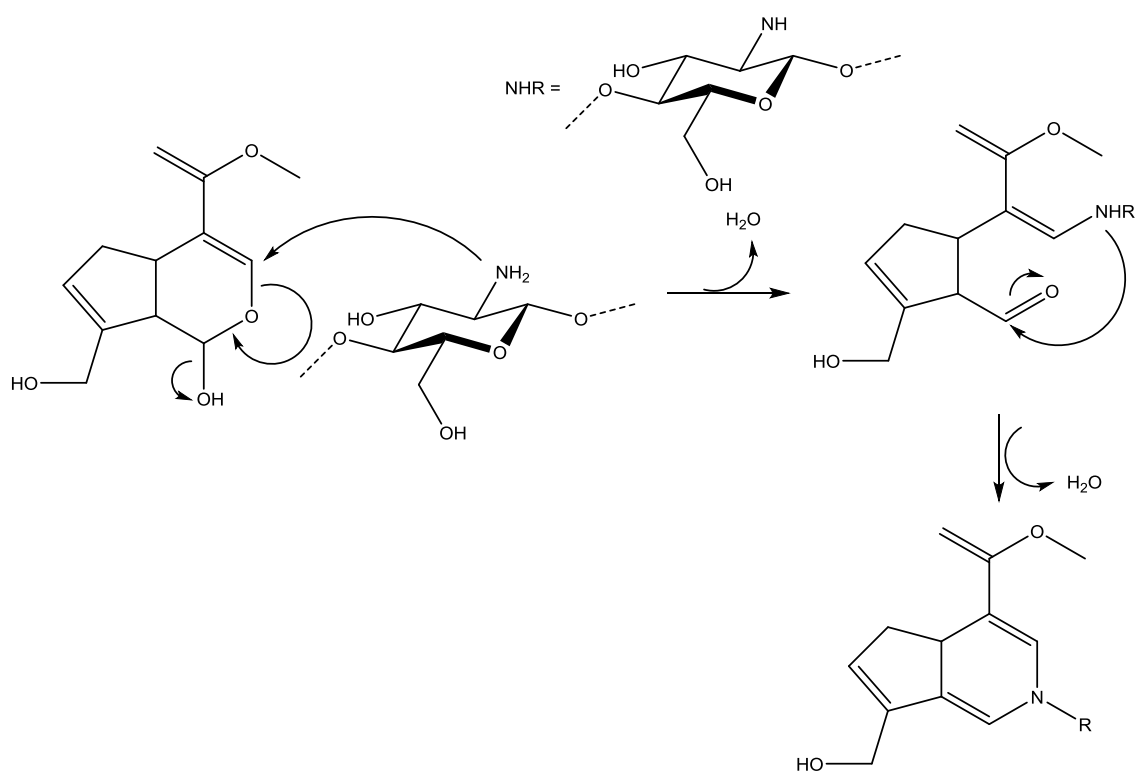


**Figure 2.20** Proposed reaction mechanism between chitosan and genipin (Chen et al., 2005)

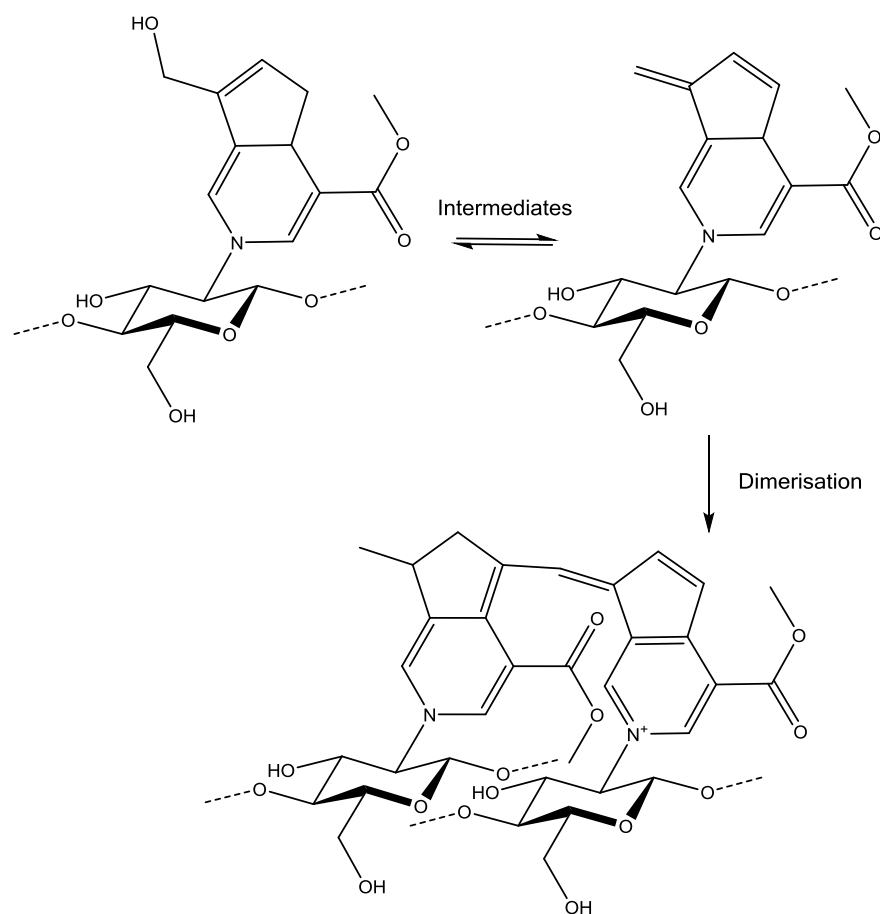


**Figure 2.21** Proposed reaction mechanism between chitosan and genipin to form a conjugated genipin derivative (Chen et al., 2005).

In order to control the porosity of chitosan structures, polymers such as PVP (Khurma et al., 2005) or PEG (Khurma and Nand, 2008) have been added to form a hydrogel. Without addition of a crosslinking agent such as genipin, combination of chitosan and PVP forms a polymer blend (Zeng et al., 2004, Sakurai et al., 2000). Polymer blends are usually multiphase systems owing to a low mixing entropy where the porous morphology is correlated with the phase separation structure of the blend membrane (Zeng et al., 2004). The formation of a miscible blend requires specific interactions between the polymers such as hydrogen bonds. These could form between the amine, residual amide or hydroxyl groups of chitosan with the amide of PVP (Fang and Goh, 2000). The drying regime was found to be important as this can also affect hydrogel porosity and therefore swelling kinetics and drug release (Risbud et al., 2000).

## **2.4.2 Antibacterial properties**

Further to using hydrogels as drug carriers, these polymer networks can also be engineered to be antibacterial in their own right. Such materials could find applications in hospitals in order to prevent the development of nosocomial infections (hospital-acquired infections). For example, bactericidal gels could form a coating on the surface of catheters and medical implants (Malmsten, 2011). Chitosan hydrogels with high quaternisation have been demonstrated to be a particularly effective against multiple Gram-positive and Gram-negative bacteria whereby detrimental electrostatic interactions with the cell wall result in cell leakage and eventual death (Li et al., 2011). It has therefore been shown that some hydrogels are able to deliver antibiotic drugs to combat infections as well as exhibiting innate antibacterial properties towards the causative strain of the same infection, thereby enhancing the overall efficacy (Buhrman et al., 2013).

## **2.4.3 Tissue engineering**

Each year millions of patients suffer the loss or failure of an organ or tissue due to accidents or disease. Tissue or organ transplantation is the generally accepted treatment, although this approach is extremely limited by a donor shortage. One way to treat such patients is to engineer man-made organs and tissues. This can be achieved by combining appropriate cell lines with polymeric hydrogels in order to mimic natural extracellular matrices found in tissues (Lee and Mooney, 2001, Drury and Mooney, 2003). Current limitations include successful in vivo integration and proliferation of desired cell lines. One way to tackle such challenges is to incorporate appropriate cell modifying peptides into the hydrogel matrix composed of natural polymers with high mechanical strength that are unlikely to illicit an immune response. Such protein scaffolds could aid cell growth on the polymer (Roque et al., 2014). Furthermore, some hydrogels have been engineered to be specifically responsive to cell growth. For example, matrix metalloproteinase-sensitive gels have been engineered to release vascular cells and small peptides (such as thymosin), resulting in human umbilical vein endothelial cell adhesion, survival, migration and organisation (Kraehenbuehl et al., 2009).

#### 2.4.4 Other applications

Hydrogels have also been utilised in separation science by conjugating specific amino acids able to bind to recognition proteins (Hoffman, 2000). Polymer gels that are responsive to pH have been utilised in sensing applications (Bashir et al., 2002, Vanblarcom and Peppas, 2011). As hydrogels can be engineered to be of a small size (millimetre scale), mass transfer and chemomechanical responses are typically faster than larger counterparts (Richter et al., 2008). Consequently by utilising a range of sensor transducers, the free swelling of responsive hydrogels can be monitored or the mechanical work of the hydrogel can be used further (Tokarev and Minko, 2009). Hydrogels have also been shown to be capable of autonomous control of local flow via incorporation into microfluidic systems (Beebe et al., 2000). Upon swelling, fluid flow is restricted and when collapse is induced, the local fluid is able to pass.

#### 2.5 Synthesis of smart hydrogels

As a hydrogel is a network of polymers, it is important to appreciate the physical properties of the constituents prior to synthesis. Most notably, the molar mass of individual polymers can have pronounced effects on the gelation, rheological and mechanical behaviours of hydrogels (Shen et al., 2010, Wang and Li, 2005). In linear polymers, the individual polymer chains do not have an identical molar mass but instead there is a molar mass distribution around an average value, which denotes the relationship between the number of moles of each polymer species ( $N_i$ ) and the molar mass ( $M_i$ ) of that polymer species. In practice, four averages are employed. The number average molar mass ( $M_n$ ) (Equation 2.22) is the statistical average molecular mass of polymer chains in a sample. The weight average molar mass ( $M_w$ ) (Equation 2.23) also takes into account the molecular weight of a chain when determining contributions to the average molecular mass (a more massive chain will contribute further to  $M_w$ ). The z-average molar mass ( $M_z$ ) (Equation 2.24) is particularly sensitive to high molecular mass polymers. The viscosity average molar mass ( $M_v$ ) was established based on the principle that larger polymers essentially make a solution more viscous than smaller equivalents (Equation 2.25 where  $\underline{a}$  is the exponent of the Mark-Houwink equation (Equation 2.26), which links intrinsic viscosity ( $[\eta]$ ) to molar mass ( $\underline{K}$  is also a Mark-Houwink parameter)). The

dispersity of a specimen (or polydispersity index) is defined as  $M_w$  divided by  $M_n$  and details how narrow the molar mass distribution is. A “perfect” polymer would have a polydispersity of 1.00. A higher polydispersity value indicates a wider distribution of polymer masses. One result of a narrow molar mass distribution in a polymer is often a high extent of three-dimensional long range order in the solid, leading to a higher density and melting point (Atkins and de Paula, 2006).

$$M_n = (\sum M_i N_i) / \sum N_i \quad (2.22)$$

$$M_w = (\sum M_i^2 N_i) / (\sum M_i N_i) \quad (2.23)$$

$$M_z = (\sum M_i^3 N_i) / (\sum M_i^2 N_i) \quad (2.24)$$

$$M_v = [(\sum M_i^{1+a} N_i) / (\sum M_i N_i)]^{a-1} \quad (2.25)$$

$$[\eta] = K M_i^a \quad (2.26)$$

Gel permeation chromatography (GPC) can be used to analyse the molar mass distribution of polymers by separating the analytes on the basis of their size. This technique involves passing a polymer solution through a matrix of crosslinked polymer particles. For polymers with a high molecular mass, the accessibility of stationary phase pore volume for the polymer molecules is limited, resulting in shorter elution times compared to polymers with a lower molecular mass. This leads to separation and detection is subsequently performed on the basis of concentration and molar mass. Following such preliminary polymer characterisation, gel synthesis can then be instigated.

Hydrogels synthesised from one polymer typically suffer from poor mechanical attributes (they often fail at a tensile stress lower than sub-MPa and strain lower than 100%) in the hydrated state leading to difficulties when surgically removing non-biodegradable networks and in drug delivery, insufficient mechanical strength may lead to the formation of voids or channels where the impregnated therapeutic can quickly diffuse out as opposed to at the intended target site (Zhang et al., 2004). In order to address this problem with stability, interpenetrating networks (IPNs) can be prepared to increase the polymer mass per unit volume. IPNs are defined as a mixture of two or more crosslinked networks that are held together by permanent entanglements (Bajpai et al.,

2008). IPNs allow for the incorporation of unique properties from individual polymers to form one hydrogel that possesses all the desired attributes (Myung et al., 2008).

The two main types of IPN this review will focus on are full IPNs and semi IPNs (Figure 2.22). Full IPNs are composed of two juxtaposed networks (Figure 2.22 (a)) whereas in a semi-IPN, one polymer is crosslinked to form a network whilst the other component is a linear polymer (Figure 2.22 (b)). Other IPNs such as homo-IPNs, latex IPNs and thermoplastic IPNs are also common. Besides superior mechanical properties, as IPNs are insoluble in bodily fluids, these hydrogels are suitable for targeted drug delivery and can be synthesised to be environmentally-sensitive (Risbud et al., 2000, Matricardi et al., 2013). To confirm the formation of IPNs when new hydrogels are synthesised, a wide range of techniques can be used. Fourier Transform Infrared Spectroscopy (FTIR) analysis can be conducted. For example, it can be determined as to whether a polymer has been successfully crosslinked during gelation (Bhattacharai et al., 2005).

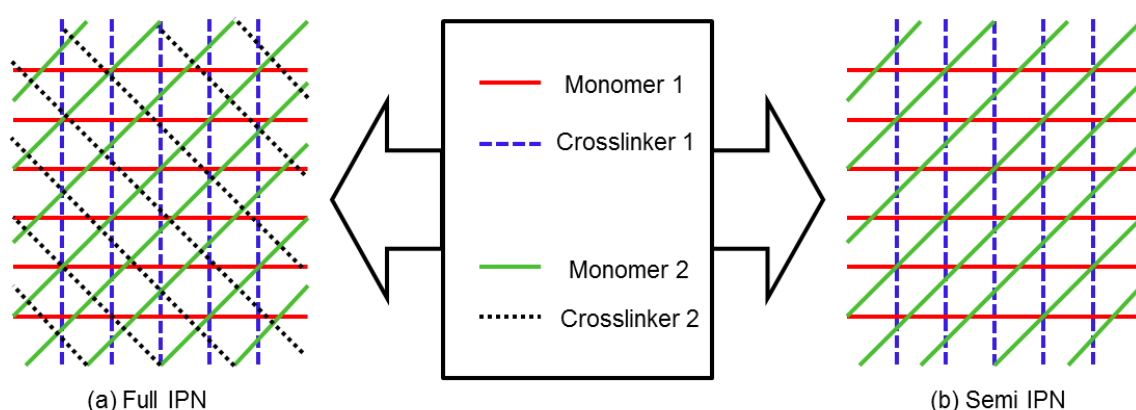


**Figure 2.22** Schematic representation of: (a) full IPN and (b) semi-IPN (Bajpai et al., 2008).

Another class of polymer gels with exceptional mechanical properties are double-network (DN) gels, which are very different from conventional IPN gels as they consist of two types of polymer components with opposite physical natures (Figure 2.23). As opposed to developing gels with a homogeneous structure, a strong degree of heterogeneity is incorporated into the material. The minor component forming the rigid skeleton is synthesised with abundantly crosslinked polyelectrolytes whilst the major component representing a ductile

substance is comprised of poorly crosslinked neutral polymers. Such DNs possess hardness (0.1-1.0 MPa), strength (failure tensile stress 1~10 MPa, strain 1000-2000%, failure compressive stress 20-60 MPa, strain 90-95%) and toughness (tearing fracture energy 100-1000 Jm<sup>-2</sup>) (Tsukeshiba et al., 2005, Na et al., 2006, Huang et al., 2007a, Tanaka et al., 2005, Na et al., 2004, Nakajima et al., 2009, Gong, 2010). Such impressive mechanical properties are akin to that of rubber or tissues, making DNs appealing for use in tissue engineering and as drug carriers. Studies have shown that the toughening behaviour exhibited by DN gels is based upon a local yielding mechanism (Brown, 2007). This is based upon the formation of multiple cracks in the initial stiff network upon stress application. Such cracks are thought to be held together by the second network. Surrounding each crack, a multiply cracked damage zone will be formed, resulting in energy dissipation and shielding of the second network (Brown, 2007).

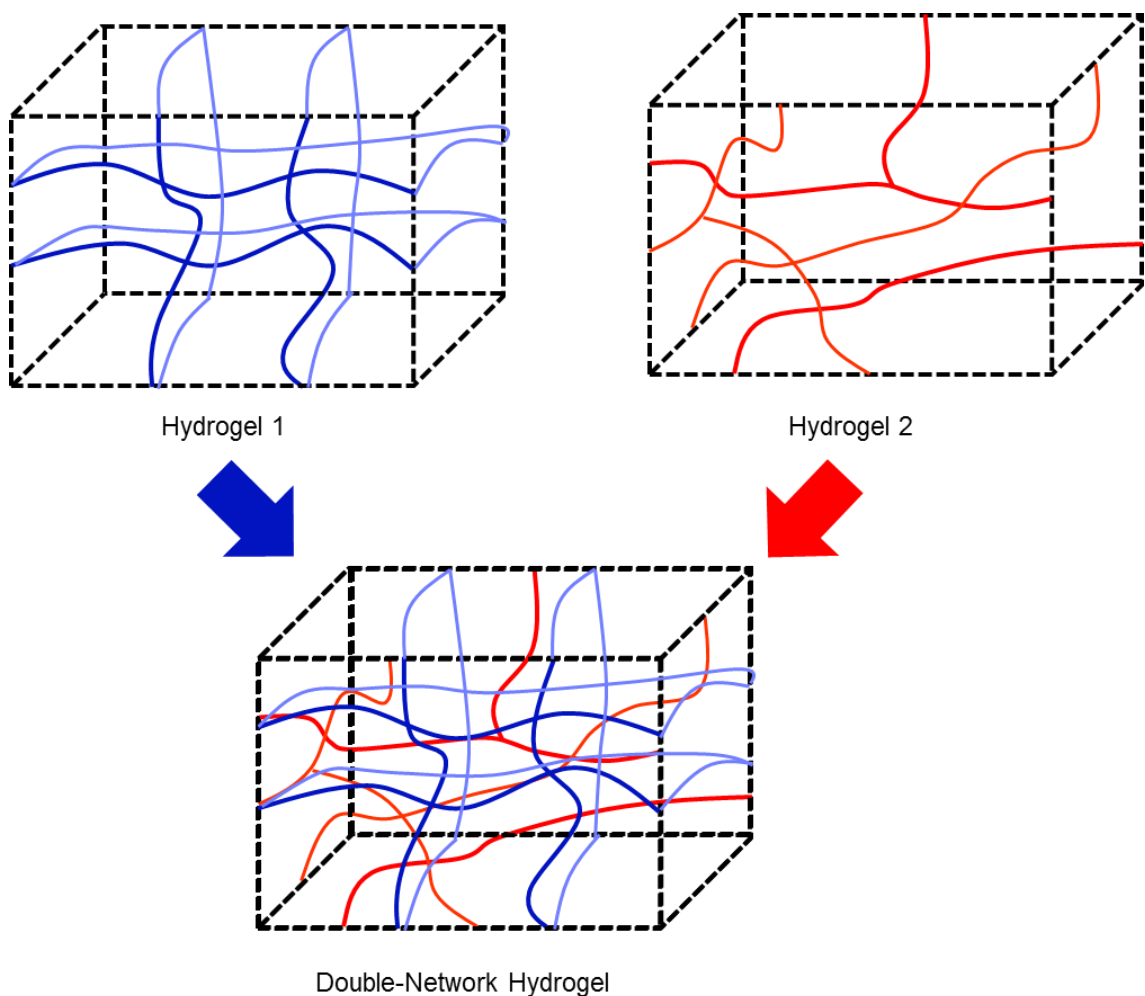


**Figure 2.23** Schematic of a DN gel displaying the opposite physical natures of polymer components in the structure (Gong, 2010).

An additional method to improve the stability of hydrogels is to carefully freeze and thaw the polymer networks following synthesis. As mentioned, although increasing the amount of crosslinking agent / tuning the hydrophobicity of the matrix can lead to enhanced mechanical attributes, this typically results in a concomitant decrease in swelling potential. The mechanism by which this process enhances stability is unclear, although for physically-crosslinked poly (vinyl alcohol) (PVA) hydrogels, increased freezing and thawing led to reinforcement of existing crystals within the porous network, resulting in stability enhancement (Hassan and Peppas, 2000). Such freezing of absorbed liquids could facilitate the formation of ice crystals within the network, resulting in crystallisation within the pores (Holloway et al., 2013). The enhancement in ultimate tensile strength and Young's modulus as a function of freeze thaw cycles was then demonstrated quantitatively where the presence of larger sized crystallites was thought to contribute to the overall strength of the network (Nugent and Higginbotham, 2006, Gupta et al., 2012). A more recent article argues that crystallisation does not play the only role in enhancing the stability of freeze-thawed hydrogels but phase separation into a PVA-rich phase and a water-rich phase is a crucial component to the overall mechanism. By forming regions of high PVA concentration following freezing, PVA chains come into close contact with one another, facilitating crystallite formation and hydrogen bonding. Hence, it is claimed that phase separation is a prerequisite for the formation and increased development of crystalline regions within the network, which ultimately increase the overall stability (Holloway et al., 2013). Figure 2.24 depicts the variation in microstructure as a function of freeze thaw cycles for hydrogels with polymers with different percentage weights via optical microscopy. Increasing porosity and phase separation (depicted via thickening of PVA-rich regions) are shown with an increasing number of freeze thaw cycles (and as expected, with increasing polymer concentration).

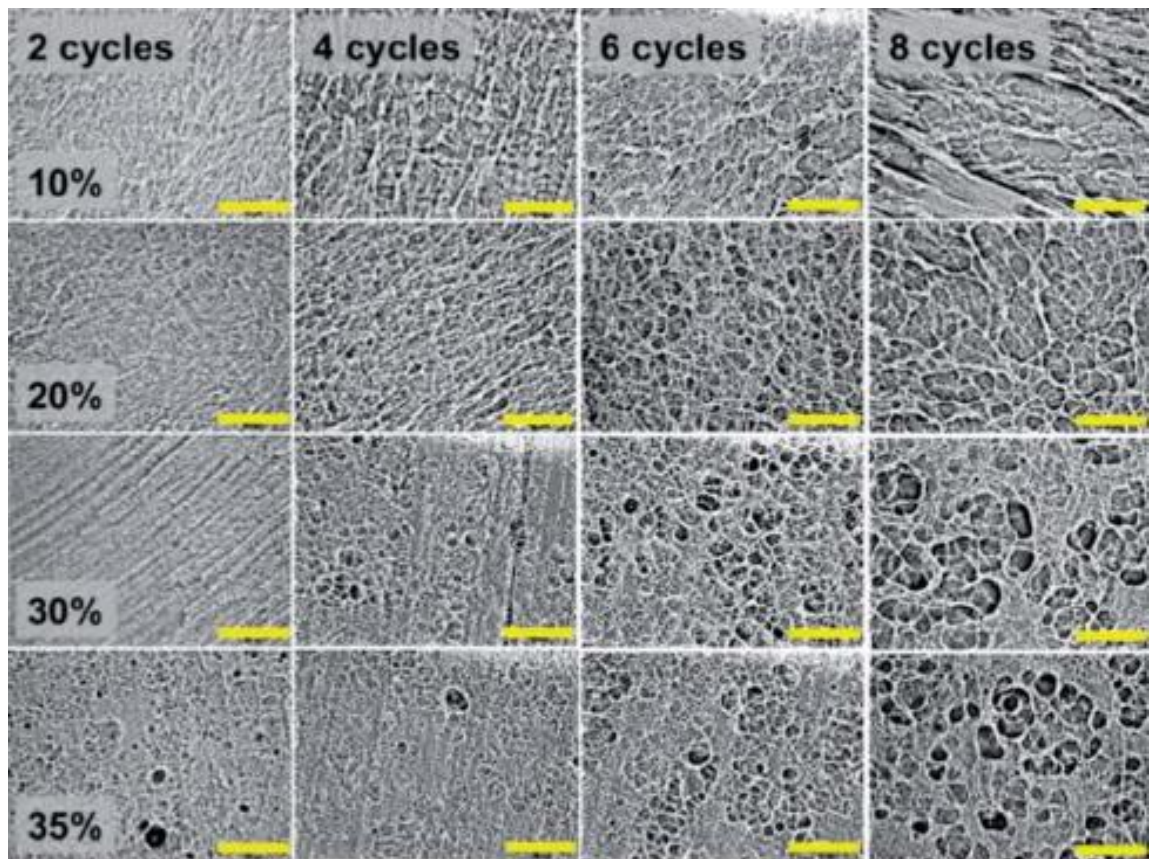


**Figure 2.24** Optical micrographs of freeze-thawed PVA hydrogels showing the increase in polymer densification and porosity with increasing freeze thaw cycles and polymer concentration. The scale bars represent 80  $\mu\text{m}$  (Holloway et al., 2013).

Taking this evidence into account, it would seem that an appropriate representation of what is occurring during freeze-thawing of PVA hydrogels is shown in Figure 2.25. This involves initial phase separation into a PVA-rich and water-rich phase. Upon freezing, PVA is expelled, forming regions of high PVA concentration, facilitating the formation of hydrogen bonds, leading to crystallite formation and densification (Holloway et al., 2013). Such a facile synthetic manipulation offers an attractive route to engineering stable hydrogels for a multitude of applications.

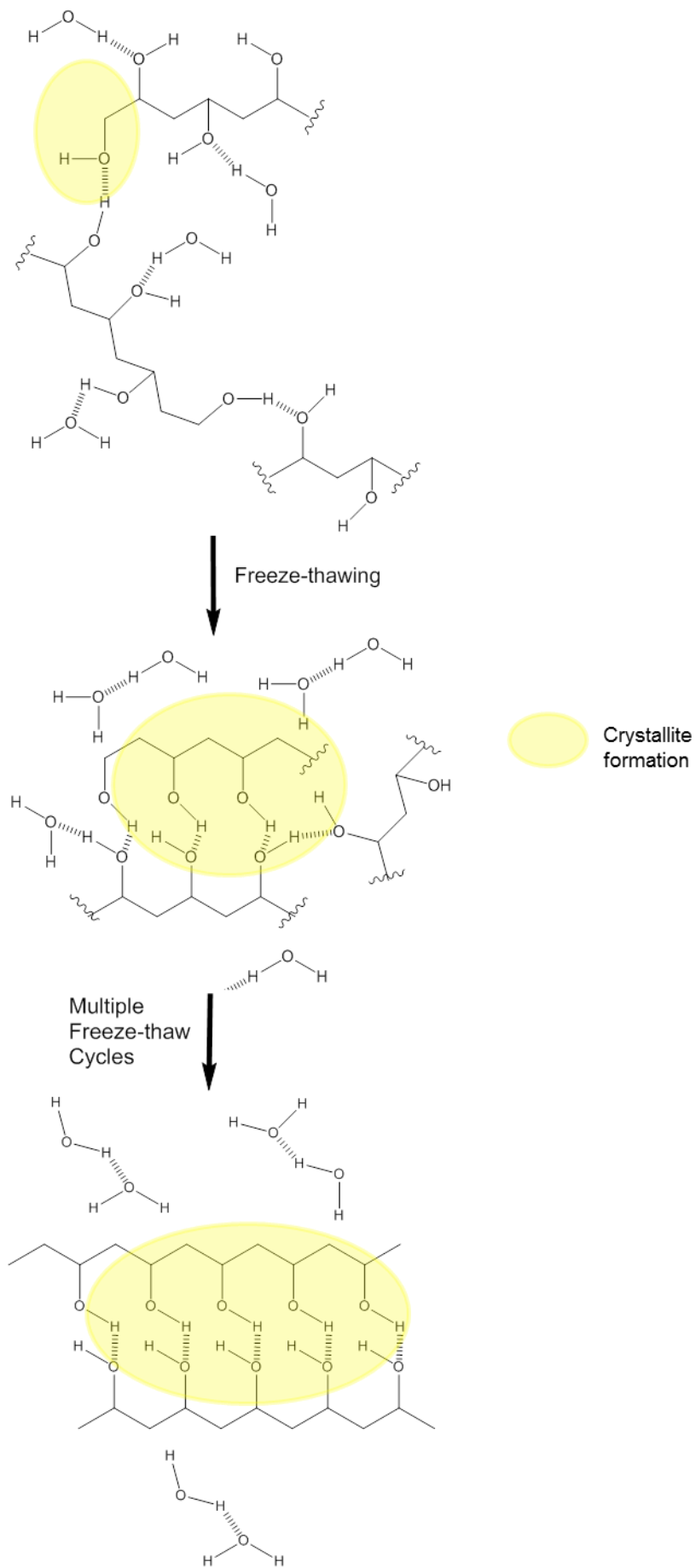


**Figure 2.25** Schematic of the probable freeze-thawing mechanism of PVA.

## 2.6 Characterisation techniques of smart hydrogels

There is a wide range of techniques to study polymer hydrogels. An overview with specific reference to how they have been used in the literature is provided below.

### 2.6.1 Swelling behaviour of smart hydrogels

The swelling ratio ( $\phi/\phi^*$ ) details how much a gel can increase in volume from an initial to a final state. In some cases this could be the final equilibrium swelling degree of the network where a plateau is reached. This informs experimenters how responsive the hydrogel is and to what extent the network can increase in size. The ratio may be determined by examining the variation in mass or volume (via surface area and height calculations over time).

The swelling ratio ( $\phi/\phi^*$ ) is dimensionless and denotes the final equilibrium volume fraction of a network and can be observed by measuring the initial ( $d^*$ ) and final ( $d$ ) diameter of the gel where  $d$  and  $d^*$  are in millimetres (mm) (Equation 2.27).

$$(\phi/\phi^*) = (d-d^* / d^*)^3 \quad (2.27)$$

It can also be found by determining the initial area ( $a^*$ ) and height ( $h^*$ ) (Equation 2.28) coupled with the final area ( $a$ ) and final height ( $h$ ) measurements (Equation 2.29) in order to achieve the relative volumetric swelling ratio (Equation 2.30) where  $V^*$  and  $V$  are the initial and final gel volumes respectively. In Equations 2.28-2.30,  $h$  and  $h^*$  are in mm,  $a$  and  $a_0$  are in millimetres squared ( $\text{mm}^2$ ) and  $V$  and  $V^*$  are in millimetres cubed ( $\text{mm}^3$ ).

$$V^* = a^* \cdot h^* \quad (2.28)$$

$$V = a \cdot h \quad (2.29)$$

$$\phi/\phi^* = (V-V^*) / V^* \quad (2.30)$$

This could be determined, using a microscope, micrometer or cameras (Ohmine and Tanaka, 1982). An alternative method is to measure the change in weight of the hydrogel according to Equation 2.31 where  $W_s$  is the weight of a swollen

hydrogel (wet weight – dry weight) and  $W_d$  is the dry weight of the hydrogel (Zhang et al., 2004). Both  $W_s$  and  $W_d$  were measured in grams (g). Typical behaviour could be an initial sharp increase in swelling (e.g. due to ionisation of corresponding functional groups owing to the pH of the surrounding environment) with an eventual plateau (e.g. all functional groups have been ionised to induce swelling).

$$\phi/\phi^* = W_s / W_d \quad (2.31)$$

Oscillatory swelling experiments can also be conducted to investigate how hydrogels respond upon repeatedly changing the local environment (e.g. switching between pH values whilst studying a pH-sensitive hydrogel) (Bell and Peppas, 1996, Özyürek et al., 2000). Further to demonstrating the reversibility of the swelling process, these studies can also be useful to ascertain whether the hydrogel will be suitably responsive for combination with an oscillatory reaction exhibiting similar changes in the appropriate stimulus.

On the microscale, the use of microelectromechanical systems can be used to elucidate the degree of swelling in hydrogels via the deflection length of a cantilever on the surface of samples (Bashir et al., 2002). Microcantilevers are particularly suited for this application as they provide mechanical amplification of a signal due to the change in surface properties and as such, upon implementing with a pH-sensitive hydrogel, during a pH variation, a maximum deflection sensitivity of 18.3  $\mu\text{m}$  during a change of one unit of pH can be achieved. This can be extended for use on the nanoscale utilising atomic force microscopy (AFM) to evaluate volume and topography changes during swelling (Caldorera-Moore et al., 2011, Mabilleanu et al., 2006).

At the molecular level, the change in swelling causes fluctuations in the distances between hydrophobic moieties in gel networks. This separation can be monitored by small-angle X-ray scattering (SAXS) and a correlation can be drawn between molecular and macroscopic events (Ryan et al., 2005b). SAXS records elastic scattering of X-rays at very low angles ( $0.1-1^\circ$ ) to determine structural data on the nanoscale. The X-ray source can be a laboratory source or synchrotron light (emission of light when charged particles are accelerated radially), which provides a higher X-ray flux. SAXS has the advantage over

X-ray crystallography in that for analysing biological moieties such as proteins, a crystalline sample is not required. It is possible to monitor the *in situ* hydrogel response by using laser light scattering through imprinted polymeric diffraction gratings where scattering patterns are generated by interference of wavefronts produced by differing refractive indexes within the sample (Swann et al., 2010). This technique overcomes the problem encountered in visualising hydrogels using an optical microscope whereby as the gel swells, the refractive index becomes similar to that of the solution making it increasingly difficult to visualise the sample.

In the case of hydrogels being engineered to form thin films, further to the relevant aforementioned characterisation techniques, a quartz crystal microbalance (QCM) can be used to measure exceptionally small mass changes over time (mass densities can be recorded to  $1 \mu\text{g cm}^{-2}$ ) (Gabai et al., 2001).

FTIR analysis may also be performed on hydrogels during swelling in order to determine specifically what changes are occurring on the molecular level. For example the degrees of protonation of chemical moieties along polymer chains can be studied as a function of pH (Topham et al., 2013).

### **2.6.2 Force response testing**

Measurement of the force response of a network is strongly related to the swelling capabilities and techniques described above. One method to do this is to place a hydrogel in solution to initiate swelling whilst maintaining contact with a static compression plate and subsequently measuring the force produced owing to swelling. This setup may be altered in order to simulate the conditions where a hydrogel may find application such as by mimicking a microfluidic device (Johnson et al., 2004). A modified Johnson-Kendall-Roberts apparatus can be also be utilised to detect force (Ryan et al., 2005b). Variations can be monitored by a balance over time and can therefore be useful for developing applications in actuation. In both methods the measured force is only a small proportion of the actual force generated as it is only recorded in one dimension, although it elegantly demonstrates the conversion of chemical potential into work (Crook et al., 2004).

### 2.6.3 Thermal behaviour

Differential scanning calorimetry (DSC) can be used to examine the thermal behaviour of temperature sensitive hydrogels (Zhang et al., 2004). DSC measures the difference in the amount of heat needed to increase the temperature of a sample compared to an appropriate reference. This thermoanalytical technique is useful for determining glass transition temperature, UCST and LCST of hydrogels. DSC can also be used to determine thermodynamic parameters such as enthalpies associated with phase transitions.

### 2.6.4 Structural characterisation

The structural morphology of hydrogels can be evaluated by numerous techniques in order to ascertain the porosity of the network and the presence of defining features such as channels or honeycomb arrangements. The porosity is an important parameter to note as it is strongly related to the associated swelling ability and mechanical attributes of polymeric hydrogels. For example as previously detailed, samples with a high porosity tend to be highly responsive but face challenges when finding applications due to insufficient mechanical properties. Scanning electron microscopy (SEM) is one technique that can be used to study the morphology of hydrogels where information about the number and size of pores can be determined. A typical SEM micrograph of a chitosan-based hydrogel is depicted in Figure 2.26.

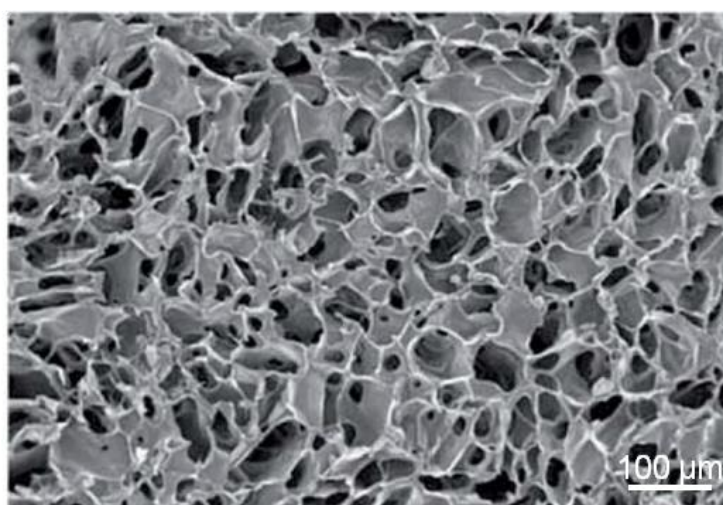


**Figure 2.26** A typical hydrogel SEM image of a freeze dried chitosan-alginate hydrogel (Levengood and Zhang, 2014).

SEM provides images of external morphology by accelerating and focussing electrons (0.5-40 keV) into a narrow beam that interacts with a sample in a controlled pattern (raster). This results in reflection of high-energy elastically-scattered electrons and deflection of inelastically-scattered secondary particles that are detected by converting and amplifying the signal to a voltage. This is applied to a cathode ray tube to determine the brightness from signal intensity and is displayed as an image.

However, before samples can be analysed, they must be prepared via drying. Two common drying techniques are critical point drying (CPD) and freeze drying (FD). CPD passes samples through the supercritical region where no phase boundary is crossed (Figure 2.28 solid arrow). FD occurs via dehydration of a sample by a sublimation process where a frozen liquid is transformed directly to the gaseous state, avoiding the liquid-gas transition (Figure 2.27, outline arrow). Such drying techniques may potentially alter the structure of these environmentally sensitive materials.

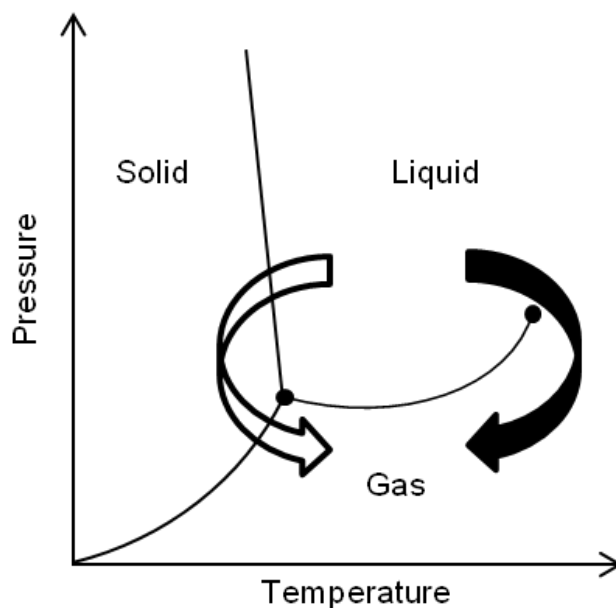


**Figure 2.27** Phase diagram illustrating how FD (outline arrow) brings the system around the triple point and how CPD (solid arrow) brings the system through the supercritical region.

Environmental scanning electron microscopy (ESEM) has been used as an alternate technique to SEM as no prior sample drying is required, (images can be collected when samples are “wet” / uncoated owing to the gaseous environment in the specimen chamber) (Gattás-Asfura et al., 2005, Lu et al.,

2010). This would allow for sample analysis to be conducted in their “native state” without specimen alteration (such as drying). However, the hydrogel cannot be immersed in liquid during analysis. It can be exceptionally difficult to elucidate structural details from images collected via this technique due to the inherent “wet” nature of the samples. An example is shown in Figure 2.28.



**Figure 2.28** A typical hydrogel ESEM image of a hydrogel (Bai et al., 2012).

Transmission electron microscopy may also be used to study the features of hydrogel networks at the nanoscale (although analysis cannot be performed whilst the sample is in an aqueous environment) (Maity et al., 2014).

Optical microscopy can also be used as an imaging technique, although shows more promise as a tool to follow the overall change in surface area as opposed to probing the porous morphology. This technique uses visible light and a system of lenses to magnify small specimens. On compound microscopes, a combination of convex lenses allow for specimens to be analysed up to 1000 x. As such, this technique has previously been used to analyse the structural properties of hydrogels (Yokoyama et al., 1986).

A good alternative to the aforementioned techniques is confocal laser scanning microscopy (CLSM) allowing the hydrogel to remain submerged in (transparent) fluid during analysis. This technique has been used to analyse the structure of hydrogels and can be operated in both bright-field and fluorescence modes, following successful conjugation of a fluorescent tag to the network (Bodugoz-

Senturk et al., 2009, Fergg et al., 2001, Woerly et al., 2008). A hydrogel studied via this method is shown in Figure 2.29.

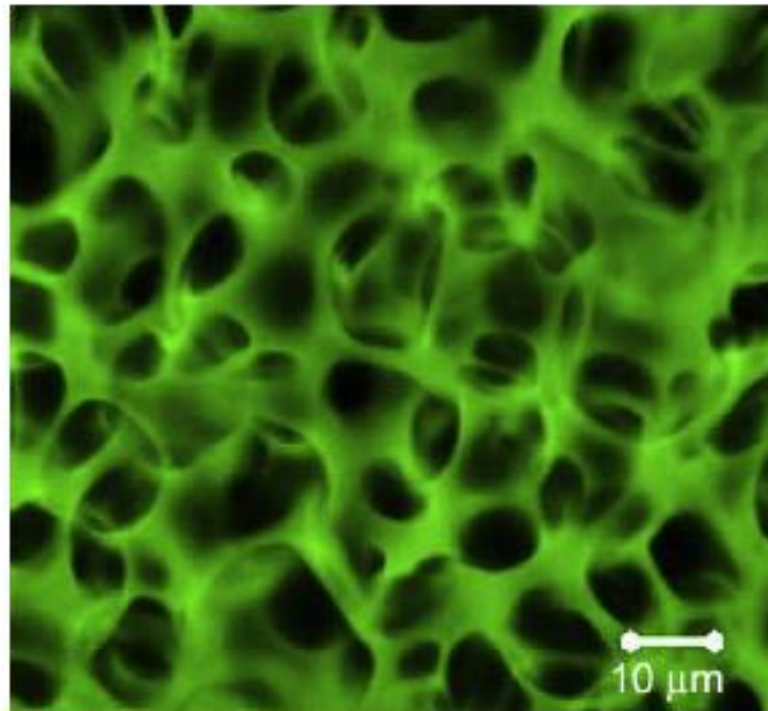


**Figure 2.29** Confocal microscopy image of a PVA-PEG hydrogel (Bodugoz-Senturk et al., 2009).

Fluorescence is radiation emitted by substances due to the incident radiation of a shorter wavelength (and therefore higher energy). Upon sample irradiation, electrons are excited from the ground state to an excited state (Figure 2.30 *blue square dotted lines*) and as the excited electron relaxes to a lower energy level, energy is emitted. This is called the energy emission due to fluorescence (Figure 2.30 *orange round dotted lines*). The curved arrow in Figure 2.30 indicates a non-radiative transition whereby transitions between energy levels are not associated with the emission of light. Examples of non-radiative transitions include vibrational relaxation, internal conversion and intersystem crossing.

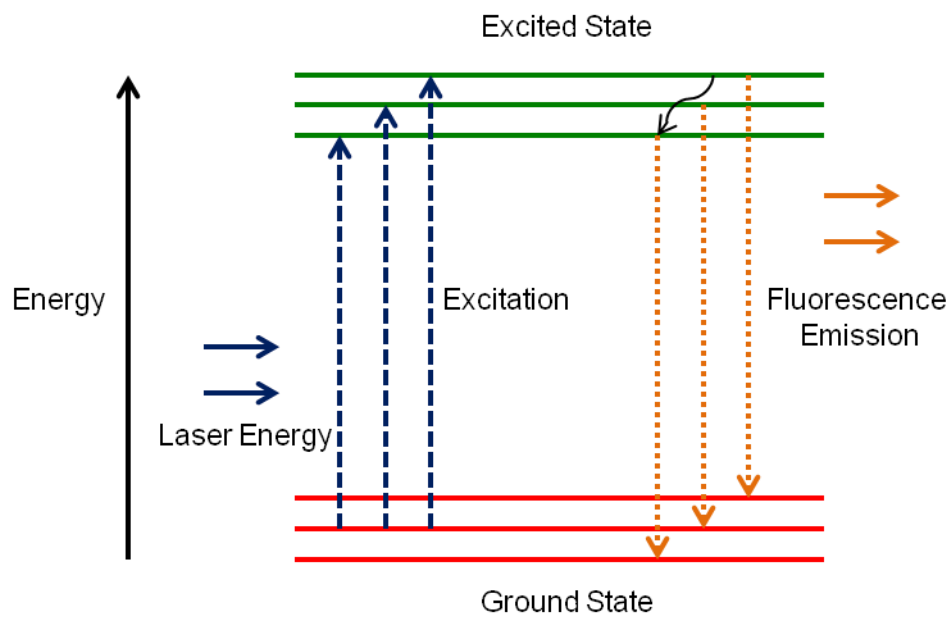


**Figure 2.30** A Jablonski diagram illustrating the transitions between electronic states.

Fluorescence microscopes function by illuminating a specimen causing the fluorophores to emit light of a higher wavelength. This light is collected using a dichroic spectral emission filter allowing an appropriate passband to be transmitted to the detector in order to generate an image.

CLSM can be used to obtain high-resolution optical images with depth selectivity by utilising optical sectioning in order to clearly examine focal planes within samples. As images are acquired point-by-point, upon reconstruction with a computer, three dimensional (3-D) images can be generated, which also facilitates topographical specimen examination (Cremer and Cremer, 1978). Operational principles include passing a laser beam through an aperture, which is focused by an objective lens onto a sample. Scattered and reflected light is recollectd by the objective lens, distributed by a beam splitter into an appropriate filter to transmit fluorescent light through a pinhole for it to be detected by a photomultiplier tube, transforming the light into an electrical signal recorded by a computer (Paddock and Eliceiri, 2014, Paddock, 2000). If the CLSM was utilised in reflectance mode, the same setup would apply with the exception of the presence of fluorescent excitation and emission filters. It is the pinhole that allows high-resolution images to be obtained at multiple depths. By altering the microscope stage or objective lens height, information can be collected from multiple focal planes. A computer can then construct a stack of images from such planes to generate a 3-D picture.

As CLSM can function via optical sectioning, a 3-D representation of the whole sample can be constructed. An alternative method for ascertaining a 3-D representation of the network is via X-ray microtomography where X-rays create cross-sections of the matrix, which are used to create a 3-D model (Figure 2.31).

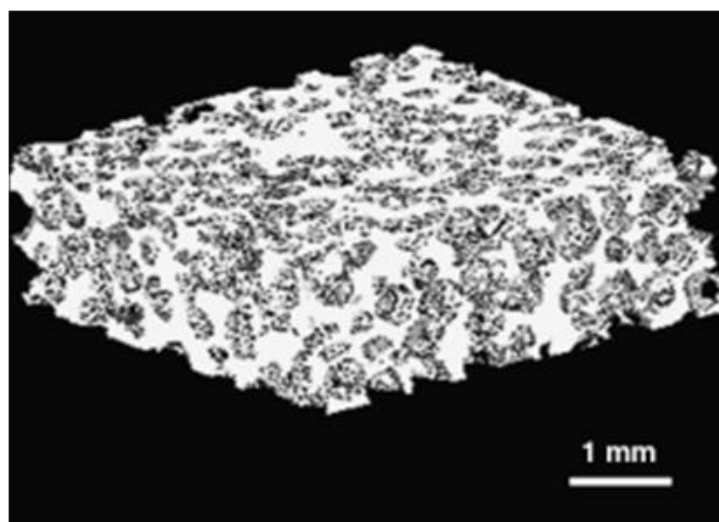


**Figure 2.31** X-ray microtomography image of a poly (epsilon-caprolactone fumarate) hydrogel (Kim et al., 2009).

As previously mentioned, on the nanoscale, AFM can be used to investigate the surface roughness of hydrogels whilst contained in aqueous environments (Mabilleau et al., 2006). However, the technique is limited as it can only image a maximum height of 10-20  $\mu\text{m}$  and a maximum scanning area of approximately 150x150  $\mu\text{m}$ . It is expected that as swelling occurs, owing to the penetration of water into the network, chain relaxation occurs leading to a decrease in surface roughness. AFM provides images by profiling surfaces with a sharp probe tip (with a radius of curvature approximately 13 nm) held at the top of a cantilever. Forces between the tip and the sample surface cause the cantilever to bend and this deflection can be measured to produce a topographical image (using a position sensitive photodetector) (Wilson, 2004, Elings, 1994). It is suggested that this technique is not appropriate for highly hydrated samples as the probe can be engulfed in the highly swollen layers of the sample (Guryča et al., 2004).

Hydrogel porosity can also be quantified by using mercury intrusion porosimetry (Kim and Chu, 2000). Porosity is determined by the amount of external pressure required to force mercury into a void against the opposing force of the surface

tension. This method is advantageous over calculating the porosity manually from images collected as a physical measurement is actually recorded as a function of pressure for the whole network as opposed to determining the average porosity based on images forming part of the overall sample. However, depending on the drying regime employed, unreliable mercury intrusion porosimetry results can be collected that do not represent the porous architecture of hydrogel samples (Romn et al., 2011).

### 2.6.5 Mechanical characterisation

The mechanics of materials can be investigated by examining the behaviour of solid objects subject to stresses and strains. When a sample is subjected to an applied load, internal forces called stresses are created within the specimen, which induce deformation of the material (strain). Such loads can be axial whereby the applied forces act to stretch (via tension) or shorten (via compression) the sample (Beer et al., 2014). Uniaxial stress ( $\sigma$  in units of  $\text{Nm}^{-2}$  or Pa) can be calculated according to Equation 2.32 where  $F$  is the force (N) acting on a deformation area,  $A$ , ( $\text{m}^2$ ).

$$\sigma = F / A \quad (2.32)$$

Compressive stress is induced when an applied load reduces the length of a sample along the axis of the applied load whereas tensile stress occurs when the specimen elongates along the axis of the applied load. As previously mentioned, strain is the resultant deformation of a material following application of a load to induce stress. Strain is defined as the deformation per unit length (Beer et al., 2014). Based upon this, strain can be represented in the form of the engineering strain as expressed in Equation 2.33 where  $\epsilon$  is strain (no units),  $L^*$  is the original length of the material and  $L$  is the final length of the specimen (both can be given in mm).

$$\epsilon = L - L^* / L^* \quad (2.33)$$

Stress and strain can be plotted against one another to produce a stress-strain curve (Figure 2.32) where properties such as the elastic modulus (or Young's modulus),  $\lambda$  ( $\text{Nm}^{-2}$  or Pa), can be determined (Equation 2.34). This number measures the resistance of a material to being deformed elastically upon

application of a force and can be calculated by determining the gradient of a stress-strain graph in the elastic deformation region (Anseth et al., 1996) whereby a stiffer material will have a higher elastic modulus. Deformation is reversible in the elastic region so that when a load is no longer applied, the specimen returns to its original shape. Such linear elastic deformation is governed by Hooke's law (Equation 2.35) where  $F$  is the force (N) required to extend or compress a spring,  $K$  is the spring constant ( $\text{Nm}^{-1}$ ) and  $x$  is the extension (m). However, it is noteworthy that some elastic materials respond in a nonlinear manner in which case Hooke's law is not applicable. The elastic range ends and deformation ensues when a specimen reaches its yield strength. For specimens in the plastic region, deformation is irreversible, although samples will have initially undergone reversible elastic deformation and hence the material may return partially to its original shape. For materials under tensile stress (specifically metals) the plastic region is composed of an initial strain hardening region whereby specimens become stronger via the movement of atomic dislocations, resulting in an ultimate strength being reached, which is followed by the final necking region where the cross-sectional area of samples is reduced before eventual fracture (Armstrong et al., 2013).

$$\lambda = \sigma / \epsilon \quad (2.34)$$

$$F = - K x \quad (2.35)$$

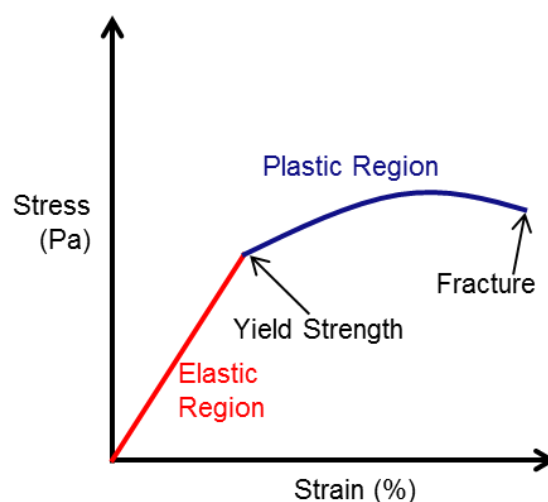


**Figure 2.32** A stress-strain graph depicting the elastic and plastic regions.

In order to appreciate the various mechanical properties of different materials, a material selection chart is often depicted (Figure 2.33). As to be expected,

heavy and stiff materials such as ceramics and metals with a high Young's modulus (10-1000 GPa) appear in the top right corner of the graph whilst polymers and wood products have an intermediate stiffness (0.1-10 GPa) with foams being the most light and flexible materials (0.01-0.5 GPa) (Ashby et al., 2009).

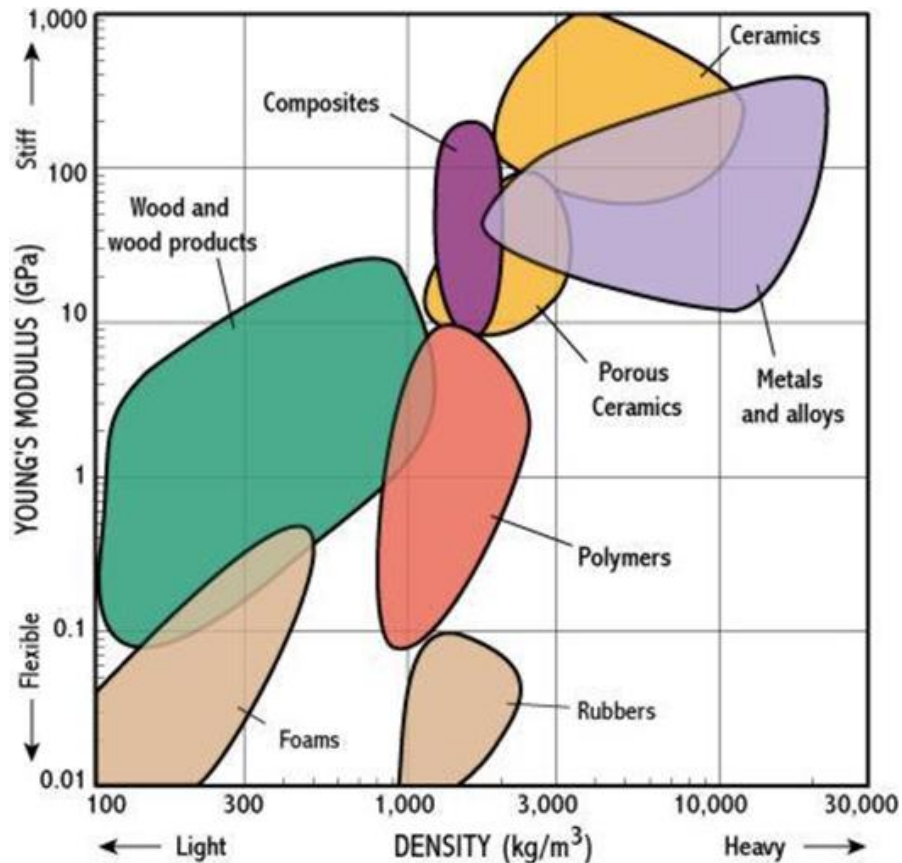


**Figure 2.33** A materials selection chart in order to compare the mechanical properties of various materials based on the Young's modulus and density (Ashby et al., 2009).

Foams are a subset of lattice-structured materials (a connected network of struts). Beyond the elastic region, plastic deformation occurs where the network collapses until opposite sides of the cells impinge where the stress rises steeply (densification) (Ashby, 2006). Gels also exhibit linear elastic behaviour up to the yield strength, although upon plastic deformation, strain hardening commonly occurs (Myung et al., 2007). This is where the strength of a material increases due to plastic deformation. The mechanisms as to why this occurs are currently unclear, however it may be due to hydrogen bond reinforcement of physical entanglements within the sample, serving to strengthen the network (Oyama et al., 1987). Gel-foams show a combination of both foam-like and gel-like behaviours depending on the density (Sehaqui et al., 2010). At low strains,

linear elastic deformation occurs and a gradual transition from linear to non-linear stress-strain behaviour (exemplified by network collapse) is common. Either a horizontal plateau region (as in foams) or a gradual increase in stress (as in gels due to strain hardening) may result. At higher strains, considerable stiffening occurs due to sample densification (Sehaqui et al., 2010). Differences between cellulose gels and foams are depicted in Figure 2.34 where Figure 2.34 (a) depicts gel-behaviour and Figure 2.34 (b) shows foam-behaviour (Sehaqui et al., 2011). Specifically the magnified sections of Figure 2.35 display typical strain hardening in image (a), which is characteristic of gel-based materials in contrast to elastic behaviour followed by densification in image (b) exhibited by foam-based specimens.

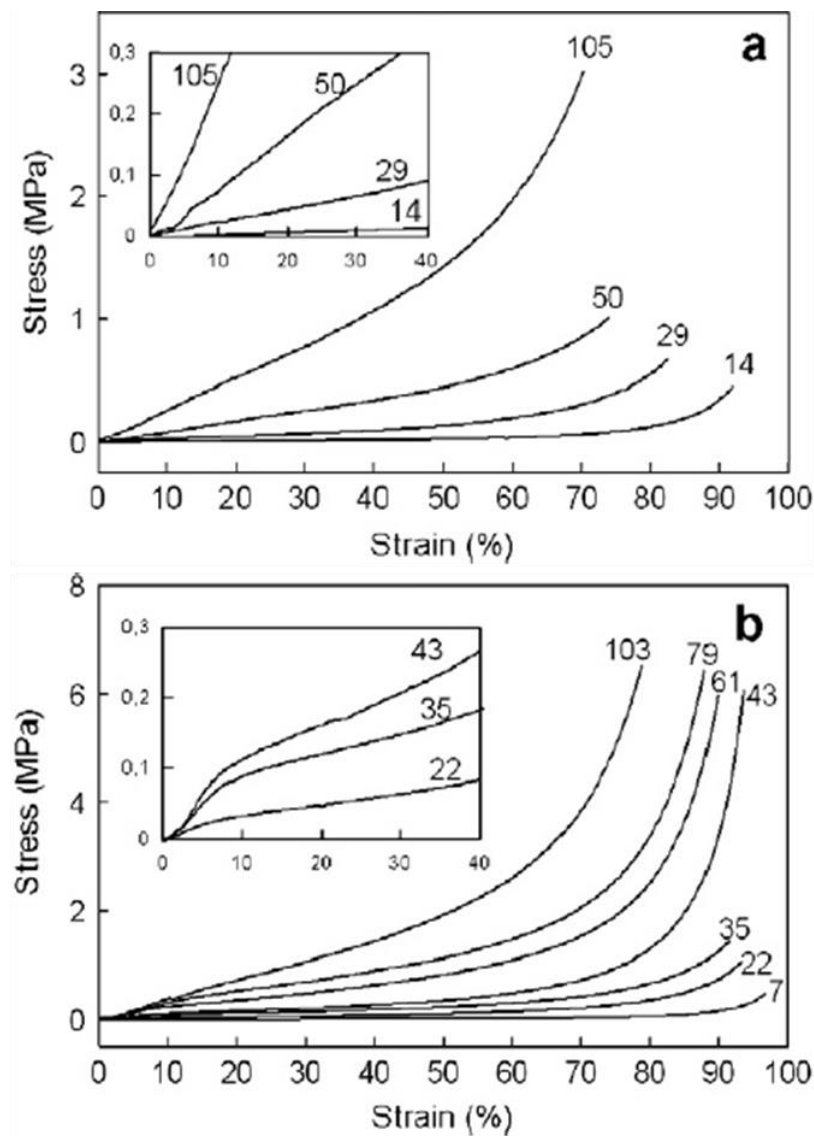


**Figure 2.34** Stress strain curves of (a) cellulose gels and (b) cellulose foams where the numbers next to each curve are density values (kg m<sup>-3</sup>). Magnified sections show strain hardening (a) and elastic behaviour followed by densification (b) (Sehaqui et al., 2011).

Two of the most common techniques used for mechanical characterisation are tensile and compression testing (Figure 2.35). Both of these techniques can be conducted using a mechanical testing frame equipped with an appropriate load cell. A load cell acts as a transducer and functions by converting the force being measured to a directly proportional electrical signal that is subsequently amplified and scaled to calculate the force applied. A strain gauge load cell is the most common form. An applied force causes a strain gauge to deform, which is measured as a variation in electrical resistance, representing the strain. Four strain gauges mounted in the same direction as the strain are arranged in a Wheatstone bridge configuration.

Dumbbell-shaped hydrogel samples are used in tensile testing so that there is minimal breakage where the hydrogel is clamped. For a uniform strip, the stress concentration would be far higher (Anseth et al., 1996, Webber et al., 2007). However, fracture still readily occurs at the grips and unless the sample is completely uniform and free of defects, repeatable results are difficult to achieve. The difficulty is compounded when the tests are conducted whilst hydrogels are immersed in aqueous solutions and hence in a hydrated state. Compression tests usually yield more reproducible results, although the bulk of the published literature examines hydrogels in a dry state such as following air-drying, freeze-drying, oven-drying, as opposed to in the aqueous solutions in which they are immersed in during application (Webber et al., 2007, Huang et al., 2007b, Zhang and Chu, 2002). Clearly this needs to be addressed and mechanical characterisation must be conducted in aqueous solutions.

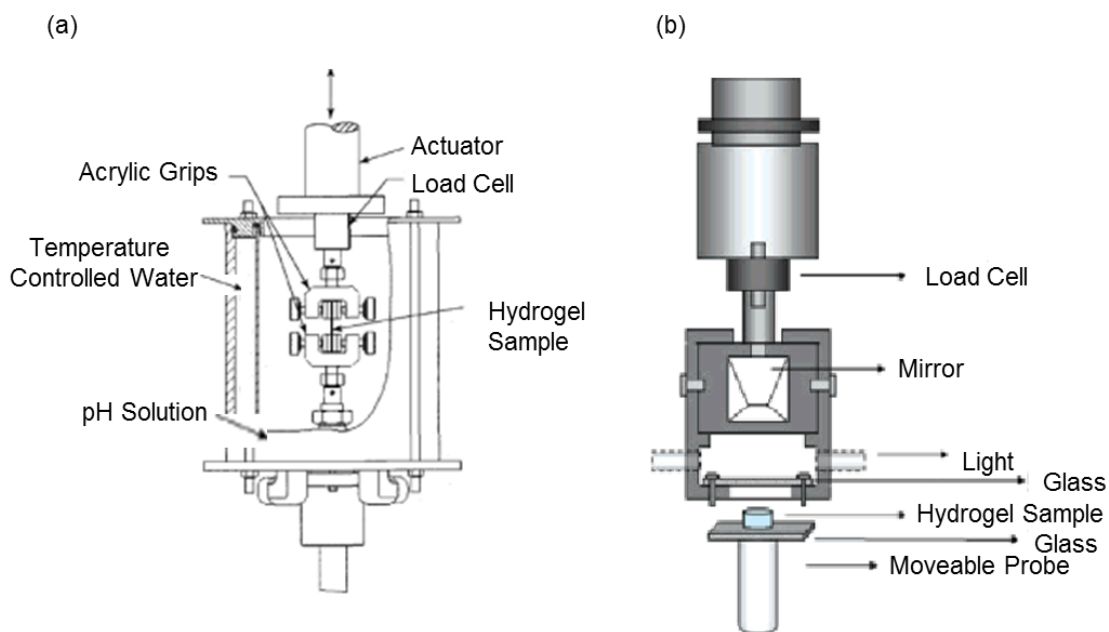


**Figure 2.35** Schematics of (a) tensile testing (Johnson et al., 2004) and (b) compression testing of hydrogels (Webber et al., 2007).

Further insights into the bulk mechanical properties, gelation mechanisms and the behaviour of hydrogels before and after flow can be explored via evaluating the rheological properties using a rheometer (Yan and Pochan, 2010). Small-amplitude oscillatory shear (SAOS) is a common rheological technique to characterise hydrogels and can be performed at variable temperatures. Less than 1 g of the sample to be tested is required. A small-amplitude torsional oscillation induces shear flow within the specimen (Zuidema et al., 2014). During frequency sweeps, it is possible to analyse the degree of crosslinking, entanglement, glass transition temperature and acquire information about the chain architecture. SAOS is particularly useful for determining the equilibrium shear modulus of a gel, providing a measure of the stiffness of these soft materials. This is achieved by finding the limiting value of the dynamic moduli in the linear-viscoelastic region at low frequency (Zuidema et al., 2014). The process of gelation can also be investigated using the SAOS frequency sweep to measure the lower frequency limit at which solid behaviour is observed. Upon determining this, it is possible to monitor the sol-gel transition (Yan and Pochan, 2010). However, evaluation of particularly fragile specimens is difficult as SAOS requires a mechanical perturbation of the system, hence imposed stresses and strains must be kept at a minimum during testing (Zuidema et al., 2014).

Other common techniques for evaluating the mechanical properties, particularly for thin films include AFM and indentation (Selby et al., 2014, Drira and Yadavalli, 2013). For example, AFM can be used to determine the local surface modulus. This is achieved in contact mode where the probe is lowered to and then retracted from the gel surface in order to acquire force against distance data (Kloxin et al., 2010). Indentation techniques measure the force required to indent a hydrogel surface at a single point to a specific depth. The elastic modulus of the material can then be determined from the force-displacement curve (Oyen, 2014).

In order to synthesise a hydrogel, it is always essential to consider the mechanical properties, and there is often a trade-off between extent of swelling and mechanical strength. For example, by increasing the hydrophobicity, cross-linking density, gelation time and gelation temperature, the pore sizes decrease and therefore degree of swelling will also decrease, resulting in increased mechanical properties and vice versa (Anseth et al., 1996). It is clear that the challenge is to carefully tune these parameters in order to produce the optimum hydrogel composition for the desired application.

### **2.6.6 Release of biomaterials**

To evaluate the release kinetics of hydrogels, model proteins and drugs are often loaded into the networks and discharge can be subsequently monitored using (for example) a UV spectrophotometer (Risbud et al., 2000, Zhang et al., 2004). This method is complimentary to fluorescence where transitions from the excited state to the ground state are observed compared to UV-visible spectroscopy where absorption measures transitions from ground to excited states. Fluorescence could also be used for this purpose if the drug or protein is fluorescently labelled. High-Performance Liquid Chromatography-Mass Spectrometry is another potential analytical technique that could also be used to monitor drug release from polymer gels (Jeong et al., 2000).

The remainder of Chapter 2 will focus on discussing oscillatory chemical reactions and how they can/have been applied in combination with smart polymeric systems.

## **2.7 Oscillatory chemical reactions**

Oscillatory chemical reactions (such as the Belousov-Zhabotinsky (BZ) reaction) are those where the concentration of some of the constituents increases and then decreases over time, exhibiting non-equilibrium behaviour. Some of these reactions generate oscillations in the relevant stimuli to induce a volume change within a responsive polymer gel.

### **2.7.1 Belousov-Zhabotinsky reaction**

In the 1950s, Boris Belousov discovered oscillatory behaviour in a reaction consisting of bromate and cerium ions with citric acid in sulfuric acid, although he was rejected by numerous journals on the grounds that it was not possible (Winfree, 1984). At the time, scientists related oscillators to the pendulum where the oscillations of the position overshoot the equilibrium position due to the mechanical inertia of the system (De Kepper et al., 2009). Furthermore, as thermodynamics dictates that chemical reactions cannot overshoot their equilibrium position, no homogeneous reactions could oscillate across an equilibrium position. Consequently, it was believed that the observed oscillatory reactions were due to an “extra physical mechanism” to allow for the periodic overshooting of the equilibrium position (De Kepper et al., 2009). Soon after, Anatol Zhabotinsky refined the reaction by replacing citric acid with malonic acid and using ferroin instead of a cerium moiety to produce a more dramatic effect. Furthermore, Zhabotinsky showed that in an unstirred system, the reaction spontaneously gave rise to target patterns or spirals from an initially homogenous solution (Figure 2.36) (Zaikin and Zhabotinsky, 1970). It is these observations that led to this class of reaction being named the Belousov-Zhabotinsky or BZ reaction. The essence of the BZ reaction is oxidation of an organic substrate (e.g. citric acid) by an oxidising agent (bromate) in the presence of a metal catalyst in an acidic environment (Yoshida et al., 2002).

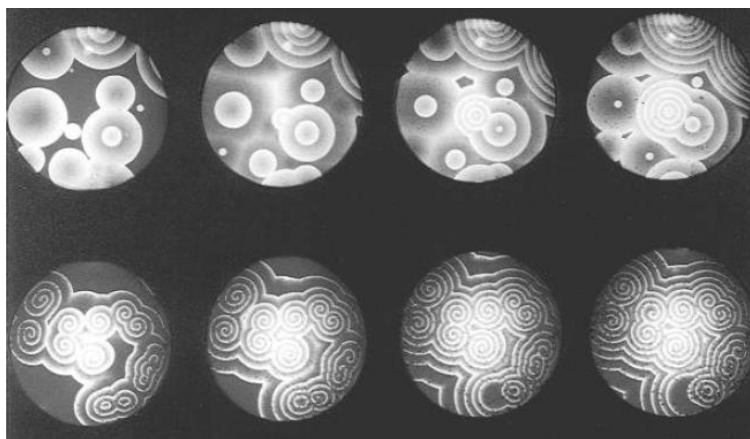
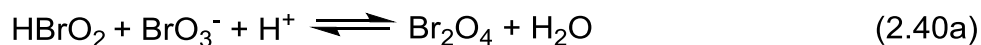
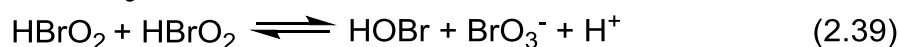
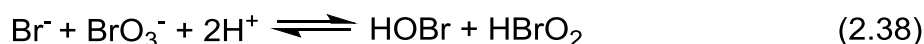
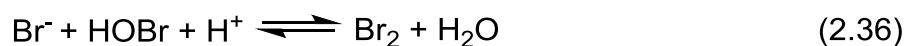
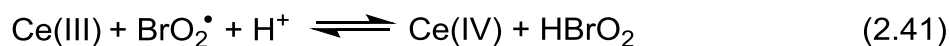


**Figure 2.36** Image showing chemical waves in the BZ reaction. Target patterns and spiral waves are displayed in the top and bottom rows respectively (Epstein and Showalter, 1996).

The currently accepted mechanism for the BZ reaction is shown in Equations 2.36-2.42 (Field and Försterling, 1986).



$$(2.40) = (2.40a) + (2.40b)$$



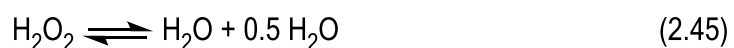
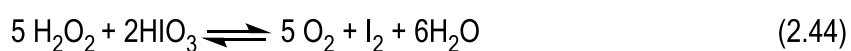
An early model of the BZ reaction called the Brusselator predicted a range of different spatial and temporal phenomena that were coined dissipative structures and the proposed mechanism stated that a reaction product acted as both a catalyst and a reactant simultaneously (Prigogine and Lefever, 1968, Prigogine and Nicolis, 1967). It was only after these theoretical studies detailing that periodic dynamic solutions could occur in homogeneous chemical kinetic systems if the reaction occurred away from equilibrium and comprised of sufficient nonlinear mechanisms, that it became accepted such oscillatory reactions could occur. This was further developed by Field, Körös and Noyes to produce the Oregonator, which describes the chemistry of BZ reactions rather

succinctly while permitting detailed numerical investigation (Epstein and Showalter, 1996, Field and Noyes, 1974).

One of the key features of oscillatory systems is multistability. It is the ability for systems to coexist in multiple states (such as steady state, oscillation, chaos) under the same set of external variables or bifurcation parameters (such as temperature and input concentrations). By varying these parameters, the state of the system can be tuned (Epstein et al., 2010). The development of a continuous-flow, stirred tank reactor (CSTR) allows an oscillatory system to be maintained far from equilibrium by constantly supplying the system with fresh reactants and allowing reacted matter to be expelled, ensuring the total volume is constant (Horváth et al., 2009, Epstein and Showalter, 1996). It is also even possible to couple multiple oscillators together, either physically or chemically, resulting in entrainment (when both systems adapt to oscillate at the same frequency), compound oscillation (when two waves merge to give a single periodic mode), oscillation death (when two oscillations combine to result in stationary behaviour) or rhythmogenesis behaviours (when oscillation is induced in systems that only show steady state behaviour when uncoupled) (Boukalouch et al., 1987, Crowley and Epstein, 1989).

### 2.7.2 Other oscillatory reactions

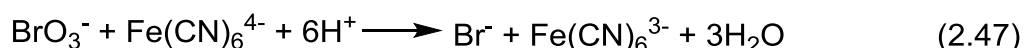
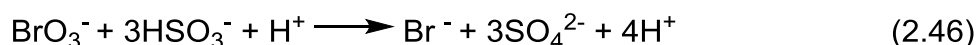
The first homogenous kinetic oscillatory reaction was actually discovered by William Bray in 1921, before what is now known as the BZ reaction (Bray, 1921). Bray was studying hydrogen peroxide as an oxidising agent and a reducing agent where he observed oscillations in the evolution of oxygen gas from the mixture. The reactions considered were the oxidation of iodine to iodic acid (2.43) and the reduction of iodic acid to iodine (2.44) where under suitable conditions the reaction would catalyse the decomposition of hydrogen peroxide (2.45).



The mechanism of the oscillatory reaction was further studied and subsequently named the BL reaction (Bray and Liebhafsky, 1931).

The Briggs-Rauscher (BR) reaction was later discovered combining parts of the BZ and BL reactions in the form of replacing bromate in the BZ reaction with iodate and adding hydrogen peroxide (Briggs and Rauscher, 1973). The BR reaction serves as an excellent classroom demonstration of oscillatory reactions owing to the striking colour changes due to the oscillatory behaviour of the evolution of oxygen and carbon dioxide gases together with the concentrations of iodine and iodide ions. Details of the mechanism, which is very similar to that of the BZ reaction applied to an iodate-hydrogen peroxide system have been published (Cooke, 1979, Furrow and Noyes, 1982a, Furrow and Noyes, 1982b, Noyes and Furrow, 1982, De Kepper and Epstein, 1982).

Building on from the aforementioned iodate-based reactions (BL / BR for example), new oscillators were reported using Landolt-type reactions, which are autocatalytic oxidations of substrates by iodate (Edblom et al., 1986, Gáspár and Showalter, 1987). It was then predicted that by replacing the iodate ion of the mixed Landolt reaction with bromate that oscillatory behaviour could be demonstrated. This was shown and large changes in pH over periods of approximately 30 minutes were identified and are depicted in Figure 2.37 (Edblom et al., 1989). This system was coined the bromate-sulfite-ferrocyanide (BSF) reaction. The mechanism can be thought of as two subsystems where the first is the oxidation of sulfite by bromate (2.46) and the second being the oxidation of ferrocyanide by bromate (2.47). The first system produces protons (positive feedback) while the second consumes protons (negative feedback). Due to the large pH change, ability to sustain oscillations at room temperature and extremes being maintained for an approximately equal time, this reaction shows good promise to be coupled to polymers (Crook et al., 2002).



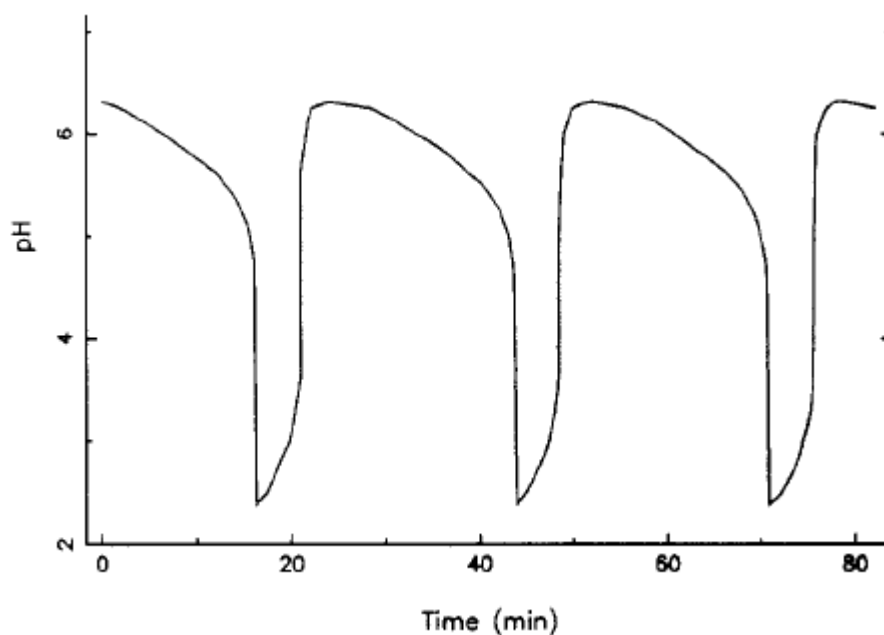


**Figure 2.37** Oscillations in pH recorded from the bromate-sulfite-ferrocyanide reaction (Edblom et al., 1989).

Other oscillatory reactions without the requirement of halogens such as the palladium catalysed phenylacetylene oxidative carbonylation (PCPOC) reaction were later reported. This reaction is a novel pH and temperature oscillator operating in a stirred batch reactor (Malashkevich et al., 1997, Novakovic et al., 2007, Novakovic et al., 2009, Novakovic and Parker, 2011) that can be controlled to be chemoselective towards specific commercially-valuable organic products (Figure 2.38) and used to optimise industrial carbonylation processes (Novakovic et al., 2008, Parker and Novakovic, 2013). Compared to aforementioned reactions, the PCPOC reaction is an oscillating system of higher complexity, and likely higher potential. However, in order to aid the development of the reaction towards a prospective application, efforts have been made to simplify the experimental procedure to obtain oscillations (Donlon et al., 2014). There are also simpler purely organic oscillatory chemical reactions generating large and periodic fluctuations in pH (Kovacs et al., 2007).

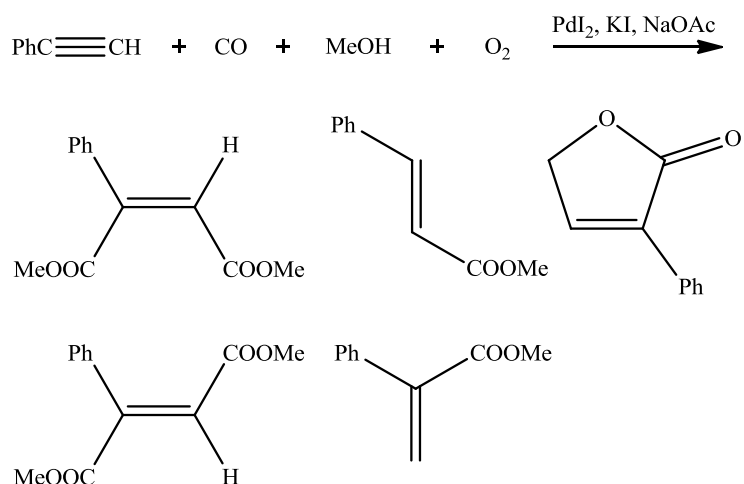


**Figure 2.38** Reaction scheme of PCPOC reaction (Novakovic et al., 2008).

## 2.8 Some applications of oscillatory chemical reactions

As well as being fascinating systems to study, oscillatory chemical reactions have also found practical applications. Perhaps most famously to date, Alan Turing described how non-uniformity (stripes, spots and spirals) can naturally arise from a uniform and homogenous state to produce Turing patterns (Turing, 1952). It is believed that Turing patterns are the basis for processes governing animal skin and pigmentation variations (Kondo et al., 2009, Nakamasu et al., 2009).

Currently, oscillatory reactions show promise upon combination with polymers in order to develop novel drug delivery systems, modes of actuation, biomimetic structures as well as other applications that could contribute to addressing current global challenges. Combination of oscillatory reactions and polymers will be discussed in detail in the next section.

### 2.8.1 Polymer gels and oscillatory reactions – experimental studies

Much of the innovative work to combine smart polymer gels and oscillatory reactions has been conducted by Ryo Yoshida. Using PNIPAAm gels seeded with tris (2,2'-bipyridyl) ruthenium (II) (Figure 2.39) coupled to the BZ reaction, autonomous swelling-collapse oscillations can occur without the requirement of external stimuli (Figure 2.40) (Yoshida et al., 2002, Yoshida et al., 1996). PNIPAAm was chosen because it is a thermosensitive polymer exhibiting a LCST of approximately 32 °C whereby the homopolymer gel undergoes a transition at that temperature. Upon oxidation of the metal catalyst, the polymer

interior becomes more hydrophilic, allowing the gel to swell and collapse when the catalyst is periodically oxidised and reduced respectively (Jeong and Gutowska, 2002). However, this method is limited by the concentration of the ruthenium catalyst which needs to remain relatively small in order to observe sustained oscillations (Yoshida et al., 2003).

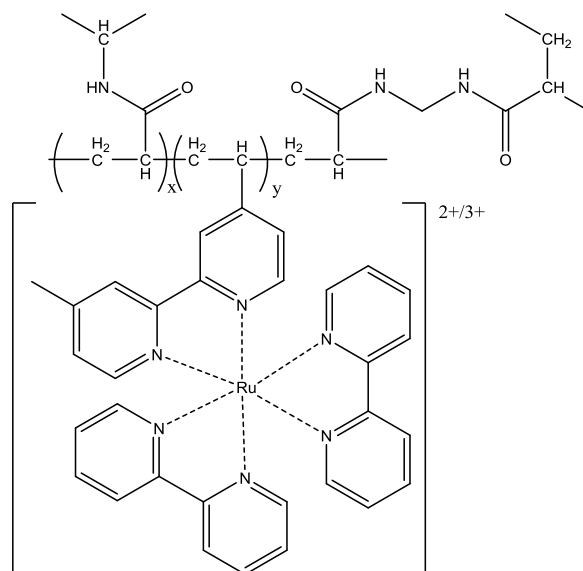


**Figure 2.39** A tris (2,2'-bipyridyl) ruthenium (II) BZ reaction catalyst grafted onto a thermosensitive PNIPAAm backbone.

It is possible to tune the value of the LCST by varying the hydrophobicity of the gel constituents. Therefore, oxidation of the metal catalyst not only causes an increase in the swelling degree of the network, but also results in a rise in the LCST. These chemical oscillations are converted into mechanical oscillations, resulting in periodic volume changes in the gel synchronised with the BZ reaction at an intermediate temperature. The thermosensitivity of PNIPAAm can be further capitalised upon by modulating the temperature of the external environment in order to also gain on-off control of the self-oscillation (Ito et al., 2003). Systems have been designed with a range of gels so that the onset of a phase transition occurs close to body temperature (Hidaka and Yoshida, 2011). These systems are particularly relevant for the development of actuators (e.g. for artificial muscles) and self-regulated drug delivery systems.

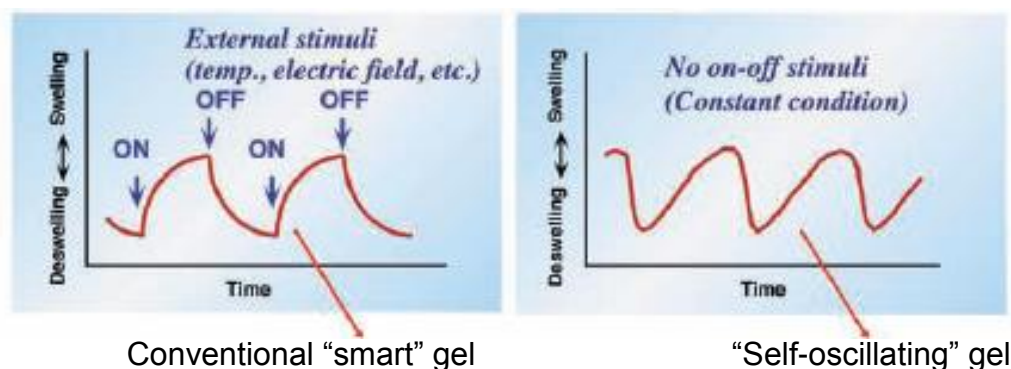


**Figure 2.40** A scheme to compare a “smart” gel and a “self-oscillating” gel (Yoshida, 2011).

The Ru-seeded PNIPAAm gel can also exhibit peristaltic motion on the macroscale when coupled to the BZ reaction (Figure 2.41) (Maeda et al., 2008, Shiraki and Yoshida, 2012). The propagating chemical waves travel through the gel at a constant velocity in the direction of the gel length (Yoshida, 2010). In Figure 2.41 the orange (Ru (II)) and green (Ru (III)) regions represent the shrunken and swollen parts respectively, and as these parts move with the chemical wave, the peristaltic motion of living worms can be mimicked. This study has been extended to mimic the motion of the intestine by creating tubular gels by fabricating the self-oscillating gel in a tubular shape (Shiraki and Yoshida, 2012). It was important to ensure that the outer layer of the tube maintained a constant diameter so that peristaltic motion only occurred on the inner surface of the gel. This was achieved by making the material non-oscillatory on the outer surface and oscillatory on the inner surface. This was realised by introducing an IPN into the material in the form of a non-oscillatory PAAm polymer coupled to the oscillatory ruthenium-seeded PNIPAAm network on the inner surface. Additionally, it was shown that an object (in the form of a carbon dioxide bubble) could be autonomously transported through the gel tube by the peristaltic pumping motion akin to the function of the intestine.

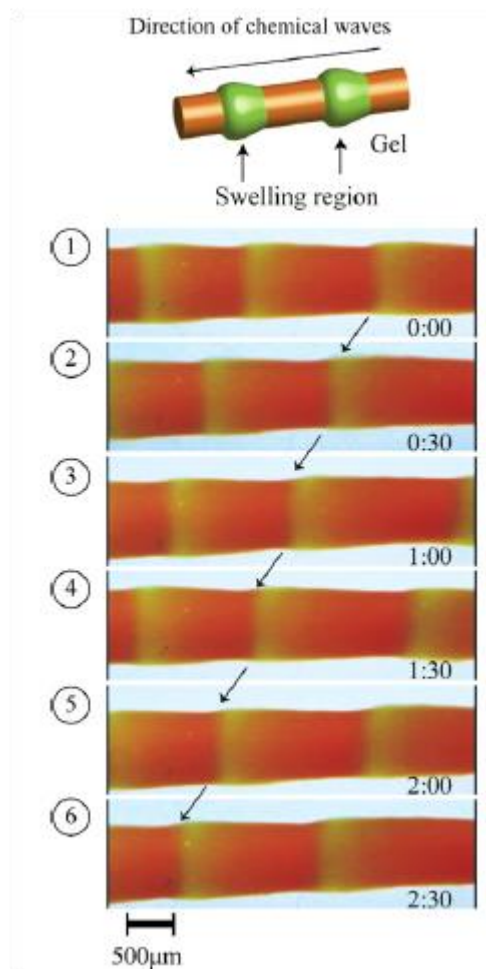


**Figure 2.41** Time course of peristaltic motion of thermosensitive PNIPAAm hydrogel immersed in the BZ reaction where the green and orange regions correspond to the oxidised and reduced states of the ruthenium catalyst in the network, respectively (Yoshida et al., 2009).

If one end of the gel is fixed and the other is free, chemical wave propagation allows the free end to move and hence the total length of the gel can be periodically changed. This wormlike motion can be controlled by irradiation with visible light, which produces bromide ions that act as inhibitors of the BZ reaction, hence local swelling can be photochemically instigated and controlled (Shinohara et al., 2008, Yamamoto and Yoshida, 2013). Oscillations can also be intrinsically varied by modulating the proximity of the catalyst to the polymer backbone, imparting a greater degree of control for application development (Zhang et al., 2012).

A biomimetic self-walking gel was even developed by inducing anisotropic swelling within the network to develop artificial muscles (Maeda et al., 2007). For this, a hydrophilic 2-acrylamido-2-methylpropanesulfonic acid (AMPS)

constituent was copolymerised into the network to lubricate the gel and induce anisotropic collapse. By initiating polymerisation when the monomer solution is in contact with two different surfaces, (one hydrophobic and one hydrophilic) a non-uniform gradient distribution of the components of the gel can be achieved across the height. Combining this polymer with a ratchet base allows the gel to move forward owing to the autonomous bending and stretching induced by the BZ reaction (Figure 2.42).

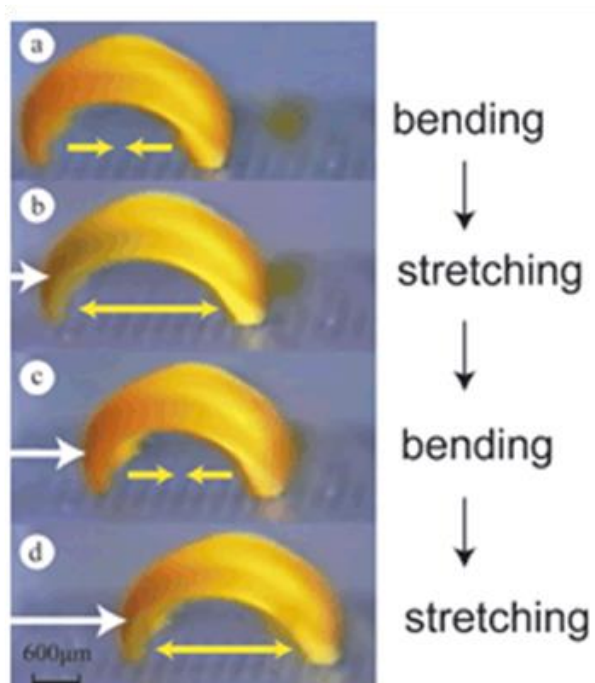


**Figure 2.42** The self-walking motion of a hydrogel in the BZ reaction. Owing to the ratchet surface base, during stretching, the front edge can move forwards on the base but the back edge is prevented from sliding backwards. The opposite is the case during bending, promoting forward motion (Maeda et al., 2007).

Ciliary motion was also realised by combining the same gel with a micro actuation array with the goal to act as a mass-transfer surface (Tabata et al., 2002). This was further developed by combining the peristaltic motion of the aforementioned poly(NIPAAm-co-Ru(bpy)<sub>3</sub>-co-AMPS) with a cylindrical PAAm model gel on the surface. Following propagation of the chemical wave, the PAAm gel was transported on the gel surface (Figure 2.43) (Murase et al., 2009, Murase et al., 2011). Potential applications include a conveyor to transport soft materials or a self-cleaning surface. The development of self-oscillating polymer brushes also shows promise for engineering a nanoscale mass transport surface in the future (Masuda et al., 2013).

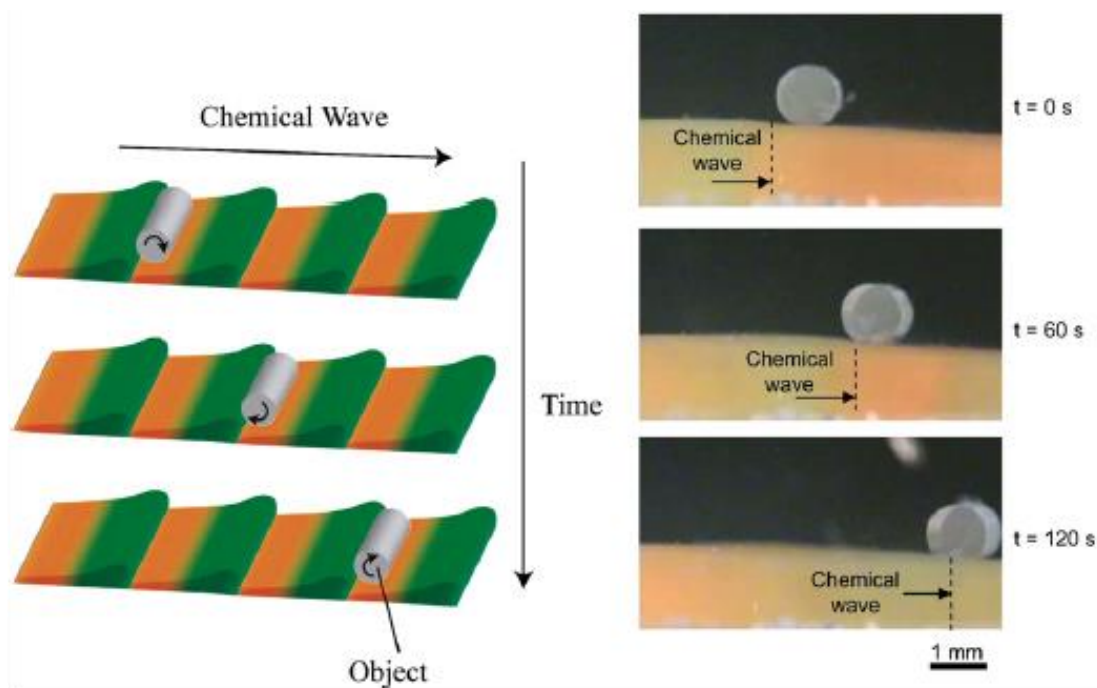


**Figure 2.43** Schematic illustration and experimental observation of the mass transport of a cylindrical PAAm gel on a poly(NIPAAm-co-Ru(bpy)<sub>3</sub>-co-AMPS) gel surface (Yoshida et al., 2009).

Autonomous oscillations in viscosity near the volume phase transition temperature were also realised, which may have application in microfluidic devices (Suzuki et al., 2009). This was later also shown to occur in gels coupled to the BZ reaction without the requirement for a thermosensitive NIPAAm polymer as the backbone but a PEG based network containing the ruthenium catalyst that exhibited reversible complex formation behaviour was shown to be sufficient (Ueno et al., 2010, Ueki et al., 2014). Furthermore, by switching the NIPAAm polymer to one with a higher LCST such as N-Ethylmethacrylamide (EMAAM), self-oscillations at higher temperatures without a decrease in the swelling-collapsing amplitude has been shown (Hidaka and Yoshida, 2011). This is because a volume phase transition of approximately 37 °C can be attained with EMAAM compared to that of 25 °C with NIPAAm.

A major drawback of all these systems is the fact that the BZ reaction occurs under strongly acidic and oxidising conditions. Currently the best solution is combination of BZ reactants onto polymer chains, excluding biorelated organic substances (Hara and Yoshida, 2008). To this end, a quaternary copolymer based on poly(NIPAAm-co-Ru(bpy)<sub>3</sub>) to include pH control from AMPS and oxidant supplying sites from positively charged

methacrylamidopropyltrimethylammonium chloride moieties was synthesised. Using this, self-oscillations under biological conditions requiring the addition of an organic acid (such as malonic acid) were achieved. However, for practical application, it would be necessary to ensure no exchange of toxic ions such as bromate occurs outside of the gel (Yoshida, 2010).

Other oscillatory reactions have also been coupled to polymer gels to investigate swelling potential. For example, oscillations in pH occurring in a bromite sulfite ferrocyanide reaction (Edblom et al., 1989) in a CSTR can be capitalised upon by combination with pH-sensitive hydrogels to exhibit periodic swelling behaviour (Crook et al., 2002). For example, a weak polyacid such as PMAA shown in Figure 2.44 partially dissociates and will hence be essentially charge neutral at a low pH, forming a collapsed gel. However upon increasing pH, dissociation of the carboxyl functional groups will occur, resulting in the gel acquiring a net charge, inducing electrostatic repulsion between polymer chains and network swelling. Such a smart material can be coupled to reactions that oscillate in pH.

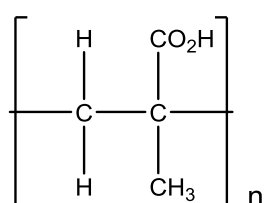


**Figure 2.44** Chemical structure of poly(methacrylic acid) (PMAA).

The response of a polymer gel can be measured visually or the force generated can be quantified demonstrating their potential use in actuation acting as a synthetic chemically driven muscle (Ryan et al., 2005b, Ryan et al., 2005a, Howse et al., 2006). However due to the macroscale size of polymer gels, long response times can occur. This effect could be reduced in severity by scaling down to the microscale using polymer brushes where a single layer of polymer molecules is end grafted to a solid substrate. In order to bridge the length scales between a macroscopic polymer gel and polymer brushes, block copolymer gels were designed where hydrophilic polyacid chains can swell and collapse and so the hydrophobic domains were unaffected, forming physical crosslinks (Figure 2.45). Upon an increase in pH, dissociation occurs leaving the carboxyl groups charged, inducing repulsion (depicted by pink arrows in

Figure 2.45) within the network and leading to swelling. Upon combination with the oscillatory BSF reaction, the gel changes from swelling to collapsing as it passes through pH 5.5, corresponding to the pKa of PMAA (Ryan et al., 2005a). This system was able to function as a free running chemical motor that generated a peak power of 20 mW kg<sup>-1</sup>. This corresponds to the power per unit mass obtained by normalising to the mass of the swollen gel (Howse et al., 2006).

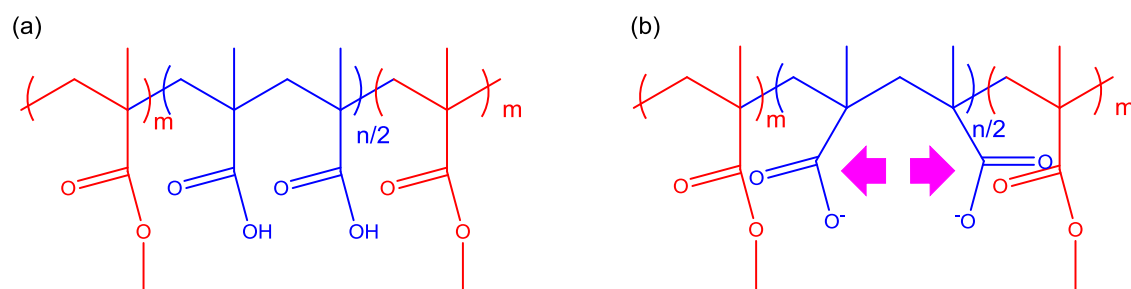


**Figure 2.45** A polyacid triblock copolymer composed of poly(methyl methacrylate)-*block*-poly(methacrylic) acid-*block*-poly(methyl methacrylate) under (a) acidic and (b) neutral/basic conditions (Topham et al., 2007a).

This can be taken further by incorporating complementary polyelectrolyte pairs of both polyacids and polybases into one bipolar material whereby as one polymer is exhibiting a positive response, the other simultaneously exhibits a negative response. Such a polybase is shown in Figure 2.46. This pairing is advantageous because at low pH, the polybase exists as the protonated form of the amine (Figure 2.46 (a)) whereby the charge density on the polymer chains induce both chain expansion and electrostatic repulsion between neighbouring chains. Meanwhile, the polyacid is charge neutral and remains in a collapsed conformation (Figure 2.45 (a)). At high pH the polyacid chains are ionised and then swell (Figure 2.45 (b)) whereas the polybase chains are deprotonated and collapse (Figure 2.46 (b)). Design of such antagonistic gels allowed for the transfer of motion from a simple linear displacement to a curved displacement, advancing the development of novel devices for actuation (Topham et al., 2007a). Upon combination with the BSF reaction, a side reaction occurred between the pendent tertiary amine groups of poly(2-(diethyl-amino)ethyl methacrylate) and the ferrocyanide ions present in the oscillatory solution, preventing reversible protonation. To negate this effect, the polymer gel was combined with a related reaction that oscillated in pH without the presence of

ferrocyanide ions (Okazaki et al., 1999). The gel was shown to respond promptly upon variation in pH during the alternative permanganate-based oscillatory reaction (Topham et al., 2007b).

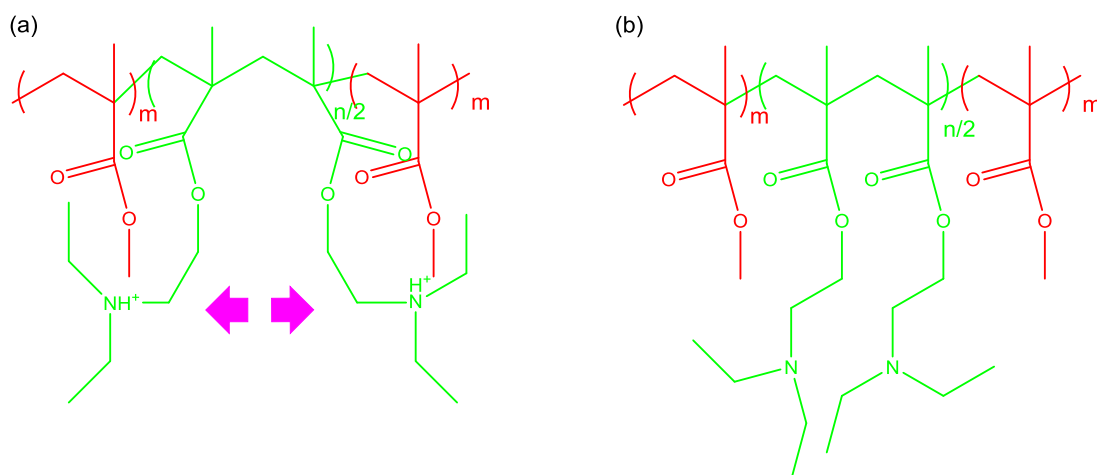


**Figure 2.46** A polybase triblock copolymer composed of poly(methyl methacrylate)-*block*-poly(2-(diethyl-amino)ethyl methacrylate)-*block*-poly(methyl methacrylate) under (a) acidic and (b) neutral/basic conditions (Topham et al., 2007a).

Variation in the polymer microstructure can be studied using SAXS and compared to macroscale results. A difference of over 300 Å between collapsed and swollen states indicates that the dimensions of smart materials may be as low as the pseudo unit cell and pH-responsive volume transitions can still occur (Topham et al., 2007b).

Another example of a polybase that has been developed for potential application in new actuation devices is poly(2-vinyl pyridine) (P2VP) with a pKa value of approximately 4.5 (Figure 2.47). Following the introduction of hydrophobic glassy end groups such as poly(styrene) to the P2VP chains in order to prevent dissolution, upon combination with a permanganate-based pH oscillatory reaction, swelling-deswelling cycles due to the reversible protonation of the amine repeat units was observed (akin to the behaviour shown in Figure 2.46) (Topham et al., 2007c).

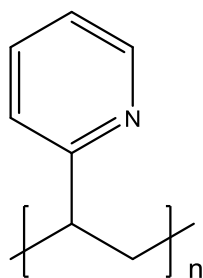


**Figure 2.47** Poly(2-vinyl pyridine)

A similar investigation using PAAc cryogels coupled to the BSF reaction produced analogous results (Bilici et al., 2010). At high pH the concentration of the mobile ions in the PAAc cryogel increases so that there is a larger difference in the mobile ion concentration inside and outside of the gel, leading to a rise in osmotic pressure and network swelling. The oscillatory BSF system circumvents the requirement to have low catalyst concentration in the BZ reaction to observe sustained oscillations. Dynamic gel deformations due to pH are also demonstrated and visualised by shadowscopy whilst a NIPAAm-acrylic acid gel is immersed in an oscillatory chlorite tetrathionate reaction (Labrot et al., 2005). Shadowscopy works by projecting a deflected light image of a gel on a screen and is hence suitable for the curvature and the zones with high gradients of refraction index in transparent objects.

### **2.8.2 Polymer gels and oscillatory reactions – modelling studies**

Modelling has become an important technique to investigate the dynamic behaviour of polymer gels coupled to oscillatory reactions. Initial studies were conducted in effectively one dimension via an algorithm based on Stefan-Maxwell equations to study diffusion in multicomponent systems. The basic assumption dictates that a deviation from equilibrium between the molecular friction and thermodynamic interactions leads to the diffusion flux (Rehfeldt and Stichlmair, 2007). Such models were able to simulate volumetric changes, although changes in sample shape could not be accounted for (Boissonade, 2005, Boissonade, 2003).

Anna Balazs has pioneered the work on modelling BZ gels in two and three dimensions, allowing variations in shape arising from the interplay between chemical reactions and mechanical action to be described (Yashin et al., 2010). This method uses the “gel lattice spring model” which combines a finite element

approach for the spatial discretization of the elastodynamic equations and a finite difference approximation for the reaction and diffusion terms. An example of the swelling dependence during the period of one oscillation is shown in Figure 2.48. The most collapsed sample corresponds to the lowest oxidised catalyst concentration (Figure 2.48 (a)) and as this concentration increases, swelling also increases (Figure 2.48 (b-d)). Similarly, as the oscillation finishes and the concentration decreases, the gel collapses (Figure 2.48 (e-f)) (Kuksenok et al., 2008). This simulation compares well with the synchronisation of chemical and mechanical oscillations observed in an experimental study by Yoshida (Yoshida et al., 2000). Furthermore, through computational modelling, gradients in crosslink density can be used to control the bending and self-propelled motion of smart gels, allowing experimenters to isolate the optimal parameters in order to tailor systems towards desired applications (Kuksenok et al., 2011). The use of modelling is important for verifying experimental observations and also as a tool for predicting the outcome of practical experiments to be conducted in the future.

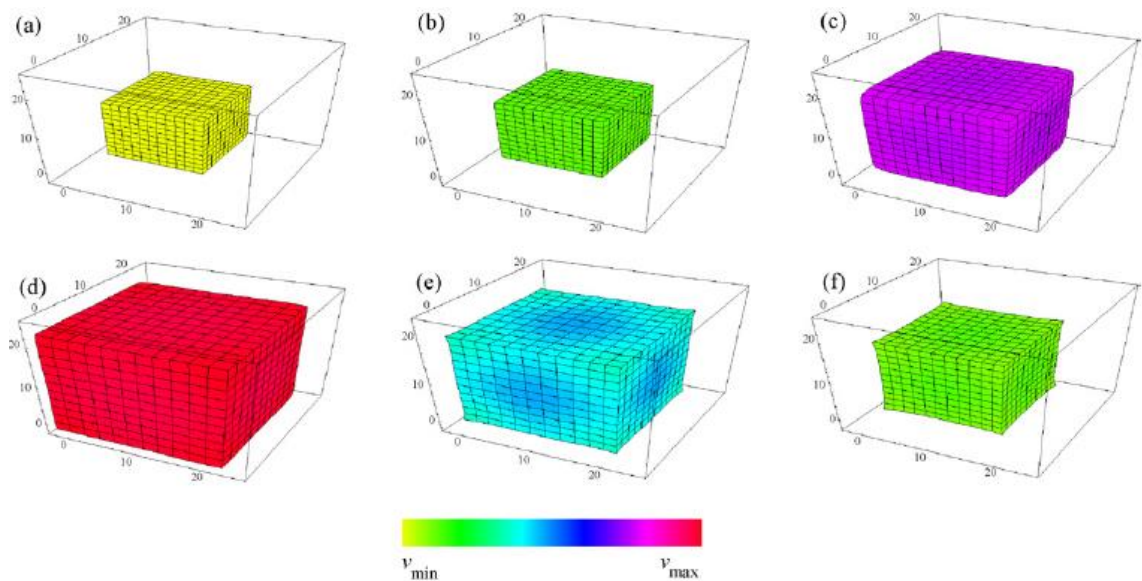


**Figure 2.48** Images of BZ gel morphology during one period of oscillation at simulation times: (a) 1761, (b) 1767, (c) 1773, (d) 1779, (e) 1788 and (f) 1794 seconds. The concentration of the oxidised catalyst,  $v$ , is represented in colour (Yashin et al., 2010).

## 2.9 Selecting and engineering a hydrogel to be combined with an oscillatory chemical reaction

The BSF and PCPOC reactions both exhibit large oscillations in the acidic region over a good time scale (tuneable to 30 min) for a smart polymer gel to be able to respond. Cationic hydrogels that are able to reversibly swell in acidic media seem to be ideal candidates for coupling to such oscillatory systems and have been utilised previously for controlled delivery of cancer cell therapeutics to tumour cells (Zhang et al., 2006, Lee et al., 2008), and release of antibiotics in the stomach due to the low pH of the target environment (Patel and Amiji, 1996). As detailed, chitosan is a cationic polymer with a pKa in the range of 6.3-6.6 that possesses good biomedical properties. To enhance stability chitosan can be combined with a natural crosslinking agent such as genipin, which causes the network to autofluoresce upon successful formation of chemical crosslinks (Figure 2.49). PVP is a physical crosslinking polymer that is neither acidic nor basic but in the presence of chitosan has been shown to raise the pKa of chitosan from 6.3 to 7.5 as determined via contact angle titration (Demirci et al., 2009).

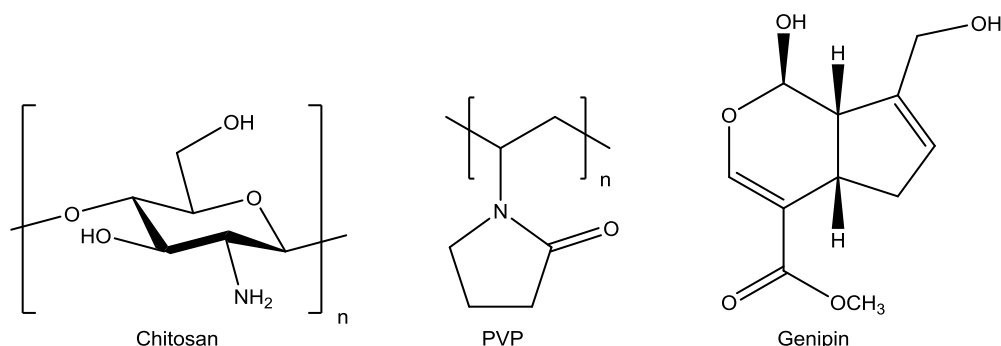


**Figure 2.49** Chemical structures of the constituents of a chitosan-PVP hydrogel crosslinked with genipin.

It is likely that the gel network formed following the crosslinking reaction of chitosan and genipin together with the hydrogen bonding between chitosan and PVP looks like the depiction in Figure 2.50. Temperature and pH sensitive behaviours of genipin-crosslinked chitosan-PVP (G-Ch-PVP) hydrogel thin films have been studied via the gravimetric swelling characterisation method (Khurma et al., 2005). Swelling was enhanced with increasing temperature due to the dissociation of intra- and inter-molecular hydrogen bonds in chitosan,

permitting more solvent to permeate into the polymer network. As expected, increased swelling is observed at low pH due to protonation of the amine groups of chitosan, inducing electrostatic repulsion between the polymer chains and associated network swelling.

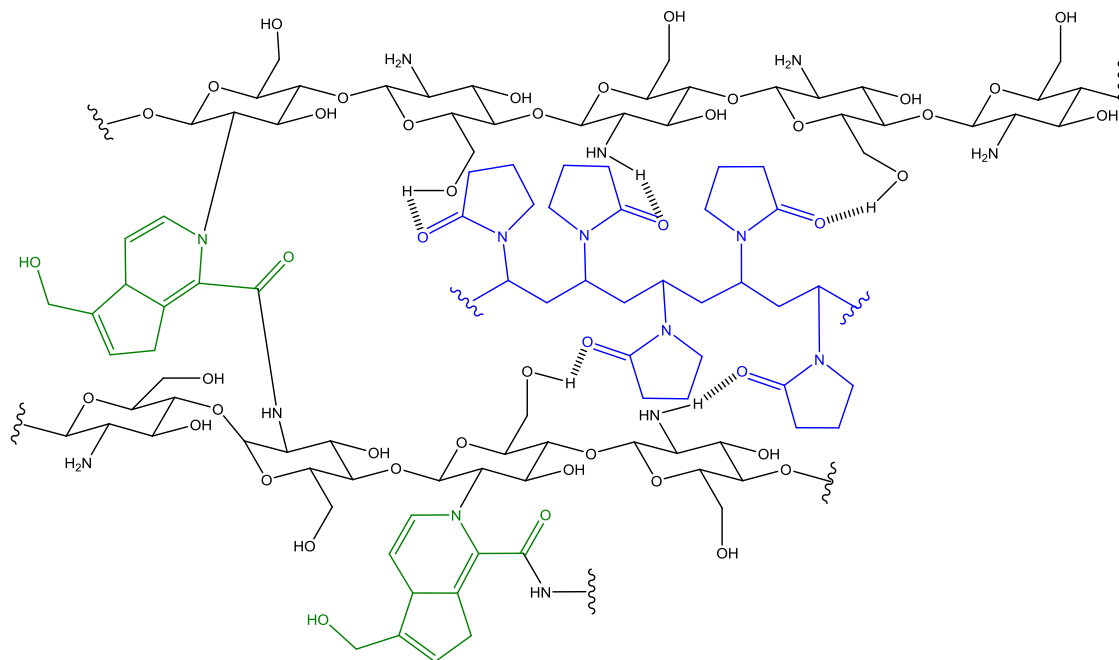


**Figure 2.50** Schematic of the probable structure of a G-Ch-PVP hydrogel where chitosan is shown in black, PVP in blue and genipin in green. Note: some bonds have been stretched in order to show the hydrogen bonding between chitosan and PVP moieties.

A study was conducted to determine the degree of swelling where the amount of chitosan, PVP and genipin within the hydrogel matrix was varied (Nwosu, 2013). A design of experiments was used where each factor (chitosan, PVP and genipin) was studied at two levels (high (H) and low (L)). A full factorial method of experimental design was employed whereby a total of  $(2)^3$  specimens were tested (Table 2.2) (Rodrigues et al., 2013). Samples were placed in an oven at 50 °C.

**Table 2.2** The code and composition of G-Ch-PVP hydrogels synthesised from following a full factorial method of experimental design (Nwosu, 2013).

Gel Code	Independent Factors					
	Chitosan		PVP		Genipin	
	Level	Volume ( $\mu\text{L}$ )	Level	Volume ( $\mu\text{L}$ )	Level	Volume ( $\mu\text{L}$ )
HHH	H	500	H	500	H	100
HHL	H	500	H	500	L	40
HLL	H	500	L	200	L	40
LLL	L	200	L	200	L	40
LLH	L	200	L	200	H	100
LHL	L	200	H	500	L	40
HLH	H	500	L	200	H	100
LHH	L	200	H	500	H	100

Optical cameras were used to record the change in both surface area and height of the samples, allowing a full representation of the swelling to be achieved whilst the gel was immersed in a pH 2 glycine buffered solution. Glycine is amphoteric such that it contains ionising groups with both acidic and basic pKa values (Figure 2.51). At low pH, the amino group can be protonated with a pKa of approximately 9.6 and at high pH the carboxyl group can be deprotonated at a pKa of 2.4.

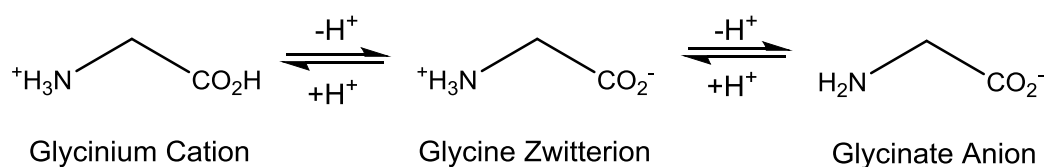


**Figure 2.51** Ionic forms of glycine.

The swelling response of the gel compositions in Table 2.2 is depicted in Figure 2.52. The highest degree of swelling, by quite some margin, was recorded for the LHL sample (165%) followed by the LHH sample (75%) and the LLL sample (57%). Remaining LLH, HHH and HLH specimens attained a swelling ratio of 50% followed by HHL and HLL achieving 44 and 40% respectively. The blend of a sample containing a high PVP content together with low chitosan and genipin (LHL) elicited a far superior swelling response owing to the hydrophilicity of PVP and that specimens were lightly crosslinked owing to a small amount of genipin (Khurma et al., 2005). Both of these factors greatly increase the accessibility of the network, promoting swelling. The importance of a high PVP and low

chitosan content is further demonstrated in the LHH sample reaching a 75% swelling degree. The lowest degree of swelling is noted in samples containing a high amount of chitosan and a low level of genipin regardless of the amount of PVP present. This could be due to chitosan forming a dense layer in and around the matrix, restricting the accessibility and hence resulting in a low degree of swelling (50%).

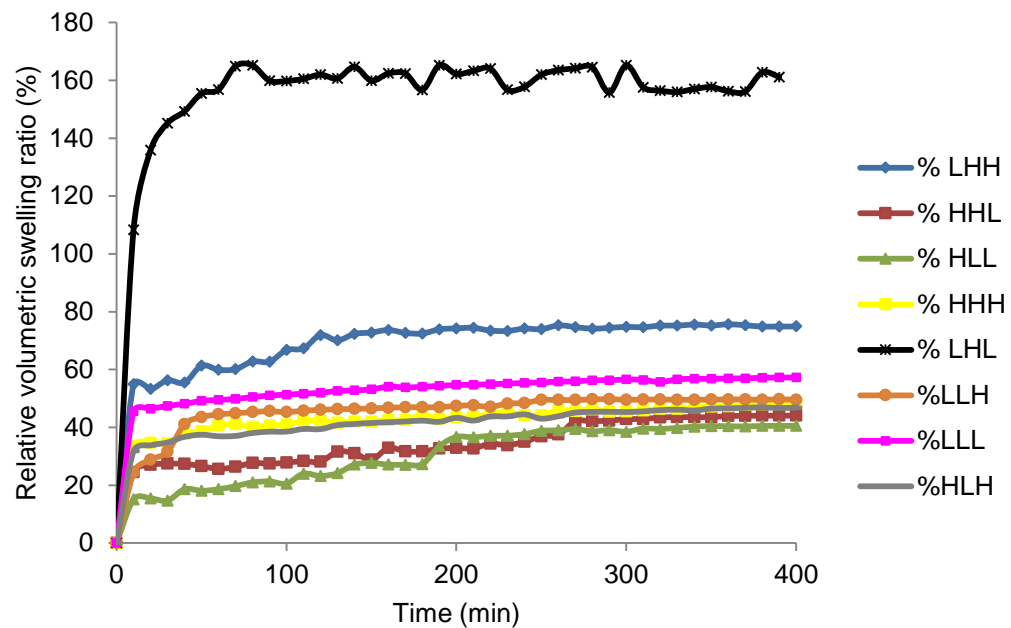


**Figure 2.52** Optical measurement of the change in diameter and thickness to calculate the variation in volume when G-Ch-PVP hydrogels were swollen in a pH 2 glycine buffered solution (Nwosu, 2013).

From Figure 2.52, it is clear that the specimen with the gel code LHL is the most responsive. The effects of varying the gelation temperature and nature of freezing / thawing on the swelling potential of LHL hydrogels were investigated according to Table 2.3. Specimens were prepared at a range of gelation temperatures (30, 40 and 50 °C) and were subsequently subjected to freezing or freeze-thawing at -10 °C.

**Table 2.3** Process parameters used to study the effects of varying gelation temperature and various post-synthetic treatments on the responsiveness of G-Ch-PVP hydrogels synthesised according to the LHL composition (Nwosu, 2013).

<b>Gel Code</b>	<b>Gelation Temperature (°C)</b>	<b>Freezing Time at -10 °C (h)</b>
LHL1	30	72
LHL2	30	3 freeze-thaw cycles: 24 h freezing and 3 h thawing each
LHL3	40	72
LHL4	40	3 freeze-thaw cycles: 24 h freezing and 3 h thawing each
LHL5	50	72
LHL6	50	3 freeze-thaw cycles: 24 h freezing and 3 h thawing each

The swelling potential of the hydrogels listed in Table 2.3 was evaluated optically as before, via immersion in a pH 2 glycine buffered solution (Figure 2.53). All LHL samples responded promptly to the pH immersion environment displaying a significant swelling response (50-145%). However in all cases, all specimens exhibited a lower swelling response than the untreated LHL sample (165%, Figure 2.52). Similarly, in all cases, samples that were continuously frozen as opposed to being freeze-thawed swelled to a greater extent with the highest swelling measured for samples placed in an oven at 30 °C (145%: LHL1). There were significant differences in the swelling ratio of continuously frozen and freeze-thawed specimens. For example, at 50 °C (LHL5 and LHL6) there was a 75% difference between specimens compared to at 40 °C (LHL3 and LHL4) where the difference was 30% and finally at 30 °C (LHL1 and LHL2) where there is a 55% difference. Additionally, it was observed that as the gelation temperature is increased, the swelling ratio reduces for samples that were freeze-thawed, although this dependence was not observed for samples which were continuously frozen.

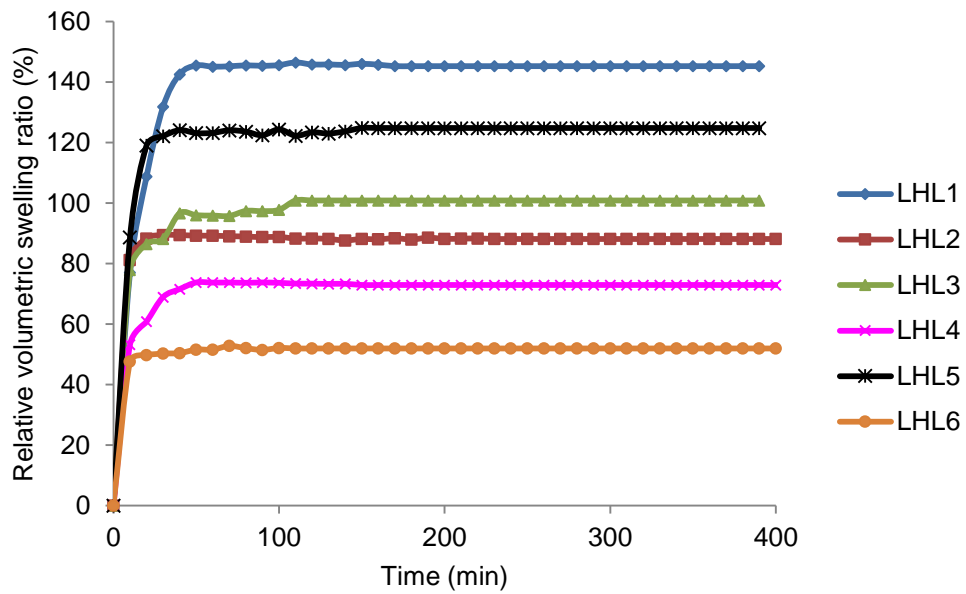


**Figure 2.53** Optical measurement of the change in diameter and thickness to calculate the variation in volume when G-Ch-PVP hydrogels synthesised according to the LHL gel code were swollen in a pH 2 glycine buffered solution (Nwosu, 2013).

Previous reports on the mechanical properties of genipin-crosslinked chitosan hydrogels show promise towards applying the networks in a biomedical setting, although the long-term stability remains a challenge (Moura et al., 2007).

After reviewing the literature, such G-Ch-PVP polymeric hydrogels (Figure 2.49) seem good candidates for coupling to oscillatory chemical reactions such as the BSF and will form the topic of this thesis.

## Chapter 3 – Methodology

This chapter details the materials, equipment and methods used to perform the synthesis, characterisation and combination of the polymeric hydrogel with an oscillatory chemical reaction, in particular with regard to swelling ability in response to a pH change of the immersion environment, morphology and mechanical attributes.

### Materials

Chitosan ( $M_w$ : 428,180  $\text{g mol}^{-1}$  as determined by GPC (Section 3.2)), PVP ( $M_w$ : 40,000  $\text{g mol}^{-1}$ ) and genipin were supplied from Sigma-Aldrich in the United Kingdom. Similarly, glacial acetic acid, n-butylamine (99%), ethylacetate (99%), hydrochloric acid (37%), sodium chloride (99%), citric acid (99%), phosphoric acid (99%), sulfuric acid (95%), sodium bromate (99%), sodium sulfite (98%), potassium hexacyanoferrate (II) trihydrate (98%), amoxicillin (potency of >900  $\mu\text{g}$  per mg), fluorescein isothiocyanate (FITC)-dextran ( $M_w$ : 10,000  $\text{g mol}^{-1}$ ) were also supplied from Sigma-Aldrich in the United Kingdom. Glycine, phthalate, phosphate and borate buffers were supplied from Fisher Scientific in the United Kingdom.

### **3.1 Preparation of genipin-crosslinked chitosan-poly (vinyl pyrrolidone) hydrogels**

Following close examination of the literature, pH-sensitive, cationic, G-Ch-PVP hydrogels seem ideal candidates for coupling to pH oscillators (Khurma et al., 2005). Three aqueous solutions of chitosan, PVP and genipin were made and combined. Gelation was then allowed to occur at various temperatures and timescales forming a disc-shaped gel.

Chitosan was dissolved at room temperature in a 1% aqueous acetic acid solution (pH 2.61) with continuous mechanical stirring for 24 h to obtain a 1.5% (w/v (weight by volume)) pale yellow, viscous solution. The molecular mass determination of chitosan is detailed in Section 3.2. PVP was dissolved in distilled water at 85 °C with continuous mechanical stirring for 1 h to yield a 5% (w/v), transparent, homogenous solution. Genipin solution (0.5% (w/v)) was produced by dissolving genipin in distilled water for 15 min using a sonication

bath at room temperature. Varying amounts of chitosan, PVP and genipin solution were combined in a cylindrical polyethylene vial (internal diameter: 13 mm, capacity: 5 mL). The pH of this mixture was 4.18. The genipin solution was added last and in small portions over a period of 30 min with continuous mechanical stirring at room temperature. Gels were synthesised in vials as opposed to being cast as a sheet so that upon simply inverting the vial, it would be immediately apparent as to whether a gel has been formed depending upon whether the sample flows under its own weight. It is assumed that specimens with a high yield stress will not flow (gel) whereas inelastic samples will exhibit appreciable flow (sol) (Dimonte et al., 1998). Samples were then placed in an oven for a range of time scales and temperatures to form a viscous gel. The gels were removed from the vials by inserting a cork borer through the container after the base was cut off. A cylindrical gel was then cut into discs (12 mm in diameter and 3 mm in thickness) using a sharp blade and a microtome (Figure 3.1). The bottom of the original gel specimen was used in all cases (as opposed to the top/middle). Gel samples were stored at 2°C before use.

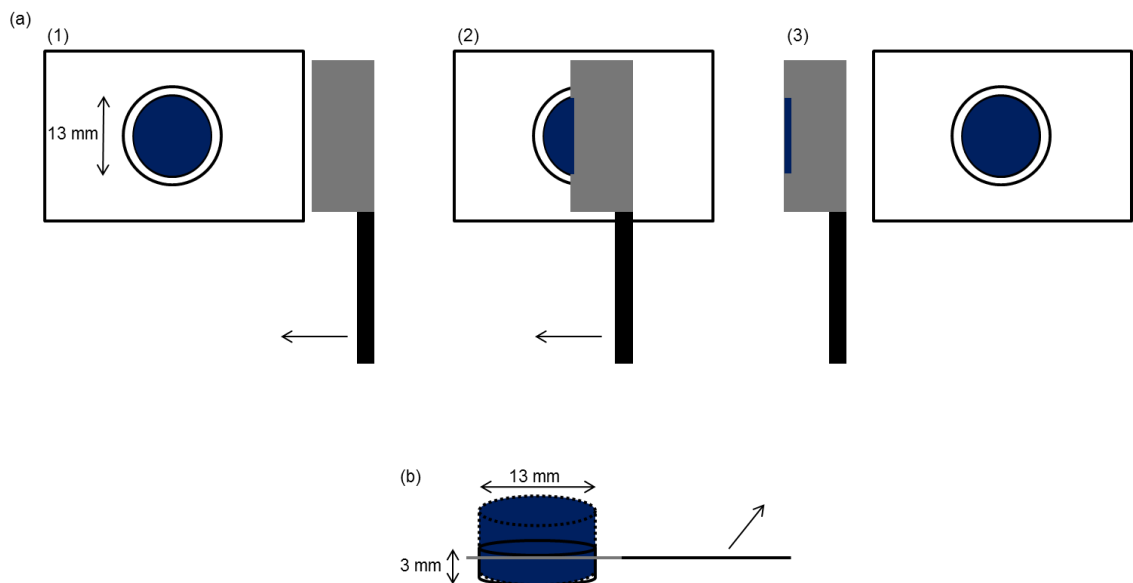


**Figure 3.1** Schematic depicting how the blue hydrogel is cut into discs using a sharp blade that is shown to be slicing the specimen from right to left (top view as shown in (a)) in order to produce a consistent thickness of 3 mm (side view as shown in (b)).

In some cases, following gelation, specimens were frozen in a freezer at -10 °C and slowly thawed at 2 °C before use. The duration and number of freeze-thaw cycles was varied.

### **3.1.1 Control reactions of genipin with n-butylamine and chitosan with ethylacetate**

As genipin has two functionalities that are capable of reacting with amine groups, genipin was combined with two equivalents of a simple amine. 10 mg of genipin ( $4.42 \times 10^{-5}$  mol) was dissolved in 2 mL of 2 M hydrochloric acid solution with a pH of 2.76. This was reacted with two equivalents of n-butylamine (8.73  $\mu$ L,  $8.84 \times 10^{-5}$  mol) for 24 h at room temperature. Following this, the lid of the reaction vessel was removed, allowing water in the reaction solution to evaporate. The solid remaining in the reaction vessel was then re-suspended in aqueous solutions of hydrochloric acid and sodium hydroxide with a pH of 2.0, 6.5 and 12.0. The pH of the resulting solution was subsequently adjusted with either addition of 2M sodium hydroxide or 2M hydrochloric acid so that the pH values were maintained at 2.0, 6.5 and 12.0 respectively.

Finally, the 80% deacetylated chitosan was calculated to contain 0.00475 moles of amine group per gram. As such, 0.02 g of chitosan was reacted with 9.3  $\mu$ L of ethyl acetate, equating to a 1:1 ratio between the number of chitosan amine groups and ethyl acetate molecules. The reaction was carried out in 2 mL of 2M hydrochloric acid solution with a pH of 2.76, in which the chitosan had been dissolved in via immersion in a sonication bath. After 24 h at room temperature, the solvent was allowed to evaporate and the solid residue was re-suspended in pH 2.0, 6.5 and 12.0 according to the above.

These gel components reacted with simple compounds were analysed via FTIR according to the method in Section 3.3.

### **3.2 Gel permeation chromatography**

Chitosan was characterised by GPC where the system comprised of two columns (TSK gel 5000 and TSK gel 6000) both set to 40 °C. The eluent was 0.1 M citric acid and was pumped at a flow rate of 0.5 mL min<sup>-1</sup>. Ethylene glycol was employed as an internal marker for flow rate correction and calibration was achieved against polyethylene oxide. A chitosan solution (0.1% (w/v)) was injected into the system (0.1 mL volume) and GPC curves were constructed utilising Program GPC, which was made using Labview software in the

Department of Chemistry at the University of Manchester. This experiment was performed by Keith Nixon in the Department of Chemistry at the University of Manchester.

### **3.3 Fourier-Transform Infrared spectroscopy**

Fourier Transform Infrared (FTIR) spectroscopy was used to determine the functional groups present in the gel constituents together with understanding as to how the spectra change upon network swelling.

Each FTIR spectrum was recorded between 4000-400  $\text{cm}^{-1}$  using a Perkin Elmer UATR Two FTIR (single reflection diamond) with a resolution of 4  $\text{cm}^{-1}$  and averaged over 25 scans.

### **3.4 Ultraviolet-visible spectroscopy of genipin-crosslinked chitosan-poly (vinyl pyrrolidone) hydrogels**

Various G-Ch-PVP hydrogels were prepared in a cuvette and allowed to undergo gelation at specified temperatures. At pre-determined time intervals, a scanning UV-Vis spectrum was recorded 300-800 nm using a Shimadzu UV-1800 spectrometer. Distilled water was used as a reference in all cases.

UV-Vis spectra were also recorded to analyse wash solutions in order to determine the presence of residual gel constituents. As previously, a UV-Vis spectrum was recorded 300-800 nm using a Shimadzu UV-1800 spectrometer with distilled water as a reference.

### **3.5 Fluorescence spectroscopy of genipin-crosslinked chitosan-poly (vinyl pyrrolidone) hydrogels**

Fluorescence spectroscopy was utilised to record the excitation and emission spectra of G-Ch-PVP hydrogels placed in a cuvette using a Shimadzu fr5301 fluorescence spectrometer. The excitation spectrum was recorded using 462 nm as the emission wavelength while scanning the excitation wavelength from 250-800 nm. The emission spectrum was recorded utilising 360 nm as the excitation wavelength while scanning the emission wavelength from

250-900 nm. Both excitation and emission spectra were recorded using a slit width of 5 nm.

### **3.6 Morphological evaluation of genipin-crosslinked chitosan poly(vinyl pyrrolidone) hydrogels via scanning electron microscopy**

Morphology was studied using SEM methods as described below using different methods of sample preparation.

#### **3.6.1 Critical point drying sample preparation**

Hydrogel samples were fully swollen in distilled water and subsequently dehydrated by being subjected to a series of graded ethanol solutions, culminating with drying using a critical point dryer (Baltec). Liquid carbon dioxide was added to the ethanol-filled pressure chamber containing the samples cooled to 10 °C. Upon mixing, the ethanol was replaced with liquid carbon dioxide and the chamber was heated to 41 °C past the critical point of carbon dioxide. Excessive pressure was vented and the samples were immersed in carbon dioxide gas, without being subjected to harmful surface tension forces (Yeong et al., 2007).

#### **3.6.2 Freeze drying sample preparation**

Hydrogel samples were fully swollen in distilled water, rapidly frozen in liquid nitrogen and then dried in a freeze-dryer (Edwards / Labconco, Freezone 1) with the ice condenser temperature at -55 °C for 48 hrs, until all the solvent sublimed.

#### **3.6.3 Scanning electron microscopy analysis**

Following drying, each sample was mounted on a carbon disk supported by an aluminium stub and coated with a 15 nm layer of gold (Polaron SEM Coating Unit). Representative images of interior polymer gel structure were taken on a scanning electron microscope (Cambridge Stereoscan 240). Where relevant, porosity analysis was performed using the public domain ImageJ program where images were converted to a binary format allowing individual pore areas to be determined. Such areas were summated and divided by the total area of

each SEM image to produce a percentage surface porosity. This process was repeated for each image.

### **3.7 Environmental scanning electron microscopy**

Hydrogel morphology was characterised using an ESEM (FEI XL30 ESEM-FEG) operated at 15 kV in “wet mode”. Samples were mounted on a carbon disk supported by an aluminium stub (Agar Scientific) and were placed on the ESEM cooling stage adjusted to 3-5 °C and maintained above a saturated water pressure of 0.76-0.84 kPa. The images were subsequently observed at a vapour pressure of 0.33-0.56 kPa (Kishi et al., 2009). A gaseous secondary electron detector was used to collect the images.

### **3.8 Optical microscopy**

Hydrogels were characterised using a Leica ICC50 HD optical microscope with a 10x magnification. Samples that were both equilibrated in water (or an appropriate buffer solution) were placed on a glass microscope slide and the porous structure was analysed. Images were collected and interpreted using ImageJ as previously described.

### **3.9 Confocal laser scanning microscopy utilising bright-field and fluorescence illumination**

Owing to the autofluorescent nature of genipin upon the formation of crosslinks, by measuring the fluorescence intensity of the network, it is possible to gain an understanding of the degree of crosslinking. Furthermore, it is anticipated that by using a confocal laser scanning microscope CLSM in fluorescence mode, a more detailed analysis of the porous structure can be achieved. Utilising a dipping lens allowed the network to be examined whilst the hydrogel is in a hydrated environment.

#### **3.9.1 Crosslinking analysis**

Fluorescence microscopy was conducted using a Leica TCS SP2 UV (Leica Microsystems Heidelberg) confocal microscope. Samples placed in an oven for various time durations at 37 °C were excited at a fixed wavelength with 488 nm light and emission was collected with a 500-550 nm filter using a 20 x 0.70

numerical aperture HL Plan Apo Lens. The microscope was set using the brightest sample and settings were kept consistent throughout the duration of the experiment. The control for this experiment was a mixture of chitosan and PVP in the appropriate ratio without combination with genipin. Fluorescence intensities were determined using LCS Software Version 2.61 where the pixel intensities of the whole of each individual image of the same area (0.25 mm<sup>2</sup>) were calculated.

### **3.9.2 Pore structure analysis**

The porous morphology was examined using a Leica TCS SP2 UV (Leica Microsystems Heidelberg) confocal microscope. Samples swollen and immersed in distilled water were examined using a 20x dipping lens in reflectance and fluorescence modes. Throughout the experiments, the entire sample was fully submerged in the transparent solution. During sample scanning, cross-sectional images of the hydrogel morphology along the z-plane were taken to construct the native three-dimensional network structure. A slice of 100 µm was taken in all experiments. For fluorescence measurements, samples were excited using a fixed wavelength of 488 nm light in the presence of a 500-550 nm filter.

### **3.10 Swelling measurements of genipin-crosslinked chitosan-poly(vinyl pyrrolidone) hydrogels**

Swelling measurements were determined optically and gravimetrically using a range of techniques. Hydrogel specimens were immersed in various buffers to include glycine (Table 3.1), phthalate (Table 3.2), phosphate (Table 3.3) and borate (Table 3.4).

#### Glycine buffered solution

*pH range: 1.98-2.02*

*pKa values: 2.34 and 9.60 (Dawson, 1959)*

*Ionic strength: 0.36 mol kg<sup>-1</sup>*

**Table 3.1** Composition of glycine buffered solution.

Component	Weight %
Glycine	< 1
Sodium Chloride	< 1
Hydrochloric Acid	< 0.5
Water	> 98
Mercuric Chloride	< 0.01

Phthalate buffered solution

*pH range: 3.98-4.02*

*pKa values: 2.89, 5.51 (Brown et al., 1955)*

*Ionic strength: 0.36 mol kg<sup>-1</sup>*

**Table 3.2** Composition of phthalate buffered solution.

Component	Weight %
1,2-Benzenedicarboxylic acid, monopotassium salt	1
Water	98.999
Mercuric Chloride	0.001

Phosphate buffered solution

*pH range: 6.98-7.02*

*pKa values: 2.12, 7.21, 12.67 (Kumler, 1943)*

*Ionic strength: 0.36 mol kg<sup>-1</sup>*

**Table 3.3** Composition of phosphate buffered solution.

Component	Weight %
Sodium Phosphate Dibasic	< 1
Dihydrogen Potassium Phosphate	< 1
Sodium Chloride	< 1
Water	> 98
Mercuric Chloride	< 0.01

Borate buffered solution

*pH range: 9.98-10.02*

*pKa values: 9.14 (Housecroft and Constable, 2006)*

*Ionic strength: 0.36 mol kg<sup>-1</sup>*

**Table 3.4** Composition of borate buffered solution.

Component	Weight %
Sodium Hydroxide	< 0.5
Boric Acid	< 0.5
Potassium Chloride	< 0.5
Water	> 99

#### Buffers of customisable pH and ionic strength

Other buffer solutions were synthesised where both the pH and ionic strength could be customised. A 5 M solution of phosphoric acid (pKa values of 2.15, 7.20 and 12.32 (Housecroft and Constable, 2006)) was titrated against a 1 M solution of sodium hydroxide and the pH was measured using a pH electrode. Twelve solutions differing by one pH unit from 2 to 13 were prepared (along with three replicates). For a given pH, the pKa values of the acids present in solution were used to calculate the concentration of all of the species participating in the dissociation of that acid (for example for phosphoric acid, the concentrations of  $\text{H}_3\text{PO}_4$ ,  $\text{H}_2\text{PO}_4^-$ ,  $\text{HPO}_4^{2-}$  and  $\text{PO}_4^{3-}$  were calculated). The pH of the solutions together with the ionic product of water (Equation 3.1) was used to determine the concentrations of  $[\text{OH}^-]$  and  $[\text{H}_3\text{O}^+]$ . From this, the concentration of  $\text{Na}^+$  was found using the volume of 1 M NaOH added to the solution.

$$K_w = [\text{H}_3\text{O}^+] [\text{OH}^-] \quad (3.1)$$

The ionic strength of the buffer solution was then calculated using Equation 2.20. At this stage, there were four identical buffer solutions for each pH from 2 to 13. Calculated masses of sodium chloride were then added to three of the identical buffer solutions to raise their ionic strength by 25%, 50% and 75% respectively. Therefore for each pH, a buffer solution of 0%, 25%, 50% and 75% additional ionic strength was produced according to Table 3.5.

**Table 3.5** Buffer solutions synthesised upon titrating 5 M phosphoric acid against 1 M sodium hydroxide and adding sodium chloride to tailor the ionic strength.

pH	Ionic Strength with 0% NaCl added (mol kg <sup>-1</sup> )	Ionic Strength with 25% NaCl added (mol kg <sup>-1</sup> )	Ionic Strength with 50% NaCl added (mol kg <sup>-1</sup> )	Ionic Strength with 75% NaCl added (mol kg <sup>-1</sup> )
2	0.92	1.15	1.38	1.61
3	1.74	2.17	2.61	3.04
4	1.89	2.36	2.83	3.31
5	1.96	2.45	2.93	3.42
6	2.14	2.67	3.20	3.74
7	3.96	4.95	5.94	6.93
8	5.99	7.49	8.99	10.49
9	5.57	6.95	8.35	9.74
10	5.60	7.01	8.41	9.81
11	7.58	9.48	11.37	13.27
12	6.74	8.42	10.11	11.79
13	6.71	8.39	10.06	11.74

The above process was repeated using citric acid (pKa values of 3.13, 4.76 and 6.39 (Housecroft and Constable, 2006)) and sodium hydroxide to produce the solutions outlined in Table 3.6.

**Table 3.6** Buffer solutions synthesised upon titrating 5 M citric acid against 1 M sodium hydroxide and adding sodium chloride to tailor the ionic strength.

pH	Ionic Strength with 0% NaCl added (mol kg <sup>-1</sup> )	Ionic Strength with 25% NaCl added (mol kg <sup>-1</sup> )	Ionic Strength with 50% NaCl added (mol kg <sup>-1</sup> )	Ionic Strength with 75% NaCl added (mol kg <sup>-1</sup> )
2	0.21	0.26	0.31	0.36
3	0.96	1.20	1.44	1.69
4	2.15	2.68	3.22	3.76
5	1.41	1.76	2.12	2.47
6	6.08	7.59	9.11	10.63
7	8.82	11.02	13.22	15.43
8	9.85	12.31	14.77	17.24
9	9.92	12.40	14.88	17.36
10	9.93	12.41	14.89	17.38
11	9.80	12.25	14.70	17.15
12	9.71	12.14	14.57	16.99
13	8.75	10.94	13.12	15.31

### 3.10.1 Hand-held microscope

Swelling equilibrium was determined by measuring the change in diameter of hydrogel samples using a Scalar USB microscope M2 equipped with ProScope HR image analysis software. The microscope was secured on a retort stand at

a fixed height throughout all experiments. Samples were immersed in glycine (pH 2), phthalate (pH 4), phosphate (pH 7) and borate (pH 10) buffers and maintained at a constant temperature (37 °C) using a water bath. This was confirmed using pH and temperature probes. At pre-determined time intervals and temperatures, images were captured and the change in diameter of swollen hydrogels was measured. The swelling ratio was determined according to Equation (2.26).

### **3.10.2 Digital cameras**

Gels were fixed to the base of a Petri dish using the minimal amount of fluid resistant glue or by placing a magnet under the Petri dish and a small piece of magnetic tape being positioned on the specimen surface. The Petri dish was placed on a custom made stand on an optical bench. Two cameras, Nikon D7000 and D5100, with AF-S micro Nikon 40 mm DX 1:2.8 G lenses were set to take images of the surface area and height of the gel as a function of time. The interval timers on both cameras were set to record images every 5 min. After the timers were simultaneously initiated and the first shots were taken, a buffer was added to the Petri dish and images were obtained. Optical studies were performed at room temperature. The images were analysed using ImageJ software (<http://rsbweb.nih.gov/ij/download.html>) and the surface area and height of the hydrogels were quantified. A calibration was initially conducted by determining the length (in pixels) of a photograph of an object where the actual length is known (in this case graph paper). Measurements of the change in gel surface area and height could subsequently be performed. An example of this is shown in Figure 3.2. The swelling ratio was recorded according to Equations 2.27-2.29.

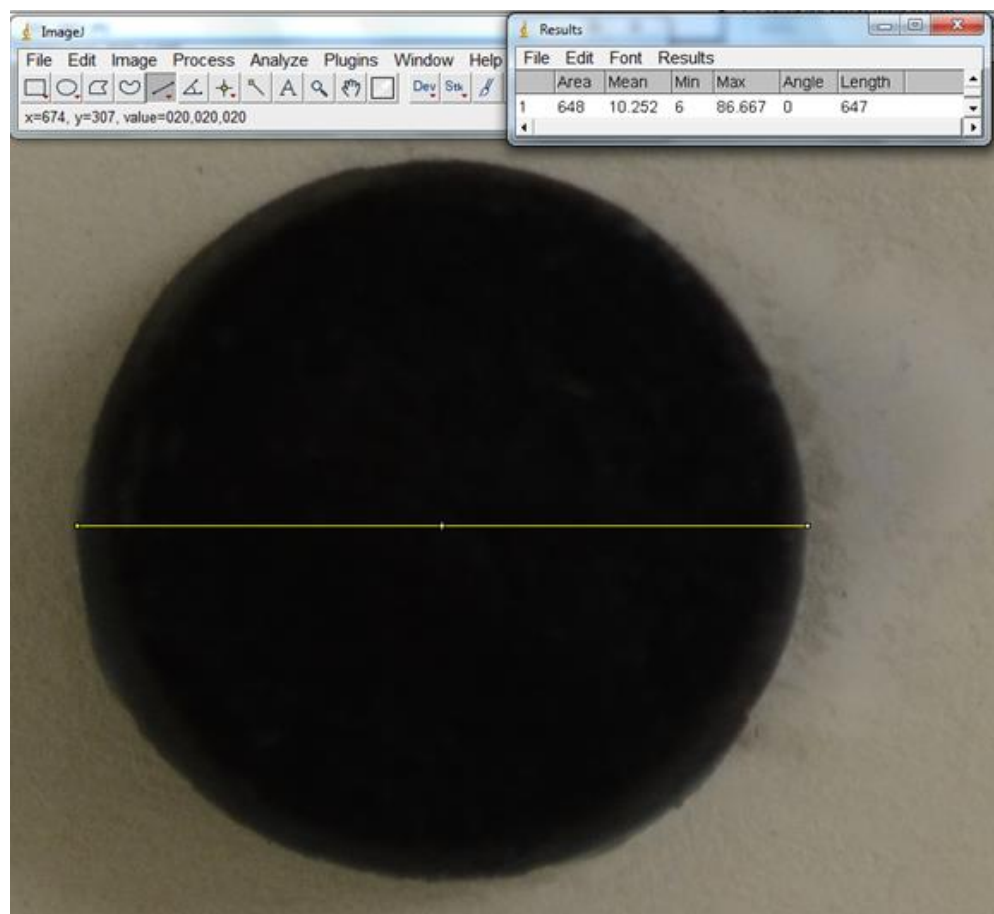


**Figure 3.2** Screenshot of the process of measuring the diameter of a hydrogel sample using ImageJ.

### 3.10.3 Macroscale swelling analysis via fluorescence microscopy

Smart behaviour was determined by measuring the change in surface area of hydrogel samples using a Nikon AZ100 microscope using a 0.5 x 0.05 numerical aperture AZ Plan Apo lens equipped with a green excitation fluorescence filter with an excitation wavelength range between 510-560 nm and a dichromatic mirror with a 575 nm cut-on value. Samples were immersed in transparent buffers and maintained at a constant temperature (20 °C). At pre-determined time intervals, the change in surface area of the samples was measured. The swelling ratio ( $\phi/\phi^*$ ) was determined according to (Equation 3.2) where the initial and final surface areas of the gel are ( $a^*$ ) and ( $a$ ) respectively. The units of area are  $\text{mm}^2$  as previously defined in Equations 2.27-2.28.

$$\phi/\phi^* = (a-a^*) / a^* \quad (3.2)$$

Variation in fluorescence intensity was determined using LCS Software Version 2.61.

#### 3.10.4 Microscale swelling analysis via confocal laser scanning microscopy

Microscale swelling was examined using a Leica TCS SP2 UV (Leica Microsystems Heidelberg) confocal microscope. This was done with the assistance of the Bio-Imaging Unit at Newcastle University. Samples were swollen and immersed in a transparent glycine solution for 30 min and were examined using a 20x dipping lens in reflectance mode (Figure 3.3). An image recorded at 0 min acted as the reference for the experiment.

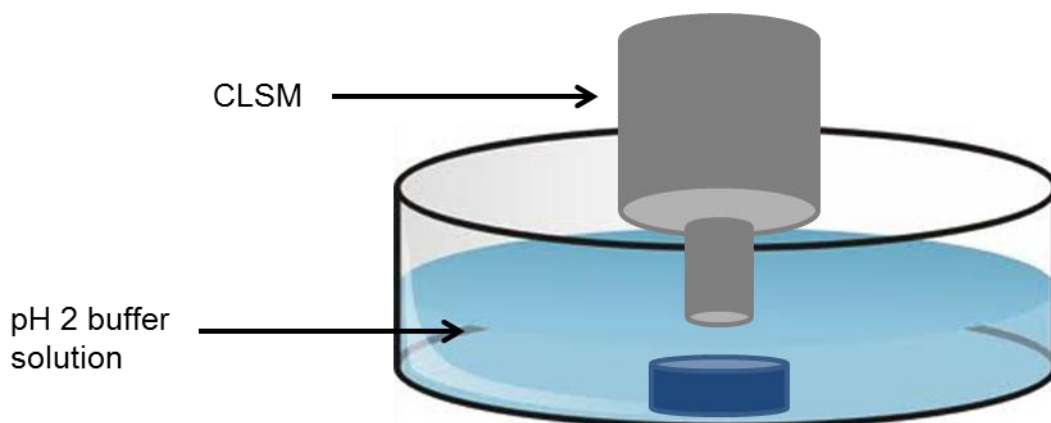


**Figure 3.3** Experimental setup to study microscale swelling via CLSM.

Images were acquired every 5 min. Throughout the experiments, the entire sample was fully submerged in the transparent solution. During sample scanning, cross-sectional images of the hydrogel morphology along the z-plane were taken to construct the native three-dimensional network structure. The sample penetration depth was 100  $\mu\text{m}$  in all experiments. The process of optical sectioning is shown in Figure 3.4 where the signal generated from the sample (shown in green) is measured within a specific focal plane. Out-of-focus light is rejected by the use of a pinhole aperture.

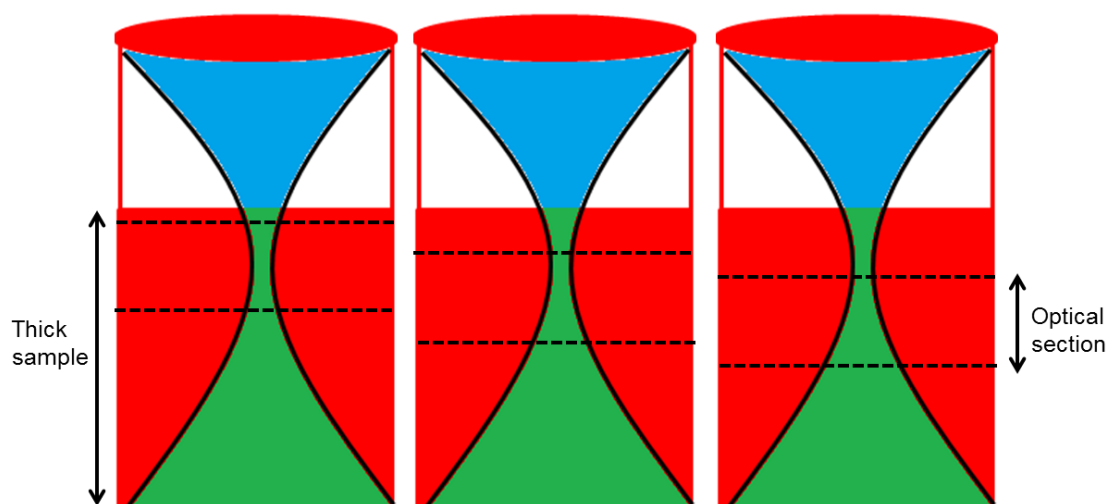


**Figure 3.4** Optical sectioning within a thick sample (green refers to the signal generated from the sample).

Pore analysis of samples acquired in reflectance mode was performed using ImageJ (<http://rsbweb.nih.gov/ij/>). Porosity was determined using the associated Measure and Label plug-in. Individual pore areas were summated and divided by the total area of each image as detailed in Section 3.5.3.

### 3.10.5 Gravimetric swelling analysis

Swelling of samples was measured gravimetrically by immersing pre-weighed hydrogels in an appropriate buffer at a constant temperature (20 °C). At pre-determined time intervals, swollen hydrogels were removed and excess solution was blotted from the sample surfaces. To facilitate transfer of the samples from solution to weighing scales, hydrogels were enclosed in a cubic poly(tetrafluoroethylene) (PTFE) cage (Figure 3.5). The change in mass was then recorded and the gravimetric swelling ratio was calculated according to Equation 2.30.

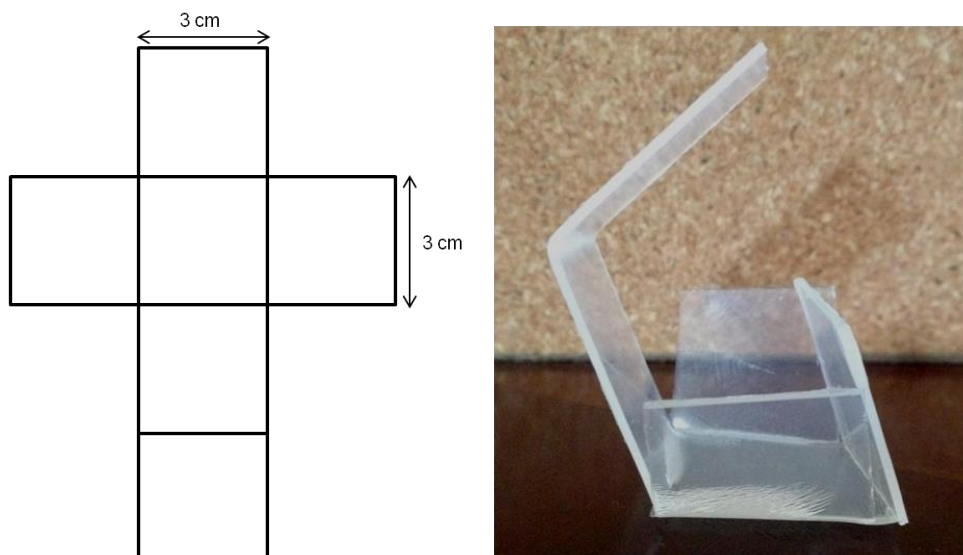


**Figure 3.5** Net and photograph of cubic PTFE cage.

### **3.11 Oscillatory swelling measurements of genipin-crosslinked chitosan-poly(vinyl pyrrolidone) hydrogels**

The oscillatory response of G-Ch-PVP hydrogels was assessed by manually alternating the pH between 2 and 4. It was envisaged that if an appropriate response could be measured in this pH range, when the polymeric system is coupled to a reaction exhibiting even larger variations in pH (e.g. 3-7 for the BSF reaction), the volume change will be even greater. The time period for the manually induced oscillations was 15 min because again this is faster than what is required for when it will be applied to a real oscillatory system. However, in some instances, the time period was lengthened to investigate oscillatory behaviour at equilibrium.

Pre-weighed hydrogels enclosed in a PTFE cage were immersed in a buffer (glycine) at a constant temperature (20 °C). This temperature was selected owing to the sensitivity of the BSF reaction to temperature (an increase in 20 °C results in almost a 4-fold increase in reaction rate) (Edblom et al., 1989). Therefore in order to achieve a time period to allow a enough time for a smart hydrogel to respond to (e.g. a time period of approximately 30 min), a low temperature (approximately 20 °C) is necessary (Edblom et al., 1989). After 15 min, the hydrogel and cage were removed. Excess solution was blotted from the sample surface and the mass was recorded. The hydrogel and cage were then placed for a further 15 min in a different solution (phthalate) and the mass

was determined as described. This process was continued in an alternate fashion for 3 h.

### 3.12 Oscillatory force response measurements of genipin-crosslinked chitosan-poly(vinyl pyrrolidone) hydrogels

Quantification of the size and response time of the force produced by a hydrogel during a volume change is of paramount importance when considering applications such as an actuator in microfluidics (Johnson et al., 2004) or in tissue engineering to stimulate cell growth (Inoue et al., 1993). Such force variations can be monitored by equipping a mechanical testing frame with a sensitive ( $\sim 5$  N) load cell with a static compression plate that is forming an intimate contact with the surface of a hydrogel immersed in an appropriate solution (Figure 3.6). Upon network swelling, a force will be exerted on the compression plate, which can be recorded as a function of time.

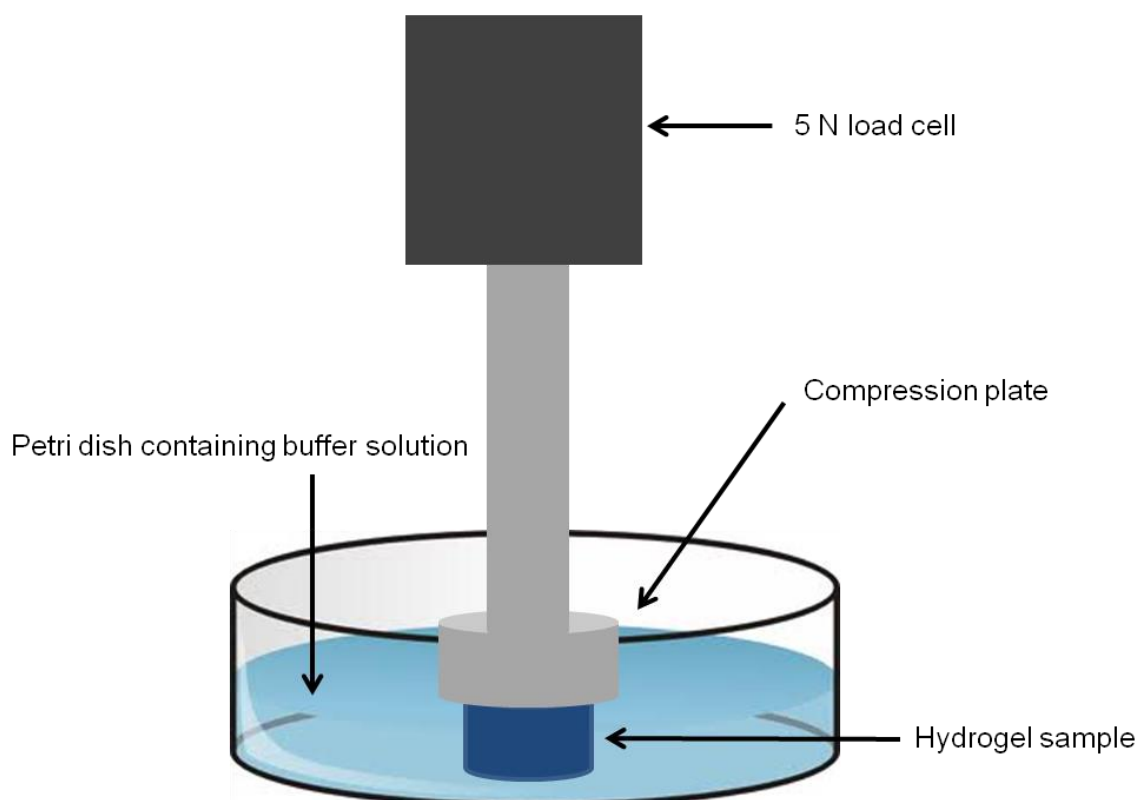


**Figure 3.6** Experimental setup for detecting the force response of a hydrogel.

A Tinius Olsen H25K-S Universal Testing Machine equipped with a 5 N load cell and a custom-built stainless steel plate (20 mm diameter) was used to measure the force response of the hydrogel at 23 °C and 43% humidity. This temperature

was selected based upon the previous oscillatory gravimetric swelling experiments outlined in Section 3.11. The height of the compression plate was adjusted using a computer-controller. The diameter (12 mm) and thickness (3 mm) of the gel was confirmed using a digital micrometer prior to the experiment. Samples were placed in a Petri dish and a pre-load of 0.150 N was applied to the gel surface to ensure a uniform contact and to ensure the gel was maintained in a stationary position for the duration of the experiment. A buffered pH solution was poured into the Petri dish and the force reading was adjusted to zero to account for buoyancy effects on the plate. In line with the previous oscillatory swelling experiment (Section 3.11) after 15 min had elapsed, the force measurement was recorded. The applied load was removed completely by taking the plate away from the sample surface via increasing the height of the plate using the computer-controller. The buffer solution was then removed from the Petri dish. A pre-load of 0.150 N was re-applied and a different buffered pH solution was poured into the Petri dish. After 15 min the aforementioned process was repeated and the buffer alternated. This process is depicted in Figure 3.7. The duration of the experiment was 3 hrs. The force was then plotted as a function of time.

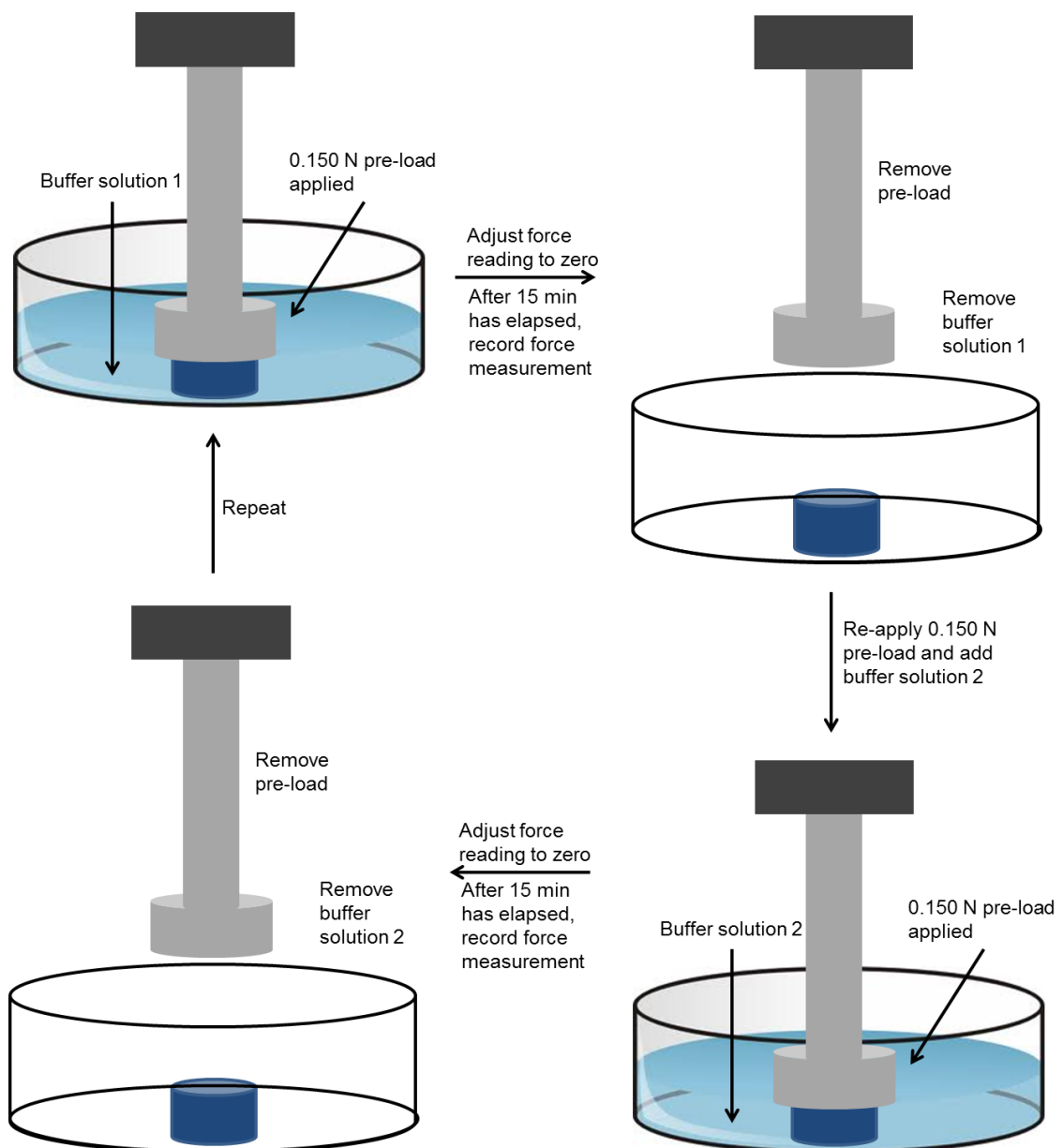


**Figure 3.7** Schematic of how to study the force variation of a hydrogel upon changing pH of the surrounding solution.

### 3.13 Compression testing

In order to synthesise a stable hydrogel that can successfully find application, it is always essential to consider the mechanical properties which are often a trade-off between extent of swelling and mechanical strength. For example, by increasing the hydrophobicity, cross-linking density, gelation time and gelation temperature, the pore sizes decrease and therefore degree of swelling will also decrease, resulting in increased mechanical properties and vice versa (Anseth et al., 1996). It is clear that the challenge is to carefully tune these parameters

in order to produce the optimum hydrogel composition for the desired application.

One way to evaluate the mechanical properties of macromolecular networks is via unconfined uniaxial compression testing. Following examination of the literature (Oyen, 2014) and availability of suitable equipment, it was concluded that compression testing conducted on triplicate samples and averaged would be the most appropriate method to determine the mechanical properties. An identical setup to that previously described in Section 3.12 for the force response testing was constructed with the exception that the compression plate moved at a defined velocity as opposed to being static. Following testing, average stress-strain curves were plotted and comparisons can be made between different specimens.

Triplicate hydrogel samples were synthesised and tested, with the diameter and thickness of all specimens being accurately determined using a digital calliper. A Tinius Olsen H25KS mechanical test frame equipped with a 100 N load cell was used to compress specimens to 50% of their original thickness at a rate of  $0.5 \text{ mm min}^{-1}$ . Samples were compressed to 50% of their original thickness in accordance with the published literature and to ensure that consistent contact was maintained with the specimen throughout the compression (Hunter et al., 2002). A slow rate of  $0.5 \text{ mm min}^{-1}$  was used to compress specimens in order to collect a sufficient amount of data during mechanical testing to accurately represent the strength of the samples (Behravesch et al., 2002). This was conducted at  $23 \text{ }^{\circ}\text{C}$  and 43% humidity. A pre-load of 0.050 N was applied to each sample to ensure an evenly distributed contact between the compression plate and the hydrogel. A lower pre-load than the oscillatory force measurements (0.150 N in Section 3.9 compared to 0.050 N) was utilised as it was not required to stir the solution that specimens were immersed in unlike when recording variations in force when the sample is contained in an oscillatory reaction. When stirring was required, a higher pre-load was needed to ensure the specimen remains stationary. By lowering the pre-load in such a way impact damage to hydrogel samples prior to compression testing would be reduced, hence the mechanical behaviour recorded would be more representative of the actual specimen compared to if a higher pre-load had been applied (Zhang et al., 1999). Average stress-strain curves were

subsequently plotted to compare the mechanical behaviour of individual samples.

### 3.14 Release of chemical moieties from hydrogels

To evaluate the release kinetics of hydrogels, model compounds equipped with a fluorescent tag, such as FITC, are often used to monitor discharge (Luo et al., 2000). Dextrans (Figure 3.8) are examples of a branched glucans used as an antithrombotic agents. They are often coupled with a FITC tag and make ideal candidates for studying permeability and transport in cells and tissues as they exist via varying molecular masses.

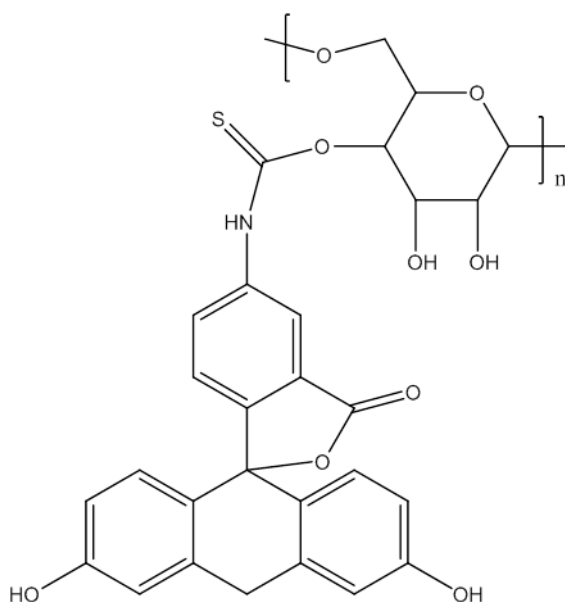


**Figure 3.8** Chemical structure of FITC-dextran.

One way to qualitatively visualise release on the macroscale is to use a setup incorporating appropriate excitation and emission filters, a light source and a digital camera (Schwaebel et al., 2013). This is depicted in Figure 3.9. Microscale visualisation can also be achieved using a CLSM in fluorescence mode corresponding to the appropriate excitation and emission wavelengths. Such wavelengths were determined by recording excitation and emission spectra of a sample of FITC-dextran solution ( $10 \text{ mg mL}^{-1}$ ) using a Shimadzu fr5301 fluorescence spectrometer. The excitation spectrum was recorded using 524 nm as the emission wavelength while scanning the excitation wavelength from 250-800 nm. The emission spectrum was recorded utilising 495 nm as the excitation wavelength while scanning the emission wavelength from

250-900 nm. Both spectra were acquired using a slit width of 5 nm for excitation and emission.

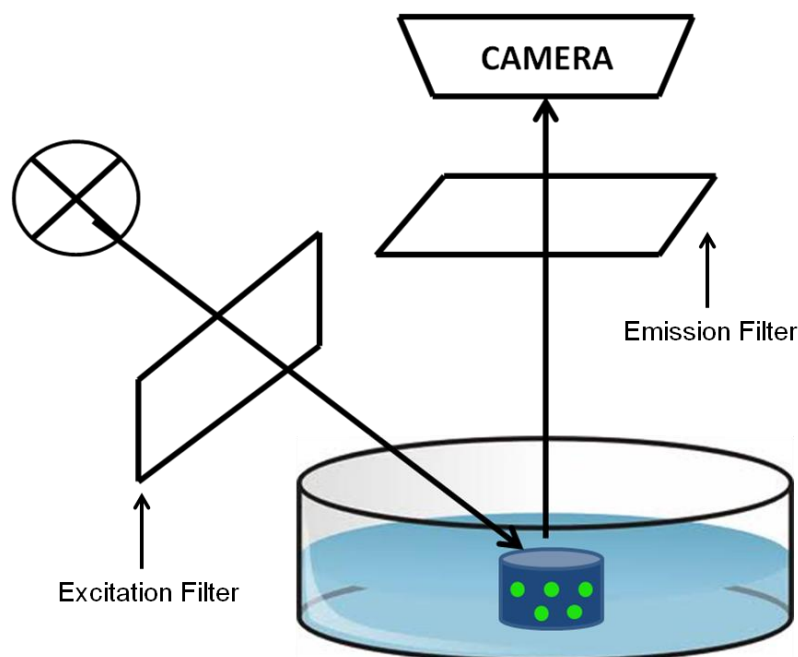


**Figure 3.9** Experimental setup for the macroscale visualisation of FITC-dextran release from a polymeric hydrogel.

### 3.14.1 Macroscale visualisation of fluorescein isothiocyanate-dextran release

A hydrogel equilibrated in a pH 7 phosphate buffer was transferred to a FITC-dextran solution ( $10 \text{ mg mL}^{-1}$ ) for 24 h at  $5 \text{ }^\circ\text{C}$  in a dark environment. The setup depicted in Figure 3.9 was followed containing a 6 W light emitting diode, a 495 nm excitation filter, 519 nm emission filter and a Nikon D7000 camera with AF-S micro Nikon 40 mm DX 1:2.8 G lenses. The hydrogel was taken out of the FITC-dextran solution, placed in a Petri dish and forced to collapse in an alkaline pH 10 borate buffer solution whilst images were taken every 5 min for 3 h. Using ImageJ, the size of the sample was interpreted as outlined in Section 3.9.2 and the fluorescence intensity was determined by measuring the variation in pixel intensity across the surface area of the gel.

### **3.14.2 Microscale visualisation of fluorescein isothiocyanate-dextran release**

A hydrogel equilibrated in a pH 7 phosphate buffer was transferred to a FITC-dextran solution ( $10 \text{ mg mL}^{-1}$ ) for 24 h at  $5 \text{ }^{\circ}\text{C}$  in a dark environment. The hydrogel was taken out of the FITC-dextran solution, placed in a Petri dish and forced to collapse in an alkaline pH 10 borate buffer solution whilst images were taken every 5 min for 40 min. Images were captured utilising a Leica TCS SP2 UV (Leica Microsystems Heidelberg) confocal microscope with a 20x dipping lens. Samples were excited using 488 nm light for the gel and 495 nm light for the FITC-dextran (fixed wavelengths) in the presence of a 500-550 nm emission filter. The resultant fluorescence intensity was interpreted using LCS Software Version 2.61 as in Section 3.8.1.

### **3.14.3 Ultraviolet-visible spectroscopy for characterisation of amoxicillin release**

Prior to gelation, 10 mg of amoxicillin with a potency of  $\geq 900 \text{ } \mu\text{g}$  per mg was incorporated into a mixture of chitosan, PVP and genipin, which was placed in an oven at  $37 \text{ }^{\circ}\text{C}$  for 24 h, subsequently freeze-thawed for 30 min and freeze-dried at  $-55 \text{ }^{\circ}\text{C}$  for 24 h. Enzyme-free simulated gastric fluid (pH 2.0) was prepared by dissolving 1.03 g of sodium chloride in 50 mL of distilled water. Following this, 870  $\mu\text{L}$  of 3 M hydrochloric acid was added to the sodium chloride solution. This was then diluted to 200 mL with distilled water to form the GI fluid (Bergstrand et al., 2012). The ionic strength was  $0.10 \text{ mol kg}^{-1}$ . A Shimadzu UV-1800 spectrometer was used to determine the wavelength at which the absorbance was greatest for amoxicillin in aqueous solution. This was found to be 276 nm (Risbud et al., 2000). A calibration curve of absorbance against amoxicillin concentration was constructed and is shown in the Appendix (Figure A1).

Freeze-dried G-Ch-PVP hydrogels were subsequently placed on a PTFE base where they were pierced with a needle. A small rubber stopper was fastened to the top of the needle to prevent the gel floating. The gel was suspended in a beaker containing the simulated GI fluid with mixing at  $37 \text{ }^{\circ}\text{C}$ . At 10 min intervals, 500  $\mu\text{L}$  samples of the solvent were taken and analysed via UV-Vis

spectroscopy at 276 nm. To maintain a constant immersion volume, a 500  $\mu\text{L}$  aliquot of fresh simulated GI fluid was added to replace the amount extracted for analysis each time. The experiment was conducted for 3 h. Images of the surface area and height of the hydrogel were taken using Nikon D7000 and D5100 cameras fitted with AF-S micro Nikon 40 mm DX 1:2.8 G lenses. ImageJ was then used to determine the increase in network volume.

### 3.15 The bromate-sulfite-ferrocyanide reaction as a pH oscillator for cationic hydrogels

As detailed in chapter 2, the BSF reaction is an ideal oscillatory system for coupling to smart hydrogels that are able to reversibly swell and collapse upon variation in pH in the acidic region (Ryan et al., 2005b, Ryan et al., 2005a, Crook et al., 2002). The hydrogel response could be monitored by determining force oscillations as depicted in Figure 3.10.

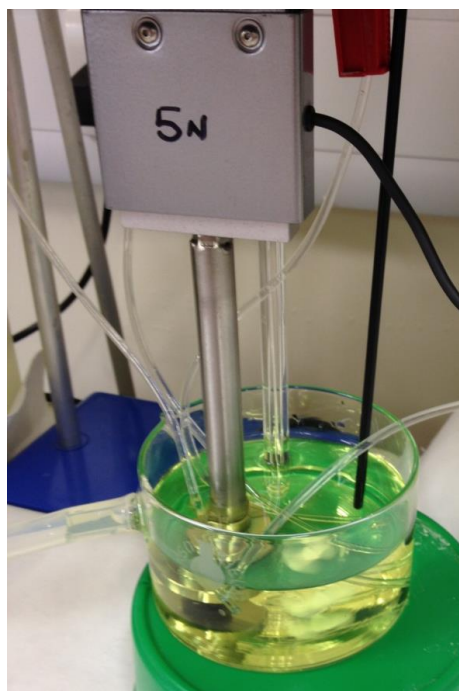


**Figure 3.10** Experimental setup for measuring the force oscillations of hydrogels during the bromate-sulfite-ferrocyanide reaction.

This reaction exhibits pronounced pH oscillations between 3 and 7 at room temperature (approximately 20 °C). Ordinarily, peristaltic pumps are used to deliver four reactant feed solutions into a continuously stirred reactor (CSTR)

equipped with an appropriate overflow to ensure a constant volume of liquid (Edblom et al., 1989, Bilici et al., 2010). However, it is also possible to gravimetrically deliver the reactants into a CSTR using appropriately sized syringes and tubes provided the liquid level in the syringes is regularly replenished. This setup is more financially viable than the use of peristaltic pumps and ensures that the reactants are not delivered in small pulses; but instead, via a simpler continuous flow regime. Temperature and pH may also be recorded using appropriate probes according to the setup depicted in Figure 3.11.

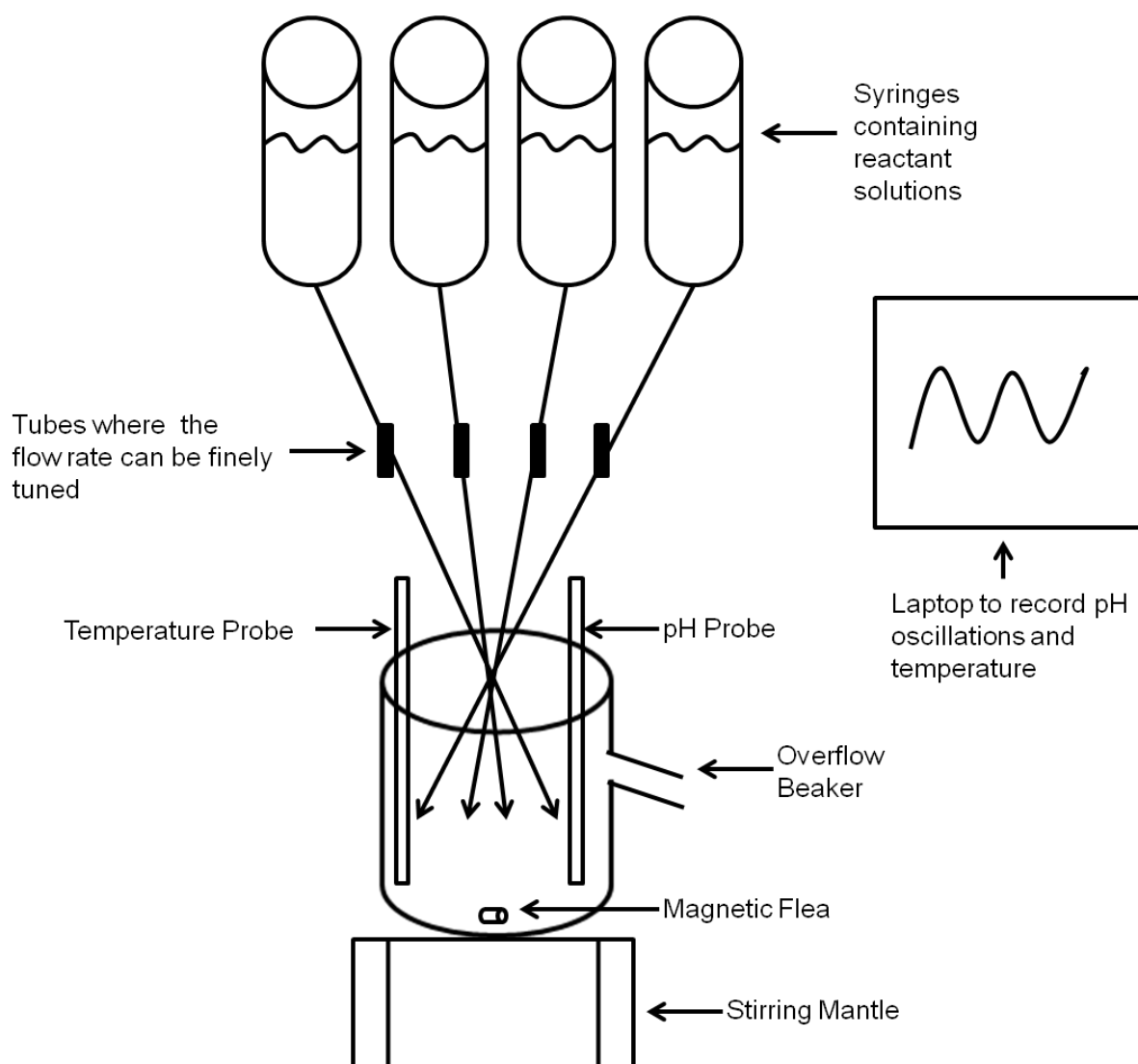


**Figure 3.11** Experimental setup for recording the temperature and pH changes due to the bromate-sulfite-ferrocyanide reaction.

According to Figure 3.11, a 150 ml glass beaker with an overflow at approximately 70 mL was used as a CSTR for the oscillatory reaction. The

reactor containing a small magnetic flea was placed on a magnetic stirring mantle and four feed solutions were allowed to flow into the reactor from a syringe through tubes at a rate of 4 mL/min. The flow rate was calibrated prior to the experiment. The four feed solutions were sodium bromate (0.065 M), sodium sulfite (0.075 M) potassium hexacyanoferrate (II) trihydrate (0.020 M) and sulfuric acid (0.010 M). pH measurements were collected using a pH electrode. This data was displayed via a personal computer. Measurements were taken every 20 seconds for periods from 3 and up to 6 hours depending on the experiment.

### **3.16 Force response in real-time of a hydrogel immersed in a bromate-sulfite-ferrocyanide oscillatory reaction**

As described in Section 2.6.2, it is possible to measure the oscillatory force response of a hydrogel using a compression plate equipped with an appropriately sensitive load cell (5 N) to determine the variation in force as the network swells and collapses. As opposed to physically changing the pH via the addition and removal of buffer solutions, an oscillatory chemical reaction such as the BSF reaction can automatically provide variation in a stimulus to induce a concomitant volume change. The variation in pH during the reaction can be subsequently monitored using a pH electrode connected to a computer. An appropriately designed CSTR was used (Figure 3.10) in order to accommodate the gel, a temperature probe, a pH electrode, a compression plate equipped with a load cell and a magnetic flea to ensure sufficient stirring. The overflow on the CSTR was engineered so that a constant volume of 165 mL was maintained.

The pre-equilibrated hydrogel was initially placed into the CSTR and a pre-load of 0.150 N was applied (as in Section 3.12) in order to ensure the specimen was stationary for the duration of the experiment and that an equal contact was achieved between the sample and compression plate. As mentioned in Section 3.13, this is more difficult to attain in an oscillatory environment when stirring of the surrounding solution is required. Hence, a pre-load such as 0.05 N is, in this case, insufficient to ensure the specimen remains stationary. The force was zeroed and the BSF reaction was initiated according to the method previously described. When the contained solution began to overflow, the force was

re-zeroed and the subsequently recorded every 5 min for 3 hrs. The force and pH were plotted as a function of time.

## **Chapter 4 – Results and Discussion: Synthesis and Characterisation of Genipin-Crosslinked Chitosan-Poly(vinyl pyrrolidone) Hydrogels**

From Chapter 2, it was identified that pH-sensitive G-C-PVP cationic hydrogels are good candidates for combination with reactions that exhibit oscillations in pH in the acidic region together with development for use in bio-related environments such as drug release. This chapter details how work from the literature was adapted to produce hydrogel discs as opposed to films. In order to record a swelling response, especially upon investigating height changes according to Equations 2.27 and 2.28, discs are thought to be easier to visualise than films. Furthermore, it is exceptionally difficult to collect reproducible data when performing tensile testing of hydrogel films, mainly due to fracture upon gripping. As an alternative, unconfined uniaxial compression testing of hydrogel discs does not require samples to be physically gripped as in tensile testing. Finally hydrogel discs can be easily manufactured using readily available vials of fixed diameter. Subsequent characterisation studies are performed to evaluate the swelling potential, morphology and mechanical properties where various parameters are changed.

### **4.1 Chitosan molecular weight determination**

Following the procedure outlined in Section 3.2, the molar mass distribution of chitosan is shown in the Appendix (Figure A2) along with the molecular mass data tabulated in Table A.1. Throughout all experiments, this was the only batch of chitosan used.

### **4.2 Hydrogel preparation**

As per the method described in Section 3.1, 1 mL chitosan (1.5% w/v) was combined with 1 mL PVP (5% w/v) and 100  $\mu$ L genipin (0.5% w/v) to form a smart gel. Following the procedure described in the published literature (Khurma et al., 2005), gels were synthesised in a polyethylene vial freely exposed to air to produce a thin film or “xerogel”. Considering visualisation and recording a response from the hydrogel with an oscillatory reaction, a disc shape was preferred so that swelling could be easily visualised and mass measurements could be performed using a mass balance as opposed to using

a quartz crystal microbalance. Based on the literature, the reliability of assessing the mechanical properties via compression testing as opposed to tensile testing where samples commonly fracture when gripped also made disc-shaped hydrogels that can easily be compressed more appealing. Finally, with a view towards the development of prospective applications in drug delivery, with the most convenient administrative route being oral, disc-shaped hydrogels are preferred (Li and Tanaka, 1990, Shibayama et al., 1992). Consequently, by ensuring that gelation vials were sealed, minimising evaporation, a viscous gel was formed.

### 4.3 Visual observations and UV-vis spectroscopy of hydrogels

The effects of varying gelation time and temperature on the visual appearance of hydrogels were evaluated (Table 4.1) in order to determine what initial conditions confer good sample stability, and to understand how crosslinking may occur. For example, it is important to know how long is required for gelation to occur when the mixture is subjected to certain conditions.

**Table 4.1** Effects of gelation time and temperature on the colour of G-C-PVP hydrogels.

Gelation Temperature (°C)	Gelation Time (h)							
	0	3	6	12	24	48	72	96
37	Colourless	Pale yellow	Green-blue	Blue-green	Dark blue-green	Dark blue	Dark blue	Dark blue
50	Colourless	Green-blue	Blue-green	Dark blue-green	Dark blue	Dark blue	Dark blue	Dark blue

The results in Table 4.1 show that at a constant temperature, as gelation time is increased, the colour of the hydrogel changes from colourless to a green hue and finally, a dark blue pigment. These results were quantified by utilising UV-Visible spectroscopy according to the method outlined in Section 3.4. For samples placed in an oven at 37 °C, the spectra recorded for the first 5 h of incubation is shown in Figure 4.1. The rise of the band between 320-430 nm is indicative of the increasingly deeper green hue observed in the initial stages of gelation. The band at 610 nm is likely due to the incorporation of a blue pigment

into the sample. It is this band that the discussion will focus on considering the visual observations depicted in Table 4.1 show that the “final” colour of the gel is dark blue.

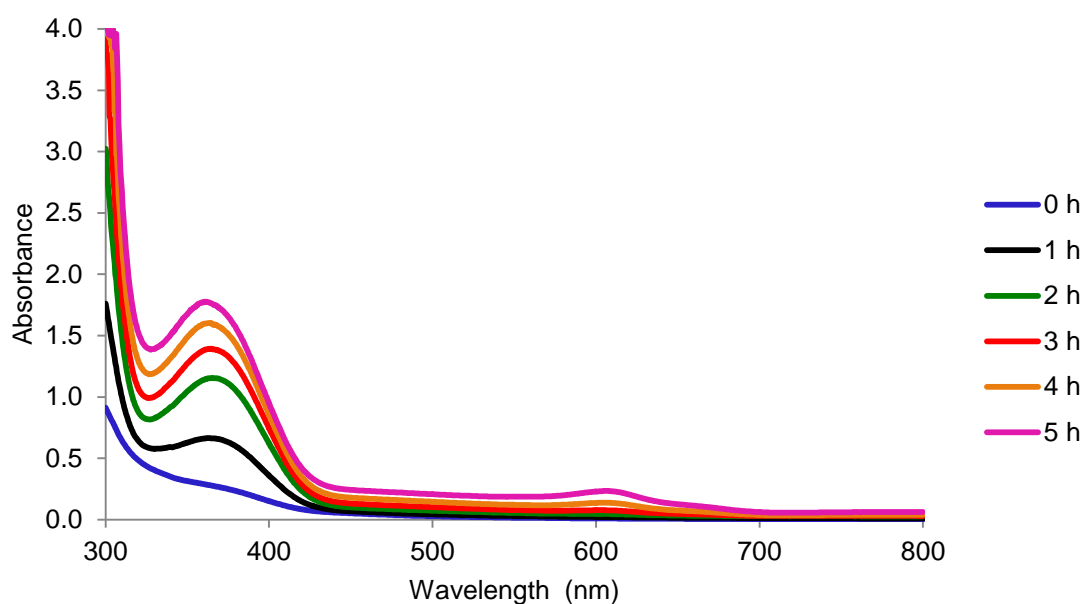


**Figure 4.1** Time-resolved UV-Visible spectra of G-Ch-PVP hydrogels placed in an oven at 37 °C.

The band at approximately 610 nm was analysed for the remaining duration of the gelation experiment at 37 °C (Figure 4.2). As shown, and in agreement with the visual observations recorded in Table 4.1, with increasing gelation time, the specimen develops a dark blue pigmentation. The final dark blue colouration of the networks is indicative of oxygen-radical induced polymerisation of genipin and its reaction with amino groups (i.e. contained in chitosan) when exposed to air (Muzzarelli, 2009, Mi et al., 2005). It is useful that the hydrogel has a dark blue pigmentation because it may be easier to optically observe changes in the shape of the specimen during swelling compared to if it were transparent. This is because the boundary between the circumference of the gel and the surrounding solution could be more easily visualised if the sample is coloured. Over time, more crosslinks within the polymer network are formed, which will presumably lead to fewer and smaller pores in the gel. At 120 h of gelation, the magnitude of absorbance is very similar to that at 96 h. This may indicate that all the crosslinks in the gel network have been formed.

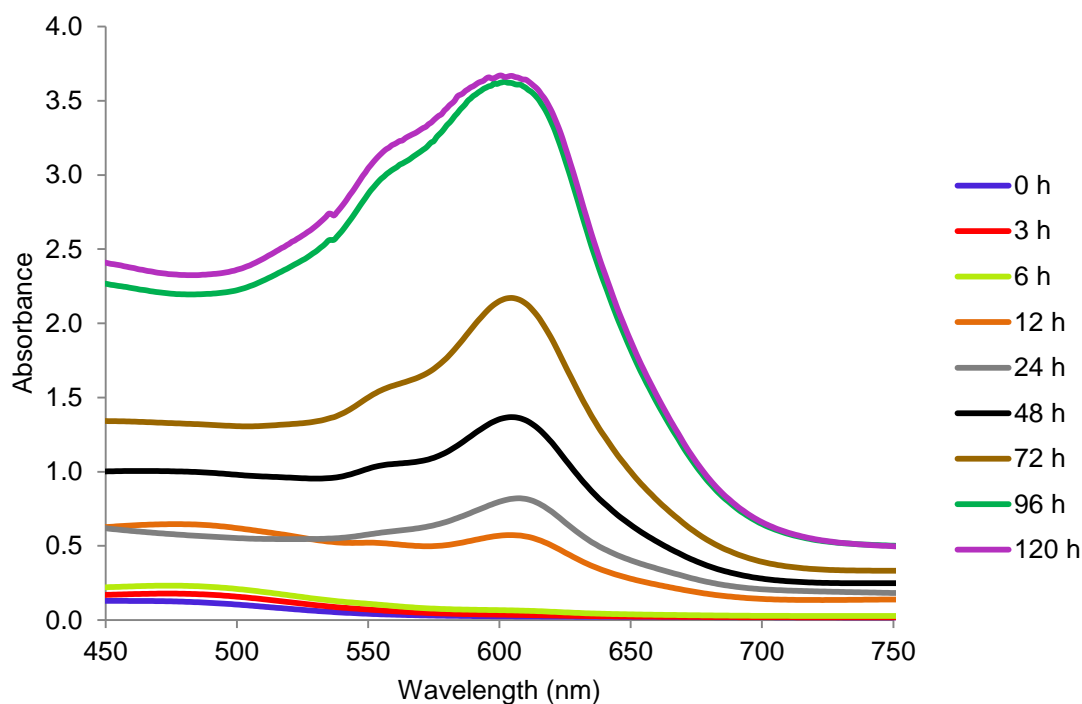


**Figure 4.2** Time-resolved UV-Visible spectra of G-Ch-PVP hydrogels placed in an oven at 37 °C focusing on the band at 610 nm.

The band at 610 nm was also investigated when gelation was initiated at 50 °C to study temperature-dependency (Figure 4.3). The absorbance at approximately 610 nm also increases with gelation time (as also observed in Figure 4.2) up to a point (96 h). Following this, there is a drop in the absorbance value recorded (120 h). This may be due to the high temperature denaturing the hydrogel network. At temperatures in excess of 40 °C, chitosan hydrogels have been shown to degrade over a period of time (Holme et al., 2008). This could be due to, for instance, physical interactions such as hydrogen bonding, Van der Waals and electrostatic attractions being destroyed at high temperature, or potential cleavage of the glycosidic bonds of chitosan (Holme et al., 2008, Kim, 2010).

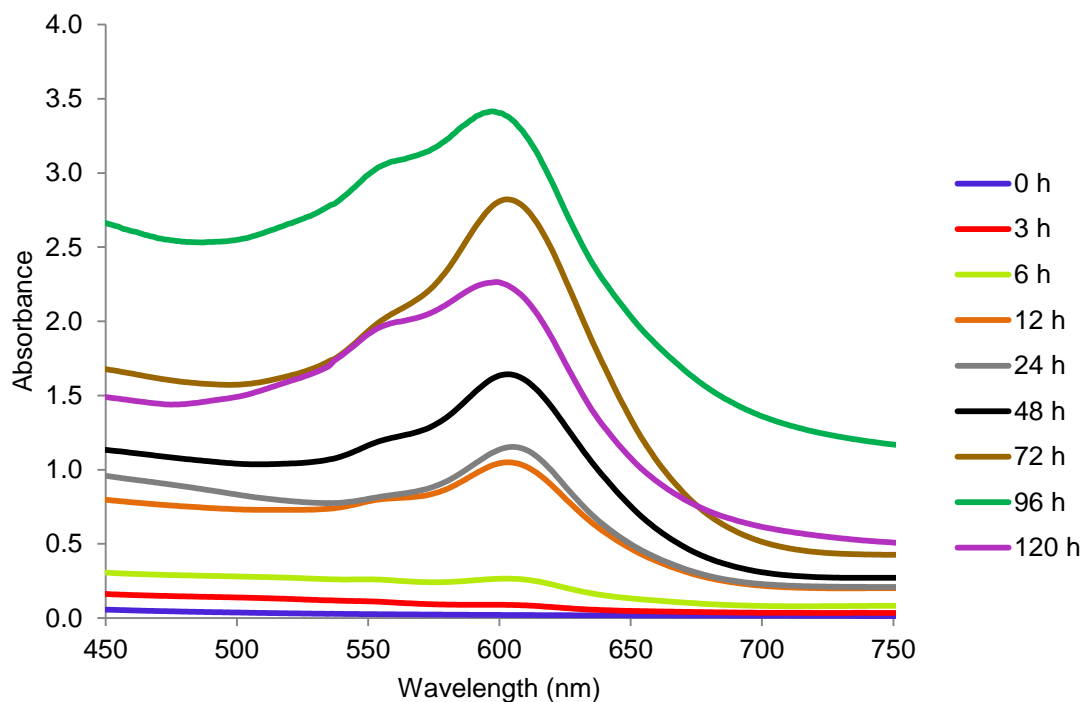


**Figure 4.3** Time-resolved UV-Visible spectra of G-Ch-PVP hydrogels placed in an oven at 50 °C focusing on the band at 610 nm.

A comparative plot of the absorbance maxima at 610 nm for G-Ch-PVP hydrogels placed in an oven at 37 and 50 °C for various time durations is shown in Figure 4.4. The rate of crosslinking shows some dependence on temperature, where a higher temperature appears to slightly increase the reaction rate. Reaction rate is related to temperature according to the Arrhenius equation (Equation 4.1) where  $\underline{A}$  is the pre-exponential factor, R is the universal gas constant, T is temperature in Kelvin and  $E_a$  is the activation energy ( $\text{kJ mol}^{-1}$ ).

$$k = \underline{A}e^{-(E_a/RT)} \quad (4.1)$$

At all time points up to and including 72 h of gelation, the specimen absorbance is slightly greater for samples placed in the oven at 50 °C. However, after this gelation time, potential denaturation of the gel incubated at 50 °C occurs.

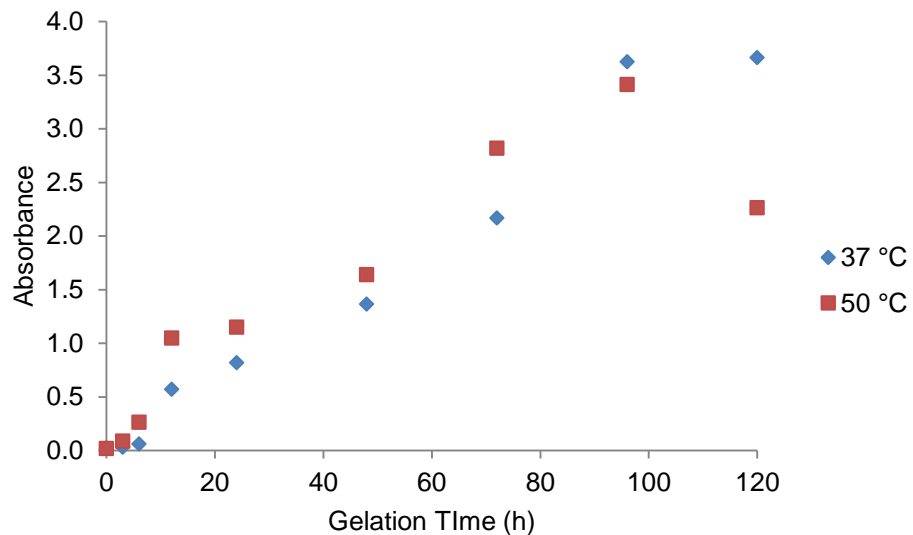


**Figure 4.4** Comparative plot of the absorbance maxima at 610 nm for G-Ch-PVP hydrogels placed in an oven at 37 and 50 °C.

Design of experiment (DOE) is a systematic method for measuring the relationship between factors affecting a process and the results of that process and could also be used in order to determine the statistical significance of the data collected (Stanojević et al., 2006). The observations have not been tested for statistical significance.

#### **4.4 Utilising confocal laser scanning microscopy with fluorescence to investigate crosslinking**

It is known that when combined with chitosan, genipin networks fluoresce and it is possible to follow the extent of crosslinking as a function of fluorescence intensity (Chen et al., 2005, Hwang et al., 2011). Gelation time of G-Ch-PVP hydrogels was found to strongly influence the fluorogenic properties of the network (Figure 4.5). Pixel intensity can be used to determine the local concentration of fluorophores in a specimen and hence measure the local fluorescence intensity because each pixel represents a finite sized area in a specific location in the sample being analysed. During image acquisition the photons that are detected at each pixel are converted to an intensity value that is correlated to, but not equal to, the number of photons detected (Pawley, 2006). Therefore it can be inferred that the pixel intensity is related to the number of fluorophores present at the corresponding area in a sample (Waters, 2009).

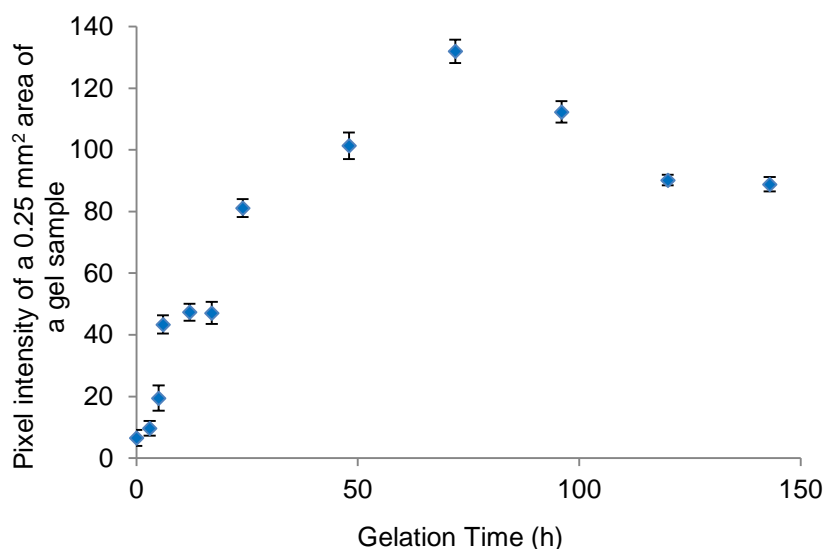


**Figure 4.5** Fluorescence intensity profile of G-C-PVP hydrogels synthesised as a function of time at 37 °C.

The data presented in Figure 4.5 are the average pixel intensities recorded following three experiments using fresh gels. The error bars were calculated according to the standard error (this was determined by calculating the standard deviation of the mean pixel intensities and dividing by the square root of the number of measurements that form the mean (in this case three)). Gelation was conducted at 37 °C so as to minimise potential denaturation. The control sample (chitosan and PVP without genipin) was analysed to have a pixel intensity of 4.2. The initial increase in fluorescence intensity up to 72 h gelation time could be due to the spontaneous reaction of genipin with primary amine groups, producing a conjugated and crosslinked hydrogel (Chen et al., 2005). A proposed mechanism for this reaction is shown in Figure 4.6. The C3 carbon of genipin is involved in nucleophilic attack from primary amines (e.g. in chitosan) leading to the dihydropyran ring opening to form an aldehyde. The secondary amine group subsequently attacks the aldehyde followed by dimerisation formed by a radical reaction (Muzzarelli, 2009). The subsequent decrease in fluorescence intensity may be attributed to the formation of a chitosan-PVP complex as a result of hydrogen bonding. This could cause a reduction of electron density on the nitrogen heteroatom of the amine groups present, decreasing intramolecular charge transfer, leading to fluorescence quenching (Mi, 2005). Towards the end of gelation, a plateau shape was observed, which may indicate the end of the crosslinking reaction where most of the amine groups have reacted. This could be studied further via FTIR. Alternatively, this

may also indicate the onset of denaturation, although given the data collected at 37 °C shown in Figure 4.4, this is unlikely as a decrease in the absorbance recorded at 650 nm is not observed for the duration of the experiment (120 h).

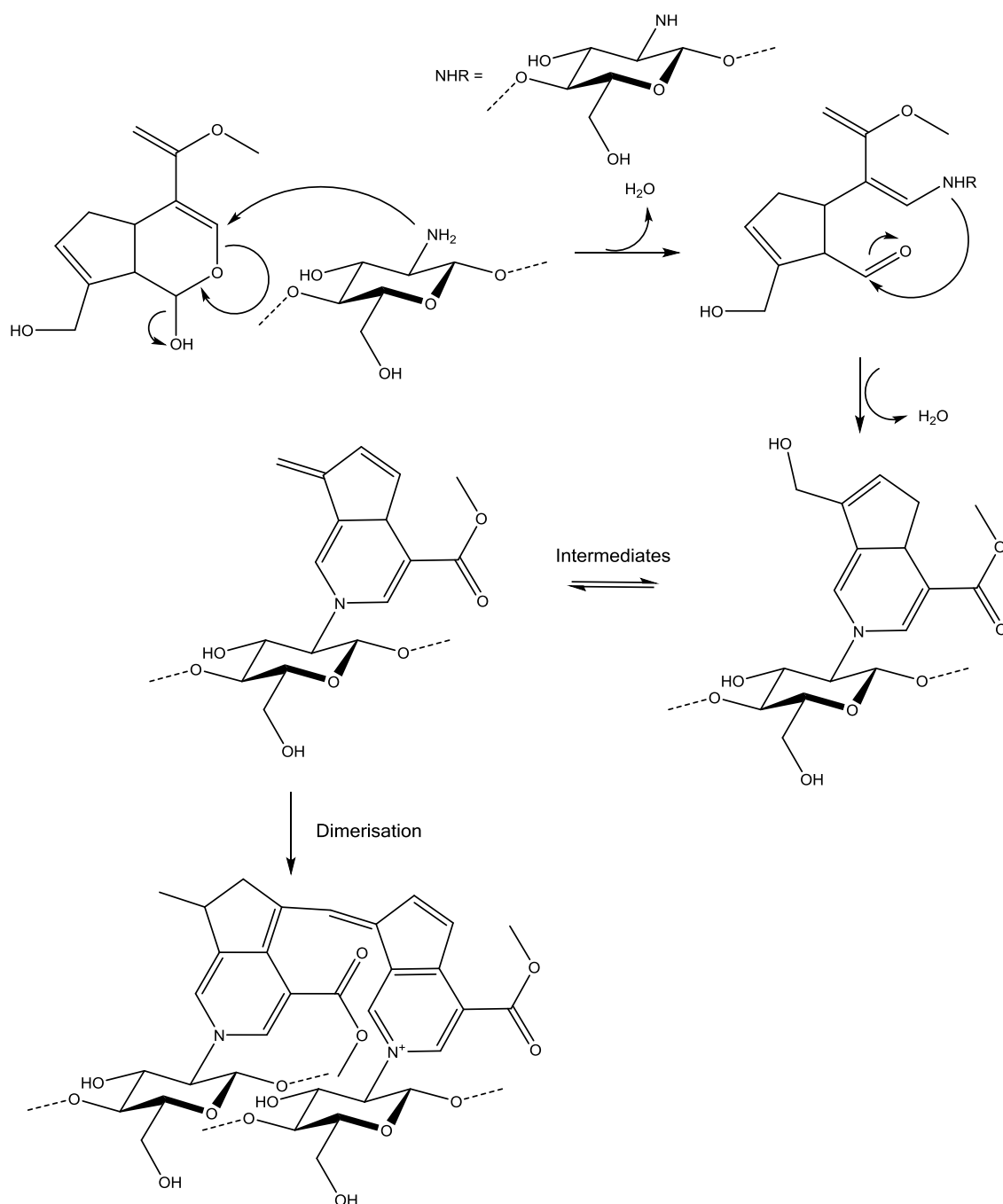


**Figure 4.6** Proposed reaction mechanism between chitosan and genipin to form a conjugated genipin derivative (Chen et al., 2005).

As genipin is being utilised as a crosslinking agent, not a fluorescent tag, no structural alteration to the hydrogel occurs as is normally the case upon the introduction of fluorescent markers (such as FITC for example) to polymers. The fluorescence is instead inherent within the gel. Addition of a large chemical

moiety in the form of a biomarker may have a detrimental effect on the mechanical integrity of the material. Furthermore, typical fluorescence markers react with nucleophilic functional groups present in polymers, which may compromise the degree of crosslinking, hence affecting both the degree of swelling and the mechanical attributes of the network. As genipin is specifically selective towards primary amines and is in itself both a crosslinking agent and serves as a fluorescent tag upon network formation, such common problems are not an issue for this system.

#### **4.5 Scanning electron microscopy analysis of the effects gelation time has on network porosity**

The variation in porosity and gel morphology with gelation time at 37 °C was studied via SEM where two drying regimes (CPD and FD) were employed in order to visualise the networks. Details of the method employed are shown in Section 3.6.

##### **4.5.1 Effect of freeze drying**

Representative electron micrographs of freeze-dried hydrogels that were placed in an oven at 37 °C for 6 h (a), 12 h (b), 48 h (c), 72 h (d) and 96 h (e) are depicted in Figure 4.7. All samples appear to exhibit quite a high porosity indicating that FD preserves the native gel structure well. Despite it being difficult to differentiate between images obtained for various incubation periods, by comparing extremes (i.e. 6 h and 96 h) it can be noted that as gelation time increases, the structural density of the hydrogels also appears to increase. Although less apparent throughout the range of samples, it may also be the case that the number and size of pores in the network decrease with increasing gelation time. This is in agreement with prior results in Section 4.4 that a longer gelation time leads to a greater degree of crosslinking and hence a less porous morphology.

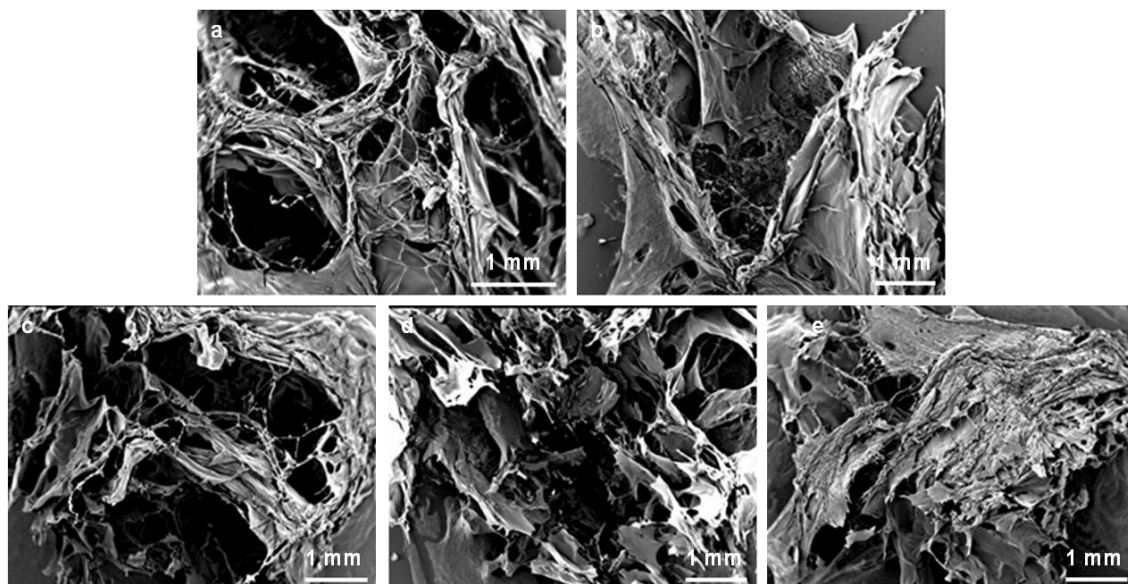


**Figure 4.7** Electron micrographs of freeze-dried G-C-PVP hydrogels synthesised for (a) 6 h, (b) 12 h, (c) 48 h, (d) 72 h and (e) 96 h at 37 °C.

ImageJ software was used to evaluate the porosity of the surface of hydrogel samples qualitatively analysed by SEM prepared via FD (Figure 4.7). Details of the method are described in Section 3.6.3. Results are presented in Table 4.2. Strong correlations between quantitative and qualitative findings were found. Following FD, the results show a sharp initial decrease from 33.8% to 11.2% surface porosity followed by smaller fluctuations and an eventual drop to 5.0% porosity as gelation time is increased. This is in agreement with the qualitative analysis performed (Figure 4.7) in that it is possible to observe the differences between samples placed in the oven for short (6 h) and long (96 h) periods of time but it is harder to distinguish morphological variations between intermediate specimens (12-72 h).

**Table 4.2** Surface porosities of freeze-dried G-Ch-PVP hydrogels determined via the analysis of SEM images using ImageJ software.

Gelation Time (h)	Surface Porosity (%)
6	33.8
12	11.2
48	16.0
72	14.4
96	5.0

This study was repeated whereby freeze-dried specimens were cut in half using a scalpel and the internal morphology was examined (Table 4.3). Results indicate a broad agreement with the data collected when the surface porosity was evaluated whereby an increase in gelation time, leads to a decrease in the porosity of the network.

**Table 4.3** Internal porosities of freeze-dried G-Ch-PVP hydrogels determined via the analysis of SEM images using ImageJ software.

Gelation Time (h)	Internal Porosity (%)
6	41.2
12	29.9
48	20.4
72	28.1
96	11.1

Regarding prominent morphological features of the freeze-dried specimens, Figure 4.8 (a) depicts channel-like structures whilst the network interior is displayed in Figure 4.8 (b) exemplifying the layers of crosslinks present.

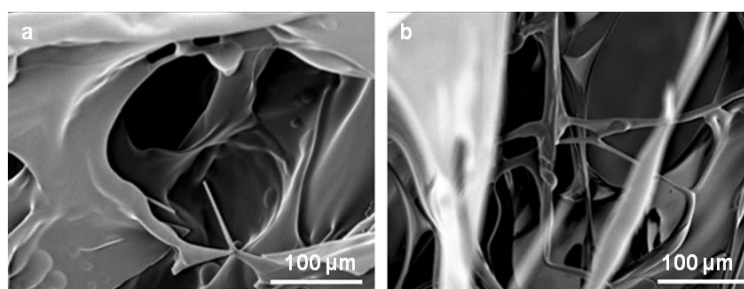


**Figure 4.8** Electron micrographs of freeze-dried G-C-PVP hydrogels depicting (a) the channels and (b) the interior structures present.

#### 4.5.2 Effect of critical point drying

Representative electron micrographs of hydrogels placed in an oven for 24 h (a,d), 48 h (b,e) and 72 h (c,f) at 37 °C that have been critically point dried are shown in Figure 4.9. As the gelation time is increased, a decrease in both the size and the amount of pores on the surface of the hydrogel is observed. Figure 4.9 (a) displays a sample with the largest pores, both in size and number, after 24 h of gelation. This is expected, as only a small amount of gelation may occur at 37 °C in such a short time period. Figure 4.9 (b) and (c) representing gelation times of 48 and 72 h respectively, show a correspondingly lower number of pores and also smaller pore sizes than the sample in Figure 4.9 (a) which was

placed in an oven for 24 h. This is consistent with a longer period of gelation, leading to more crosslinking and fewer pores.

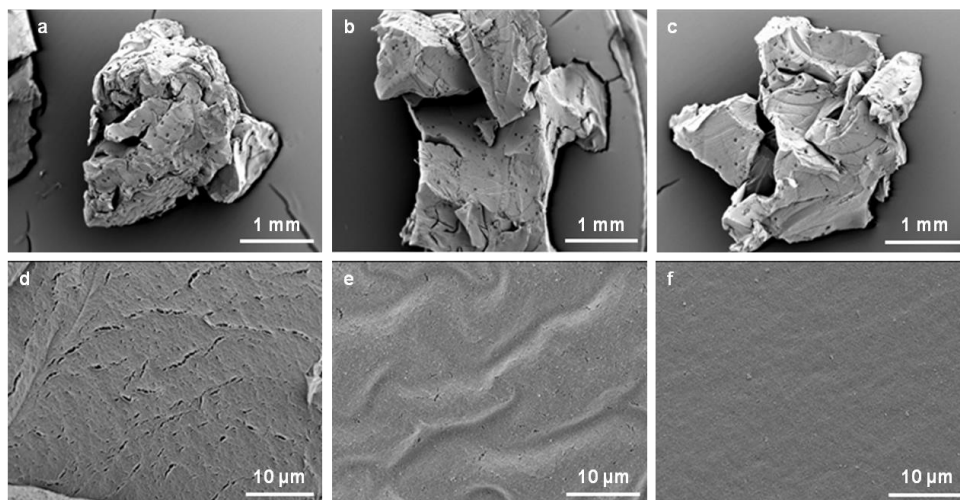


**Figure 4.9** Electron micrographs of G-C-PVP hydrogels that have been critically point dried following incubation at 37 °C for 24 h (a,d), 48 h (b,e) and 72 h (c,f).

These observations show a far more discernible trend than samples that were freeze-dried; indicating CPD is a better preparatory technique for this purpose and that the duration of incubating the specimens at 37 °C has a profound effect on the morphological structure. A dense outer layer, indicative of a polymer network in the collapsed state (Matsuo and Tanaka, 1988), is shown in Figure 4.9 (a-c). The same relationship between gelation time and the number / size of pores is exemplified in Figure 4.9 (d-f) where smaller pores within the same gel samples are examined at a higher magnification. The presence of both large (a-c) and small (d-f) pores indicates a high interface area for exchange of both absorbed and surrounding solvent.

In comparison to freeze-dried specimens, the surface porosities of all critically point dried samples decreased with increasing gelation time on both macro and micro length scales (Table 4.4). This indicates that CPD may be a better preparatory technique than FD for monitoring subtle hydrogel morphological variations with incubation time. In agreement with qualitative observations, freeze-dried samples were more porous on the surface than those prepared via CPD (Cauch-Rodríguez et al., 2001, Yeong et al., 2007, Trieu and Qutubuddin, 1994).

**Table 4.4** Surface porosities of critically-point dried G-Ch-PVP hydrogels determined via the analysis of SEM images using ImageJ software.

Preparatory Technique	Gelation Time (h)	Surface Porosity (%)
CPD Macro Scale	24	0.9
	48	0.6
	72	0.4
CPD Micro Scale	24	4.2
	48	0.6
	72	0.1

The samples in Figure 4.9 were fragmented using a scalpel and the porosity of the inner morphology was evaluated as before (Table 4.5). The data collected was loosely consistent with observations on the surface of the gel, corroborating the effect that increasing gelation time results in a decrease in network porosity. This relationship was more apparent on the macro scale compared to the micro scale.

**Table 4.5** Internal porosities of critically-point dried G-Ch-PVP hydrogels determined via the analysis of SEM images using ImageJ software.

Preparatory Technique	Gelation Time (h)	Internal Porosity (%)
CPD Macro Scale	24	1.4
	48	1.2
	72	0.9
CPD Micro Scale	24	0.6
	48	0.6
	72	0.5

The interface between the dense surface layer and dilute inner sphere is displayed in Figure 4.10 (a), while (b) is a good example of the channels present in the networks, which can enhance the mass transfer rate throughout the gel leading to excellent accessibility (Antonietti et al., 1999). The outer surface layer actually forms the channels, serving as a wall to strengthen the internal structure (Yeong et al., 2007). Figure 4.10 (c) displays a honeycomb structure of pores, which is characteristic of advanced mechanical properties and good storage and transfer of hydrogel contents during swelling and collapse. These features are all necessary in applications such controlled drug delivery (Kato et al., 2003).

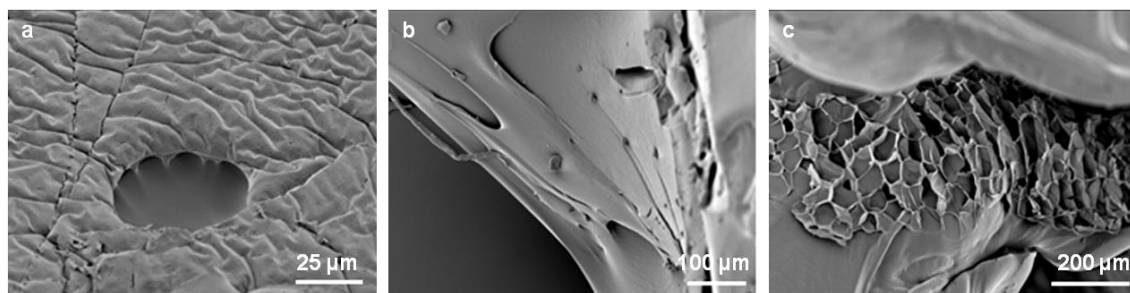


**Figure 4.10** Electron micrographs of G-Ch-PVP hydrogels subjected to critical point drying illustrating (a) the boundary between the surface layer and the inner sphere of hydrogels, (b) the channels formed as part of the skin and (c) the honeycomb morphology.

Compared to FD (Figures 4.7 and 4.8), the images after CPD (Figures 4.9 and 4.10) show collapse of the surface layer. This volume reduction is most likely the effect of dehydration in ethanol, although it may be due to gel collapse during exchange of ethanol with carbon dioxide (Trieu and Qutubuddin, 1994).

#### 4.6 Swelling measurements

The swelling potential of G-Ch-PVP hydrogels in acidic media (pH 2 glycine buffer) was evaluated optically according to the method in Section 3.7.1 (Figure 4.11). Samples were studied at 37 °C with the view that the hydrogels may eventually find application in the body. Clearly, the hydrogels do swell throughout the duration of the short experiment. This phenomenon was previously observed in acidic media and is due to protonation of the nitrogen moieties of chitosan and PVP, leading to electrostatic repulsion within the gel network and subsequent swelling (Khurma et al., 2005).

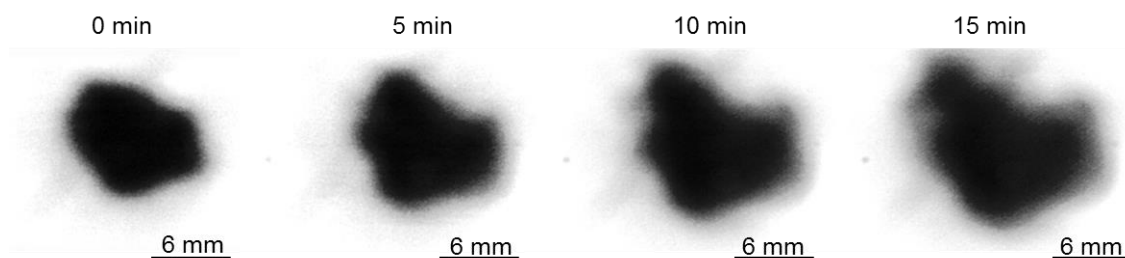


**Figure 4.11** Swelling of G-Ch-PVP hydrogels placed in an oven for 24 hours and immersed in a pH 2 glycine buffered solution in a temperature-controlled water bath at 37 °C. Images were collected using a USB microscope adjusted to a constant height away from the sample.

Even though swelling is illustrated in this simple experiment, there are many obvious shortcomings. The USB microscope used for analysis does not have sufficient contrast to accurately determine variations in sample shape, producing a blurred image that is difficult to interpret. Throughout the experiments, the position of the gel in the beaker was not static, making it hard to obtain good images that can subsequently be interpreted. One way to overcome this problem is to fix the gel to the base of the vessel it is contained in using a cyanoacrylate (Strange and Oyen, 2012). However, this approach does elicit problems. Firstly, the composition of the hydrogel may be modified owing to fixation and secondly, the swelling is restricted in the vertical direction and hence this is an inaccurate representation of how the network would behave in a target environment. It is also clear that the geometries are not in the shape of a disc and hence swelling cannot occur uniformly in all directions. This lack of shape retention following gelation and the freeze-dried SEM images are indicative that this particular gel formulation suffers from inadequate mechanical properties. Such poor stability can be improved by increasing the hydrophobicity of the network (for example by decreasing the amount of PVP), although this will result in a diminished swelling response. It is therefore important to determine the optimum formulation for both good swelling and mechanical attributes.

A further inherent problem of using an optical microscope to characterise hydrogel behaviour is that as swelling occurs and the network absorbs more of the surrounding fluid, the refractive index of the gel begins to approach that of the solution (Swann et al., 2010). This makes it difficult to visualise the hydrogel owing to the refractive indexes of the gel and the solution being very similar. This is exemplified in Figure 4.11 by the boundary between the gel surface and the buffered solution becoming increasingly unclear during swelling. Furthermore, as most oscillatory reactions do not remain colourless for the whole time duration, it will be difficult to visualise highly hydrated samples within the reaction solution. Therefore it was concluded that swelling should not be characterised using a USB microscope due to the aforementioned issues.

As G-Ch-PVP hydrogels are autofluorescent, it is advantageous to monitor the variation in surface area using a fluorescent microscope where the sample is immersed in buffer solutions during the experiment. This is reported in Section

5.2. Another method discussed in Section 2.6.1 monitors the change in weight of hydrogel samples as a function of time. As this does not involve visualisation issues, G-Ch-PVP hydrogels were subsequently characterised gravimetrically as described in the following section.

#### **4.7 Gravimetric swelling measurements**

Initial swelling tests were conducted as per the published literature where samples were removed from buffer solutions and the variation in mass was determined using a mass balance (Zhang et al., 2004, Risbud et al., 2000). Details of the method employed are shown in Section 3.10.5. However, this proved to be a poor technique owing to sample fragmentation upon transferring the hydrogel from the buffer medium to a balance, producing inaccurate measurements. A possible solution was found where a steel mesh cage was used to minimise direct handling of the samples (Khurma et al., 2005). Using this cage led to more reproducible data.

The swelling response of G-Ch-PVP gels after equilibration for 24 h was evaluated as a function of pH with both phosphoric acid and sodium hydroxide (Figure 4.12) according to the method in Section 3.10.5. The data collected are an average of three trials and the error bars represent the standard error. It is clear that upon decreasing the pH (specifically below 6, which is in agreement with the pKa of chitosan being 6.3-6.6), there is a sharp rise in the swelling ratio of the gels in all solutions. This is most likely due to protonation of the amine functional groups within the network, inducing further electrostatic repulsion between such moieties and resulting in gel swelling. As there is such a large difference in the swelling ratio between pH 6 and 4 (approximately 70%), it would be highly desirable to couple the gel with a reaction that oscillates within this pH range in order to illicit a prominent response from the material. Upon decreasing the pH further (to 2), in all cases the gel does swell, although to a lesser extent (10-20% between pH 2 and 4) as the remaining amine groups become protonated. At a neutral pH, minimal gel swelling is observed and this also seems to remain the case up to pH 13. In some cases there may be a slight increase in the swelling ratio as the pH is increased from pH 6, although this is very minor. A possible reason could be the presence of electrostatic repulsions at high pH, leading to gel swelling or hydroxide moieties disrupting

the crosslinked network, which could create more vacancies within the network, aiding diffusion and hence enhancing the degree of swelling.

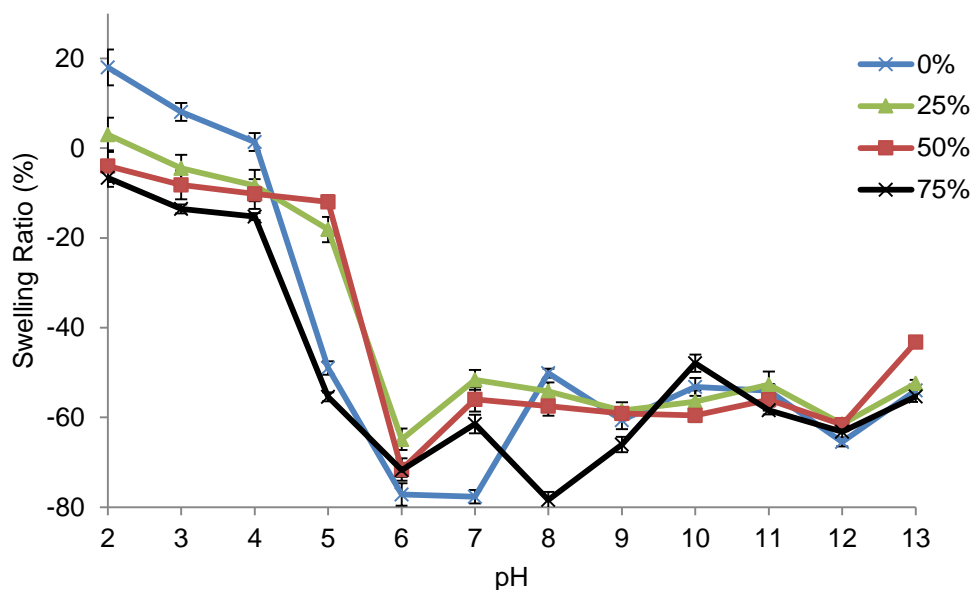


**Figure 4.12** Gravimetric swelling measurements of G-Ch-PVP hydrogels synthesised at 37 °C. Gels were immersed in various mixtures of phosphoric acid and sodium hydroxide solutions that were either unmodified or adjusted with sodium chloride to a higher ionic strength (25%, 50% and 75%) and monitored at 37 °C.

Upon comparing the effect of varying the ionic strength on the hydrogel swelling ratio (Figures 4.12 and 4.13), at low pH, it is clear that a higher ionic strength, results in a lower degree of gel swelling. This is most likely due to the increased development of ionic atmospheres, enhancing the amount of charge screening, which results in a decrease in the ionic Coulomb potential (and hence charge distribution within the network). This would in turn lower the Donnan potential (electrical potential between the gel and the surrounding buffered solution), decreasing the exerted osmotic pressure and resulting in a lower overall swelling ratio. This trend is not observed at a higher pH and could be due to the lack of charged species present part of the gel framework (e.g.  $-\text{NH}_3^+$  groups would be  $-\text{NH}_2$  at higher pH).

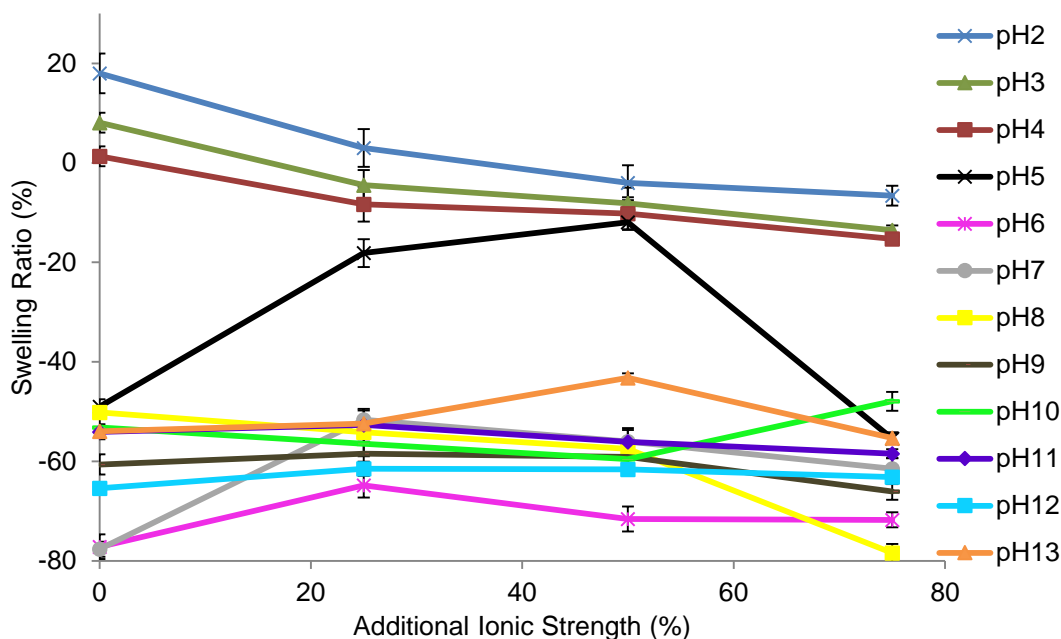


**Figure 4.13** The effect of ionic strength of the surrounding buffer solution during gravimetric swelling measurements of G-Ch-PVP hydrogels synthesised at 37 °C. Gels were immersed in various mixtures of phosphoric acid and sodium hydroxide solutions that were either unmodified or adjusted with sodium chloride to a higher ionic strength (25%, 50% and 75%) and monitored at 37 °C.

The aforementioned experiment was repeated using citric acid and sodium hydroxide to form the buffer solutions (Figure 4.14). Citric acid is weaker than phosphoric acid (first pKa is 3.13 compared to 2.15 for phosphoric acid), although the second and third pKa values are 4.76 and 6.39 for citric acid compared to 7.20 and 12.32 for phosphoric acid. Not all buffer solutions could be successfully made (e.g. pH 8-13 with an additional 75% ionic strength) due to the sodium chloride not dissolving in the citric acid and sodium hydroxide mixture. A similar trend was observed with the majority of gel swelling occurring at low pH with the swelling ratio beginning to increase at pH 6 and climbing constantly. This is unlike when the gels were previously immersed in phosphoric acid based solutions whereby after pH 4 there was a steady decrease in the degree of swelling observed. This may be due to the pKa values of citric acid all being within a low and narrow range (3.13, 4.76 and 6.39). In agreement with the gels immersed in phosphoric acid based solutions, an increase in the swelling ratio is observed in very high pH, which again may suggest disruption of the network by sodium hydroxide.

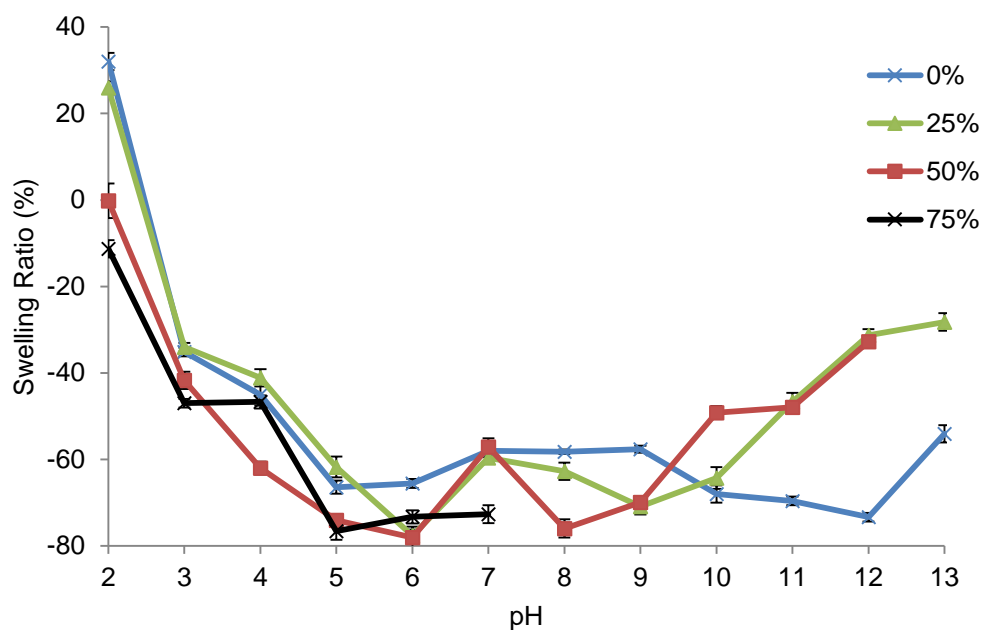


**Figure 4.14** Gravimetric swelling measurements of G-Ch-PVP hydrogels synthesised at 37 °C. Gels were immersed in various mixtures of citric acid and sodium hydroxide solutions that were either unmodified or adjusted with sodium chloride to a higher ionic strength (25%, 50% and 75%) and monitored at 37 °C.

Finally, the effects of varying ionic strength on the gel swelling ratio (Figure 4.14 and 4.15) are consistent with those observed with phosphoric acid based buffer solutions where a higher ionic strength tends to result in a lower swelling ratio. This is again particularly prevalent at lower pH values where the gel is swollen owing to electrostatic repulsion.

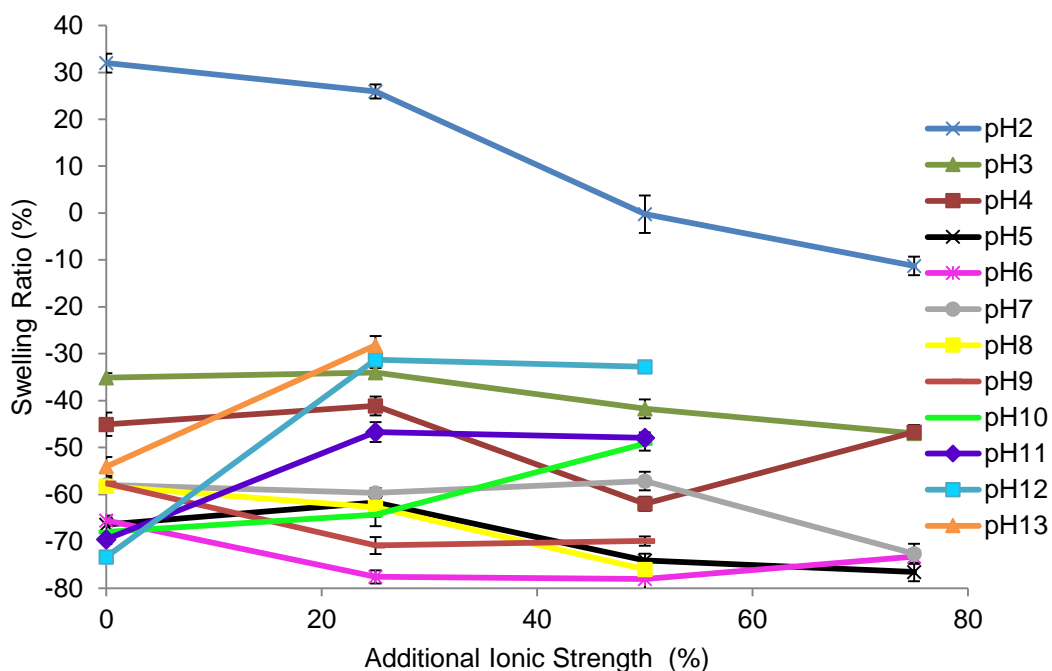


**Figure 4.15** The effect of ionic strength of the surrounding buffer solution during gravimetric swelling measurements of G-Ch-PVP hydrogels synthesised at 37 °C. Gels were immersed in various mixtures of citric acid and sodium hydroxide solutions that were either unmodified or adjusted with sodium chloride to a higher ionic strength (25%, 50% and 75%) and monitored at 37 °C.

#### 4.8 Utilising Fourier-Transform Infrared spectroscopy to study the protonation and deprotonation of network moieties

In an attempt to understand how the aforementioned swelling behaviour arises from changes to the network on the atomic/molecular level, a study of the protonation/deprotonation of gel constituents using FTIR has been conducted. Ahead of this, aqueous solutions of individual gel constituents together with citric acid were analysed to determine the functional groups present. The FTIR spectra of chitosan, PVP, genipin and citric acid (Figures A3-A7) together with spectral assignment (Tables A2-4) are shown in the Appendix.

FTIR spectra were collected of all the samples in Figure 4.14 where gel specimens were equilibrated for 24 h in solutions of citric acid and sodium hydroxide, which were tailored to be of customisable ionic strength with sodium chloride according to Table 3.6., The N-H stretch of chitosan at approximately  $3300\text{ cm}^{-1}$  (Table A2) is the most appropriate spectral feature to examine during a protonation/deprotonation study of the gel network (Figure 4.16).

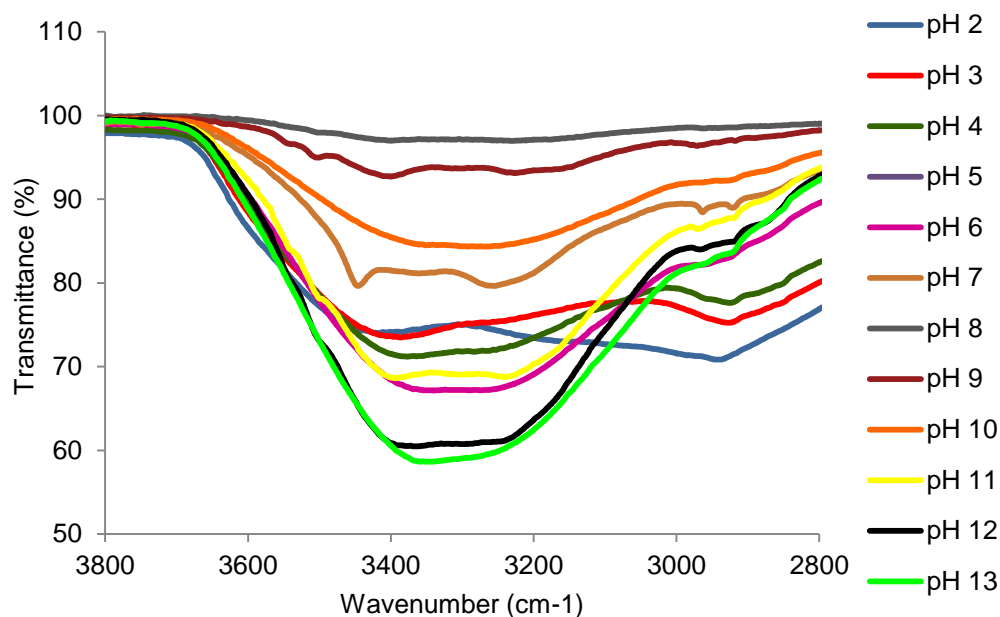


**Figure 4.16** FTIR spectrum of G-Ch-PVP hydrogels immersed in various mixtures of citric acid and sodium hydroxide solutions with an unmodified ionic strength (0%).

Following normalisation to a peak at  $1078\text{ cm}^{-1}$  that was unaffected by deprotonation, the data was analysed for variation in transmittance (Figure 4.17) and wavenumber of the N-H stretch (Figure 4.18) as a function of pH. Buffer solutions with four different ionic strengths were used in each case. It is noteworthy that throughout analysis, the O-H stretches made it difficult to interpret the position of the N-H stretch. From the transmittance data, unfortunately no clear trends could be observed linking transmittance to pH in all of the solutions tested. This was the same case when investigating if the N-H stretch had been blue-shifted following protonation, although once again no clear trends could be concluded from the data (Figure 4.18).

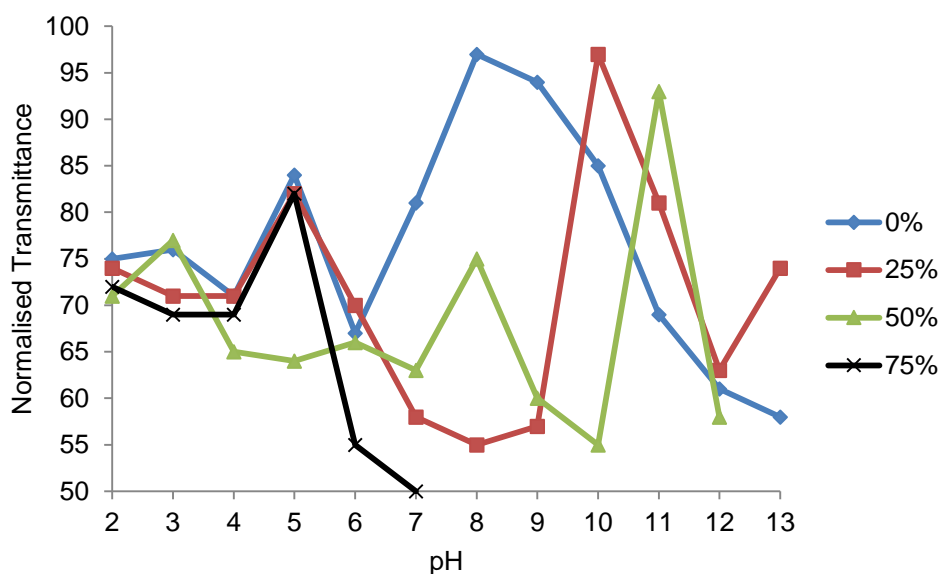


**Figure 4.17** Normalised transmittance at  $3300\text{ cm}^{-1}$  of G-Ch-PVP hydrogels immersed in various mixtures of citric acid and sodium hydroxide solutions that were either unmodified or adjusted with sodium chloride to a higher ionic strength (25%, 50% and 75%).

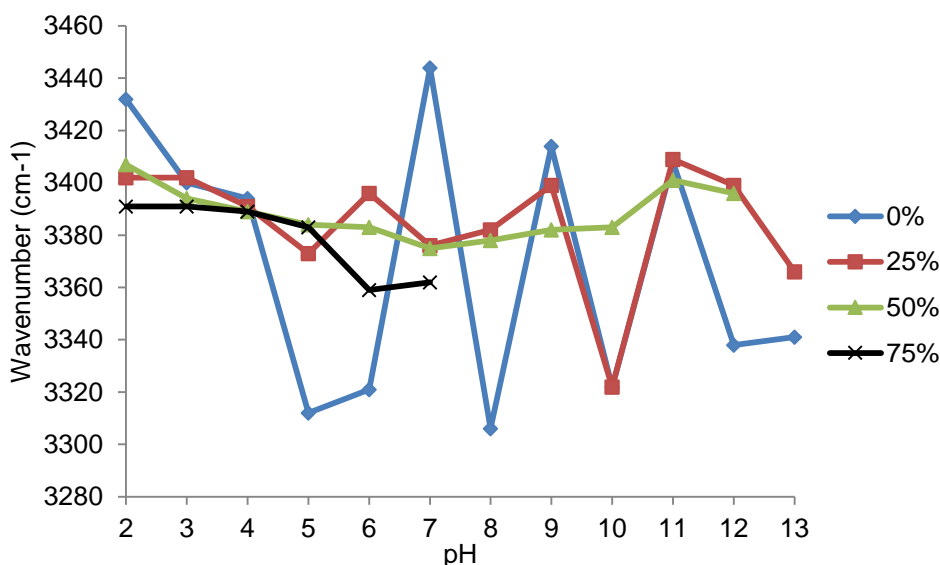


**Figure 4.18** Variation in the wavenumber recorded of the band between  $3450\text{-}3300\text{ cm}^{-1}$  of G-Ch-PVP hydrogels immersed in various mixtures of citric acid and sodium hydroxide solutions that were either unmodified or adjusted with sodium chloride to a higher ionic strength (25%, 50% and 75%).

In conclusion, the FTIR data collected for citric acid and sodium hydroxide investigations could not be correlated with gravimetric swelling behaviour. An FTIR protonation/deprotonation study was then conducted for phosphoric acid

and sodium hydroxide mixtures to explore further as to whether a link between protonation and swelling behaviour could be established. The FTIR spectrum of phosphoric acid was recorded and is depicted in the Appendix (Figure A7).

The results of the protonation/deprotonation study with phosphoric acid and sodium hydroxide-based solutions as the surrounding solvent were not positive and no discernible trends could be deduced in terms of variation in the position of the N-H band, the intensity of the band or ionic strength effects. Figure 4.19 shows how the transmittance at  $3300\text{ cm}^{-1}$  varies as a function of pH while Figure 4.20 shows how the position of the band between  $3500\text{-}3100\text{ cm}^{-1}$  (N-H stretch overlapping with O-H stretch) varied as a function of pH. Unfortunately, no meaningful conclusions could be drawn from these datasets.

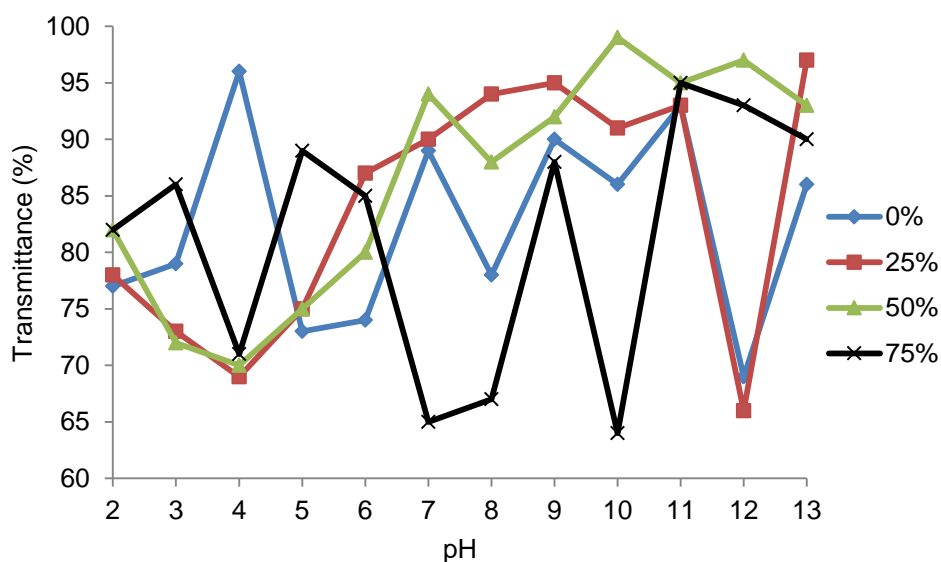


**Figure 4.19** Normalised transmittance at  $3300\text{ cm}^{-1}$  of G-Ch-PVP hydrogels immersed in various mixtures of phosphoric acid and sodium hydroxide solutions that were either unmodified or adjusted with sodium chloride to a higher ionic strength (25%, 50% and 75%).

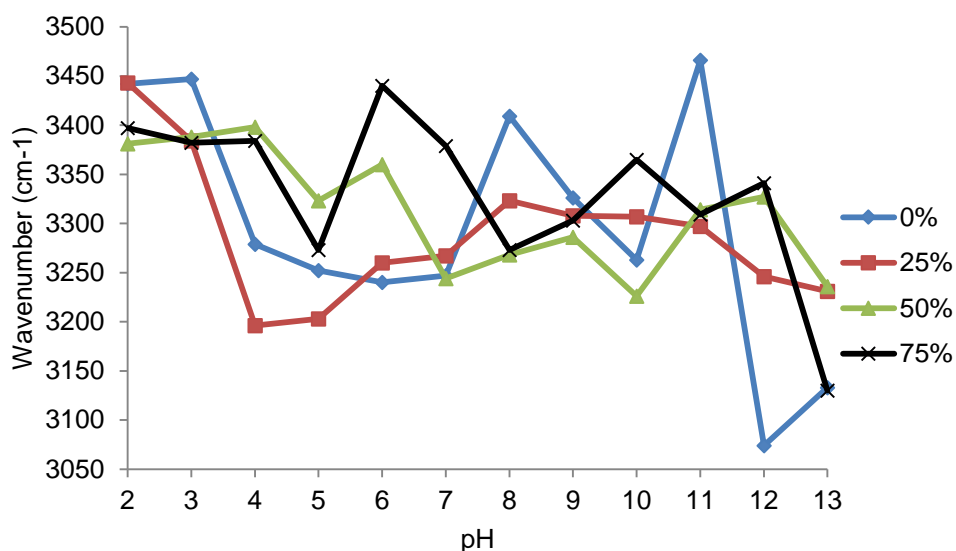


**Figure 4.20** Variation in the wavenumber recorded of the band between 3450-3100  $\text{cm}^{-1}$  of G-Ch-PVP hydrogels immersed in various mixtures of phosphoric acid and sodium hydroxide solutions that were either unmodified or adjusted with sodium chloride to a higher ionic strength (25%, 50% and 75%).

#### 4.9 Utilising optical microscopy to study gel morphology as a function of pH

In an attempt to link swelling behaviour to the porous structure, optical microscopy images were taken of gels immersed in 0% additional ionic strength citric acid/phosphoric acid with sodium hydroxide mixtures. This was performed according to the method outlined in Section 3.8. Examples of the porous architecture of G-Ch-PVP hydrogels immersed in citric acid and sodium hydroxide-based solutions are shown in Figure 4.21 revealing an open cell foam type structure.

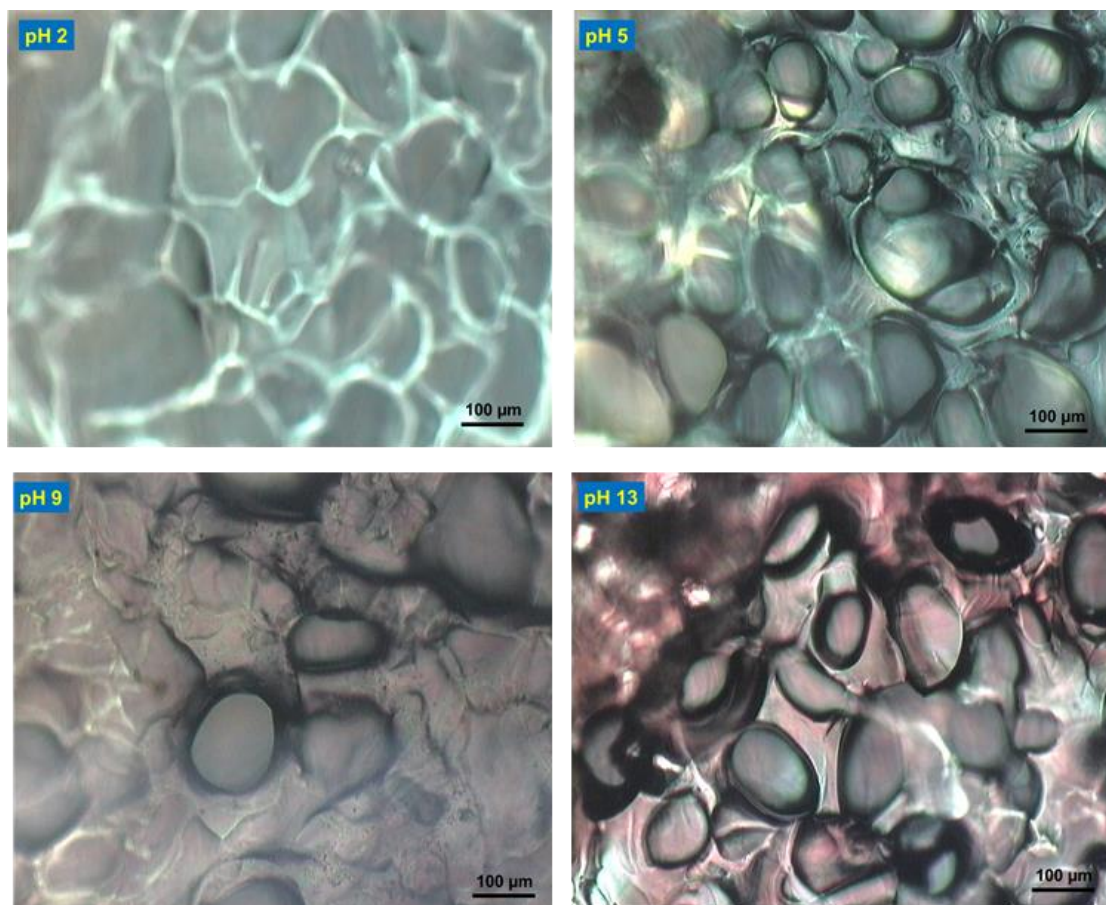


**Figure 4.21** Representative optical microscopy images of G-Ch-PVP hydrogels immersed in solutions of varying pH consisting of citric acid and sodium hydroxide mixtures.

The surface porosity of hydrogel samples was determined from the images collected via optical microscopy using ImageJ and is portrayed in Table 4.6.

**Table 4.6** Surface porosities of G-Ch-PVP hydrogels immersed in either citric acid or phosphoric acid-based solutions in combination with sodium hydroxide. Values were determined using ImageJ.

pH	Surface porosity in citric acid-based solutions (%)	Surface porosity in phosphoric acid-based solutions (%)
2	56.1	41.3
3	36.1	31.7
4	45.9	22.7
5	34.3	18.6
6	22.1	11.9
7	24.4	11.4
8	15.3	9.1
9	11.3	2.5
10	6.6	10.9
11	13.5	13.2
12	16.9	18.5
13	21.4	23.8

The data in Table 4.6 is represented graphically in Figure 4.22. In agreement with the gravimetric swelling behaviour data as the pH is increased from 2, the surface porosity decreases, hence limiting diffusion into the network due to a reduced number of protonated amine groups and aggregation of PVP moieties. This results in gel collapse. Furthermore, also in accordance with gravimetric studies the initial surface porosity of the gels immersed in citric acid at pH 2 (56.1%) is significantly higher than the counterpart submerged in phosphoric acid-based solutions (41.3%). This aligns well with a 35% swelling ratio in citric acid compared to approximately 20% in phosphoric acid, although as phosphoric acid is stronger than citric acid (with a pKa of 2.15 compared to 3.13), it is surprising that the swelling behaviour and surface porosity are not in reverse. However, the ionic strength of each of the pH 2 0% solutions must be considered. As the ionic strength of the citric acid-based solution is just 0.21 mol kg<sup>-1</sup> compared to the phosphoric acid-based solution at 0.92 mol kg<sup>-1</sup> (Tables 3.5 and 3.6), the citric-acid based solution will have a higher Donnan potential, leading to a more porous architecture that is able to swell to a greater degree. Furthermore, as the citrate anion is bigger than the phosphate anion, it will have to be accommodated in the swollen gel, which will also lead to a greater degree of swelling. Finally, also in agreement with the gravimetric swelling behaviour, the surface porosity increases at high pH (over 10 in both cases). There is some indication from the swelling studies that this may also be reflected on the macroscale.

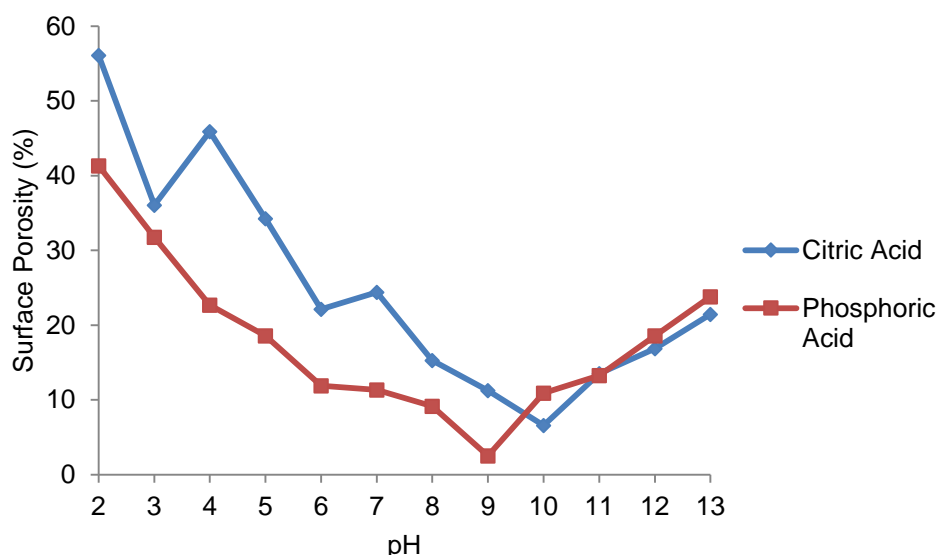


**Figure 4.22** Surface porosity of G-Ch-PVP hydrogels as a function of pH immersed in citric acid and phosphoric acid-based solutions in combination with sodium hydroxide.

#### 4.10 Study to determine the dependence of pH on fluorescence

Finally, a study was conducted to investigate as to whether there is an effect on the fluorescence spectra of G-Ch-PVP hydrogels upon varying the pH. The excitation and emission spectra for a G-Ch-PVP hydrogel directly following synthesis are shown in Figure 4.23. This was conducted according to the method in Section 3.5. In the excitation spectrum, the emission wavelength was set to 462 nm and the wavelength of the excitation maximum was 380 nm. Similarly, in the emission spectrum, the excitation wavelength was set to 360 nm with a wavelength of the emission maximum at 440 nm.

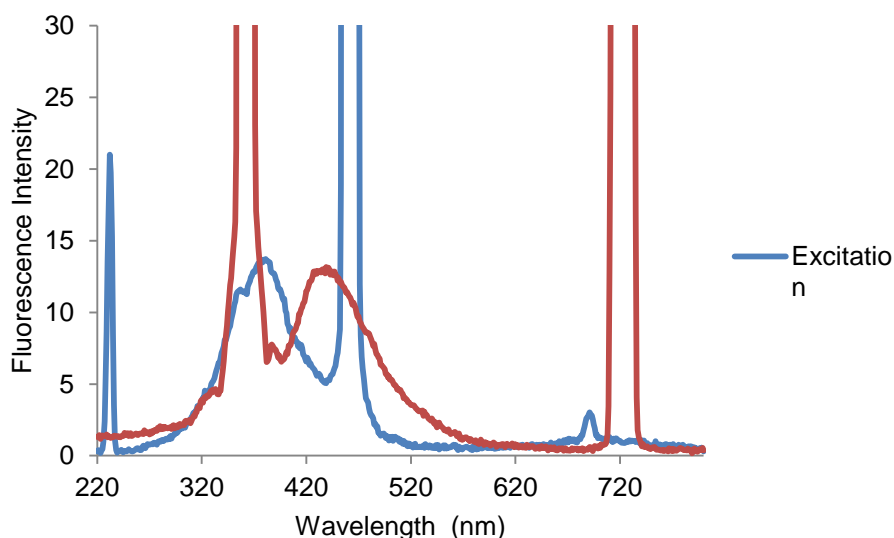


**Figure 4.23** Excitation and emission spectra of a G-Ch-PVP hydrogel.

Excitation and emission spectra were recorded as a function of the pH of the solution the gel had been equilibrated in. The variation in the excitation spectra of the citric acid and sodium hydroxide-based solutions is shown in Figure 4.24. Clearly as the pH changes there is no discernible variation in the maximum excitation wavelength. There also appears to be no trend in terms of the fluorescence intensity of the samples, although this is not unexpected as it was very difficult to examine all samples at the same thickness.

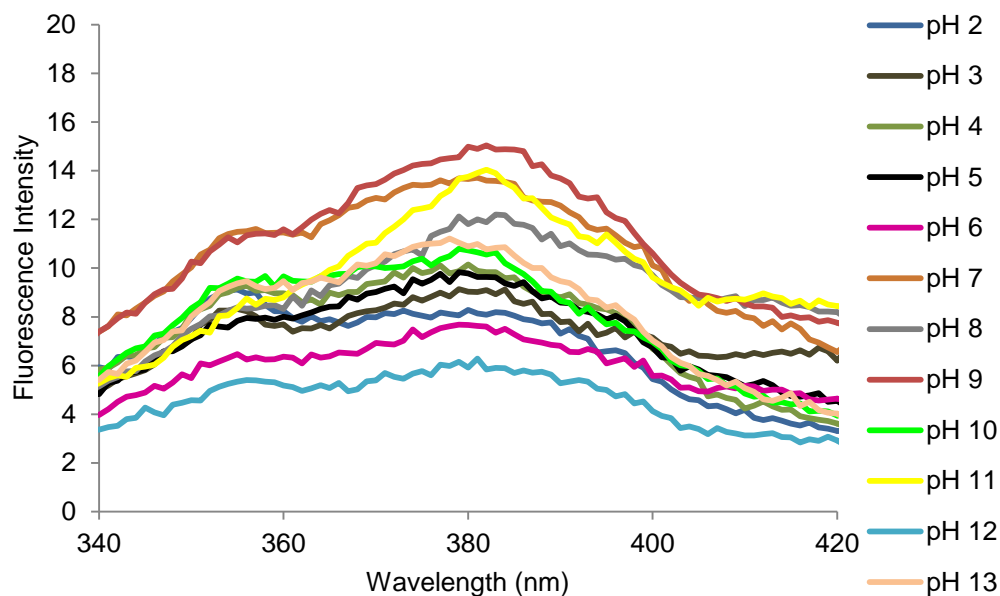


**Figure 4.24** Excitation spectra at 380 nm of G-Ch-PVP hydrogels as a function of pH immersed in citric acid solutions in combination with sodium hydroxide.

Similarly, the change in the emission spectra of the citric acid and sodium hydroxide-based solutions is shown in Figure 4.25. Akin to the excitation spectra, a variation in pH does not shift the maximum emission wavelength in a predictable manner nor is there a trend in terms of fluorescence intensity observed.

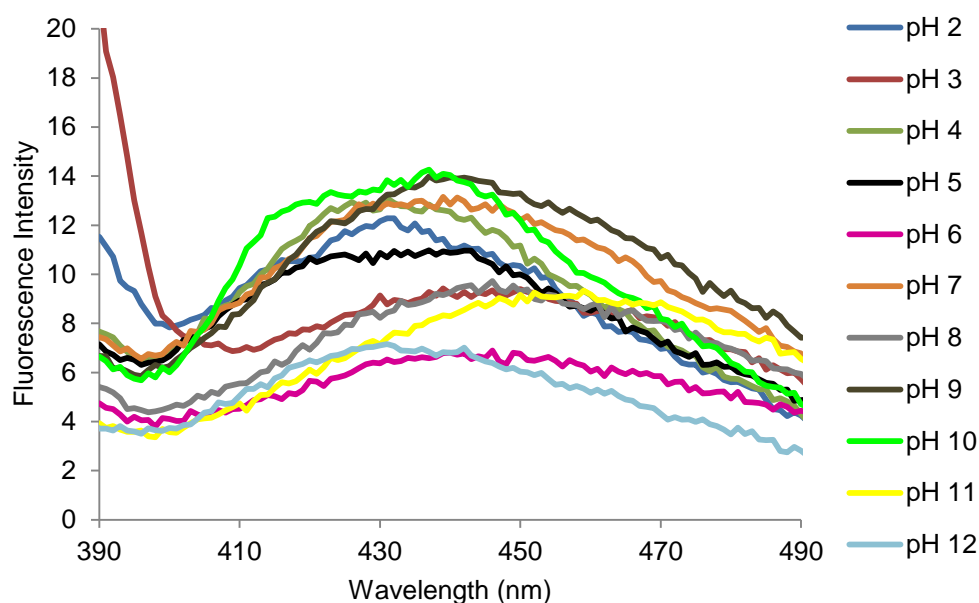


**Figure 4.25** Emission spectra at 440 nm of G-Ch-PVP hydrogels as a function of pH immersed in citric acid solutions in combination with sodium hydroxide.

There was also no observable shift in the excitation or emission spectra when G-Ch-PVP hydrogels immersed in phosphoric acid and sodium hydroxide-based solutions were investigated. The maximum emission and excitation wavelengths for the gels in each of the solutions as a function of pH are shown in Table 4.7. It can therefore be concluded that pH does not affect the fluorescence of G-Ch-PVP hydrogels to a significant extent.

**Table 4.7** Maximum excitation and emission wavelengths collected according to the method in Section 3.5 when G-Ch-PVP hydrogels immersed in citric acid or phosphoric acid-based solutions in combination with sodium hydroxide.

pH	Citric acid and sodium hydroxide-based solutions		Phosphoric and sodium hydroxide-based solutions	
	Maximum excitation wavelength (nm)	Maximum emission wavelength (nm)	Maximum excitation wavelength (nm)	Maximum emission wavelength (nm)
2	377	428	377	442
3	377	435	376	436
4	376	428	380	442
5	381	430	382	441
6	381	439	379	425
7	376	433	380	428
8	381	440	378	424
9	378	436	379	442
10	378	433	378	435
11	379	450	378	426
12	377	426	380	440
13	379	-	379	439

#### 4.11 Combination of chitosan and genipin with simple compounds to determine the behaviour of individual gel components

In order to investigate all gel components as a function of pH they were reacted with simple compounds according to the method in Section 3.1.1. Prior to this, the FTIR spectra of chitosan, PVP and genipin immersed in hydrochloric acid or sodium hydroxide-based solutions at pH 2 or 13 were recorded and compared. Chitosan is shown in Figure 4.26 and the spectra compare well with unmodified chitosan depicted in Figure A3. There seems to be a minimal shift in the wavenumbers of notable peaks, although the transmittance of the C-O-C stretch of the sample immersed in a pH 13 solution is greater than its counterpart.

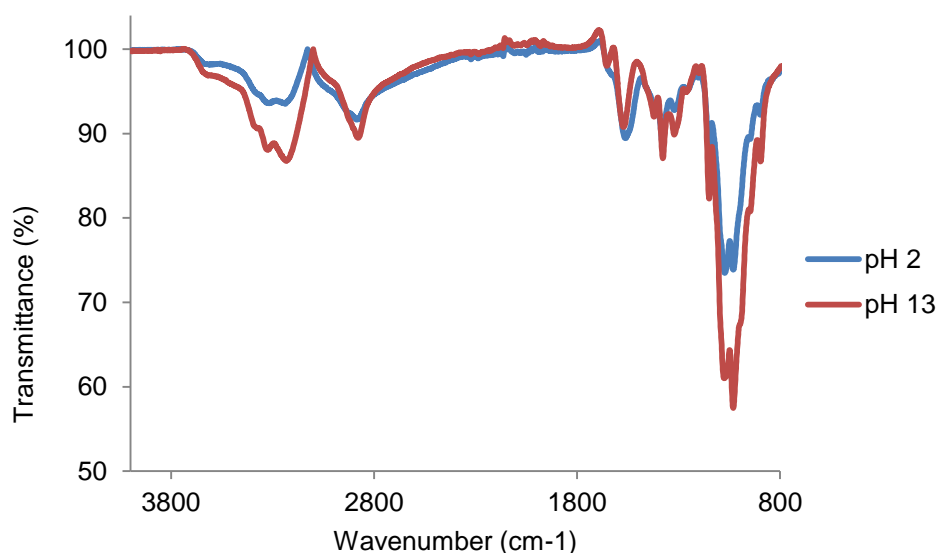


**Figure 4.26** FTIR spectra of chitosan immersed in a pH 2 and a pH 13 solution of mixtures of hydrochloric acid and sodium hydroxide.

Similarly the FTIR spectra of PVP in each of the pH 2 and pH 13 solutions do not differ considerably from one another (Figure A8) and show the same spectral features as untreated PVP (Figure A4). Unfortunately, no meaningful spectra could be collected for genipin immersed in each of the pH solutions and it was exceedingly difficult to assign the spectra (Figure A9).

Chitosan was reacted with ethyl acetate. The spectrum for ethyl acetate is shown in Figure A10 with the accompanying spectral assignment in Table A5. The FTIR spectra recorded upon combination of chitosan and ethyl acetate according to the method described in Section 3.1.1 is shown in Figure 4.27.

Upon examination it is difficult to deduce the position of the N-H stretch due to overlap with the O-H stretch.

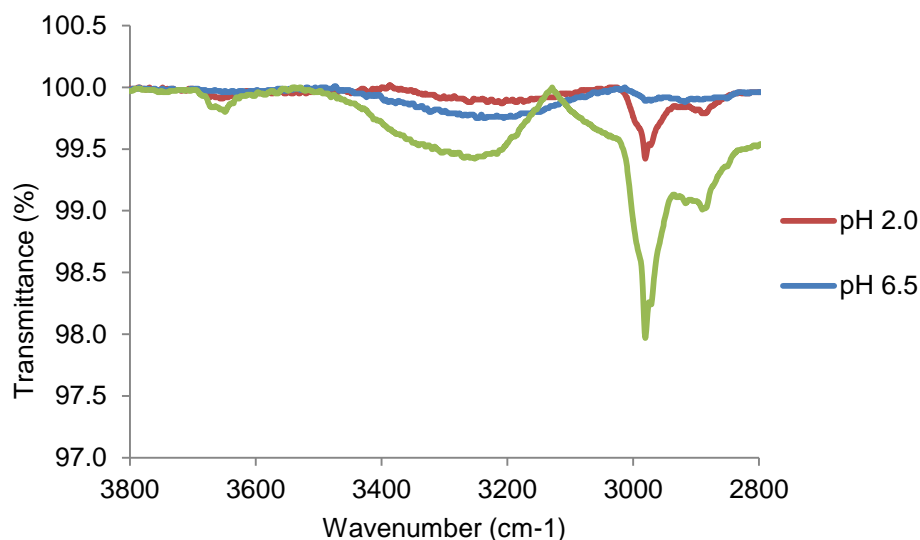


**Figure 4.27** FTIR spectra of chitosan in combination with ethyl acetate followed by immersion in various hydrochloric acid and sodium hydroxide-based buffer solutions.

Finally, genipin were reacted with n-butylamine (Figure A11 and Table A6) in place of chitosan according to the method in Section 3.1.1. PVP was not reacted with n-butylamine, as this is a physical crosslinking polymer and does not form covalent bonds with the network. The FTIR spectra of genipin reacted with n-butylamine immersed in acidic and alkaline pH buffer solutions (hydrochloric acid and sodium hydroxide-based) is shown in Figure 4.28. As with chitosan, much of the absorption bands are similar in pH 2.0, 6.5 and 12.0. In conclusion, it has also proven difficult to study the protonation and deprotonation of individual gel components via FTIR. It is most likely this is due to strong overlap of the N-H stretch with the O-H stretch.

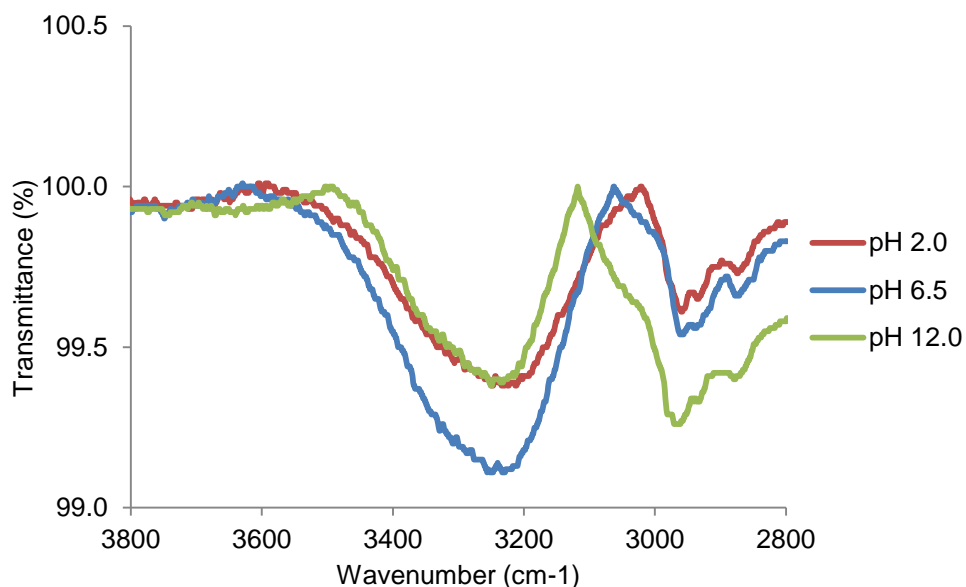


**Figure 4.28** FTIR spectra of genipin in combination with n-butylamine followed by immersion in various hydrochloric acid and sodium hydroxide-based buffer solutions.

The excitation and emission spectra of genipin in combination with n-butylamine were explored according to the method in Section 3.5 (Figure 4.29). In the same way as in the G-Ch-PVP hydrogel neither the excitation nor emission spectra changed significantly as a function of pH, confirming that the emission is not pH sensitive.

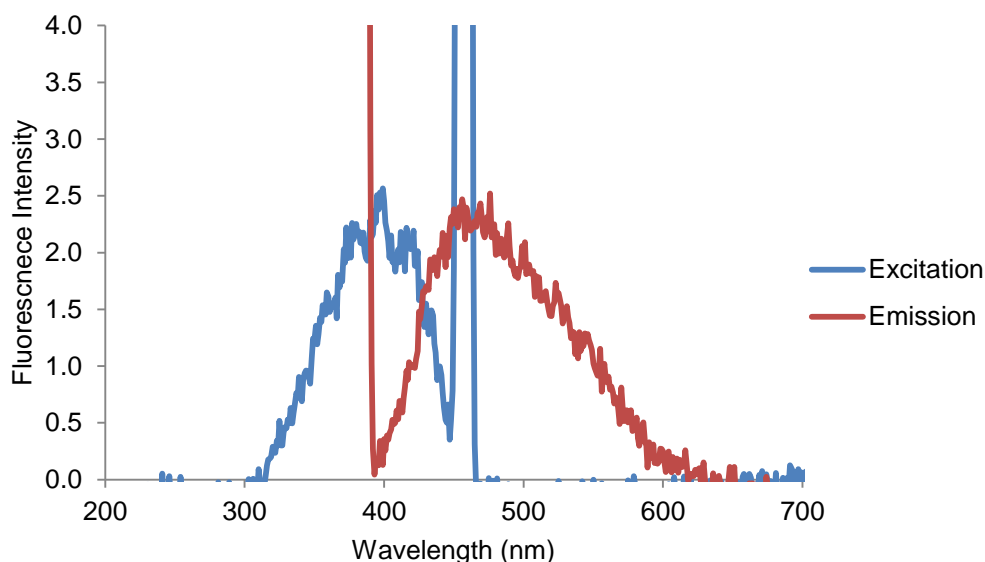


**Figure 4.29** Excitation and emission spectra of a genipin in combination with n-butylamine.

#### 4.12 Further swelling studies to understand gel behaviour

Swelling measurements of hydrogels contained in mesh cages immersed in glycine, phthalate, phosphate and borate buffer solutions (with ionic strength of  $0.36 \text{ mol kg}^{-1}$ ) are depicted in Figure 4.30 where the data collected was collected in the same way as previously as an average of three trials and the error bars represent the standard error. The ionic strength for each of the four buffers is the same and comparatively low (especially at high pH) with respect to citric acid and phosphoric acid. A lower ionic strength at higher pH was chosen in the hope of being able to observe swelling in alkaline conditions and hence be able to make good comparisons between datasets.

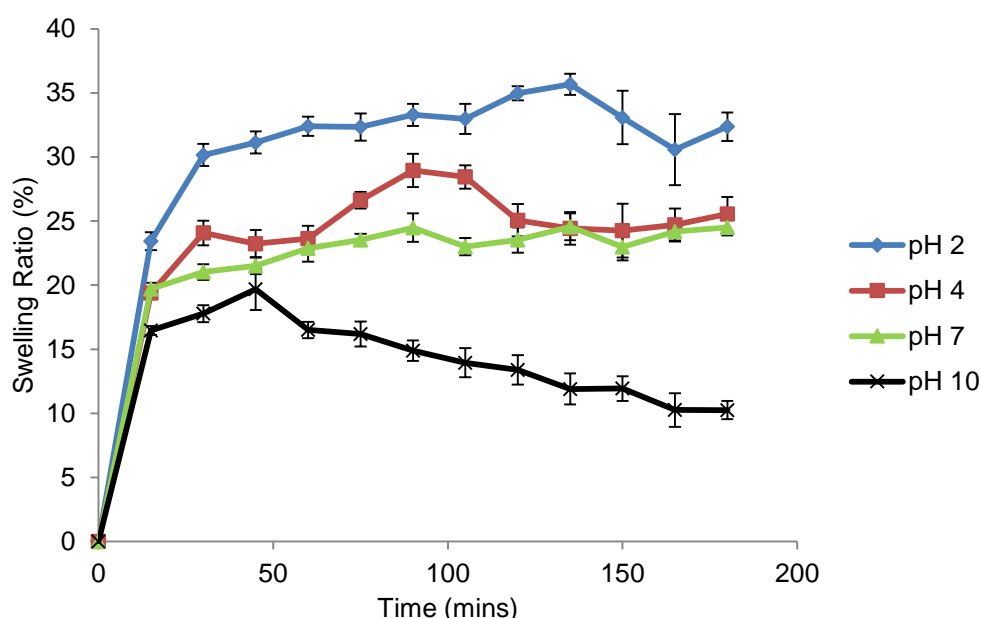


**Figure 4.30** Gravimetric swelling measurements of G-Ch-PVP hydrogels synthesised at  $37^\circ\text{C}$  contained in steel mesh cages immersed in various buffers at  $37^\circ\text{C}$ .

In good agreement with the published literature (Risbud et al., 2000, Khurma et al., 2005), pH dependent behaviour is observed and the degree of swelling increases when hydrogels are immersed in increasingly acidic media; the reasons for which have been previously detailed. As all four solutions have a lower ionic strength than those previously tested in citric and phosphoric acid-based solutions, this may explain as to why, for instance, swelling is observed when gels were immersed in pH 7 phosphate and pH 10 borate solutions compared to the aforementioned data. A plateau shape indicates that equilibrium has been reached. However, a significant reduction in mass has occurred, particularly for gels that were immersed in extreme pH environments

such as 2 and 10. This may be due to corrosion of the mesh cage. Significant rusting will affect the precision of the mass measurements and also contaminate both the hydrogel samples and buffer solutions. This could be mediated by using a plastic such as PTFE to make a cage. This was subsequently implemented as discussed later in this section. Owing to the mesh-structure of the cage, it was very difficult to remove excess buffer liquid from the container during transfer to the weighing scales. The large error bars (some in excess of 5% in total) further demonstrate low precision, potentially due to sample fragmentation, which made it even more difficult to ascertain what the equilibrium values were.

The previous experiment was repeated where samples were placed in an oven at 50 °C for 24 hours. Owing to extensive sample fragmentation, it was exceptionally difficult to record swelling measurements. It is apparent that incubating at such high temperatures destroys the network structure, resulting in synthesis of samples with very low apparent viscosity and poor stability. This agrees with the results collected using UV-Vis spectrometry as per Figures 4.3. and 4.4. In an attempt to further investigate the temperature dependence of the surrounding solution on the gravimetric swelling measurements of G-Ch-PVP hydrogels, immersed in the same buffer solutions as in Figure 4.30 but at 10 °C were recorded (Figure 4.31).

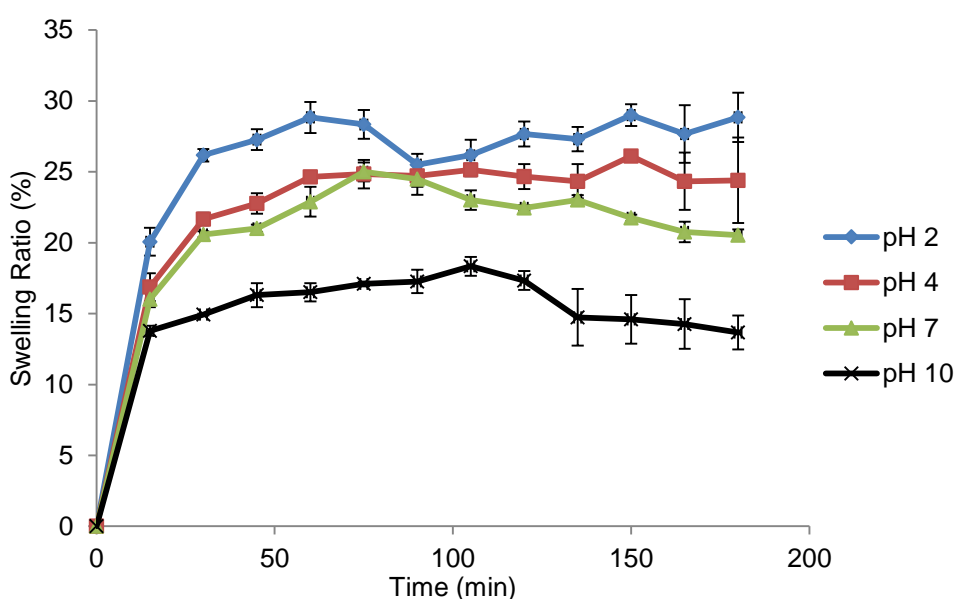


**Figure 4.31** Gravimetric swelling measurements of G-Ch-PVP hydrogels synthesised at 37 °C contained in steel mesh cages immersed in various buffers at 10 °C.

It is clear from Figure 4.32 that the pH dependence observed at 37 °C is still present at 10 °C, although the overall swelling ratio (and certainly the initial degree of swelling) is perhaps slightly lower (Table 4.8). A higher swelling ratio with increasing temperature may be due to dissociation of intra and intermolecular hydrogen bonds between gel constituents, leading to the potential to accommodate more solvent within the network (Khurma et al., 2005).

**Table 4.8** Average gravimetric swelling ratio of G-Ch-PVP hydrogels after being placed in glycine, phthalate, phosphate and borate buffers for 15 min.

Buffer Immersion Temperature (°C)	Buffer pH	Average Swelling Ratio after 15 min (%)
10	2	20
	4	17
	7	16
	10	14
37	2	23
	4	19
	7	20
	10	16

After demonstrating that G-Ch-PVP hydrogels respond differently when placed in various buffered solutions, the smart properties of the networks were subsequently evaluated with the aim to couple to reactions that oscillate in pH. Such chemical reactions often exhibit pronounced pH changes (for example the BSF reaction can be made to oscillate approximately between pH 2.5 and 6 with a time period of 20-25 min (Edblom et al., 1989)). Therefore to test whether G-Ch-PVP hydrogels can respond to changes in an oscillatory environment, samples were placed in an alternate fashion between pH 2 glycine and pH 10 borate buffered solutions (with an ionic strength of 0.36 mol kg<sup>-1</sup>) with a time period of 15 min so that hopefully a pronounced response would be observed (Figure 4.32). These results depict the average swelling ratio of three gels and the associated standard error. The starting point at 0 min was defined at the point at which the hydrogel was placed in a borate buffer solution following being pre-swollen in a pH 2 glycine buffer.

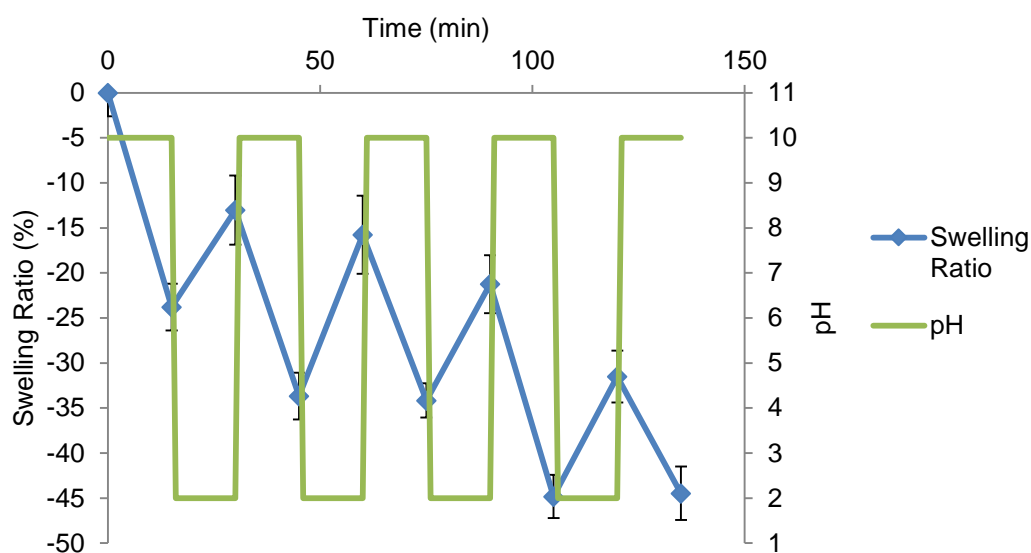


**Figure 4.32** Simulated oscillatory swelling of G-Ch-PVP hydrogel (blue line) alternately immersed in pH 2 glycine buffer and pH 10 borate buffer (green line) with a time period of 15 min.

Despite there being oscillatory behaviour observed, there is a significant reduction in the mass of the hydrogel over time due to aforementioned fragmentation issues with the steel mesh cage. A cage composed of PTFE was subsequently used to transfer samples from buffer media to weighing scales. This prevented any rusting in harsh pH conditions and as it does not have a mesh-structure, the cage could be easily drained of excess fluids. Furthermore, it is apparent from preliminary SEM testing and swelling studies that the gel in its current formulation does not exhibit adequate stability and is susceptible to fragmentation when placed in its target environment. There are two obvious and facile methods to enhance such properties. The amount of genipin can be increased, leading to a more highly crosslinked network or the amount of PVP can be decreased, producing a more hydrophobic gel. If either of the methods is employed, it is true that the mechanical properties will improve, although the swelling degree will suffer (because the network will have smaller / fewer pores owing to more crosslinking agent or the gel will be less hydrophilic and therefore be capable of absorbing a lower amount of fluid). As genipin is relatively expensive (25 mg / £67.00 Aldrich Chemicals U.K.), it is preferable to reduce PVP content. Therefore the subsequent gel formulation in this section is comprised of 1 mL chitosan (1.5% w/v), 200  $\mu$ L PVP (5% w/v) and 100  $\mu$ L genipin (0.5% w/v).

Further to this, it is also advisable to wash hydrogels following gelation to remove unreacted chemical moieties. Methanol was chosen as a suitable washing medium as it is a poor solvent, leading to the preference of polymer-polymer self-interactions, causing the network to collapse (Chen et al., 1999). This was therefore envisaged to be a suitable starting point to observe pH-dependent gel behaviour. At this point the stability of the hydrogels was still too low for the specimens to be washed in water prior to testing. Samples were placed in an oven at 37 °C for 24, 48 and 72 h, washed in methanol for 24 h and subsequently swollen in a pH 2 glycine buffer (Figure 4.33). As expected from prior experiments, in all cases samples increased in network volume in the pH 2 buffered solutions. However, it was observed that the most swelling was exhibited by the gel synthesised in an oven for 24 h, followed by that of 48 h and finally 72 h.

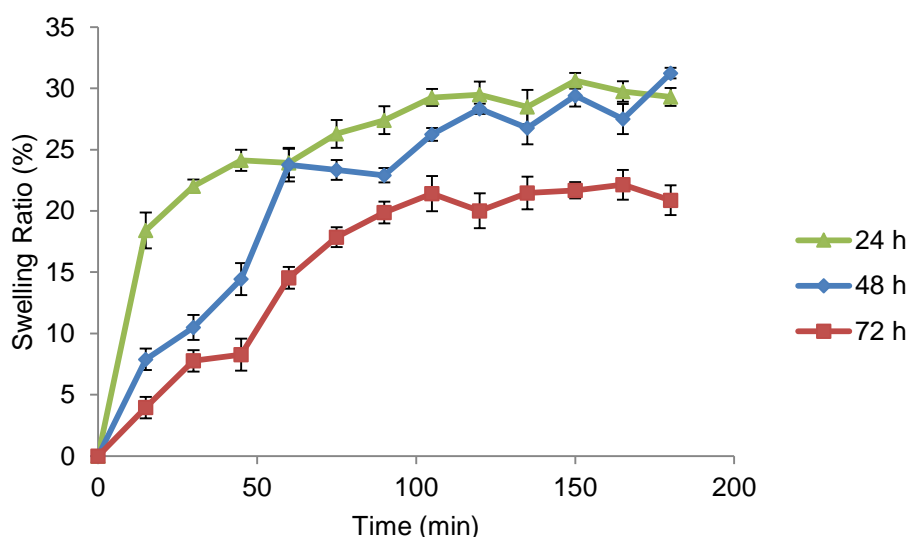


**Figure 4.33** Swelling of G-Ch-PVP hydrogels placed in an oven at 37 °C for various time periods and subsequently washed for 24 h in methanol before being immersed in a pH 2 glycine buffered solution.

The results in Figure 4.33 are in line with the UV-Vis spectroscopy, fluorescence crosslinking and SEM investigations where during longer gelation periods, more crosslinking occurs, leading to smaller and fewer pores, resulting in a lower swelling degree. To explore this structure activity relationship further, a comparative plot between the rate of swelling in the first 15 min with respect to measurements in Figure 4.33 and the porosities determined via SEM studies (Tables 4.3 and 4.4) was created (Figure 4.34). In both cases (whether surface

or internal porosity data were considered), there is a strong correlation between the porosity and the initial swelling rate whereby as gelation time decreases, porosity (both surface and internal) increases and hence the swelling rate also increases. There is a stronger dependence of porosity on the initial swelling rate when pores on the surface are evaluated ( $R^2$  value of 0.98) as opposed to those internally ( $R^2$  value of 0.87). It is likely that this is because swelling is diffusion-limited and the surrounding solvent will permeate through the pores on the surface of the gel in the first instance.

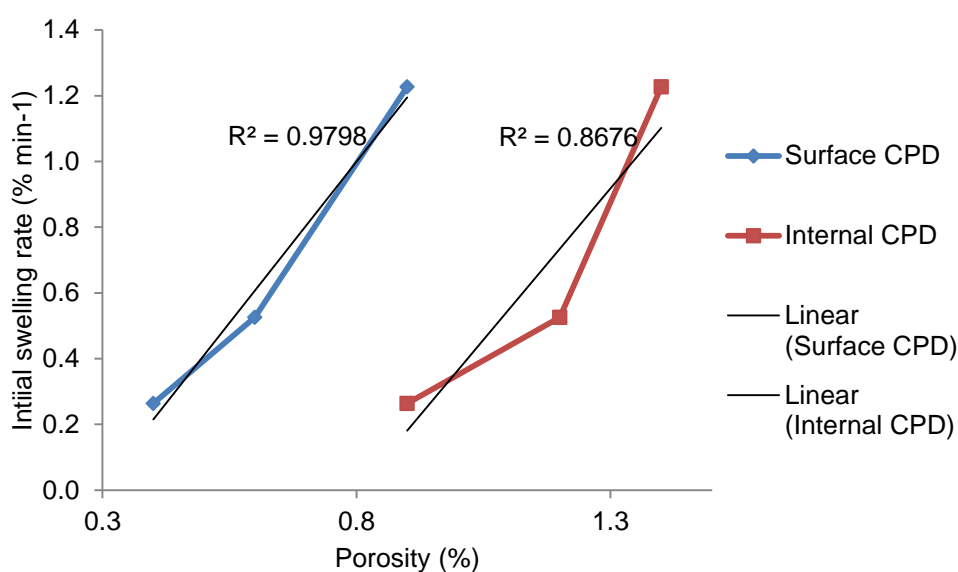


**Figure 4.34** Comparative plot of porosity determined via SEM following CPD with swelling rate during the first 15 min of G-Ch-PVP hydrogels placed in an oven at 37 °C for various time periods and subsequently washed for 24 h in methanol before being immersed in a pH 2 glycine buffered solution.

The previous gravimetric experiment was repeated, although this time gels were immersed in a pH 4 phthalate buffered solution following being washed in methanol for 24 h as depicted in Figure 4.35. The same trend is shown whereby the 24 h specimen is the most responsive followed by that of 48 h and finally 72 h. However, as most clearly depicted for the 24 h sample, there is a decrease in the degree of swelling followed by a recovery. This is indicative of an inhomogeneous gel matrix in terms of the solvent distribution and could be visually seen by a tight and swollen inner core (most likely water-containing) and a severely dehydrated periphery (probably methanol-containing). It is most likely that methanol had permeated firstly into the periphery of the matrix owing to diffusion. This inhomogeneous gel leads to unpredictable swelling. The most

likely explanation is that for the initial 45 minutes the methanol was slowly being exchanged with the buffered solution and for the remainder of the experiment, more phthalate solution was entering the matrix due to protonation of the amine moieties leading to electrostatic repulsion within the network and consequent gel swelling. By the end of the experiment, there was no discernible difference between the periphery and inner part of the gel disc indicating that it had returned to a homogenous state. This initial contraction and subsequent swelling is evident to a lesser extent in samples with a longer gelation time of 48 and 72 h. It is noteworthy that although Figure 4.35 presents a negative swelling ratio for such samples, this is relative to the starting position (after the gel had been immersed in methanol for 24 h). Overall, all the gels are still in a swollen state.

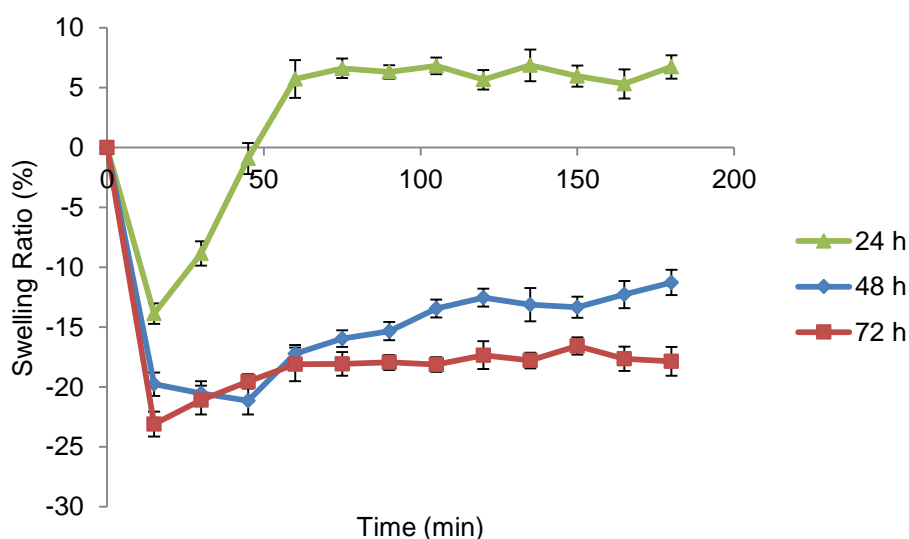


**Figure 4.35** Swelling of G-Ch-PVP hydrogels placed in an oven at 37 °C for various time periods and subsequently washed for 24 h in methanol before being immersed in a pH 4 phthalate buffered solution.

In contrast, when immersed in pH 7 (Figure 4.36) and pH 10 (Figure 4.37) buffered solutions following being washed in methanol for 24 h, no swelling is observed. At pH 7 or 10 the amine groups within the network are not protonated, hence no swelling is observed. It is thought that methanol simply diffuses out of the network and is replaced by the buffered solutions the gels are immersed in, causing the specimens to collapse further.

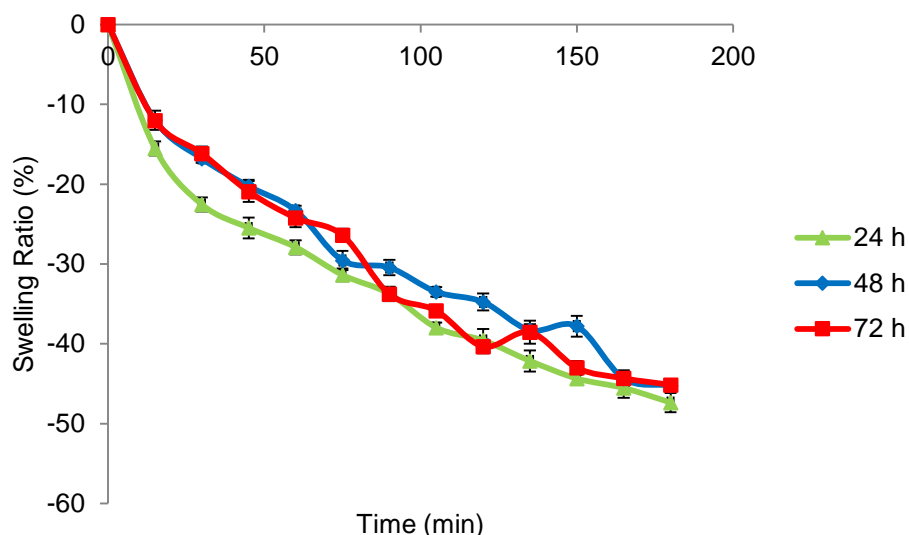


**Figure 4.36** Swelling of G-Ch-PVP hydrogels placed in an oven at 37 °C for various time periods and subsequently washed for 24 h in methanol before being immersed in a pH 7 phosphate buffered solution.

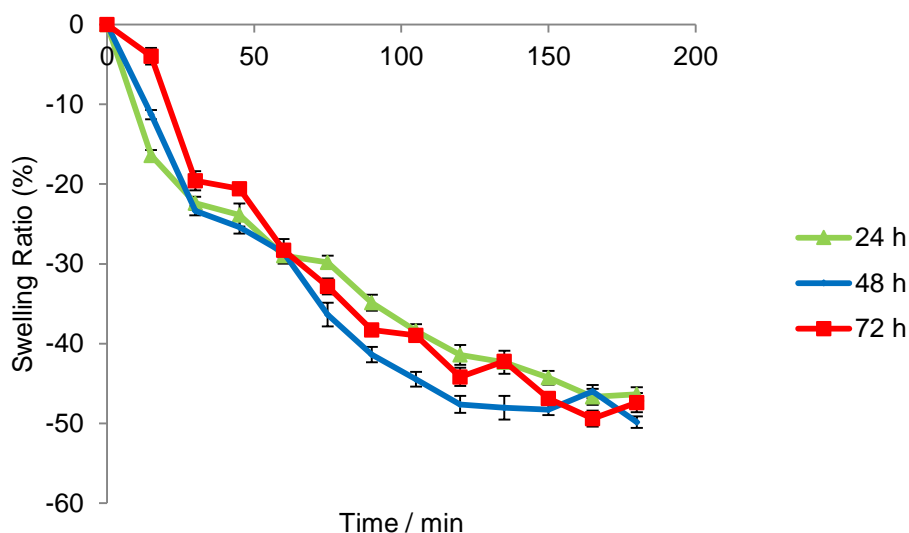


**Figure 4.37** Swelling of G-Ch-PVP hydrogels placed in an oven at 37 °C for various time periods and subsequently washed for 24 h in methanol before being immersed in a pH 10 borate buffered solution.

The same data collected in Figure 4.33 and Figures 4.35-4.37 is plotted showing how the swelling ratio when the gels are immersed in different buffers after being placed in an oven for various time periods at 37 °C is presented in Figures 4.38-4.40. As expected it is clear that when the gelation time is kept constant, the gel swells the most in a pH 2 glycine buffer. This is followed by a gel immersed in a pH 4 phthalate buffer where after an initial collapse, the

network recovers and begins to swell. Comparing Figures 4.39-4.41, it is clear that the gels placed in an oven for the shortest timescale (24 h in Figure 4.38) show the fastest recovery followed by (Figure 4.39) and (Figure 4.40) at 48 h and 72 h respectively. This may be due to the lower amount of crosslinking in the sample placed in an oven for just 24 h, meaning the network is more responsive and can more easily facilitate exchange of methanol with phthalate buffer. Finally, in all cases the gel collapses in phosphate (pH 7) and borate (pH 10) with no discernible difference between either of these buffered environments. This is expected as none of the cationic moieties will be protonated under these conditions, leading to minimal network swelling, and equally there are no anionic functional groups present, hence there is no swelling in an alkaline pH environment. Consequently, the gel is likely to exhibit similar pH-responsive behaviour whether the sample is placed in a neutral or alkaline buffered solution.

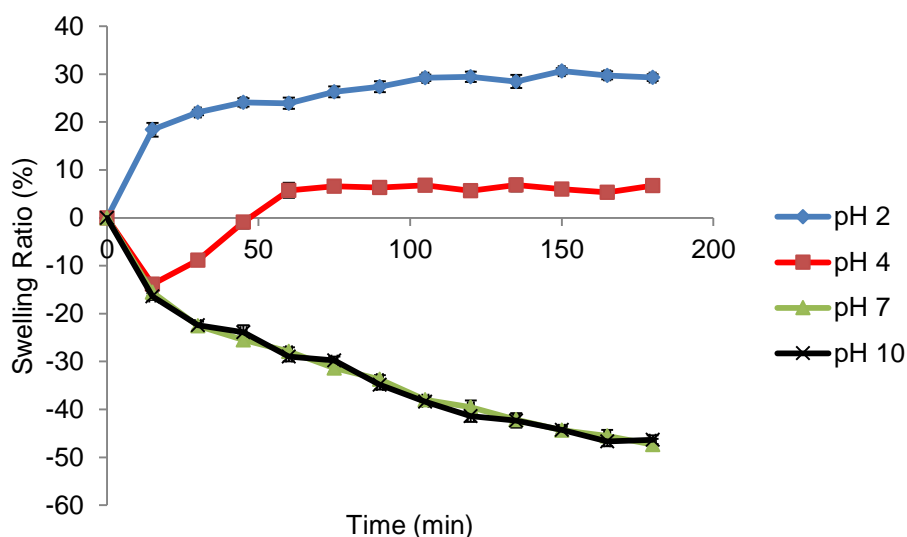


**Figure 4.38** Swelling of G-Ch-PVP hydrogels placed in an oven at 37 °C for 24 h and subsequently washed for 24 h in methanol before being immersed in various buffered solutions.

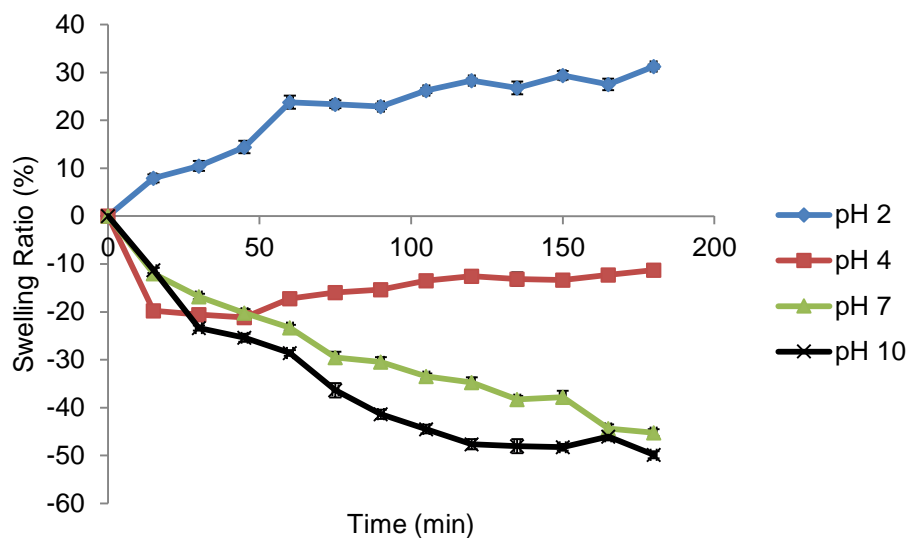


**Figure 4.39** Swelling of G-Ch-PVP hydrogels placed in an oven at 37 °C for 48 h and subsequently washed for 24 h in methanol before being immersed in various buffered solutions.

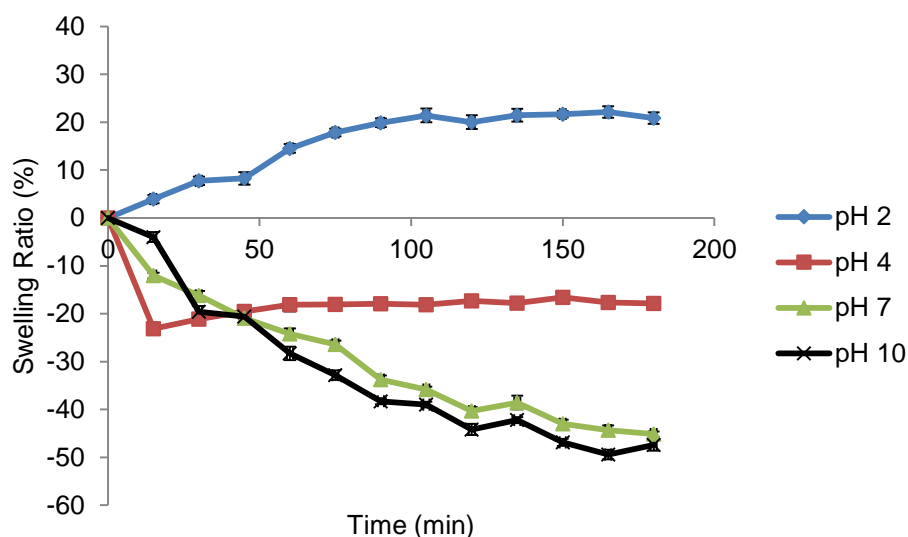


**Figure 4.40** Swelling of G-Ch-PVP hydrogels placed in an oven at 37 °C for 72 h and subsequently washed for 24 h in methanol before being immersed in various buffered solutions.

To determine as to whether an oscillatory response of such methanol-washed hydrogels could be achieved samples were immersed in pH 2 glycine and pH 4 phthalate buffer solutions for 15 min in an alternate fashion (Figures 4.41 and 4.42). Furthermore, considering the metallic moieties present in pH 2 glycine and pH 4 phthalate buffers such as mercuric chloride or monopotassium salts (Tables 3.1 and 3.2), it may be the case that non-reversible interactions

between such metals and gel constituents could form. This could occur via chelation between metal ions and chitosan/PVP moieties. Such behaviour has been exploited for the treatment of polluted water resources (Shawky et al., 2006, Jeon and Höll, 2003). If such non-reversible interactions were to occur, oscillatory swelling behaviour may not be observed.

The hydrogel placed in an oven for 24 h was used for these tests as it was found to be the most responsive. Figure 4.41 illustrates slight oscillatory behaviour where the gel was immersed in a pH 2 buffer solution first and Figure 4.42 shows oscillatory behaviour where the gel was immersed in a pH 4 solution first. Following initial swelling, oscillatory behaviour is observed as the buffer solution is exchanged between the gel matrix and the surrounding fluid, suggesting there is a minimal effect of chelation of gel constituents with buffer components. However, in both cases the gel is swelling as a function of time.

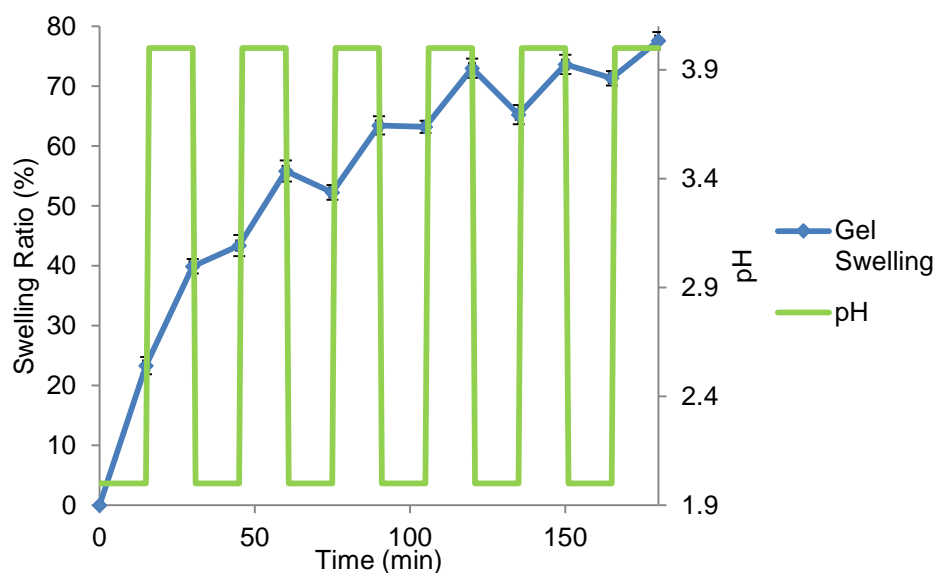


**Figure 4.41** Oscillatory swelling of hydrogels placed in an oven for 24 h at 37 °C, washed in methanol and immersed in a pH 2 glycine buffer first in an alternate fashion with a time period of 15 min at 20 °C.

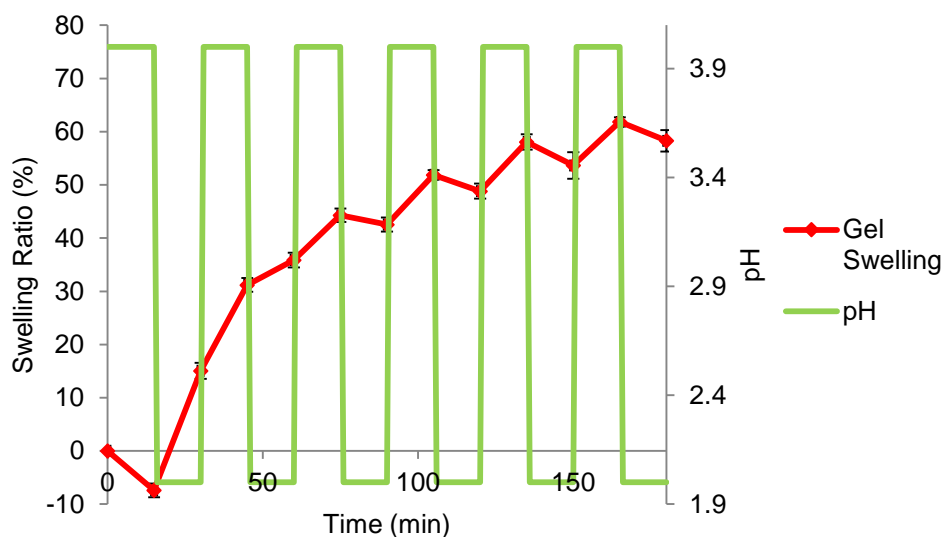


**Figure 4.42** Oscillatory swelling of hydrogels placed in an oven for 24 h at 37 °C, washed in methanol and immersed in a pH 4 phthalate buffer first in an alternate fashion with a time period of 15 min at 20 °C.

As shown in Figures 4.41 and 4.42, it takes approximately 150 min until both gels begin to stabilise in terms of swelling. Therefore in an attempt to elicit an oscillatory response without concomitant network swelling, the time period of oscillations was increased to 150 min (Figures 4.43 and 4.44). In both cases (whether the gel was placed in a pH 2 glycine buffer or a pH 4 phthalate buffer first), after just two alternations of the buffer (approximately 300 min), oscillatory behaviour with minimal overall swelling ensues. This is in comparison to 9-10 alternations when a time period of 15 min is employed (Figure 4.43 and 4.44). However, such a time period of 150 min is quite long to couple to a reaction that oscillates in pH (oscillations in the BSF reaction occur approximately between pH 2.5 and 6 with a time period of 20-25 min (Edblom et al., 1989)). Nonetheless this is an interesting and useful oscillation over a relatively small pH range.

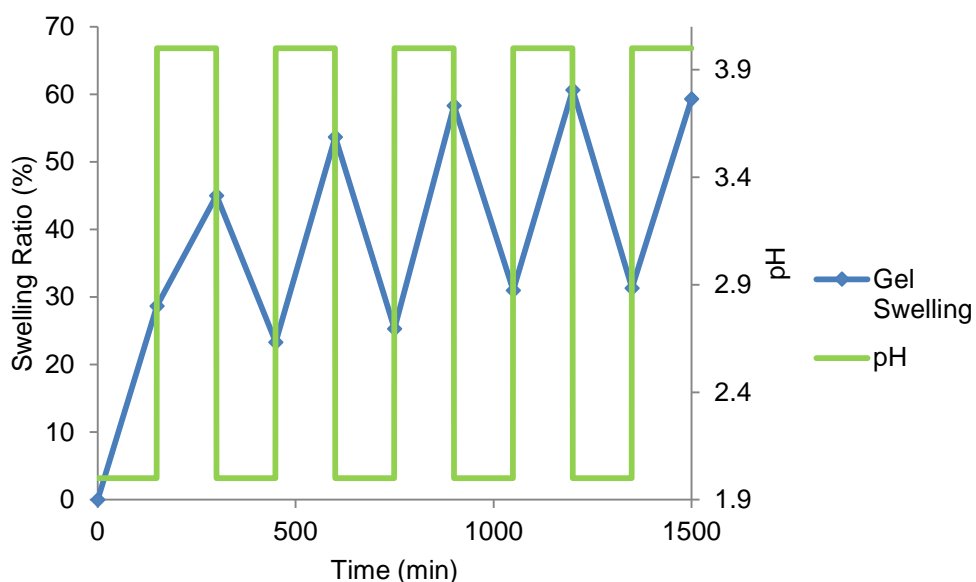


**Figure 4.43** Oscillatory swelling of hydrogels placed in an oven for 24 h at 37 °C, washed in methanol and immersed in a pH 2 glycine buffer first in an alternate fashion with a time period of 150 min at 20 °C.

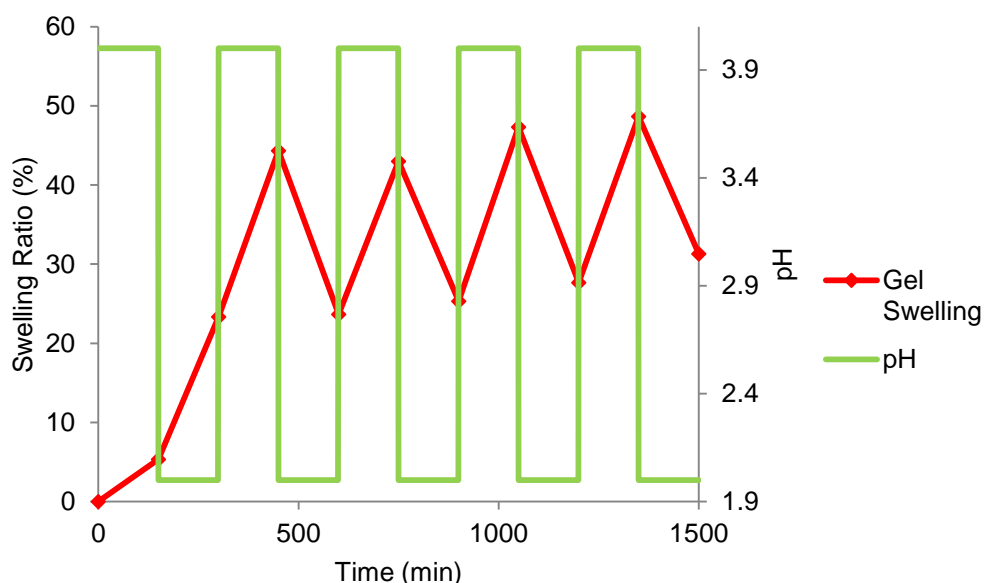


**Figure 4.44** Oscillatory swelling of hydrogels placed in an oven for 24 h at 37 °C, washed in methanol and immersed in a pH 4 phthalate buffer first in an alternate fashion with a time period of 150 min at 20 °C.

The oscillatory behaviour observed can be optimised without lengthening the time period of buffer alternation by pre-swelling the gel following methanol washing in the respective pH 2 and 4 buffers for 24 h. Following this, an oscillatory response can be induced. Figure 4.45 depicts a gel that has

pre-swollen in a pH 4 buffer solution initially and then oscillations from pH 2 every 15 minutes are initiated. It is noteworthy that the zero-position in Figures 4.52 and 4.53 does not represent the same degree of swelling for both gels as prior to the test they were immersed in different buffers and will hence be swollen to differing degrees. As expected, the gel that was immersed in a pH 4 phthalate buffer for 24 h still swells when oscillations are induced owing to the pH 2 environment, generating more electrostatic repulsion within the gel, inducing further network swelling (Figure 4.45) However, the gel that was pre-swollen in a pH 2 glycine buffered solution (Figure 4.46) does not show further network swelling. This is more desirable as the gel oscillates in volume about a set point as opposed to continuously increasing in size. It should, however, be noted that the induced changes in swelling ratio are relatively small.

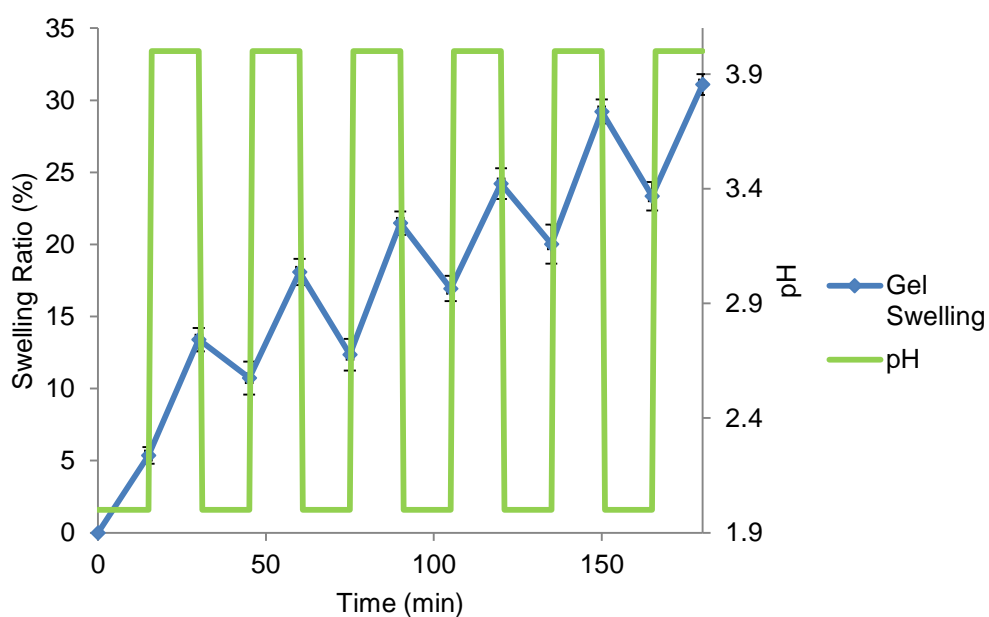


**Figure 4.45** Oscillatory swelling of hydrogels placed in an oven for 24 h at 37 °C, washed in methanol, pre-swollen in a pH 4 phthalate buffer then immersed in a pH 2 glycine buffer first in an alternate fashion with a time period of 15 min at 20 °C.

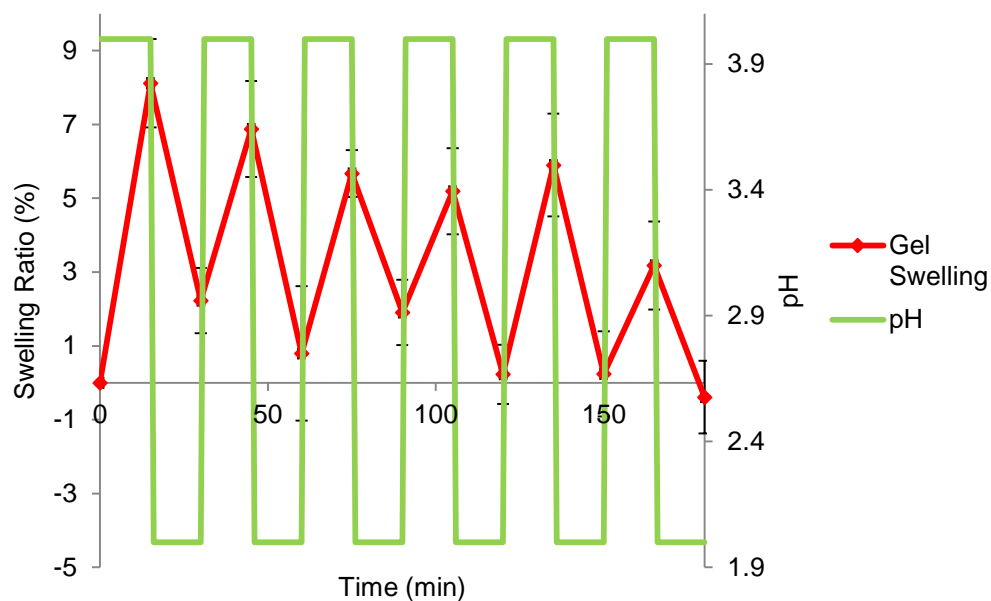


**Figure 4.46** Oscillatory swelling of hydrogels placed in an oven for 24 h at 37 °C, washed in methanol pre-swollen in a pH 2 buffer then immersed in a pH 4 buffer first in an alternate fashion with a time period of 15 min at 20 °C.

The aforementioned study where gel samples were pre-swollen prior to induction of pH oscillations was therefore repeated with a time period of 150 min (Figures 4.47 and 4.48) to further investigate as to whether the time period would have an effect of the amplitude of oscillations in gel swelling. A similar trend is exhibited in Figures 4.47 and 4.48 as to when the time period of oscillations was just 15 min (Figure 4.45 and 4.46), although as expected, the change in the swelling ratio upon varying pH is larger (approximately 25% compared to 5%). This is because the gel has a greater amount of time to reach an equilibrium state. Furthermore, as also previously exhibited in Figures 4.45 and 4.46, the gel swollen in a pH 4 phthalate buffer prior to being subjected to oscillations in pH, does not show overall gel swelling but instead desirable oscillations around a set volume.

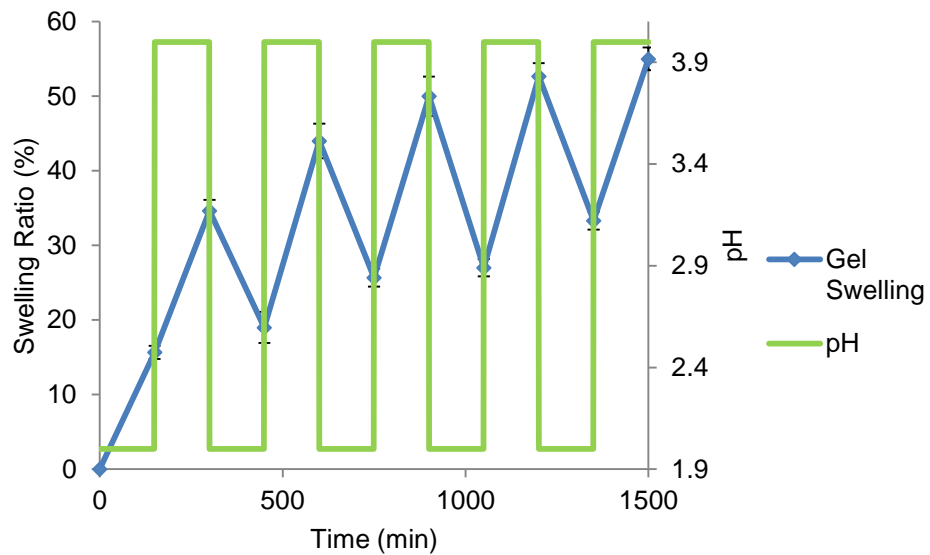


**Figure 4.47** Oscillatory swelling of hydrogels placed in an oven for 24 h at 37 °C, washed in methanol, pre-swollen in a pH 4 phthalate buffer then immersed in a pH 2 glycine buffer in an alternate fashion with a time period of 150 min at 20 °C.

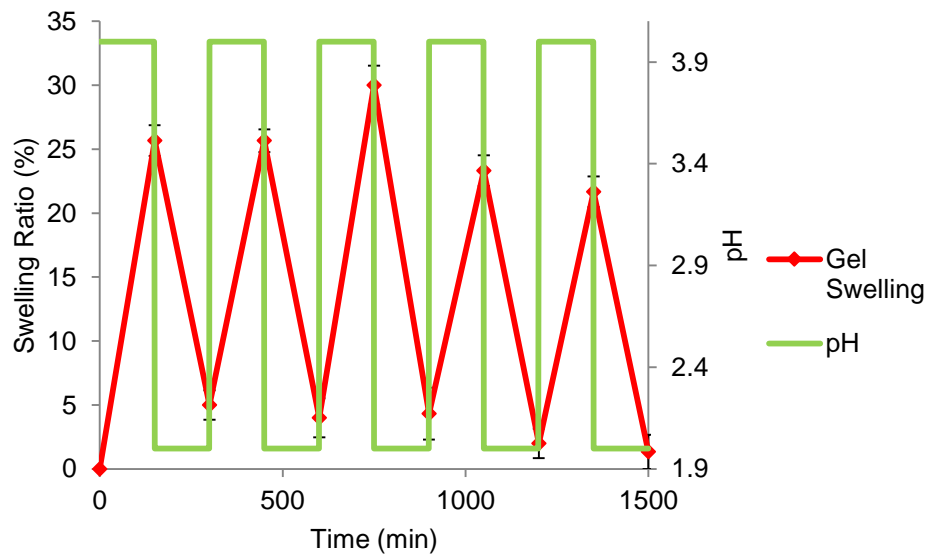


**Figure 4.48** Oscillatory swelling of hydrogels placed in an oven for 24 h at 37 °C, washed in methanol pre-swollen in a pH 2 buffer then immersed in a pH 4 buffer first in an alternate fashion with a time period of 150 min at 20 °C.

By increasing the time period of the oscillatory swelling experiments from 15 min to 150 min, it is clear that the gel response to the oscillations is diffusion limited. The increase in the amplitude of the gel swelling oscillation (e.g. comparison of Figure 4.46 with 4.48) is hence an equilibrium effect. For

example, during swelling, a variation in the pH of the surrounding solution causes a concentration difference between the inside and the outside of the gel, leading to diffusion of ions into the gel, inducing an increase in osmotic pressure inside the gel and hence network swelling. Consequently, by scaling down the size of the hydrogel, as swelling is driven by diffusion, the swelling response of the material is likely to be enhanced (De et al., 2002). To this end, the gel thickness was varied (3 mm, 2 mm and 1 mm) at a constant diameter (12 mm) and the swelling response was recorded (Figure 4.49). From Figure 4.49, it is clear that there is no significant variation in the equilibrium swelling ratio at 180 min (approximately 30%) upon varying the thickness of gel samples.

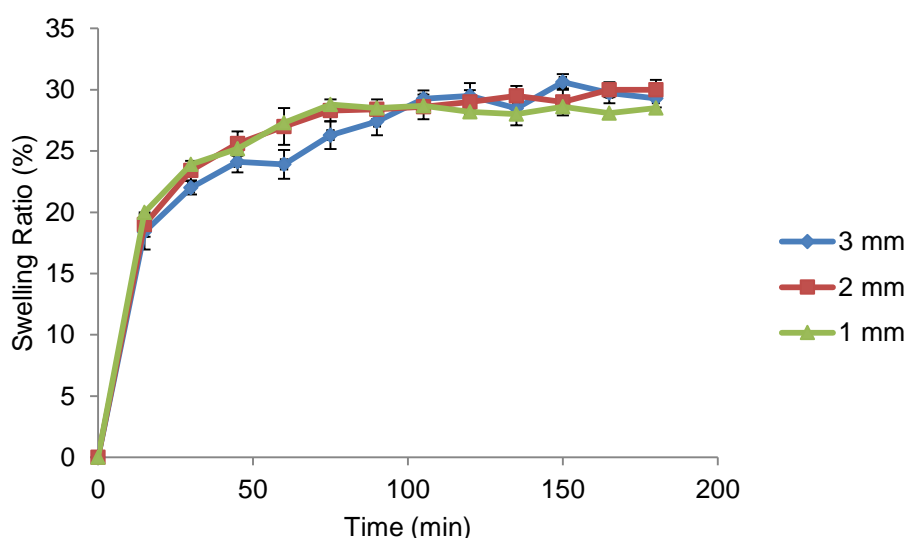


**Figure 4.49** Swelling of G-Ch-PVP hydrogels of varying thicknesses placed in an oven at 37 °C and washed for 24 h in methanol before being immersed in a pH 2 glycine buffered solution.

The effect of gel thickness on swelling was also investigated in a pH 4 phthalate buffered solution (Figure 4.50). Similar conclusions can be drawn as to when the gels were placed in a pH 2 glycine buffered solution (Figure 4.49) whereby the swelling ratio at 180 min is approximately the same irrespective of gel thickness.

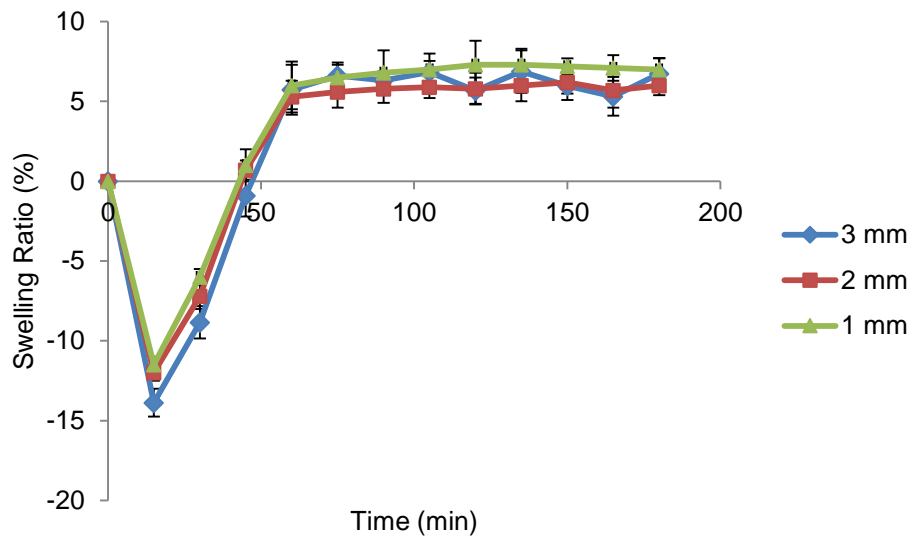


**Figure 4.50** Swelling of G-Ch-PVP hydrogels of varying thicknesses placed in an oven at 37 °C and washed for 24 h in methanol before being immersed in a pH 4 phthalate buffered solution.

Similar trends and appropriate conclusions were also found when gels of varying thicknesses were immersed in a pH 7 phosphate (Figure 4.51) and a pH 10 borate (Figure 4.52) buffer.

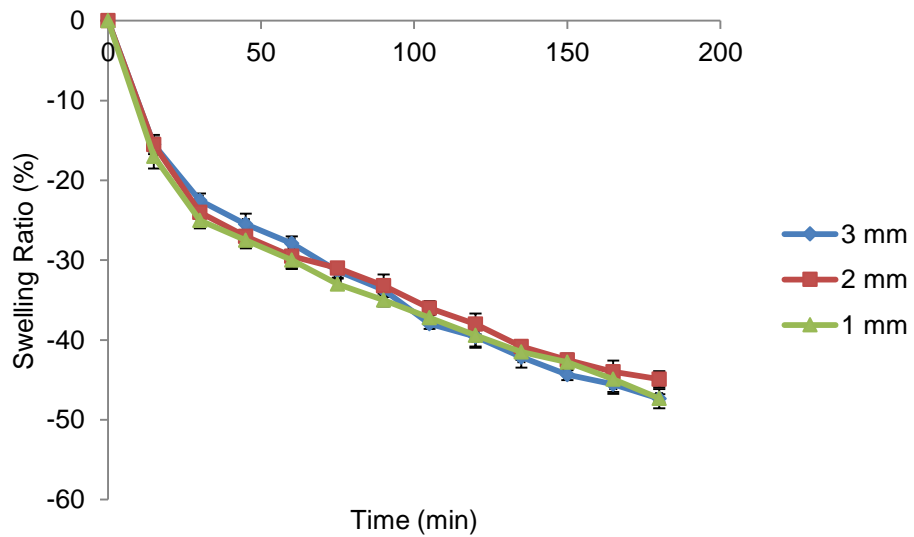


**Figure 4.51** Swelling of G-Ch-PVP hydrogels of varying thicknesses placed in an oven at 37 °C and washed for 24 h in methanol before being immersed in a pH 7 phosphate buffered solution.

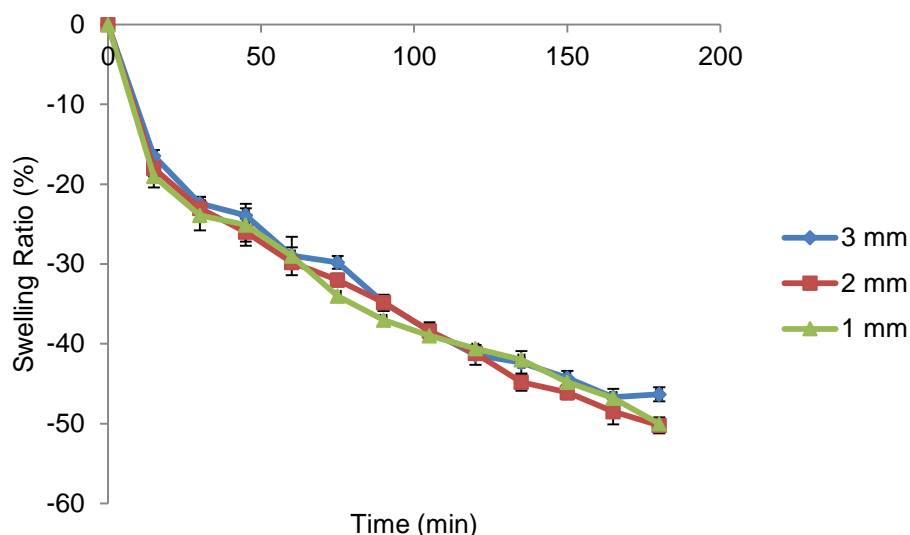


**Figure 4.52** Swelling of G-Ch-PVP hydrogels of varying thicknesses placed in an oven at 37 °C and washed for 24 h in methanol before being immersed in a pH 10 borate buffered solution.

Finally, the swelling behaviour when gels with multiple thicknesses were washed in methanol, pre-swollen in a pH 2 glycine buffer and then immersed in a pH 4 phthalate followed by a pH 2 glycine buffer under two oscillatory regimes was determined (Figures 4.53 and 4.54). Gels with a thickness of 2 mm were not tested as based upon previous results (Figures 4.49-4.52) if a difference in swelling was to be observed, this would be most prominent by studying the thinnest specimen. As shown in Figures 4.53 and 4.54, there is very little difference in terms of the swelling response between the two gel samples of varying thicknesses. This would suggest that on the timescales of the study, diffusion was not limited by sample size on the millimetre length scale. Therefore in future work, to assist in imaging the thickness of the gel on the macro scale, specimens were studied at a thickness of 3 mm.

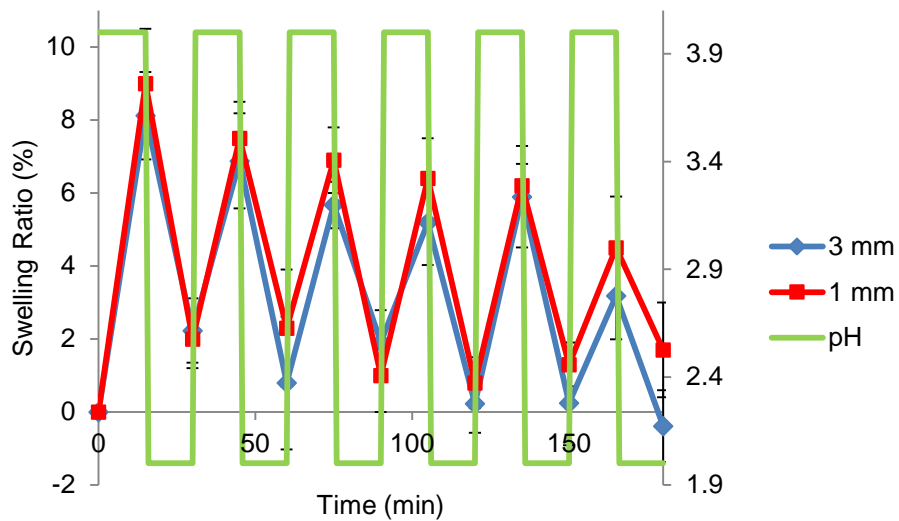


**Figure 4.53** Oscillatory swelling of hydrogels of varying thicknesses placed in an oven for 24 h at 37 °C, washed in methanol, pre-swollen in a pH 2 buffer then immersed in a pH 4 buffer first in an alternate fashion with a time period of 15 min at 20 °C.

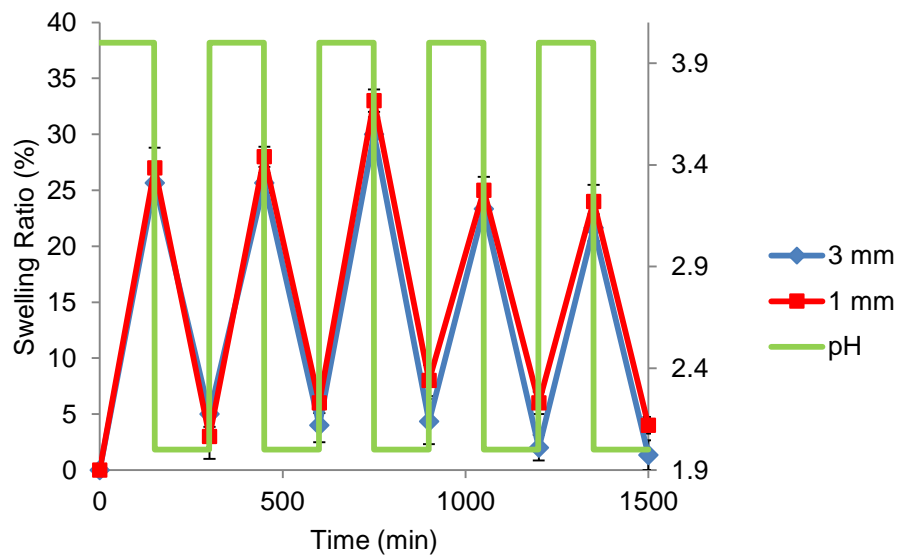


**Figure 4.54** Oscillatory swelling of hydrogels of varying thicknesses placed in an oven for 24 h at 37 °C, washed in methanol, pre-swollen in a pH 2 buffer then immersed in a pH 4 buffer first in an alternate fashion with a time period of 150 min at 20 °C.

### 4.13 Mechanical characterisation

A typical uniaxial compression was conducted on the current formulation of G-Ch-PVP hydrogels where the specimens were compressed to 50% of their original thickness. The results are shown in Figure 4.55 where stress, as detailed in Section 2.6.5 and equation 2.31 is the force per unit area (uniaxial

stress) and strain as defined in equation 2.3.2 is the deformation per unit length (engineering strain). The magnitude of the error bars was calculated according to the standard error. Error bars are displayed for data points at intervals of 5% strain for clarity. In Figure 4.55, the gel exhibits linear elastic behaviour up to approximately 20% strain and then following this plastic deformation occurs in the form of strain hardening, leading to densification. Despite the typical polymeric mechanical behaviour exhibited by the hydrogel samples, the mechanical strength of these specimens is inferior to typical gel-based materials in the literature (Oyen, 2014, Koob and Hernandez, 2003). For example the elastic modulus calculated between 0 and 20% strain in Figure 4.55 was found to be 33 Pa. In the literature, for a 3% acrylamide gel, the elastic modulus can be measured to be between 10-1000 Pa depending on the mode of preparation and analysis (Oyen, 2014). Together with prior SEM and optical swelling studies, it is clear that the mechanical stability of these smart hydrogels needs to be improved. Furthermore, as well as enhancing the stability, future tests should be conducted where the sample is hydrated and immersed in a liquid medium to more accurately simulate the conditions in which it may find application.

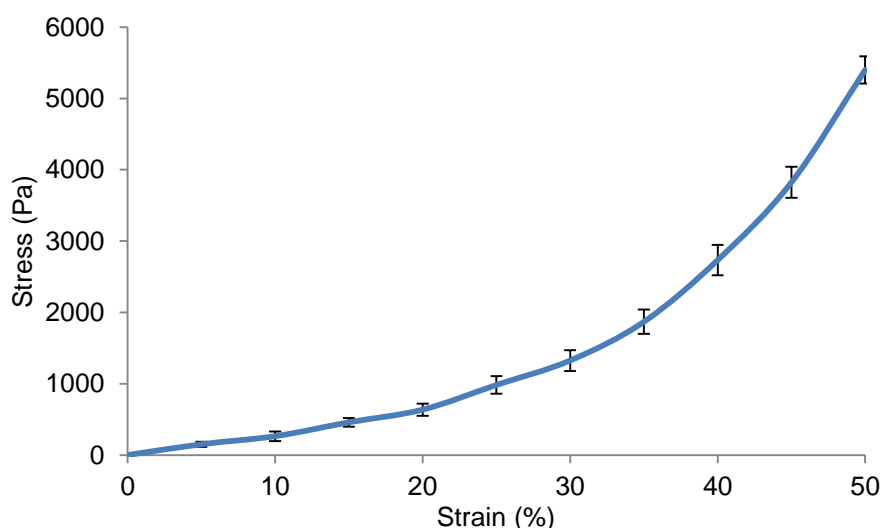


**Figure 4.55** A stress-strain graph depicting a uniaxial compression test of G-Ch-PVP hydrogels where samples were compressed to 50% of their thickness.

#### 4.14 Conclusions

Synthesis of G-Ch-PVP hydrogels was successfully achieved. UV-Vis spectroscopy, fluorescence microscopy and SEM provided insights into the morphology of the networks whilst showing the strong dependence gelation

time has on the structural properties. As the reaction time is increased, gel networks become more crosslinked, leading to smaller and fewer pores (33.8 % surface porosity of gels placed in an oven at 37 °C for 6 h compared to 5.0% surface porosity after 96 h in an oven at 37 °C). This relationship was initially found utilising CPD and FD drying techniques prior to SEM. Hydrogel structure was preserved to a greater degree following FD owing to minimal network collapse. However, it is important to use CPD in conjunction with FD to fully characterise the gel morphology. It is noteworthy that both of these preparatory techniques lead to alteration of the sample prior to analysis and hence do not represent the true sample structure, although as all specimens are altered in the same way, comparisons can be made relative to one another. As such, characterising hydrogel morphology via SEM following CPD or FD is currently common practice.

The smart nature of G-Ch-PVP hydrogels was partially confirmed during optical swelling measurements, although measuring the volume change proved to be difficult owing to the limitations of the camera and the instability of the gel sample (previously highlighted in SEM studies). Subsequent swelling experiments were conducted gravimetrically. Initial results using this technique also confirmed the smart nature of the samples, although stability continued to be problematic. Swelling behaviour was determined as a function of pH using citric acid and phosphoric acid in combination with sodium hydroxide to act as buffers. The effect of increasing the ionic strength on the degree of swelling was also demonstrated, whereby such an increase, enhances the degree of charge screening within the network, lowering the Donnan potential, resulting in a reduction in the osmotic pressure exerted and hence a lower swelling degree. FT-IR was used to investigate how a variation in pH affects gel constituents at a molecular level. Upon analysing the individual components of the gel, it was difficult to see ascertain meaningful results due to the overlap of the O-H stretch with the N-H stretch. The surface porosities of the gels were studied as a function of pH using optical microscopy and a correlation with gravimetric swelling data was found. Fluorescence spectroscopy was utilised to investigate as to whether a shift could be observed in the excitation or emission spectra of G-Ch-PVP hydrogels as a function of pH. Such a dependence was not found.

Network hydrophobicity was adjusted by varying PVP content to produce optimal structures for improved handling. Gels placed in an oven at 37 °C for 24 h and successive washing in methanol produced smart and responsive samples. Predictable swelling behaviour was observed when samples were immersed in a pH 2 glycine buffered solution with a swelling ratio of 30% after 180 min. This swelling behaviour compared well with prior surface and internal porosity measurements collected via SEM. However the results from when gels were placed in pH 4 (phthalate), 7 (phosphate), and 10 (borate) buffered solutions illustrated the inhomogeneous distribution of solvent within the gel matrix. Ideally distilled water would be used to wash the hydrogels pending an improvement in mechanical stability. This is discussed in chapter 5. Nevertheless, oscillatory behaviour was demonstrated showing that the gel response is dictated by the environment the sample has experienced in the immediate past. The effect of gel thickness on network swelling and response to oscillatory regime was shown to be negligible when comparing samples of 3, 2 and 1 mm thickness. In particular, a significant change in swelling behaviour on varying the pH from 2 to 4 (which is a relatively small change) is a positive and useful result which has been carefully optimised.

The mechanical properties of G-Ch-PVP hydrogels were briefly analysed, further indicating that the samples exhibit typical mechanical behaviour for a gel. However in comparison to literature values, the elastic modulus is rather low and there is evidence in the literature that the stability of gel samples can be enhanced by altering modes of preparation, for instance. This is studied further in Chapter 5.

## **Chapter 5 – Results and Discussion: Improving the Stability of Genipin-Crosslinked Chitosan-Poly(vinyl pyrrolidone) Hydrogels**

From Chapter 4, the morphology, swelling behaviour and mechanical properties of pH-sensitive G-C-PVP cationic hydrogels were characterised. These gels show good promise for combination with oscillatory pH reactions, although suffer from relatively poor mechanical stability. This chapter details how the gel formulation was altered in order to improve the mechanical attributes of the network whilst still remaining a responsive material. A range of further techniques are employed to study the structural properties of G-Ch-PVP hydrogels in order to understand microscale processes.

After reviewing the literature, it was identified that sample stability could possibly be improved by carefully freezing and thawing hydrogels (Nugent and Higginbotham, 2006, Gupta et al., 2012). This is because this process encourages reorganisation and the formation of more crystalline solid-like structures. Freezing and thawing was regarded as the preferred method of manipulation as no changes to the sample composition are required in order to eventually enhance the stability of the hydrogel specimens.

### **5.1 Visual and morphological characterisation of freeze-thawed hydrogels**

Upon visual inspection of a G-Ch-PVP hydrogel placed in an oven for 24 h at 37 °C, subsequently frozen at -10 °C for 30 min and slowly thawed at 2 °C for 24 h, the specimen was far more stable than its counterpart of the same composition without being subjected to a 30 min freeze-thaw cycle. This stability enhancement was observed by the fact that the gel could be immersed in distilled water for 24 h, allowing it to swell and subsequently handled without fragmentation issues. This was not the case for gels that were not freeze-thawed. A 24 h gelation time was chosen based on the fast oscillatory pH swelling response exhibited by the hydrogel sample as shown in Figure 4.57. A thawing period of 24 h at 2 °C was selected so that the thawing process would be slow in the hope of inflicting minimal damage to the gel structure and facilitating crystallite formation (as shown in Figure 2.26) compared to thawing

more quickly or at a higher temperature (Degner et al., 2013, Degner et al., 2014).

The freeze-thawed hydrogel is depicted in Figure 5.1, although, as shown, the hydrogel was not homogenous. This may be due to the polymeric domains that are created during crosslinking, leading to the formation of an inhomogeneous hydrogel microstructure. Voids in the gel microstructure (where the crosslinking agent may have aggregated) facilitate the diffusion of solvent molecules into the network, resulting in swelling. As the gel microstructure is therefore not constant, during swelling, imperfections occur when solvent diffuses into the voids. This can lead to the production of a sample that is not homogenous (Hennink and Van Nostrum, 2002).

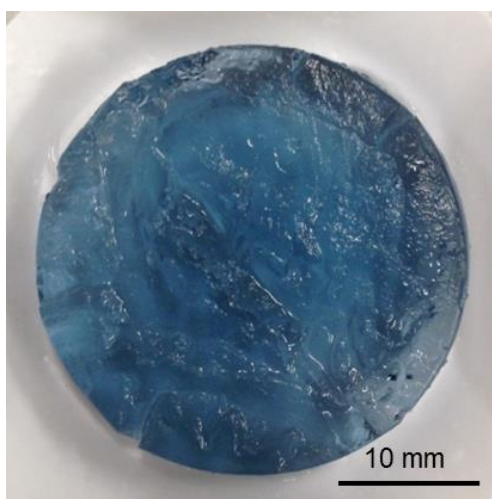


**Figure 5.1** An image of a G-Ch-PVP hydrogel placed in an oven for 24 h at 37 °C, frozen for 30 min at -10 °C, thawed for 24 h at 2 °C and swollen in distilled water for 24 h at room temperature taken with a digital camera.

The microporous morphology of such freeze-thawed G-Ch-PVP hydrogels was evaluated by a number of techniques. Optical microscopy images (Figure 5.2) were, on the whole, very unclear. It is exceptionally difficult to ascertain exactly where the pores are. The best image obtained is shown in Figure 5.2 in which and some pores can be observed together with regions of the polymer architecture.

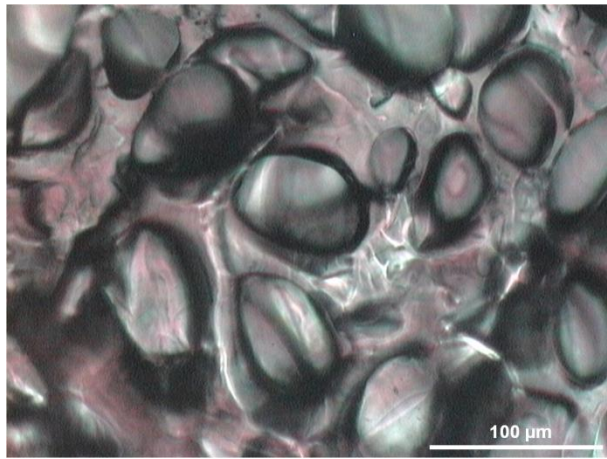


**Figure 5.2** G-C-PVP hydrogel microstructure analysed by optical microscopy.

After CPD, analysis by SEM did show porous regions in the specimens, although akin to previous tests, extensive network collapse occurred as evidenced by small pores (<10 μm in diameter) and a dense surface layer (Figure 5.3). This collapse is probably due to ethanol dehydration required before drying and/or exchange of ethanol for liquid carbon dioxide during CPD (Lamprecht et al., 2000).

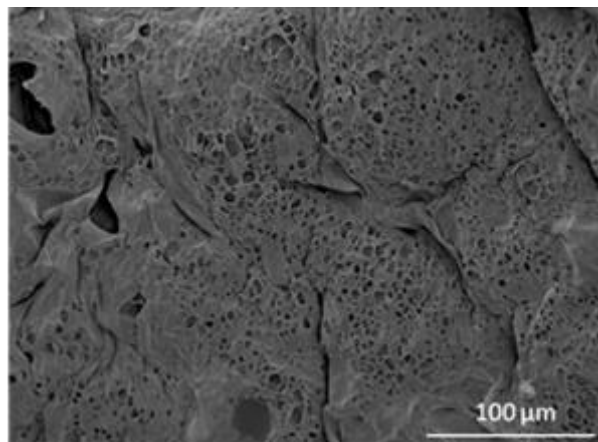


**Figure 5.3** G-C-PVP hydrogel microstructure analysed by SEM following CPD (Hurst and Novakovic, 2013).

In contrast, FD preserved the native gel structure to a greater degree (Figure 5.4) where pores are larger (50-100 μm in diameter) and the surface layer, upon visual inspection, appears to be smoother, indicating minimal collapse has occurred.

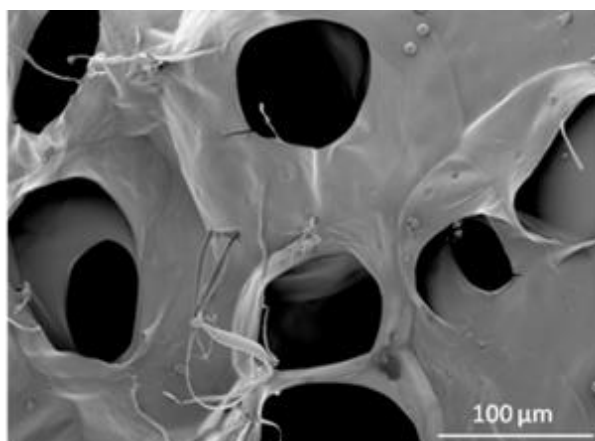


**Figure 5.4** G-C-PVP hydrogel microstructure analysed by SEM following FD (Hurst and Novakovic, 2013).

The viability of ESEM as a technique to characterise hydrogel morphology was subsequently tested as no prior drying (e.g. CPD or FD) is required before analysis. Images collected using ESEM were difficult to elucidate structural detail from (Figure 5.5). It may be argued that there is a porous architecture present with pore sizes that approximately correspond to freeze-dried samples, although it is more likely that the images acquired using this technique show an inconclusive representation of the gel morphology. This could be due to the harmful interaction of the electron beam on the surface of the hydrated network, leading to damage and local evaporation (Kishi et al., 2004). Furthermore, it may be the case that specimens have a higher mobility due to solvation, resulting in acquisition of blurred images. Additionally, sample analysis occurs in the vacuum chamber of the microscope and not in an aqueous/solvent environment where the hydrogel will be applied.

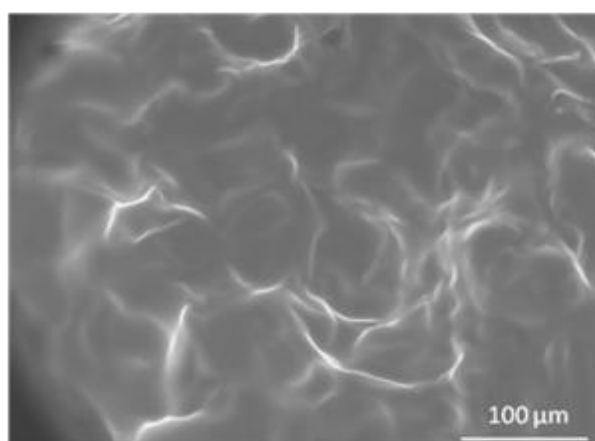


**Figure 5.5** G-C-PVP hydrogel microstructure analysed by ESEM (Hurst and Novakovic, 2013).

Due to the enhanced stability of freeze-thawed gels, CLSM could also be employed to aid sample analysis. Images acquired via CLSM in situ show a continuous, 3-D porous architecture that is a true representation of the structure of the hydrogel in the aqueous environment it will find application (Figure 5.6). As a dipping lens was utilised, the sample can be fully immersed in solution during analysis in reflectance mode.

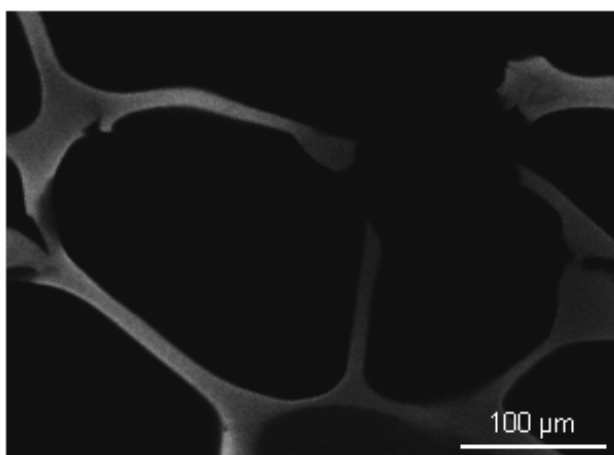


**Figure 5.6** G-C-PVP hydrogel microstructure analysed by CLSM in reflectance mode.

The microstructure of hydrogels can also be visualised utilising fluorescence. However, in most cases a fluorescent probe such as fluorescein isothiocyanate must be added to a hydrogel, which may alter the native structure of the gel network. This can occur via blending or covalent linking, potentially restricting the availability of functional groups to form crosslinks or swell (Lamprecht et al., 2000). If a fluorescent probe is simply blended, it may migrate to other parts of the sample during visualisation, leading to potentially unreliable information being acquired. However, as G-Ch-PVP hydrogels autofluoresce upon crosslink formation, combination with an external probe is not necessary and fluorescence can be used to increase the amount of structural detail during image acquisition without making any changes to the native network (Figure 5.7).

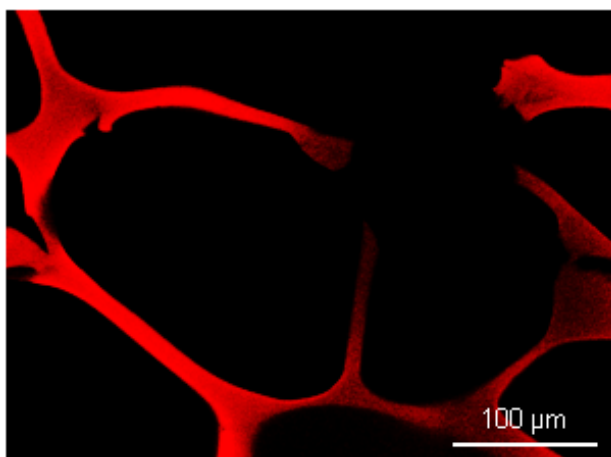


**Figure 5.7** G-C-PVP hydrogel microstructure analysed by CLSM in fluorescence mode.

## **5.2 Smart behaviour of freeze-thawed hydrogels**

The smart behaviour of freeze-thawed G-Ch-PVP hydrogels was confirmed (Figure 5.8) gravimetrically and optically (monitoring the variation in surface area by fluorescence) by immersing samples in a pH 2 glycine buffer solution. Fluorescence was used to monitor the change in surface area of gel samples to aid the identification of the boundary between the gel and surrounding solution during swelling and to simultaneously monitor the variation in fluorescence intensity of the network. As shown there is a significant difference in the swelling observed between the characterisation techniques employed. The initial swelling observed is greater during gravimetric measurement compared to using an optical technique where a gradual increase in the surface area as a function of time is continually observed for the duration of the experiment. This may be because the mass of the hydrogel represents the whole sample as opposed to optical measurement solely concerning the surface area as opposed to the total volume of the network during swelling. This is therefore expected due to the differing dimensions being measured (area compared to volume)

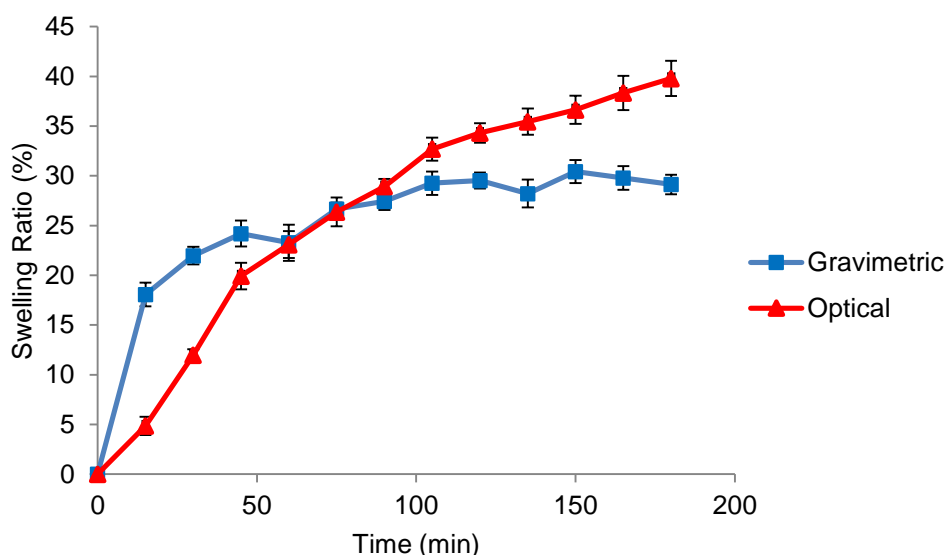


**Figure 5.8** Swelling of freeze-thawed G-Ch-PVP hydrogels in a pH 2 glycine buffer studied via gravimetric and optical techniques (Hurst and Novakovic, 2013).

As well as being able to monitor size changes in the network via fluorescence, the fluorescence intensity can also be observed during swelling (Figure 5.9). Since the crosslinks in the network give rise to the autofluorescence, during swelling, the gel volume increases (depicted in Figure 5.9), leading to a decrease in the density of the crosslinks and hence a concomitant reduction in the overall fluorescence intensity of the network (Hurst and Novakovic, 2013). Furthermore as previously investigated with citric acid and phosphoric acid solutions in combination with sodium hydroxide (Table 4.8), the fluorescence emission is not significantly sensitive to pH. As additional confirmation, the emission spectra of G-Ch-PVP hydrogels immersed in pH 2 glycine, pH 4 phthalate, pH 7 phosphate and pH 10 borate solutions that were excited at 488 nm did not show any significant differences. Therefore variations in the fluorescence are not a result of the proton concentration varying the emission spectra but instead, are likely due to the impact of swelling on the density of the fluorescent chemical moieties within the gel network.

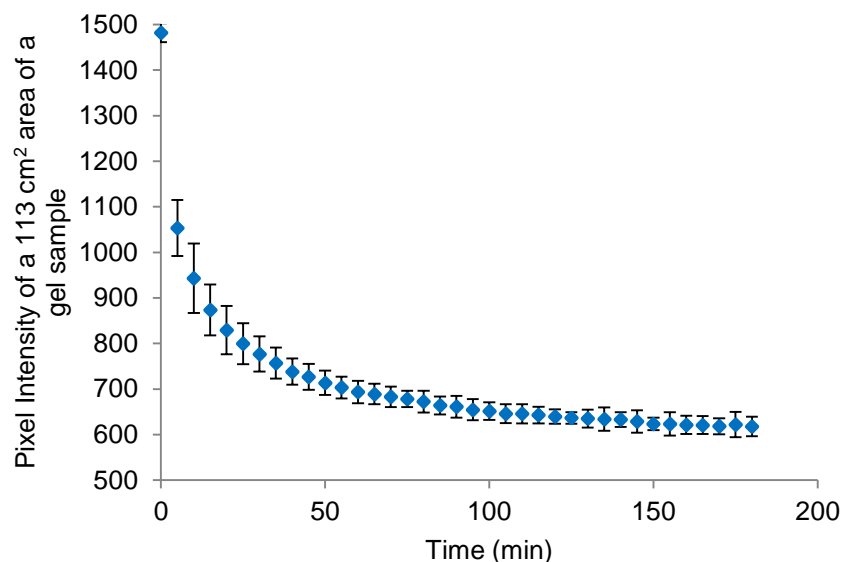


**Figure 5.9** Swelling of freeze-thawed G-Ch-PVP hydrogels in a pH 2 glycine buffer studied by determining the change in macro-fluorescence intensity over time (Hurst and Novakovic, 2013).

A normalised representation of Figure 5.9 is shown in Figure 5.10 and to investigate the effects of photobleaching, the fluorescence intensity of a freeze-thawed G-Ch-PVP hydrogel that was pre-swollen and subsequently kept in a pH 2 glycine buffer was measured at the same time intervals as in Figure 5.9. Photobleaching is the photochemical alteration of a fluorophore such that it is no longer able to fluoresce and is induced by cleavage of covalent bonds or non-specific interactions between the fluorophore and surrounding molecules. This photobleaching experiment is shown in Figure 5.11. As shown in Figure 5.12 photobleaching does occur over the time period of the experiment (decrease in pixel intensity of approximately 25% by the final measurement). However when the gel is made to swell in the same pH 2 glycine buffer, over an identical experimental time period, the pixel intensity measures decreases by approximately 60% of the original value (Figure 5.10). This indicates that it is variations in the fluorogenic properties of the sample that is inducing some of the reduction in observed pixel intensity as opposed to just photobleaching.

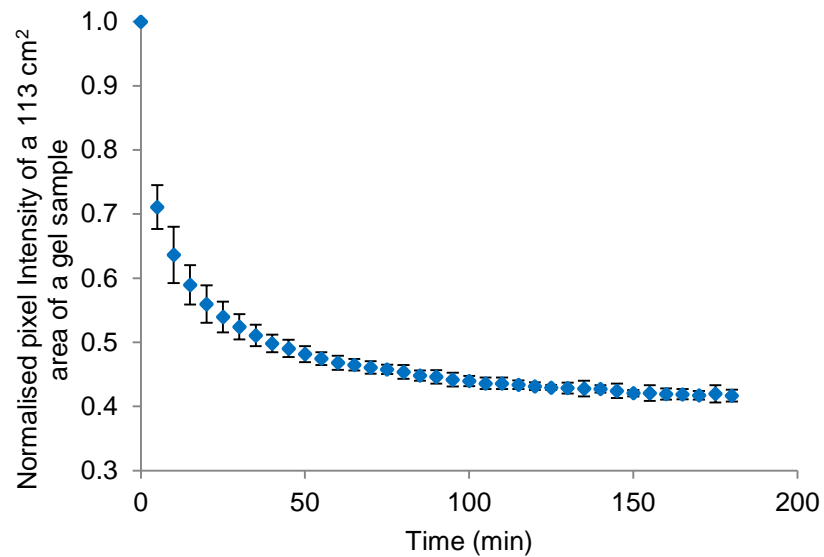


**Figure 5.10** Swelling of freeze-thawed G-Ch-PVP hydrogels in a pH 2 glycine buffer studied by determining the change in macro-fluorescence intensity over time (normalised values).

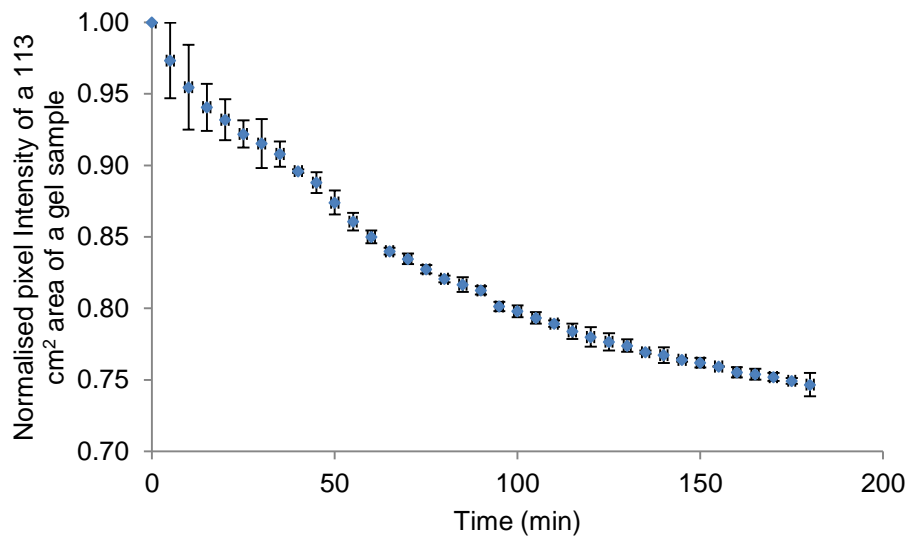


**Figure 5.11** Normalised values of a freeze-thawed G-Ch-PVP hydrogel pre-swollen in a pH 2 glycine buffer where the change in macro-fluorescence intensity was measured over time.

To determine how good the correlation was between fluorescence intensity and swelling of G-Ch-PVP hydrogels measured gravimetrically and optically, Pearson product-moment correlation coefficients were determined in each case by utilising Figure 5.12. The correlation coefficient is the covariance of the two variables (swelling ratio measured gravimetrically/optically and the fluorescence

intensity of the sample) divided by the product of their standard deviations. Values range between +1 and -1 inclusive, where 1 is total positive correlation, 0 is no correlation and -1 is total negative correlation. The correlation coefficient between the swelling ratio obtained gravimetrically and the fluorescence intensity is -0.98 compared to -0.81 when optical swelling measurements were recorded. The minus sign of the correlation coefficients indicate that, as expected, there is a negative correlation between the swelling ratio and the fluorescence intensity of gel samples whereby as the gel swells, there is a decrease in crosslink density and hence a decrease in the overall network fluorescence intensity. As the magnitude of the correlation coefficient when swelling was measured gravimetrically is closer to -1 (-0.98 compared to -0.81), this indicates that there is a stronger negative correlation between the swelling ratio and the fluorescence intensity of the gel when the swelling is evaluated gravimetrically. This enhanced negative correlation may indicate that as in gravimetric studies, the fluorescence intensity measurement is representative of the entire sample as opposed to optical studies where the surface area change is recorded.

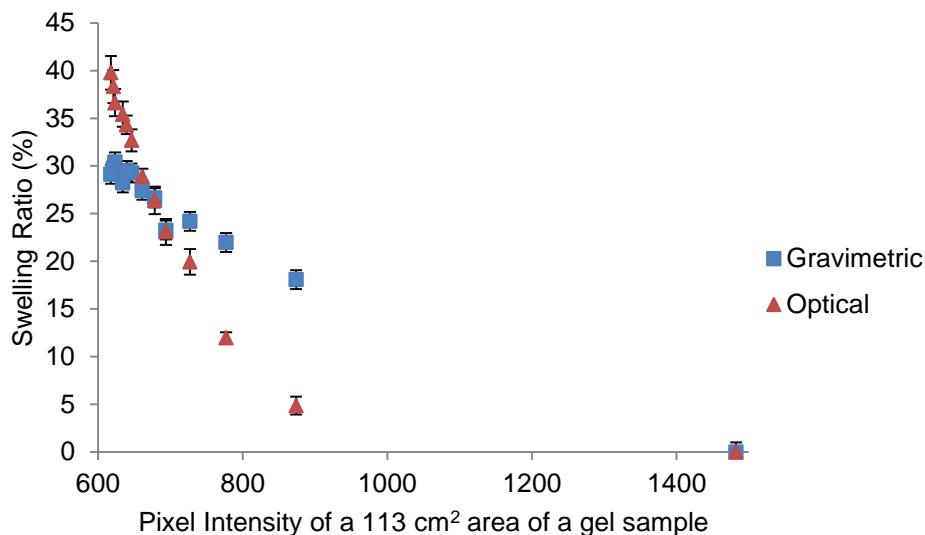


**Figure 5.12** A plot of the swelling ratio of freeze-thawed G-Ch-PVP hydrogels in a pH 2 glycine buffer determined gravimetrically and optically against the macro-fluorescence intensity.

So far tests have been conducted to determine how the network responds on a macro-scale upon swelling, although by determining the change in microporous structure during swelling, a more detailed analysis can be performed to inform

how the internal structure varies as a function of time. This can be achieved by visualising hydrogel samples during swelling using CLSM in reflectance mode (Figures 5.13-5.15). In the images collected, the white structures depict the actual gel network whilst the remaining black voids represent the pores. The images appear structured as cross-sectional images along the z-plane were taken, stacked to reconstruct the native hydrogel structure. It is clear to see that as the network swells, the size of the pores increase quite dramatically representing protonation of the amine moieties due to the low pH of the surrounding aqueous environment diffusing into the gel matrix. As this experiment was conducted in reflectance mode, CLSM may be used to monitor hydrogels that do not fluoresce, hence demonstrating the universality of the technique to monitor variation in pore structure during swelling. As an alternative to visualising how the gel network changes in conformation during swelling, the mobility of tracer molecules can also be studied to investigate diffusion kinetics during swelling (Raccis et al., 2011). However, potential tracer-polymer gel interactions may affect the diffusion behaviour observed via this technique.

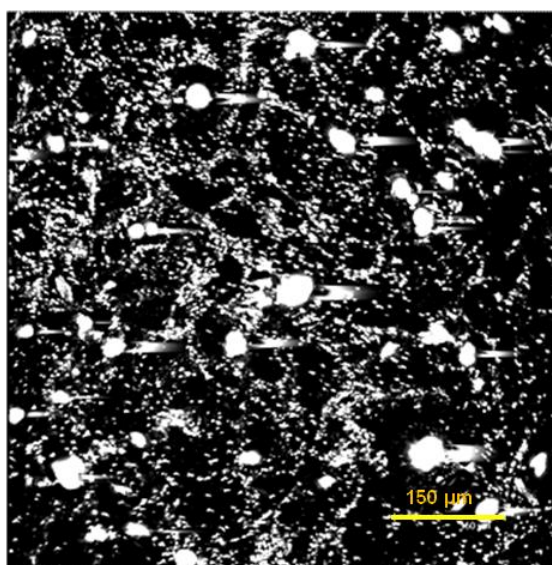


**Figure 5.13** CLSM images of freeze-thawed G-Ch-PVP swelling in a pH 2 glycine buffer at 0 min collected in reflectance mode (Hurst and Novakovic, 2013).

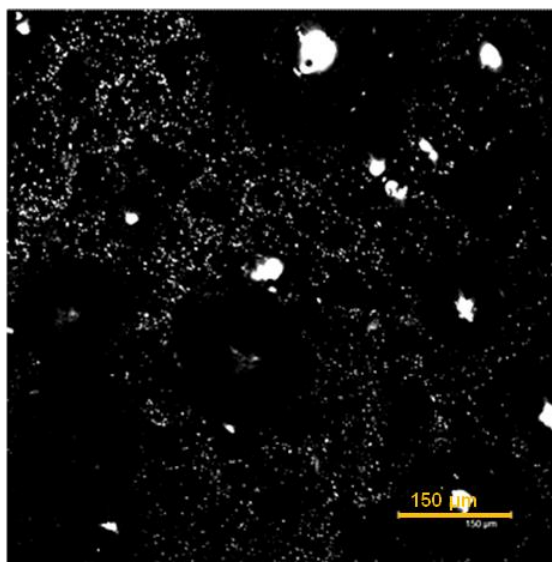


**Figure 5.14** CLSM images of freeze-thawed G-Ch-PVP swelling in a pH 2 glycine buffer at 15 min collected in reflectance mode (Hurst and Novakovic, 2013).

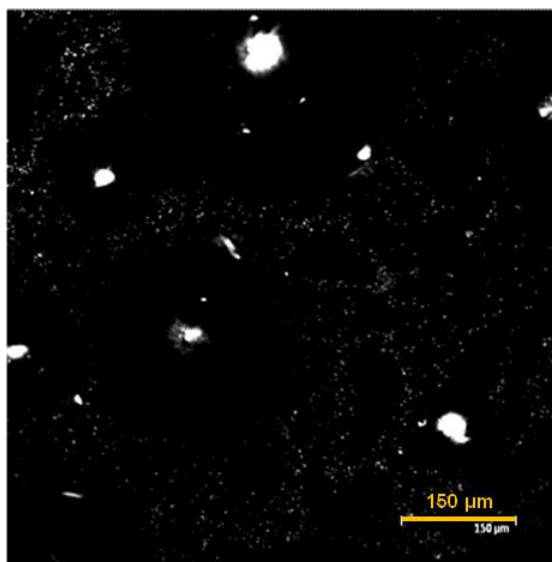


**Figure 5.15** CLSM images of freeze-thawed G-Ch-PVP swelling in a pH 2 glycine buffer at 30 min collected in reflectance mode (Hurst and Novakovic, 2013).

Variation in network porosity during the swelling experiment in Figures 5.13-5.15 is represented quantitatively in Figure 5.16 and is subsequently depicted in Figure 5.17. Porosity is the measure of the number of void spaces in the hydrogel, and is a percentage of the number of voids over the total gel volume. In the case of this experiment, the overall volume analysed was approximately  $150,000 \mu\text{m}^3$ . This was measured according to the method detailed in Section 3.10.4. The variation in the porous architecture is aligned with the macroscale gravimetric measurements. This indicates that monitoring

the porous structure could be a valid technique to determine how the overall specimen responds during network swelling.

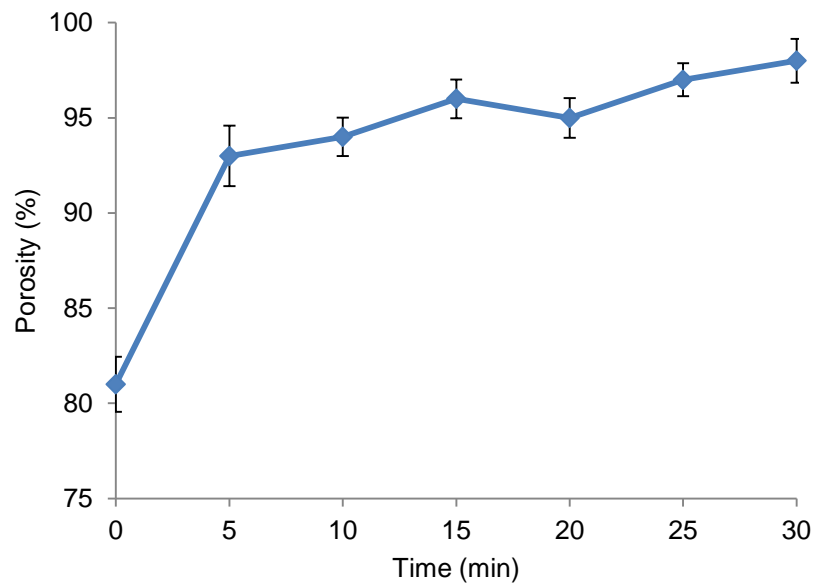


**Figure 5.16** Change in porosity of freeze-thawed G-Ch-PVP hydrogels as a function of time during swelling in a pH 2 glycine buffer (Hurst and Novakovic, 2013).

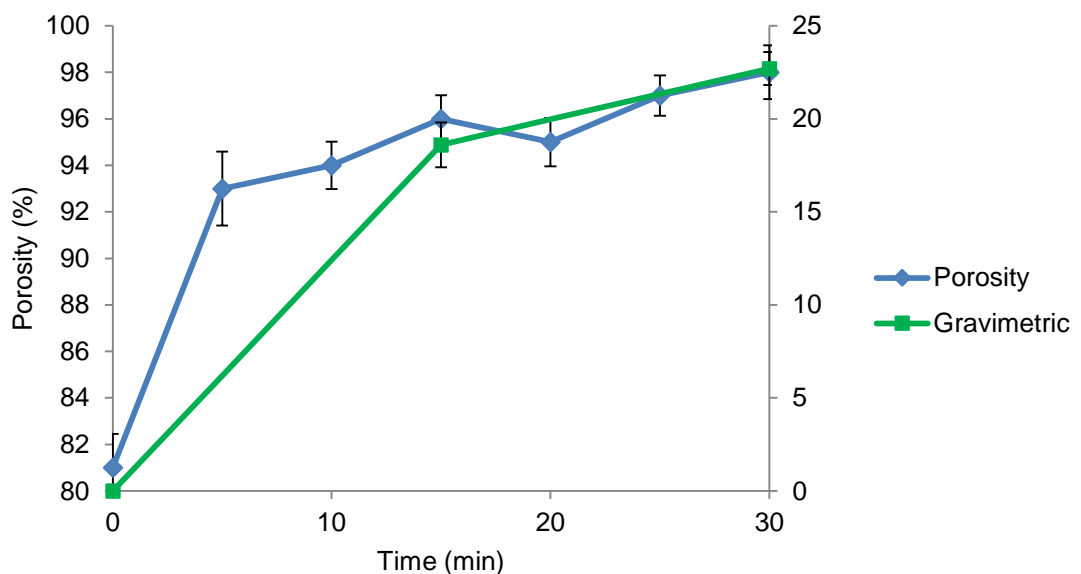


**Figure 5.17** The relationship between the porosity and gravimetric measurements of freeze-thawed G-Ch-PVP hydrogels swelling in a pH 2 glycine buffer (Hurst and Novakovic, 2013).

Changes in the porous architecture have also been monitored using CLSM with fluorescence (Figures 5.18-5.20). It is noteworthy that in all cases, the gel fluoresced red, although to enhance the contrast between the gel and the voids,

all images were equally manipulated so that areas of red fluorescence appear green. Interestingly, visualisation of the structural morphology is not as clearly defined as when reflectance was used, and hence a porosity study could not be conducted. From these results it may be concluded that reflectance is a superior technique than fluorescence when used with a CLSM to monitor how the porous network of G-Ch-PVP hydrogels vary during swelling.

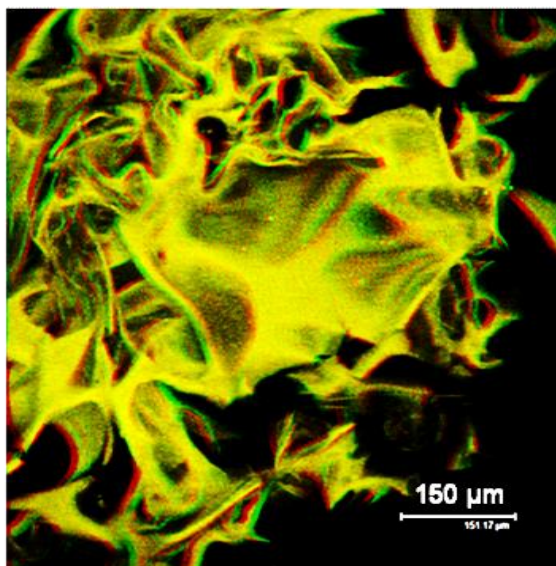


**Figure 5.18** Image collected using CLSM with fluorescence of a freeze-thawed G-Ch-PVP hydrogel swelling in a pH 2 glycine buffered solution at 0 min (Hurst and Novakovic, 2013).

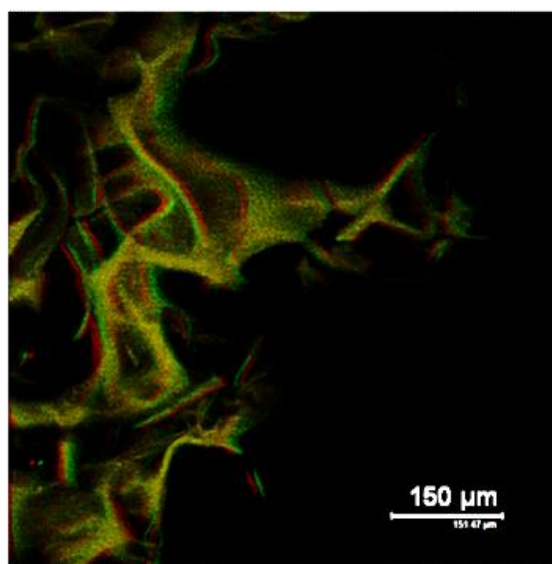


**Figure 5.19** Images collected using CLSM with fluorescence of a freeze-thawed G-Ch-PVP hydrogel swelling in a pH 2 glycine buffered solution at 15 min (Hurst and Novakovic, 2013).

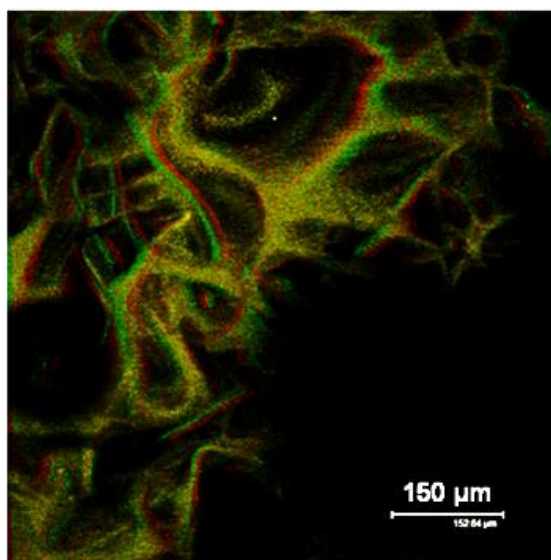


**Figure 5.20** Images collected using CLSM with fluorescence of a freeze-thawed G-Ch-PVP hydrogel swelling in a pH 2 glycine buffered solution at 30 min (Hurst and Novakovic, 2013).

In line with previous macroscale experiments (Figure 5.9), it is shown that on the microscale the fluorescence intensity decreases during swelling of the hydrogel (Figure 5.21). Additionally, there is a strong negative correlation (-0.99 correlation coefficient) between the gravimetric swelling ratio and the micro-fluorescence intensity data collected (Figure 5.22). This behaviour is expected based on previous discussions and further supports that this is an important technique to monitor hydrogel swelling on the microscale.

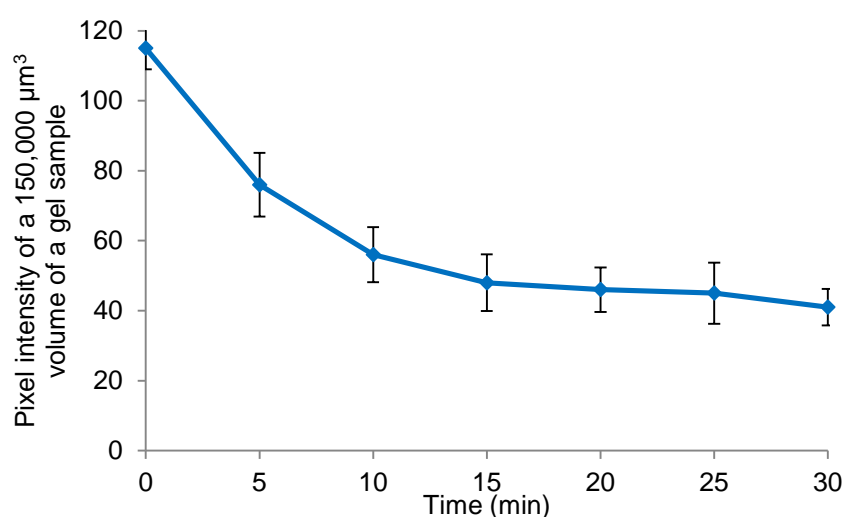


**Figure 5.21** Change in micro-fluorescence intensity of freeze-thawed G-Ch-PVP hydrogels during swelling in a pH 2 glycine buffered solution (Hurst and Novakovic, 2013).

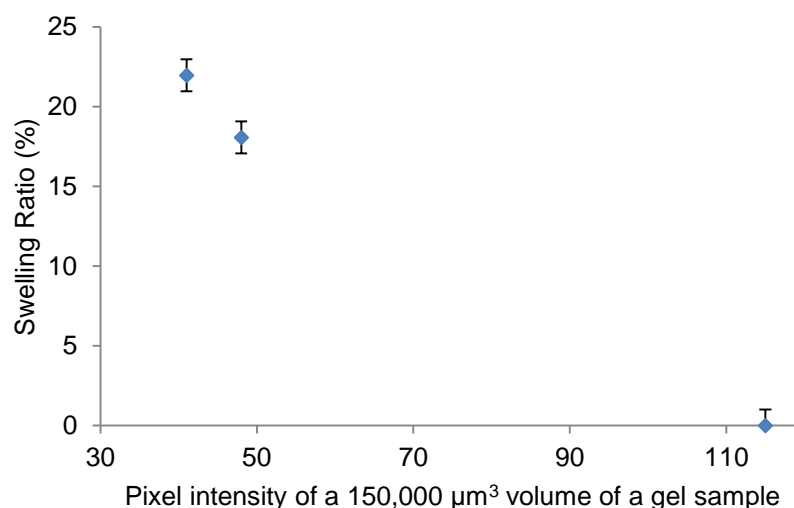


**Figure 5.22** A plot of the swelling ratio of freeze-thawed G-Ch-PVP hydrogels in a pH 2 glycine buffer determined gravimetrically and optically against the micro-fluorescence intensity.

### **5.3 Washing genipin-crosslinked chitosan-poly (vinyl pyrrolidone) hydrogels in distilled water to determine the presence of residuals**

Due to the substantially increased stability of G-Ch-PVP hydrogels following freezing and thawing, specimens could be swollen and washed multiple times in distilled water without any damage being incurred. An experiment was conducted to determine the number of washes / washing duration that was required to remove unwanted residuals from the gel. The gel was placed in distilled water and samples were taken after various time periods. UV-Vis spectroscopy was continually performed on water-wash specimens according to the method described in Section 3.4. As PVP and genipin contain chromophores, if these constituents were being washed out, there would be a detectable absorbance at 213 and 240 nm respectively as evidenced from initial calibration where varying concentrations of PVP and genipin were dissolved in aqueous solutions (Appendix Figure A12).

The number of washes required to remove residual chemical moieties from the network is shown in Figure 5.23. Wash 1 was analysed following immersion of a freeze-thawed G-Ch-PVP hydrogel in distilled water with stirring for 30 min and as shown, the absorbance for PVP increases. This is in contrast to genipin where a minimal amount is being washed out. This could be due to the physical interactions associated with incorporation of PVP in the network in contrast to the chemical crosslinking of genipin. Upon further washing the absorbance of

genipin remained low, indicating that genipin is not leaching out of the gel. After washes 2, 3 and 4 the amount of PVP coming out is greatly diminished. Wash 5 refers to 48 h and as can be seen from Figure 5.23, there is a negligible difference in absorbance between washes 4 and 5. This indicates that 4 washes after 3 hours were sufficient to remove any unwanted constituents.

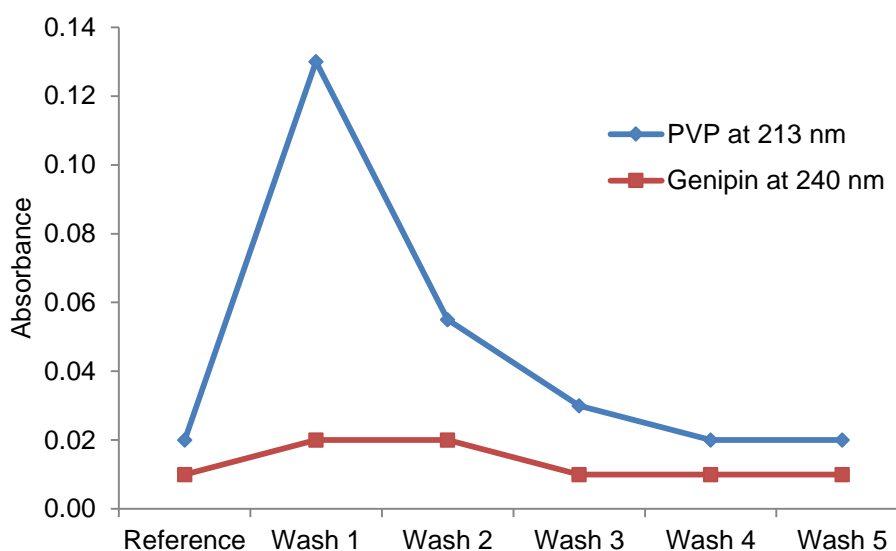


**Figure 5.23** Absorbance data to analyse for PVP (213 nm) and genipin (240 nm) from UV-Vis spectroscopy of distilled water wash solutions following immersions with a G-Ch-PVP hydrogel after 30 min (Wash 1), 1 h (Wash 2), 2 h (Wash 3), 3 h (Wash 4) and 48 h (Wash 5) to include a purely distilled water reference following no washes.

#### **5.4 A study to determine the effects of freezing and thawing on the mechanical properties of genipin-crosslinked chitosan-poly (vinyl pyrrolidone) hydrogels**

In order to investigate the effects of freezing and thawing G-Ch-PVP hydrogels on the stability of the materials, a study to determine how the mechanical strength varies as a function of the freezing and thawing times and the number of cycles can be conducted. To this end, uniaxial compression tests were performed where hydrogels were compressed to 50% of their thickness according to the method described in Section 3.10.1. An appropriate stress-strain curve could then be generated. As detailed in Section 4.13, the results presented here relate to the stress, as shown in Section 2.6.5 and equation 2.31 being the force per unit area (uniaxial stress) and the strain as defined in equation 2.3.2 being the deformation per unit length (engineering strain). The magnitude of the error bars was calculated according to the standard error.

Error bars are displayed for data points at intervals of 5% strain for clarity. In all cases, the gels tested were composed of 1 mL chitosan (1.5% w/v), 200  $\mu$ L PVP (5% w/v) and 100  $\mu$ L genipin (0.5% w/v). Gelation time and temperature also remained at 24 h at 37 °C. Parameters varied were the freezing and thawing times / number of freeze thaw cycles. Each curve on the subsequent stress-strain graphs represents an average of triplicate tests performed. The numbers in the legend represent the number of times the samples were freeze-thawed. Typical gel-like mechanical behaviour is observed in all cases with elastic behaviour at low strains (0-20%) followed by plastic deformation in the form of strain hardening (which is most likely due to reinforcement of hydrogen bonding within the network (Oyama et al., 1987)). Foam-like behaviour (elastic behaviour followed by densification) is not observed. The first batch of samples was tested in a dry environment without being immersed in any media.

#### **5.4.1 Uniaxial compression of genipin-crosslinked chitosan-poly (vinyl pyrrolidone) hydrogels evaluated in a dry environment**

Figure 5.24 depicts a stress-strain curve for samples that were frozen and thawed for 5 min. During analysis, all specimens took the form of solid gel-discs. Upon handling the samples, it was observed that all gels were particularly unstable apart from the specimens that were subjected to 4 freeze-thaw cycles. This is depicted in the graph as samples undergoing 1-3 cycles exhibit quite a low stress at high strains. It was exceptionally difficult to handle the gels and ensure a consistent shape was retained without damage being incurred. This could explain the apparent random order of mechanical strength relative to one another exhibited by these samples. In contrast, it is clear that upon freezing and thawing samples for four cycles, that there is a marked increase in sample stability. The elastic modulus calculated for all samples also supports this conclusion (Table 5.1) whereby gels that have undergone 4 freeze-thaw cycles exhibit an elastic modulus of 172 Pa and are hence stiffer compared to those that were subjected to 1-3 cycles (37-74 Pa in a random order). The effects of repeated freeze-thawing on strain hardening are also apparent whereby the transition from elastic behaviour to plastic deformation occurs at lower strains following more freeze-thaw cycles.

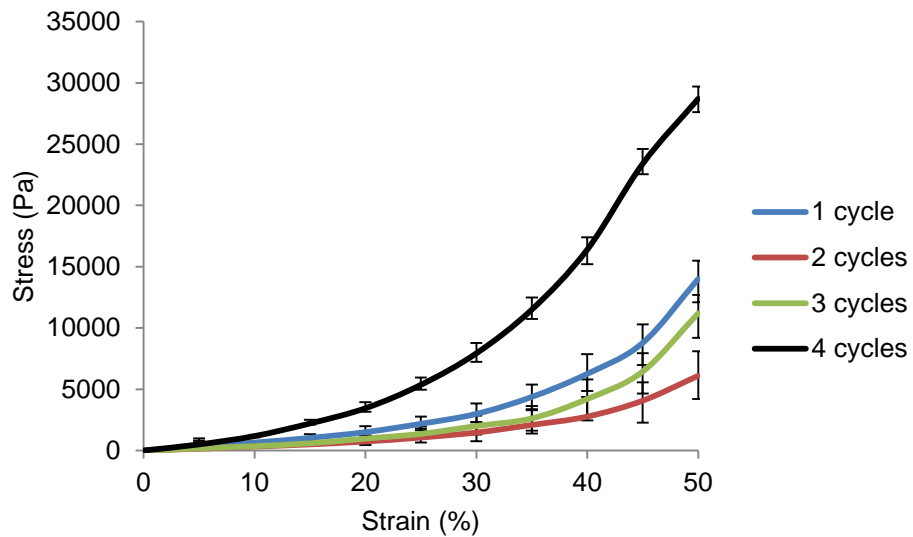


**Figure 5.24** Stress-strain graph depicting uniaxial compression tests for G-Ch-PVP hydrogels that were freeze-thawed for 5 min for a varying number of cycles.

**Table 5.1** Elastic modulus between 0-20% strain of G-Ch-PVP hydrogels that were freeze-thawed for 5 min for a varying number of cycles.

Number of cycles	Elastic Modulus (Pa)
1	74
2	37
3	47
4	172

Samples tested that were freeze-thawed for 15 min are shown in Figure 5.25. As can be seen from this data, the stability of the specimens increases in line with the number of freeze-thaw cycles ( $1 < 2 < 3 < 4$ ). This is also exemplified by the increase in the elastic modulus of samples shown in Table 5.2. This data reveals a dependence of increasing mechanical strength of specimens when subjected to more freeze-cycles during a period of 15 min. From the data there seems to be a marked increase in sample strength for specimens that undergone freeze-thawing between 2 and 3 cycles. Comparing these findings to the published literature, it seems that these results are in good agreement with observations that increasing the number of freeze-thaw cycles improves sample stability and strength by reinforcing existing crystals within the porous network (Hassan and Peppas, 2000, Holloway et al., 2013). Furthermore, comparing specimens in Figure 5.25, which were freeze-thawed for 15 min to those in Figure 5.24, which were freeze-thawed for 5 min, particularly those that had

undergone 3 and 4 cycles, it is clear there is an increase in mechanical stability. For example the stress at 50% strain for specimens treated with 4 freeze-thaw cycles of 15 min exceeded 50,000 Pa compared to their counterparts treated for 5 min where the stress was less than 30,000 Pa. This indicates that freezing and thawing time plays an important role in enhancing the stability of these materials.

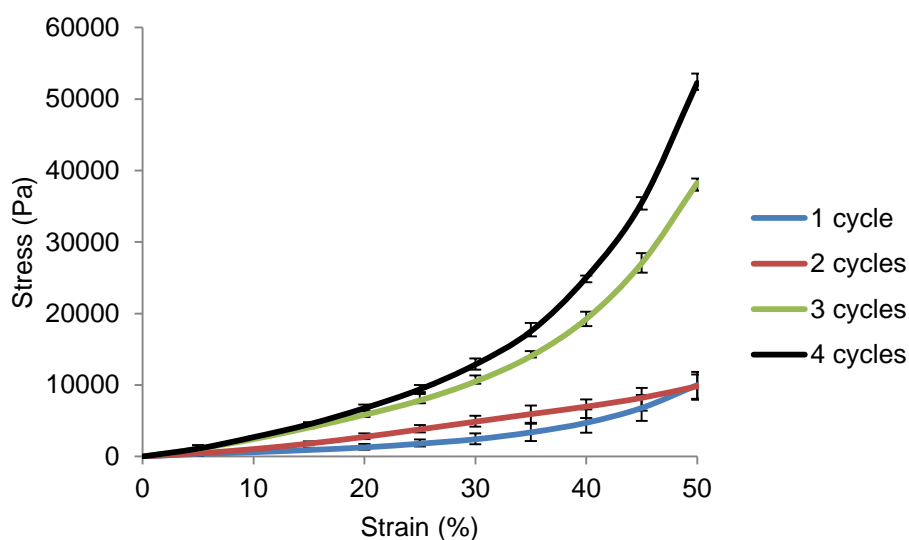


**Figure 5.25** Stress-strain graph depicting uniaxial compression tests for G-Ch-PVP hydrogels that were freeze-thawed for 15 min for a varying number of cycles.

**Table 5.2** Elastic modulus between 0-20% strain of G-Ch-PVP hydrogels that were freeze-thawed for 15 min for a varying number of cycles.

Number of cycles	Elastic Modulus (Pa)
1	62
2	137
3	292
4	338

Specimens that were freeze-thawed for 30 min are shown in Figure 5.26. Despite the trend in freeze-thaw cycles being less clear, there are important points to be noted. The sample that was freeze-thawed for just one cycle does show lower mechanical stability than those freeze-thawed for 2-4 cycles in agreement with prior results. This is also proven to be the case upon calculation of the elastic modulus (Table 5.3) where after one freeze-thaw cycle, the elastic modulus is 348 Pa compared to when the gels were subjected to multiple cycles (356-487 Pa). Compared to hydrogels tested for a lower freeze-thawing time

(Figure 5.24 and 5.25), each curve does show an increase in network strength, representing the effect of how increasing the freeze-thawing time affects the overall gel.

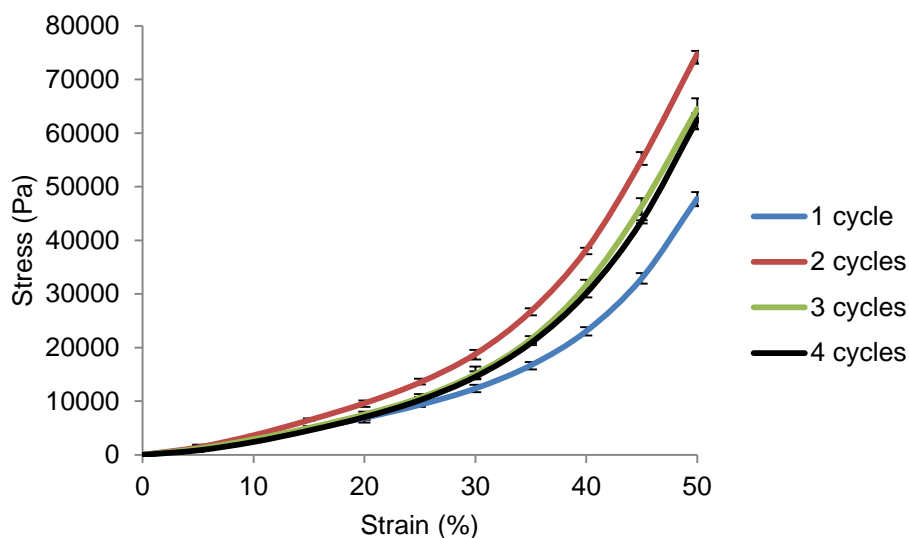


**Figure 5.26** Stress-strain graph depicting uniaxial compression tests for G-Ch-PVP hydrogels that were freeze-thawed for 30 min for a varying number of cycles.

**Table 5.3** Elastic modulus between 0-20% strain of G-Ch-PVP hydrogels that were freeze-thawed for 30 min for a varying number of cycles.

Number of cycles	Elastic Modulus (Pa)
1	348
2	487
3	380
4	356

Hydrogels that were frozen and thawed for 1 h were tested (Figure 5.27). Interestingly, a very similar trend in terms of the number of freeze-thaw cycles and the stability of the sample is observed, which is in line with the results in Figure 5.26 (1<3,4<2) and, to some extent, the elastic modulus values in Table 5.4. It seems that compared to samples freeze-thawed for 30 min, the only specimen that has shown a small noticeable improvement in mechanical strength is the hydrogel that was subjected to 2 freeze-thaw cycles. This seems to indicate that past a certain point, not only do the effects of increased cycles become negligible, but so does the freezing and thawing time.

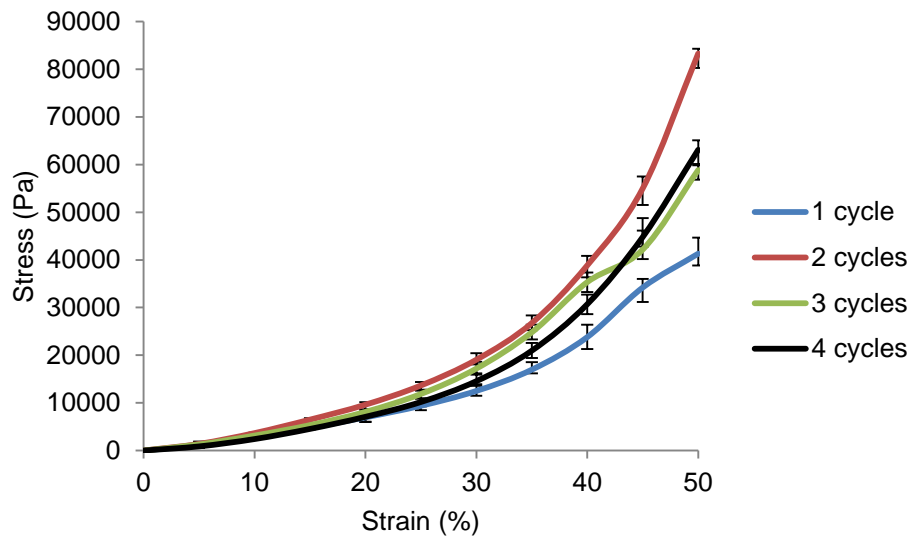


**Figure 5.27** Stress-strain graph depicting uniaxial compression tests for G-Ch-PVP hydrogels that were freeze-thawed for 1 h for a varying number of cycles.

**Table 5.4** Elastic modulus between 0-20% strain of G-Ch-PVP hydrogels that were freeze-thawed for 1 h for a varying number of cycles.

Number of cycles	Elastic Modulus (Pa)
1	352
2	487
3	406
4	356

Upon increasing the duration of freeze-thawing treatment, it is apparent that freeze-thaw time is a significant factor in enhancing sample stability, although the effects of cycling for one period of time are more dominant. This observation is depicted in Figure 5.28 where the average elastic modulus variation is higher for samples subjected to cycling (blue data points) in comparison to those subjected to increased freeze-thawing times (red data points) between 5 and 30 min. Furthermore, the distribution of sample stability between all cycles tested becomes narrower (comparison of Figure 5.26 at 30 min freeze-thawing to Figures 5.24 and 5.25 at 5 min and 15 min freeze-thawing). This is outlined in Figure 5.28 whereby past a certain time period of freezing and thawing (30 min), the effects of introducing cycles plays a diminished role (indicated by the negative gradient of the blue data points between 2 and 4 freeze-thaw cycles).

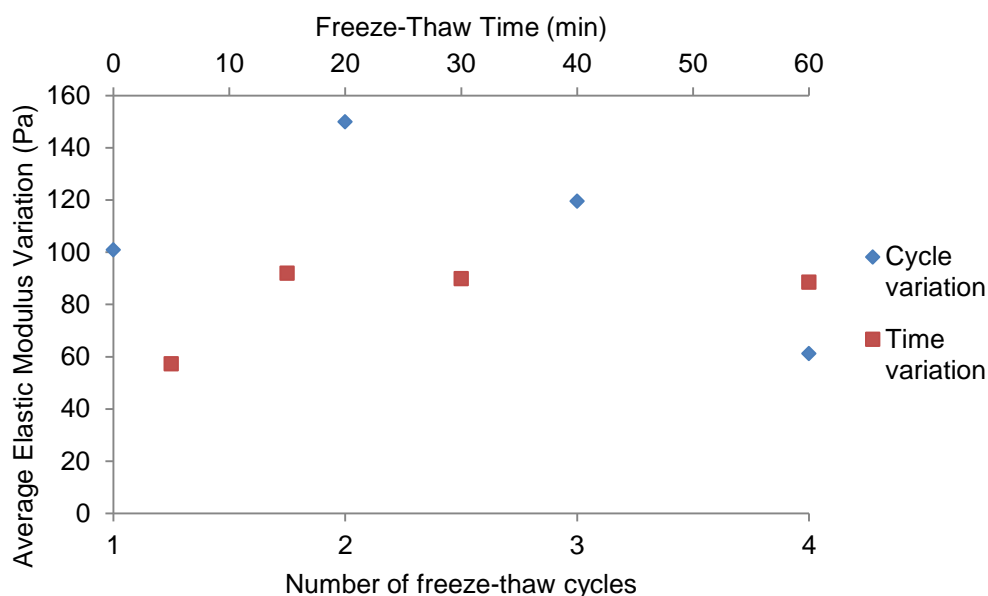


**Figure 5.28** Comparison of the effects of freeze-thaw time and the number of freeze-thaw cycles on the average variation in the elastic modulus of G-Ch-PVP hydrogels.

It is also worth noting that compared to samples tested without any freeze-thawing, the gel also exhibits linear elastic behaviour up to approximately 20% strain and subsequent plastic deformation ensues in the form of strain hardening, resulting in densification. Furthermore, without freeze-thawing, the stress was approximately 5500 Pa at 50% strain and the elastic modulus between 0-20% strain was 33 Pa (Figure 4.55), hence there is a significant enhancement in mechanical properties in all samples investigated in this section (Figures 5.25-5.28). This clearly demonstrates the positive improvement in the mechanical strength and stiffness of samples by freezing and thawing following gel fabrication.

#### **5.4.2 Uniaxial compression of genipin-crosslinked chitosan-poly (vinyl pyrrolidone) hydrogels evaluated in a wet environment**

The aforementioned samples were subsequently tested when they had been previously swollen in a pH 2 buffered solution for 24 h. It is important that the mechanical properties are evaluated with respect to where the hydrogels may find application (a hydrated environment). Surface tension was accounted for by zeroing / recalibrating the instrument when appropriate. When fully swollen, gels that were freeze-thawed for 5 min (after 1, 2, 3 and 4 cycles), were simply too unstable to take meaningful measurements. Therefore the first set of data

presented depicts the stability of samples freeze-thawed for 15 min over various cycles (Figure 5.29). Compared to the dry samples that were frozen and thawed for 15 min, these specimens were far less stable. This is to be expected owing to the higher level of hydration of the network. Akin to samples tested in a dry environment, the same trend in the effects of the number of cycles on the stability of samples was found ( $1 < 2 < 3 < 4$ ). This trend is also evident from the elastic modulus calculations (Table 5.5). These results indicate that the effects of tuning the mechanical stability in this way translate to when the gel is in a swollen state where it will be applied.

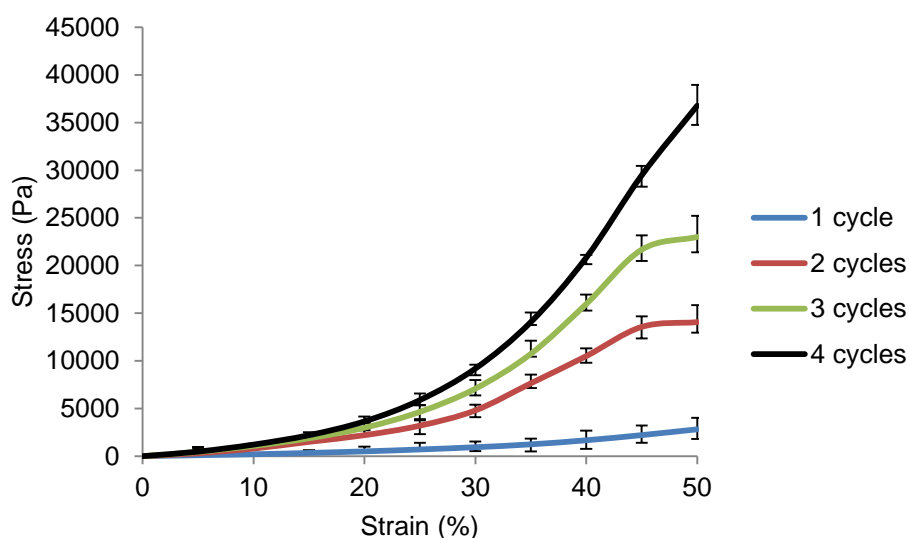


**Figure 5.29** Stress-strain graph depicting uniaxial compression tests for G-Ch-PVP hydrogels that were freeze-thawed for 15 min for a varying number of cycles and immersed in a pH 2 buffered solution during testing.

**Table 5.5** Elastic modulus between 0-20% strain of G-Ch-PVP hydrogels that were freeze-thawed for 15 min for a varying number of cycles and immersed in a pH 2 glycine buffered solution.

Number of cycles	Elastic Modulus (Pa)
1	25
2	112
3	148
4	180

Specimens subjected to 30 min freeze-thaw cycles and tested in a wet environment are shown in Figure 5.30. As in the dry state, there is a marked improvement in sample stability with freeze-thawing for a longer period of time.

The trend in improved mechanical properties of the network with more freeze-thaw cycles also remains intact as also displayed when analysing the elastic modulus data (Table 5.6). A further new observation is that the yield point is reached in all samples during this compression. The yield point is also reached at lower strains when the number of freeze-thaw cycles increases. This indicates that samples subjected to more freeze-thaw cycles for 30 min intervals are stiffer. It is known that the stiffness of networks can be tuned by varying the crosslink density (Gardel et al., 2004). Therefore it is expected as by introducing more freeze-thaw cycles, a larger degree of enforcement of existing crystals within the network will occur, leading to a stiffer polymer matrix, similar to what can be achieved by increasing the crosslink density.

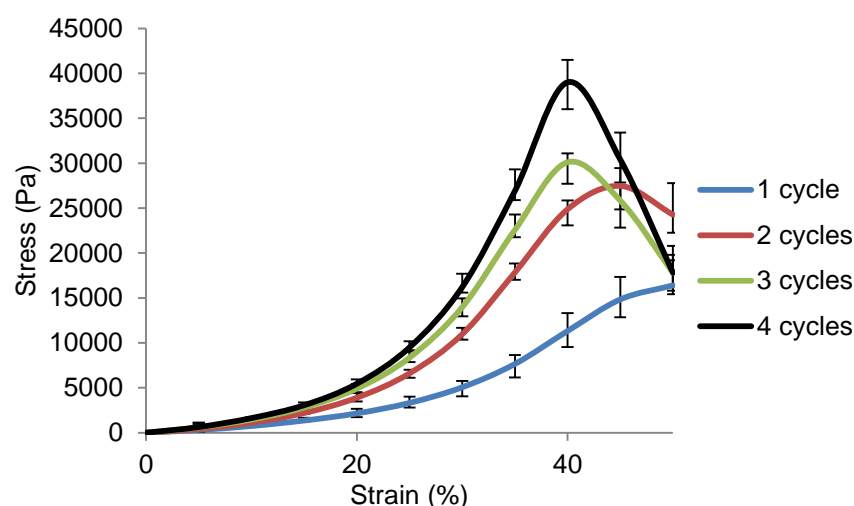


**Figure 5.30** Stress-strain graph depicting uniaxial compression tests for G-Ch-PVP hydrogels that were freeze-thawed for 30 min for a varying number of cycles and immersed in a pH 2 glycine buffered solution during testing.

**Table 5.6** Elastic modulus between 0-20% strain of G-Ch-PVP hydrogels that were freeze-thawed for 30 min for a varying number of cycles and immersed in a pH 2 glycine buffered solution.

Number of cycles	Elastic Modulus (Pa)
1	107
2	192
3	240
4	267

Finally, samples evaluated in an aqueous environment that had been freeze-thawed for 1 h were studied (Figure 5.31). As previously observed, an

improvement in the strength of all samples was shown exemplifying the effect of freeze-thawing time on stability. This can be seen by analysing the stress at 50% strain in comparison to gels that had been freeze-thawed for just 30 min (Figure 5.30). Upon examination, all gels freeze-thawed for 1 h are in the region of 34000-40000 Pa at 50% strain in comparison to gels freeze-thawed for 30 min where, for example, some gels exhibit a stress of just 16000 Pa at 50% strain. Similar to the dry state, there is a narrow distribution of mechanical properties (also shown by the elastic modulus data in Table 5.7 where there is a range of just 46 Pa across all cycles), in line with previous findings in dry conditions, which show that the number of cycles plays a diminished role with increasing freeze-thawing time. In contrast to samples freeze-thawed for 30 min (Figure 5.30), a yield point being reached followed by subsequent decrease in stress is not pronounced. This may be due to the lesser role the number of freeze-thaw cycles plays on the mechanical properties of the network at higher freeze-thaw times. Consequently, this indicates that network stiffness is more dependent upon the number of freeze-thaw cycles when they have a dominant role as oppose to the freeze-thawing time. The observations have not been tested for statistical significance, although the effects of freeze-thawing time and the number of cycles on the variation in the average elastic modulus have been investigated (Figure 5.32). In accordance with comparisons made between gels evaluated in a dry environment (Figure 5.28), freeze-thaw cycles play a dominant role in sample stability for low freeze-thawing durations.

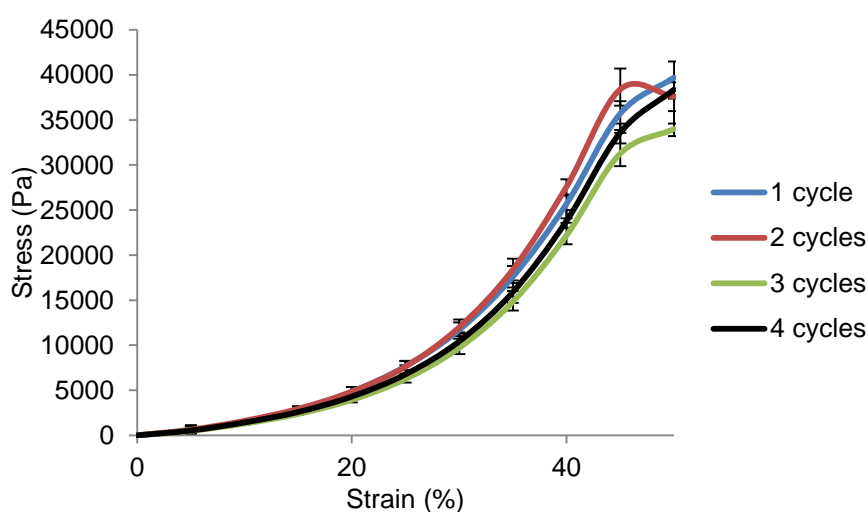


**Figure 5.31** Stress-strain graph depicting uniaxial compression tests for G-Ch-PVP hydrogels that were freeze-thawed for 1 h for a varying number of cycles and immersed in a pH 2 glycine buffered solution during testing.

**Table 5.7** Elastic modulus between 0-20% strain of G-Ch-PVP hydrogels that were freeze-thawed for 1 h for a varying number of cycles and immersed in a pH 2 glycine buffered solution.

Number of cycles	Elastic Modulus (Pa)
1	241
2	240
3	195
4	213

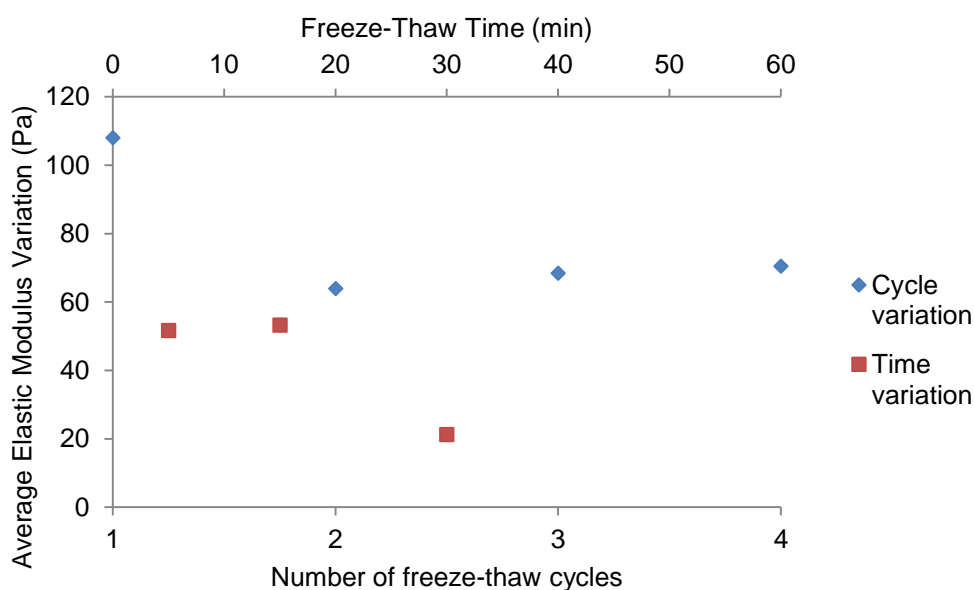


**Figure 5.32** Comparison of the effects of freeze-thaw time and the number of freeze-thaw cycles on the average variation in the elastic modulus of G-Ch-PVP hydrogels immersed in a pH 2 glycine buffered solution.

The values of elastic modulus for freeze-thawed G-Ch-PVP hydrogels can also be compared to the environment in which the compression test was conducted (Figures 5.33-5.35). As shown for all freeze-thaw timescales (15 min, 30 min and 1 h), the value of the elastic modulus is higher in all cases for those specimens evaluated in a dry environment compared to when immersed in a pH 2 glycine buffer. As previously mentioned, this is to be expected considering the higher level of network hydration when the gels are placed in such an acidic buffer compared to the dry state.

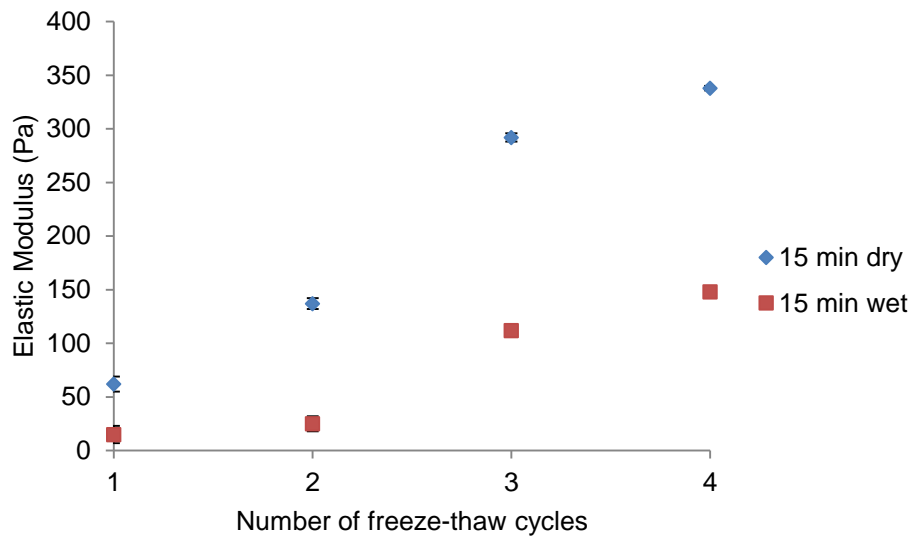


**Figure 5.33** Comparison between the elastic modulus of G-Ch-PVP hydrogels that were freeze-thawed for 15 min for various cycles and compressed in either a dry environment or via immersion in a pH 2 glycine buffer.

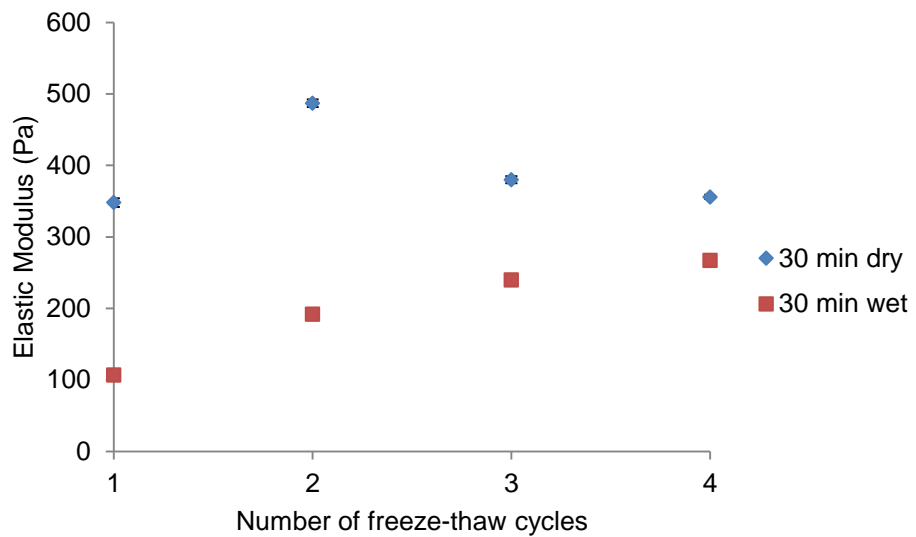


**Figure 5.34** Comparison between the elastic modulus of G-Ch-PVP hydrogels that were freeze-thawed for 30 min for various cycles and compressed in either a dry environment or via immersion in a pH 2 glycine buffer.

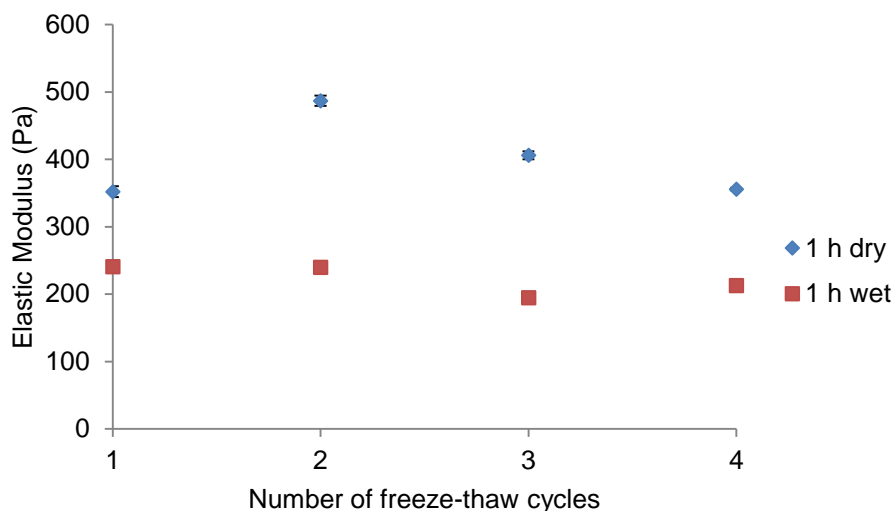


**Figure 5.35** Comparison between the elastic modulus of G-Ch-PVP hydrogels that were freeze-thawed for 1 h for various cycles and compressed in either a dry environment or via immersion in a pH 2 glycine buffer.

Finally, Figure 5.36 depicts a comparison of freeze-thaw time and elastic modulus. This is shown for samples that had undergone one freeze-thaw cycle. As expected, for hydrogel specimens evaluated in both dry and wet environments, as the freeze-thaw time increases, the elastic modulus also generally increases. This is most likely due to more efficient phase separation into the polymer-rich and water-rich phases, facilitating the formation of and enhancement in hydrogen bonding within the network.

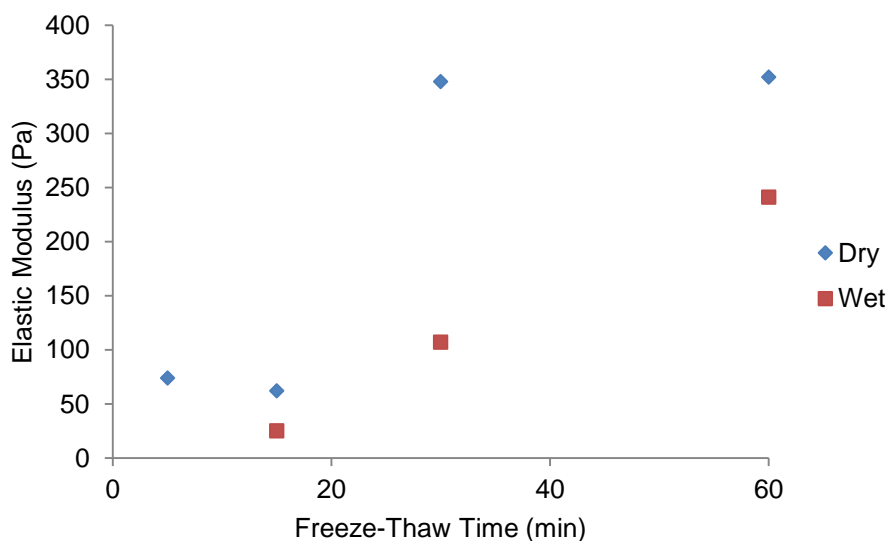


**Figure 5.36** Comparison between the elastic modulus of G-Ch-PVP hydrogels that were freeze-thawed once for various time periods and compressed in either a dry environment or via immersion in a pH 2 glycine buffer.

## 5.5 Swelling potential of freeze-thawed genipin-crosslinked chitosan-poly (vinyl pyrrolidone) hydrogels

The swelling response of freeze-thawed G-Ch-PVP hydrogels was evaluated after being collapsed in a pH 7 phosphate buffered solution and subsequently swollen in distilled water. This study was conducted gravimetrically to account for the whole network on the macroscale. Figures 5.37 and 5.38 show the response of G-Ch-PVP hydrogels swelling in distilled water without subsequent freeze-thawing. The swelling ratio (recorded as 0%) at the time point of 0 min has not been plotted as the  $\log_{10}(0)$  is undefined. Distilled water was chosen as the surrounding medium as due to the high degree of hydrophilicity in the network, an exceedingly large degree of swelling can be observed compared to immersion in a pH 2 buffered solution (due to the differing ionic strengths). This allows the differences in swelling between hydrogels with subtle structural variations to be more easily observed. As expected, initial swelling up to 120 min is quite rapid followed by a plateau effect as the surrounding solution diffuses into the porous network (Figure 5.37). However, it is particularly striking how large the error bars are for these specimens (over 80% above and below the average value recorded in some cases). This is most likely due to the large instability of the samples, making it exceptionally difficult to engineer multiple samples with very similar shapes, causing the swelling response to be non-uniform (Li and Tanaka, 1990, Shibayama et al., 1992).

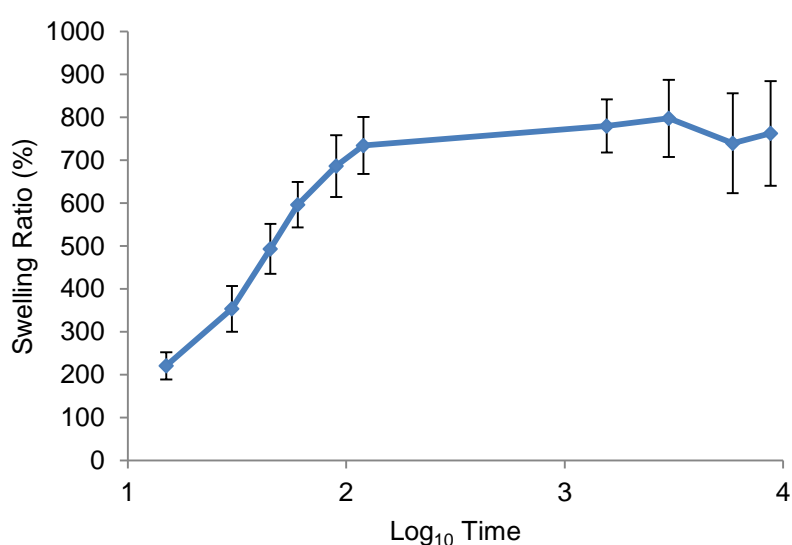


**Figure 5.37** Gravimetric swelling of G-Ch-PVP hydrogels swollen in distilled water.

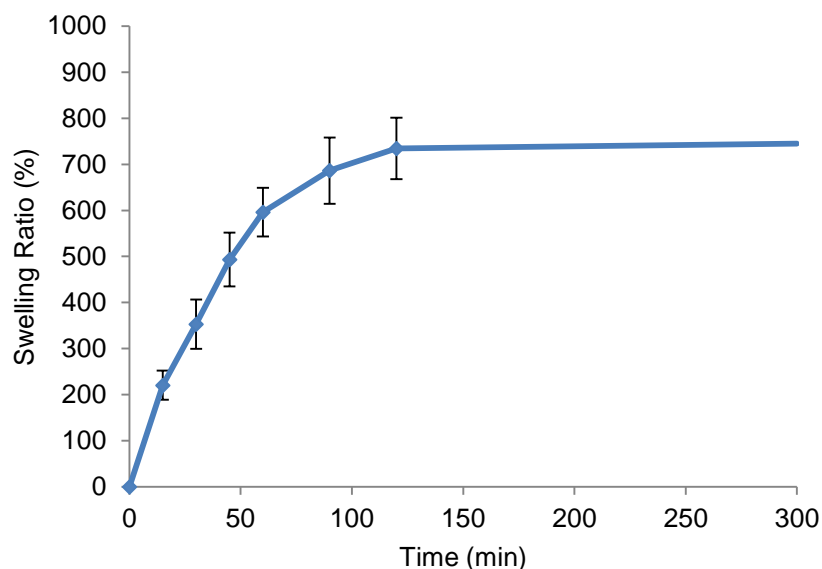


**Figure 5.38** Gravimetric swelling of G-Ch-PVP hydrogels swollen in distilled water showing the initial response.

Samples that were subjected to freeze-thaw cycles of 5 min are shown in Figures 5.39 and 5.40. In line with the compression studies in the previous sections, the gels that were frozen and thawed for 1 and 2 cycles swell noticeably more than those subjected to 3 and 4 cycles. In fact, during the first 200 min of swelling (Figure 5.40), it is clear that the gel frozen and thawed for 1 cycle was more responsive than its counterpart frozen and thawed for 2 cycles. Therefore, it seems that not only does repetitive freeze-thawing for this time interval enhance the mechanical properties; it also reduces the swelling response somewhat. This can be likened to an enhancement in the mechanical stability of hydrogel samples upon increasing the degree of crosslinking in the network, although this also typically results in a decrease in the swelling response. Both graphs in Figures 5.39 and 5.40 show curves with much smaller error bars than samples without any freeze-thawing (Figure 5.37), exemplifying the stability enhancement resulting from this post-treatment, allowing the specimens to be more easily handled and adopt a more uniform and consistent shape. Furthermore, comparing the swelling ratio at the same time intervals between freeze-thawed samples and specimens with no post-synthetic treatment, particularly those subjected to 1 and 2 cycles, there is no apparent decrease in the swelling response, despite a small enhancement in the mechanical stability.

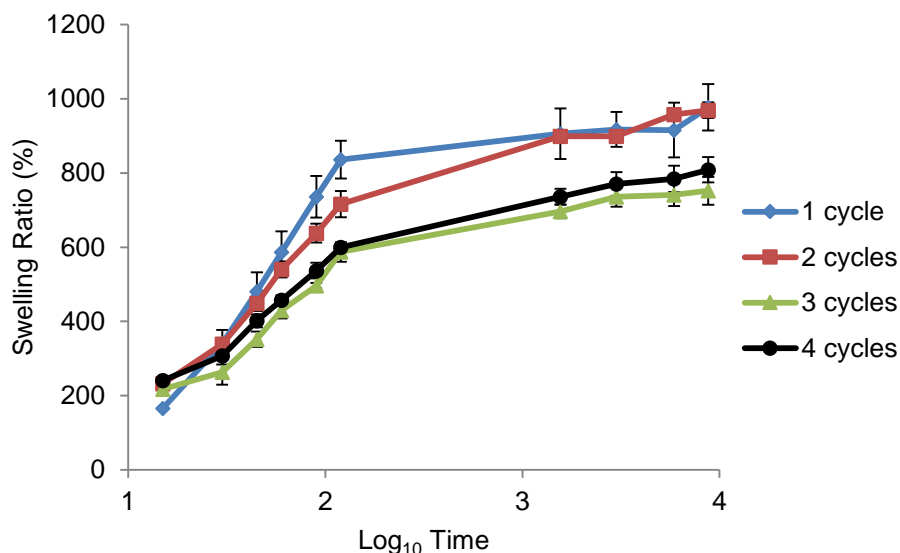


**Figure 5.39** Gravimetric swelling of G-Ch-PVP hydrogels freeze-thawed for 5 min and swollen in distilled water.

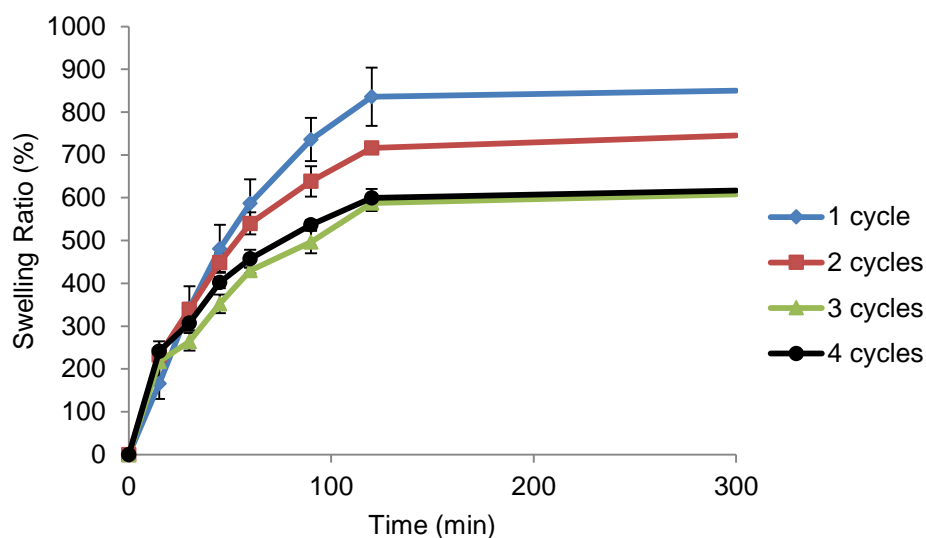


**Figure 5.40** Gravimetric swelling of G-Ch-PVP hydrogels freeze-thawed for 5 min and swollen in distilled water showing the initial response.

Specimens freeze-thawed for 15 min and swollen in distilled water are shown in Figures 5.41 and 5.42. It is very clear that samples which had undergone 1 freeze-thaw cycle were much more responsive than those subjected to 2-4 cycles. It seems there is a clear transition whereby after a certain freezing time or number of freeze-thaw cycles the accumulation of crystallite formation restricts the response of the network and simultaneously increases the mechanical stability of the overall sample as a consequence (Figure 5.29).

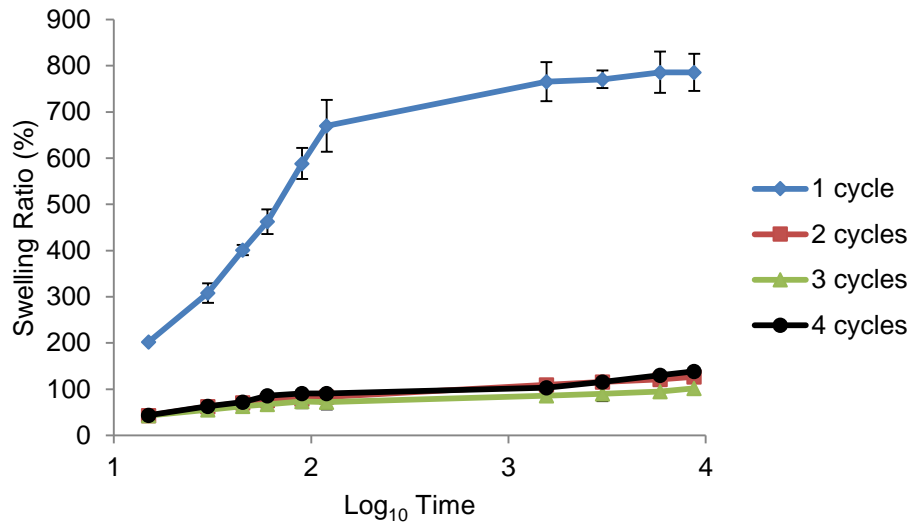


**Figure 5.41** Gravimetric swelling of G-Ch-PVP hydrogels freeze-thawed for 15 min and swollen in distilled water.

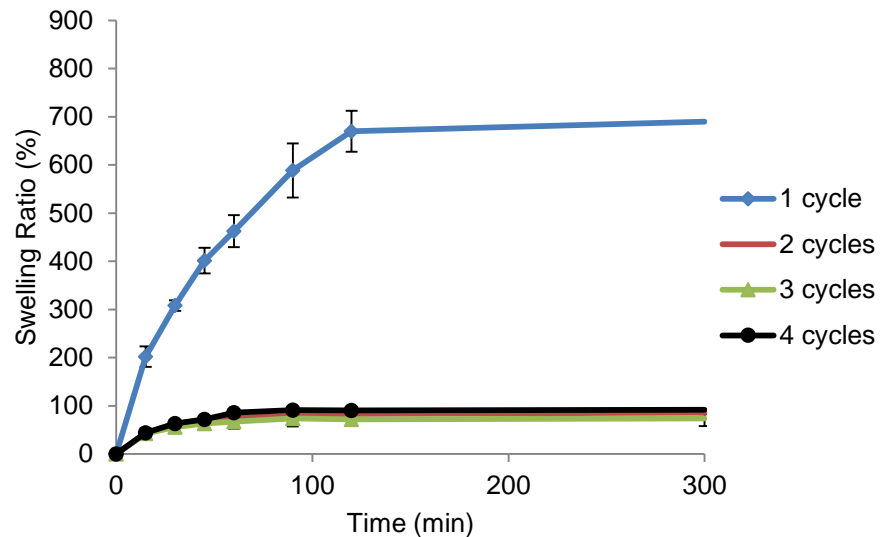


**Figure 5.42** Gravimetric swelling of G-Ch-PVP hydrogels freeze-thawed for 15 min and swollen in distilled water showing the initial response.

Studies were subsequently conducted on G-Ch-PVP hydrogels frozen and thawed for 30 min for various cycles (Figures 5.43 and 5.44). All samples, including the specimens frozen and thawed once displayed a large decrease in the swelling response compared to those treated for shorter freezing times (Figures 5.39 and 5.41). The number of cycles does play a small role as hydrogels frozen and thawed once do swell more than their counterparts. However, compared to the aforementioned studies, the difference in terms of swelling response between all four curves is much smaller, demonstrating the diminished role freeze-thaw cycling plays with increasing freezing time, as

concluded in the compression test results. It is also apparent that the size of the error bars decrease with an increasing number of freeze-thaw cycles for each time period (Figures 5.37-5.44) showing the increasing uniformity and stability due to cycling.

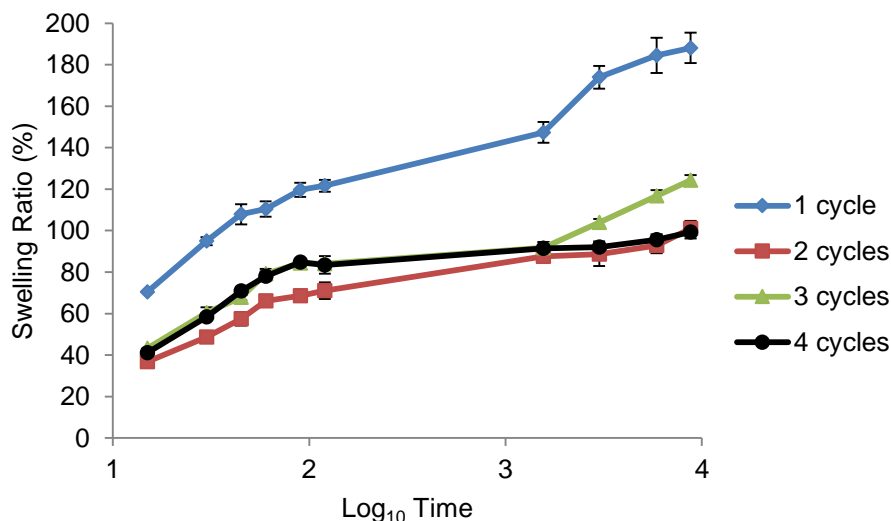


**Figure 5.43** Gravimetric swelling of G-Ch-PVP hydrogels freeze-thawed for 30 min and swollen in distilled water.

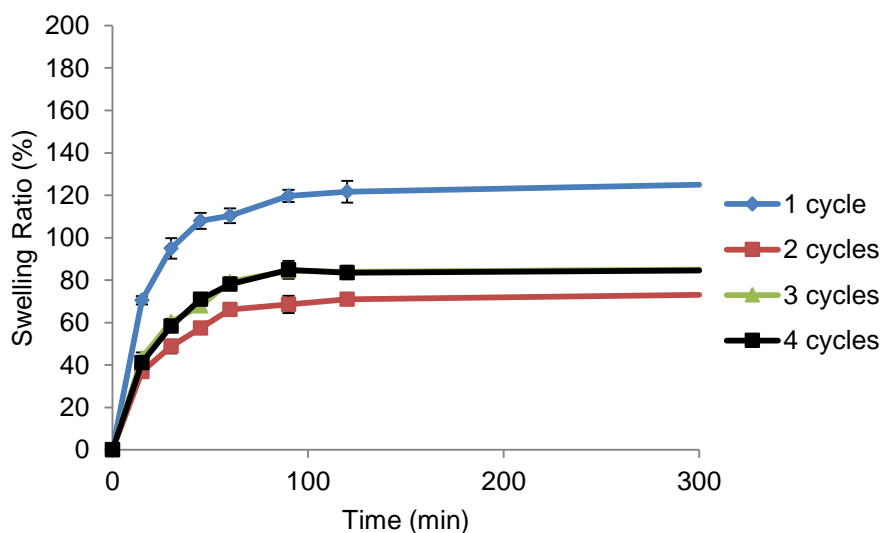


**Figure 5.44** Gravimetric swelling of G-Ch-PVP hydrogels freeze-thawed for 30 min and swollen in distilled water showing the initial response.

Lastly, hydrogel specimens were evaluated that were frozen and thawed for 1 h (Figures 5.45 and 5.46). As before, the set of samples frozen and thawed once displayed the greatest swelling response closely followed by the other specimens. Also the gap between the most and least responsive network is just

50% (approximately) further showing the small effects of the number of cycles at this freezing and thawing duration. To further substantiate this, unlike previous gels frozen and thawed for shorter time periods, there is no apparent change in the size of the error bars in Figure 5.45, which also demonstrates the minor effects of additional cycling. Finally, comparing these results to gels that were freeze-thawed for 30 min (Figures 5.43 and 5.44), there is very little swelling difference between gels that were subjected to the same number of cycles, showing the diminishing effect of freezing and thawing time too. These findings are strongly aligned with the previous compression test results.

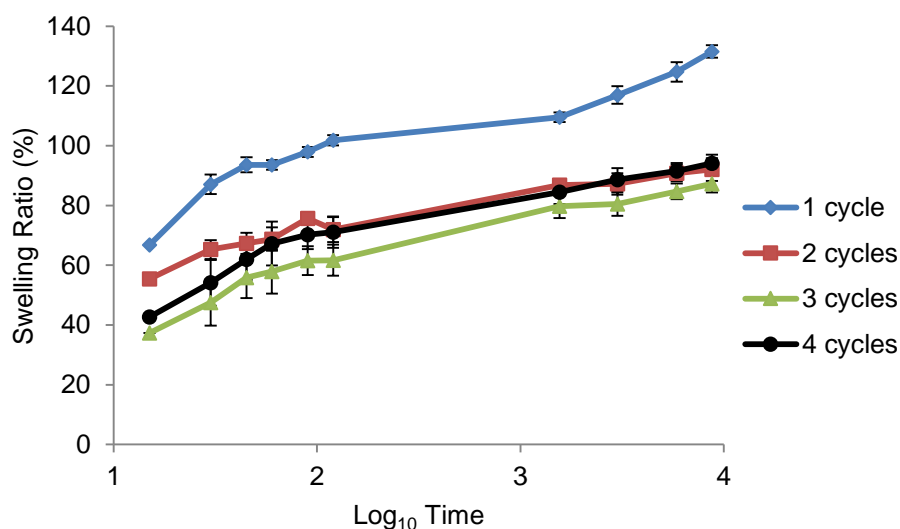


**Figure 5.45** Gravimetric swelling of G-Ch-PVP hydrogels freeze-thawed for 1 h and swollen in distilled water.

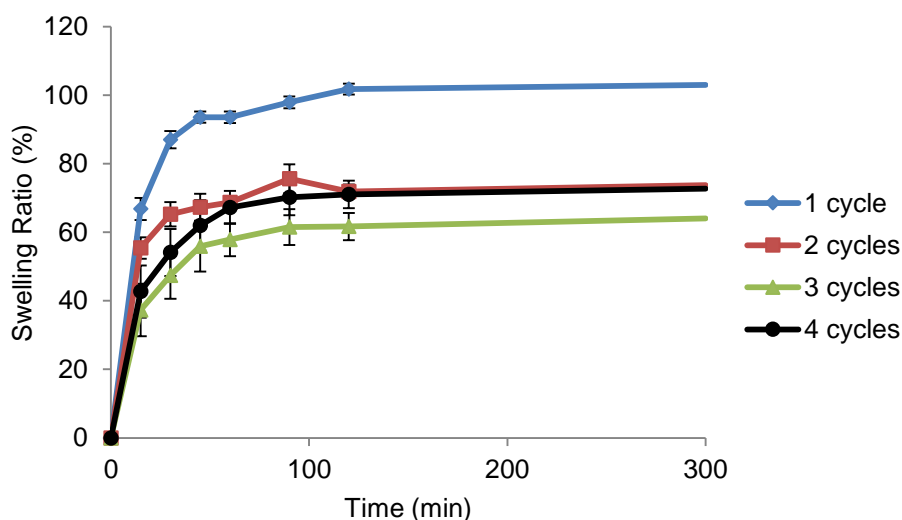


**Figure 5.46** Gravimetric swelling of G-Ch-PVP hydrogels freeze-thawed for 1 h and swollen in distilled water showing the initial response.

There is also a link between the swelling ratio and elastic modulus as represented in Figure 5.47 where the swelling ratio after the gels were immersed in distilled water from Figures 5.41, 5.43 and 5.45 is plotted against the elastic modulus from Tables 5.5-5.7 as a function of the number of freeze-thaw cycles. In general, for all freeze-thaw durations, it is clear that as the elastic modulus is increased, the swelling ratio decreases. This could be due to an enhancement in hydrogen bonding between chitosan and PVP moieties, which could impede overall swelling. Similarly, it is also evident (particularly between 1 and 2 freeze-thaw cycles) that as the number of freeze-thaw cycles is increased, a large enhancement in elastic modulus accompanied by a decrease in network swelling occurs.

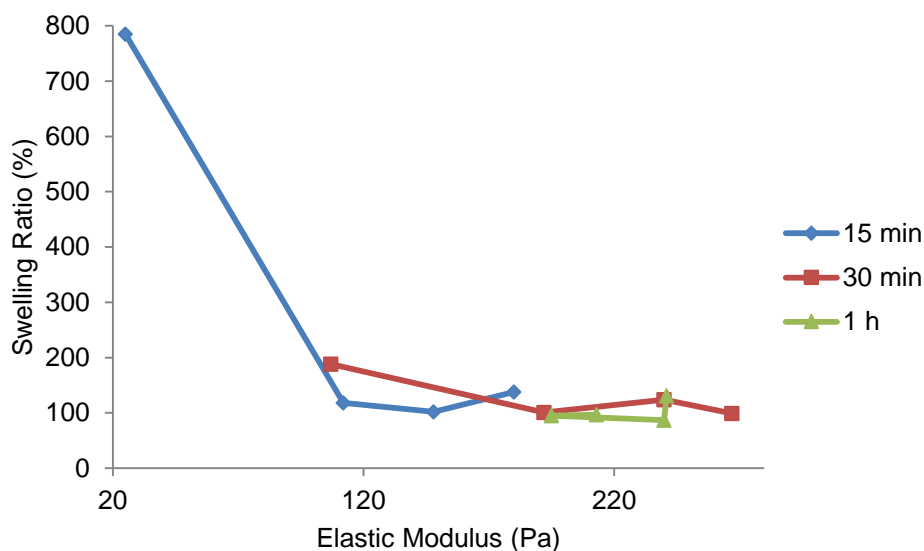


**Figure 5.47** Comparison of the swelling ratio of G-Ch-PVP hydrogels in distilled water that were freeze-thawed for various cycles and time scales with the elastic modulus.

Hydrogels freeze-thawed for 15, 30 and 60 min were placed in citric acid and sodium hydroxide solutions with an unmodified ionic strength (0%) for 24 h according to Table 3.6. The elastic modulus was then determined and plotted as a function of pH (Figure 5.48). In all cases there is a dependence of pH of the surrounding solution on the elastic modulus of the gel. In a swollen state at low pH, the elastic modulus is comparatively low (approximately 20 Pa for gels freeze-thawed for 15 min) followed by a sharp rise at pH 6 (close to the pKa of chitosan (6.3-6.6)) to approximately 145 Pa. The elastic modulus is then virtually constant when immersed in solutions up to pH 13. This general behaviour is also exhibited for gels that were freeze-thawed for 30 min and 1 h.

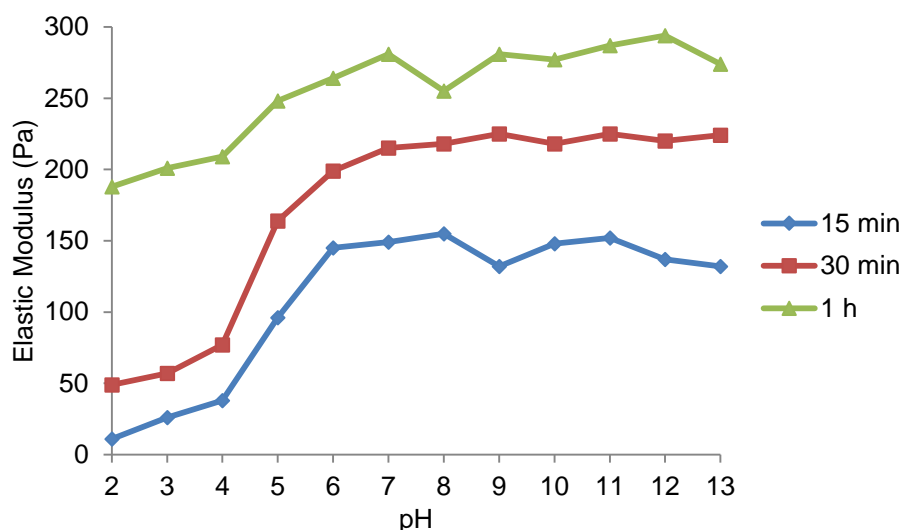


**Figure 5.48** Comparison of the elastic modulus of freeze-thawed G-Ch-PVP hydrogels as a function of pH in citric acid and sodium hydroxide-based buffer solutions.

This behaviour also correlates well with hydrogel swelling measurements (Figure 4.14) whereby a large degree of swelling was observed below pH 6 followed by collapse. Figure 5.49 illustrates the negative correlation between elastic modulus and swelling ratio. This dependence is particularly prevalent when the elastic modulus is low and is most likely due to the variation in the number of protonated amine groups present within the network. This variation is likely to occur between pH 2 and 7 (pKa of chitosan is 6.3-6.6), which from Figure 5.48, is between 20 and 150 Pa.

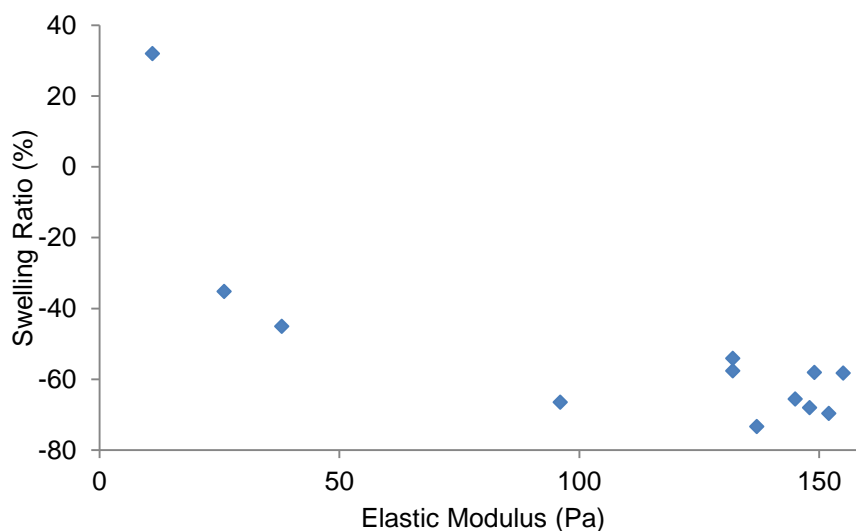


**Figure 5.49** Comparison of the elastic modulus of G-Ch-PVP hydrogels freeze-thawed for 15 min with the overall swelling ratio after 24 h in citric acid and sodium hydroxide-based buffer solutions at varying pH.

Finally, a similar link between elastic modulus and surface porosity based on the data collected in Table 4.10 is also depicted in Figure 5.50. As expected as the elastic modulus is increased, up to a point, there is a negative correlation with the surface porosity. This trend strongly agrees with protonation and swelling data and demonstrates a strong link between elastic modulus, pH, swelling and protonation.

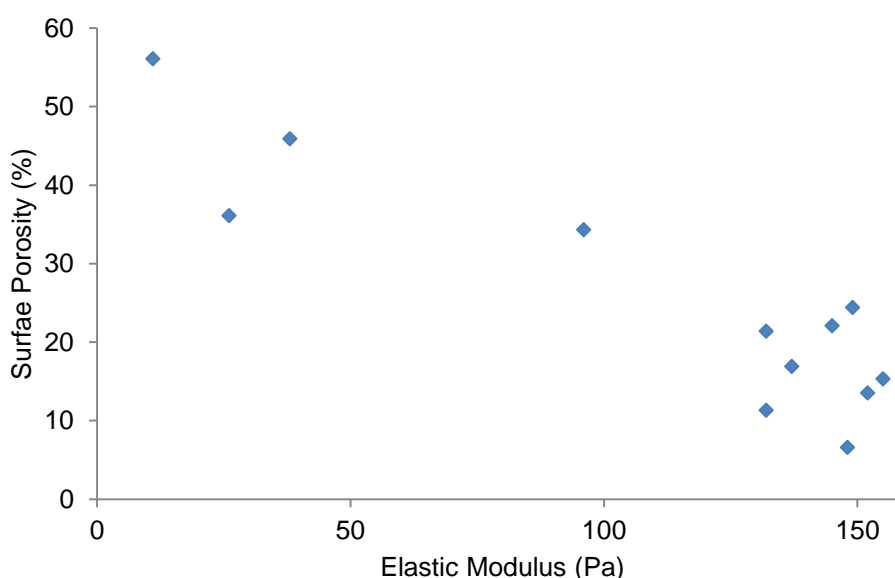


**Figure 5.50** Variation in the surface porosity of G-Ch-PVP hydrogels immersed in various mixtures of citric acid and sodium hydroxide solutions as a function of their elastic modulus.

To summarise, akin to the behaviour of PVA upon freeze-thawing (Figure 2.26), it is likely that such processing leads to an initial phase separation into a polymer-rich phase and a water-rich phase (Holloway et al., 2013). During freezing, this may facilitate the formation of highly concentrated regions of where the crosslinked polymer resides, enhancing the degree of hydrogen bonding between gel constituents, resulting in crystallite formation and densification. This could be represented by a gradual increase in the elastic modulus with freezing time and in some cases the number of freeze-thaw cycles. In turn, this results in a concomitant reduction in the swelling response of the network. Based on this, it is likely that the degree of hydrogen bonding within the network will vary according to Figures 5.51-5.53. Genipin moieties have been omitted as they are not directly involved in hydrogen bonding as depicted in Figure 2.50. Figure 5.51 details the limited hydrogen bonds between chitosan and PVP polymers prior to freeze-thawing.

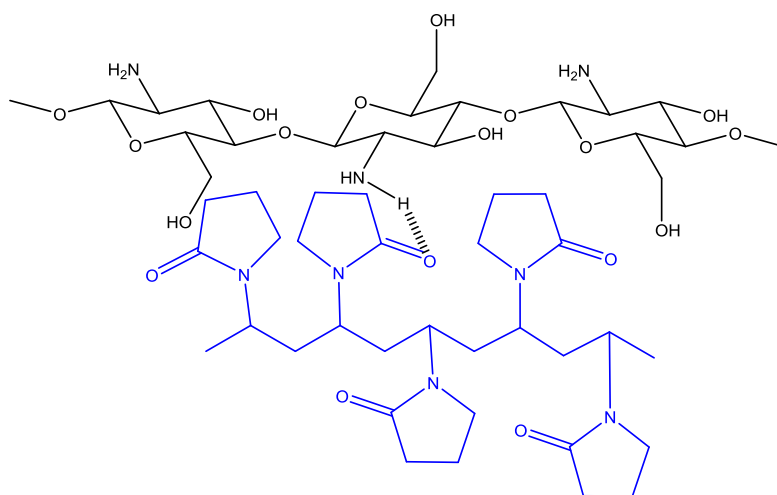


**Figure 5.51** Representation of hydrogen bonding between chitosan and PVP moieties prior to freeze-thawing. Genipin moieties have been omitted for clarity.

A depiction of how freeze-thaw processing changes the gel structure is shown in Figure 5.52. There is a higher density of chitosan and PVP moieties within close proximity owing to the enhanced degree of hydrogen bonding between the polymers.

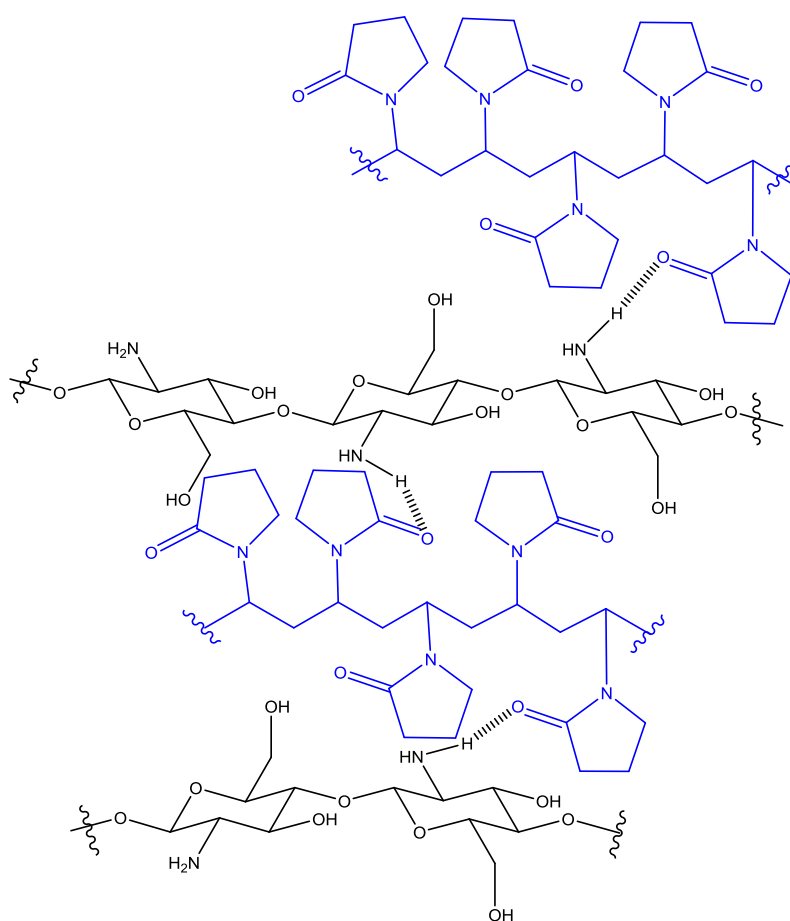


**Figure 5.52** Representation of hydrogen bonding between chitosan and PVP moieties upon freeze-thawing. Genipin moieties have been omitted for clarity.

Figure 5.53 represents what the gel structure may look like upon continued freeze-thaw treatment. An enhancement in the degree of hydrogen bonding between chitosan and PVP moieties is depicted leading to densification of the network.

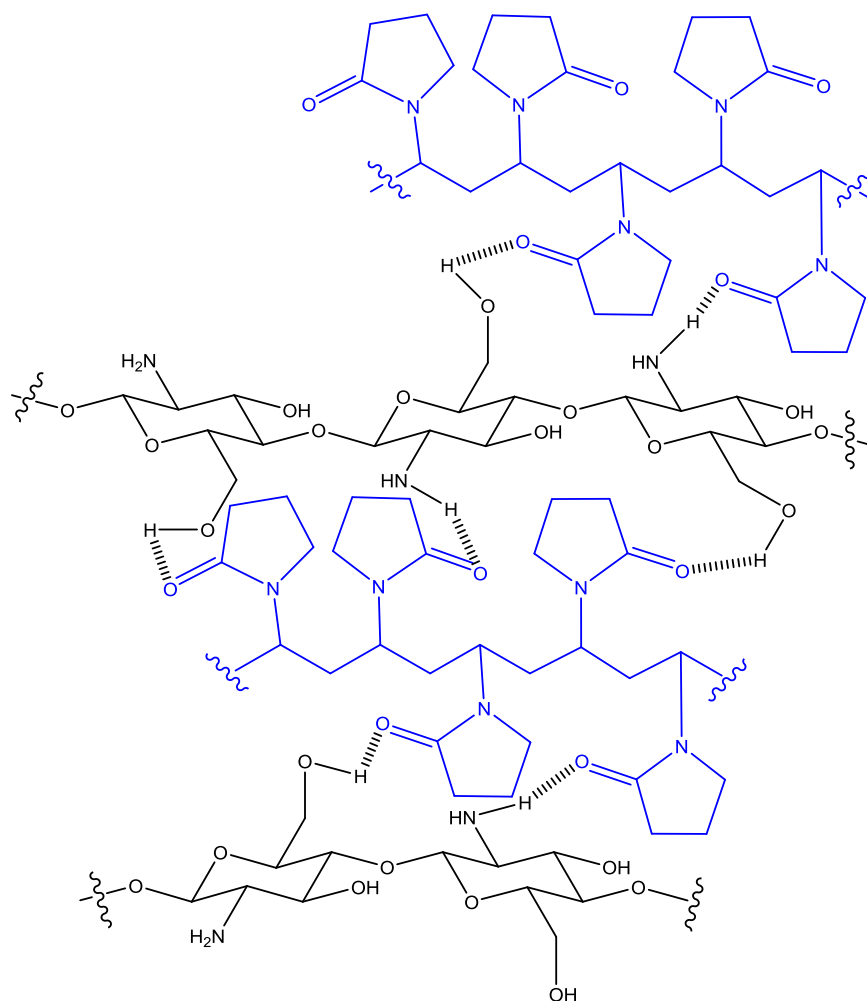


**Figure 5.53** Representation of hydrogen bonding between chitosan and PVP moieties upon continued freeze-thawing. Genipin moieties have been omitted for clarity.

## 5.6 Effect of constituents of genipin-crosslinked chitosan-poly (vinyl pyrrolidone) hydrogels on the swelling response

The amount of one chemical moiety in the hydrogel matrix was varied (higher or lower) whilst the amount of the other constituents were kept constant. The default composition remained 1 mL chitosan, 200  $\mu$ L PVP and 100  $\mu$ L genipin at the aforementioned concentrations. All samples were placed in an oven at 37  $^{\circ}$ C for 24 h. The variations of “high” and “low” are specified in Table 5.8. All samples were frozen and thawed for 30 min prior to washing, collapsed in a pH 7 phosphate buffered solution, swollen in a pH 2 glycine buffered solution and evaluated gravimetrically.

**Table 5.8** Volume of chitosan, PVP and genipin used when alterations to the default composition were made. Specimens were placed in an oven at 37 °C for 24 h.

Chemical Moiety	“High” Volume (μL)	“Low Volume (μL)	“Normal” Composition (μL)
Chitosan	2000	500	1000
PVP	400	100	200
Genipin	200	50	100

The effects of varying the amount of chitosan in the network on swelling are depicted in Figure 5.54. Clearly, varying the chitosan concentration does not have a large effect on network swelling and in the initial stages it seems that a low chitosan content is preferable for an enhanced network response. This may initially be counter-intuitive when considering more chitosan, will mean more amine groups, leading to a stronger degree of electrostatic repulsion between chains, allowing more solvent to diffuse into the pores, culminating in a greater degree of network swelling. However, a dominating effect may be that a large amount of chitosan will contribute towards forming an exceptionally dense gel, which may decrease the accessibility of the pores to the neighbouring solvent solution, hence hindering diffusion and hence swelling.

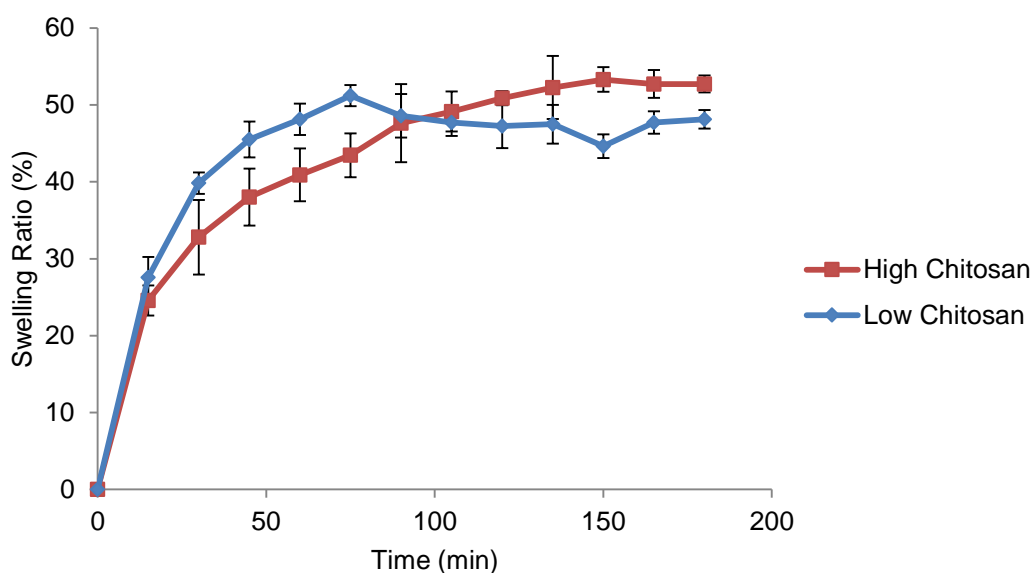


**Figure 5.54** Gravimetric swelling measurements in a pH 2 buffered solution of high (2000 μL) and low (500 μL) chitosan combined with PVP (200 μL) and genipin (100 μL) to form a hydrogel.

In contrast, varying the PVP content of the hydrogel has a pronounced effect on the swelling capabilities (Figure 5.55). This is due to the hydrophilic nature of

PVP which is likely to enhance the capability of the gel to absorb a large amount of solvent in the network (Vázquez et al., 1997). This could contribute towards the higher swelling ratio after 180 min for the gel with a high PVP content (60%) compared to the counterpart with a low PVP content (47%).

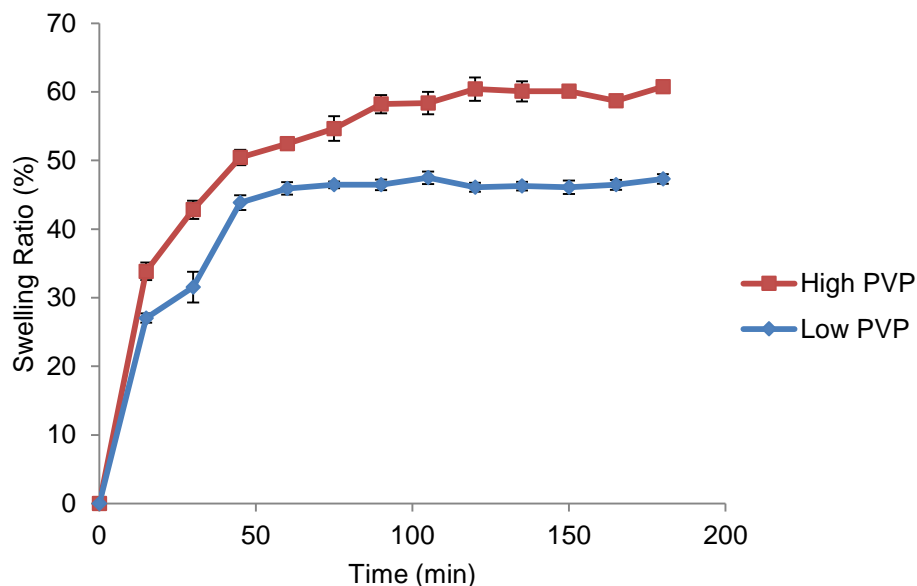


**Figure 5.55** Gravimetric swelling measurements in a pH 2 buffered solution of high (400  $\mu\text{L}$ ) and low (100  $\mu\text{L}$ ) PVP combined with chitosan (1000  $\mu\text{L}$ ) and genipin (100  $\mu\text{L}$ ) to form a hydrogel.

Finally, the effect of varying the amount of genipin in the network during swelling was determined (Figure 5.56). As expected, a higher amount of genipin results in a more crosslinked gel, leading to smaller and few pores, diminished accessibility and a lower swelling response compared to when the network is lightly crosslinked. The observations have not been tested for statistical significance.

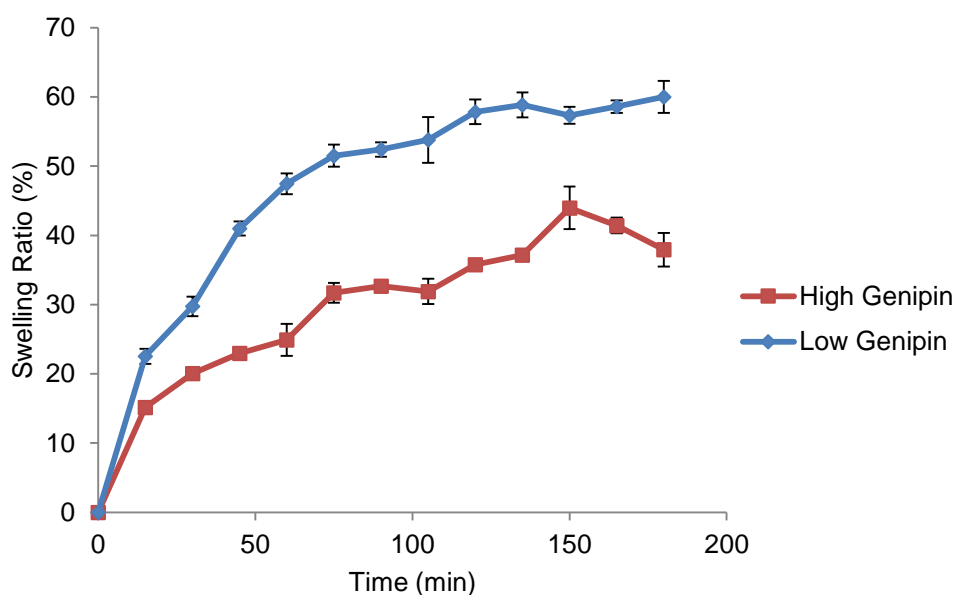


**Figure 5.56** Gravimetric swelling measurements in a pH 2 buffered solution of high (200  $\mu$ L) and low (50  $\mu$ L) genipin combined with chitosan (1000  $\mu$ L) and PVP (200  $\mu$ L) to form a hydrogel.

### 5.7 Further investigations of how varying the amount of chemical constituents in genipin-crosslinked chitosan-poly (vinyl pyrrolidone) hydrogels affects network properties

It has been noted in the previous section that varying the amount of chitosan, PVP and genipin within the hydrogel matrix has a profound effect on the swelling properties. This was further investigated by building on the previous work conducted analysing G-Ch-PVP hydrogels (reviewed in Section 2.9) (Nwosu, 2013). This study was chosen as a lower amount of genipin was employed because this crosslinking agent is very expensive, and considering future applications, it would be optimal to cut production costs. Samples were placed in an oven at 50 °C in order to speed up the rate of crosslinking, in the hope that as many amine groups as possible react to form crosslinks. No freezing or thawing was employed to enhance stability. The code and composition of gels shown in Table 2.2 is also depicted below (Table 5.9).

**Table 5.9** The code and composition of G-Ch-PVP hydrogels synthesised from following a full factorial method of experimental design (Nwosu, 2013).

Gel Code	Independent Factors					
	Chitosan		PVP		Genipin	
	Level	Volume ( $\mu\text{L}$ )	Level	Volume ( $\mu\text{L}$ )	Level	Volume ( $\mu\text{L}$ )
HHH	H	500	H	500	H	100
HHL	H	500	H	500	L	40
HLL	H	500	L	200	L	40
LLL	L	200	L	200	L	40
LLH	L	200	L	200	H	100
LHL	L	200	H	500	L	40
HLH	H	500	L	200	H	100
LHH	L	200	H	500	H	100

On gel fabrication, it was noted that all specimens did not look alike in terms of their colour. This was investigated quantitatively using UV-Vis spectroscopy by measuring the absorbance of gels synthesised according to Table 5.9 at a wavelength of 610 nm (Table 5.10) following the method outlined in Section 3.4. This wavelength was chosen due to the previous work discussed in Section 4.3. It is clear that a higher absorbance at 610 nm is linked with a more pronounced blue colouration in hydrogel specimens.

**Table 5.10** Absorbance at 610 nm of G-Ch-PVP hydrogels synthesised according to Table 5.9 as determined by UV-Vis spectroscopy.

Gel Code	Colour	Absorbance at 610 nm
HHH	Very deep blue	1.9
HHL	Light blue	0.6
HLL	Light blue	0.6
LLL	Very deep blue	2.0
LLH	Very deep blue	2.2
LHL	Very light blue	0.4
HLH	Deep blue	1.3
LHH	Light blue	0.7

To investigate as to whether the degree of crosslinking is related to the depth of the blue pigmentation observed in hydrogel specimens, the fluorescence intensity of the hydrogel samples was determined according to the method in Section 3.9.1. These results are depicted in Table 5.11.

**Table 5.11** Fluorescence intensity of G-Ch-PVP hydrogels synthesised according to Table 5.9 as determined via CLSM in fluorescence mode.

Gel Code	Average pixel intensity of a 0.25 mm <sup>2</sup> area of gel sample
HHH	277
HHL	79
HLL	88
LLL	254
LLH	310
LHL	43
HLH	157
LHH	100

In agreement with the data collected via UV-Vis spectroscopy (Table 5.10), the results collected by determining the average pixel intensity of hydrogel samples also show an increase in fluorescence intensity with a deeper blue pigmentation (and hence larger absorbance at 610 nm). This link is demonstrated in Figure 5.57 showing a linear dependence.

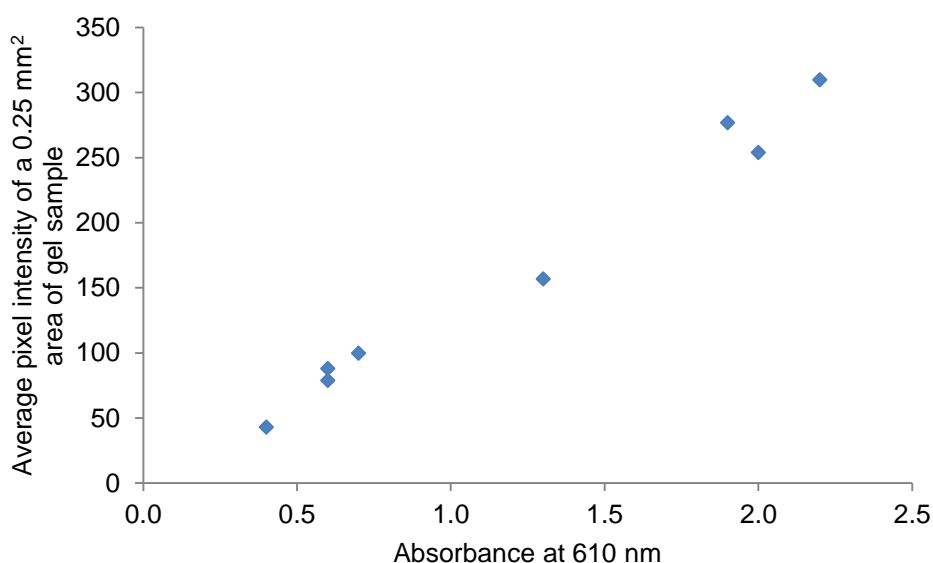


**Figure 5.57** A comparison between the average pixel intensity of 0.25 mm<sup>2</sup> samples of G-Ch-PVP hydrogels determined via CLSM in fluorescence mode and their absorbance at 610 nm as measured by UV-Vis spectroscopy.

According to the observations in Tables 4.6 and 4.7, due to the absence of amine groups in PVP and the fact that a semi-IPN is formed, the key parameter in the stability of G-Ch-PVP hydrogels is likely to be the genipin-crosslinked chitosan component of the network. High levels of crosslinking are likely to be

present in specimens with a high absorbance and average pixel intensity (HHH, HLH, LLL, LLH) as there is enough genipin to react with a comparatively high number of amine groups on chitosan to form a tight network. Samples with intermediate absorbance and intensity values (HLL, LHH) have either a low PVP content, making specimens more hydrophobic and with less voids or a comparatively high genipin to chitosan ratio, enabling a higher level of crosslinking to occur. In contrast, samples with a high amount of PVP and low amounts of genipin (HHL, LHL) exhibit a low absorbance and fluorescence intensity irrespective of the amount of chitosan present. A low crosslink density is likely to produce a highly porous network, resulting from a small amount of genipin whilst a large degree of PVP enhances the number of voids in the network, whilst making it more hydrophilic.

The swelling of the gels in Table 5.9 was monitored gravimetrically according to the method in Section 3.10.5 (Figure 5.58). Similar conclusions to when G-Ch-PVP hydrogels were evaluated optically can be constructed (Nwosu, 2013). Both the speed and degree of swelling for LHL hydrogels continues to be the greatest with a swelling ratio of 170% reached at 3 h of immersion in a pH 2 glycine buffer. This could be due to the hydrophilicity of the PVP moieties present within the sample. This is corroborated by the second, third and fourth most swollen and responsive hydrogels being LHH, HHL and HHH respectively; all of which have a “high” PVP content.

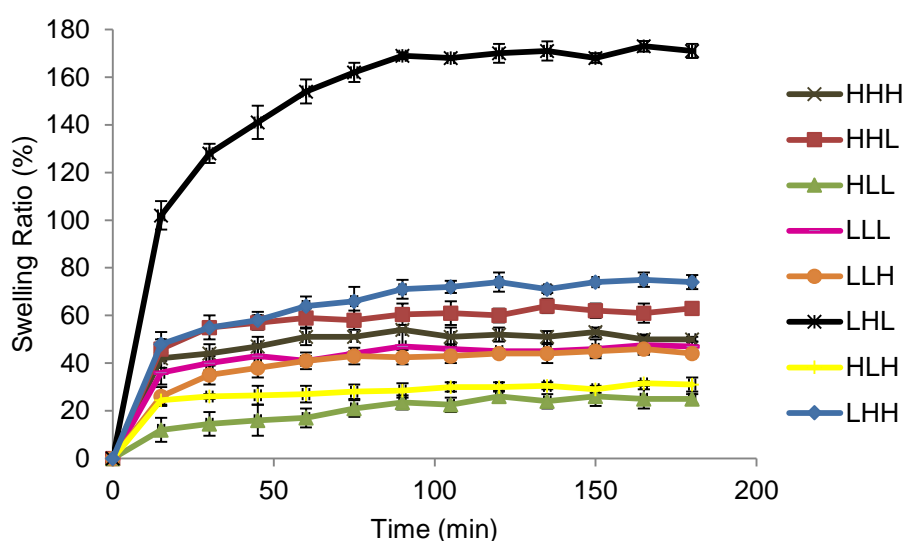


**Figure 5.58** Gravimetric swelling of G-Ch-PVP hydrogels prepared according to Table 5.9 in a pH 2 glycine buffered solution.

A statistical analysis of the experimental design was conducted using *Minitab* using 3 factors, 2 levels (high and low), 3 replicates and hence 24 runs. All terms were free from aliasing. An R-squared value of 99.47% indicates that the model successfully accounts well for the variability of the response data around its mean. All terms were statistically significant as their p-values (which are functions of the observed sample results (a statistic)) were all less than the significant level of the test (5%). This is displayed in the Pareto chart (Figure 5.59) where the absolute value of all effects (A is chitosan, B is PVP and C is genipin) is depicted. In all cases, the absolute value extends beyond the reference line at 2.12, indicating all effects are significant with respect the swelling ratio recorded at 180 min. This is inclusive of the linear effects of individual components and interactions between multiple components. As expected from the swelling data, PVP (B) is shown to be the most important variable in determining the swelling ratio at 180 min with a standardised effect value of 35. This is exemplified by the fact that based on the gravimetric swelling behaviour in Figure 5.58, all of the compositions with a high PVP content have a higher swelling ratio at 180 min than their counterparts. This highlights the important role that hydrophilicity plays in determining the swelling ability of G-Ch-PVP hydrogels. In contrast, the amount of genipin (C) is shown to have a comparatively smaller effect (standardised effect value of 16). This is represented in Figure 5.58 by the very similar swelling behaviour of HLH and HLL compositions. Upon considering multiple components together, as mentioned, all combinations are statistically significant. PVP-genipin interactions (BC) seem to affect the swelling behaviour more than chitosan combinations. Once again this demonstrated the strong effect that PVP has on the network together with showing that the degree of crosslinking does play an important role in resultant swelling behaviour.

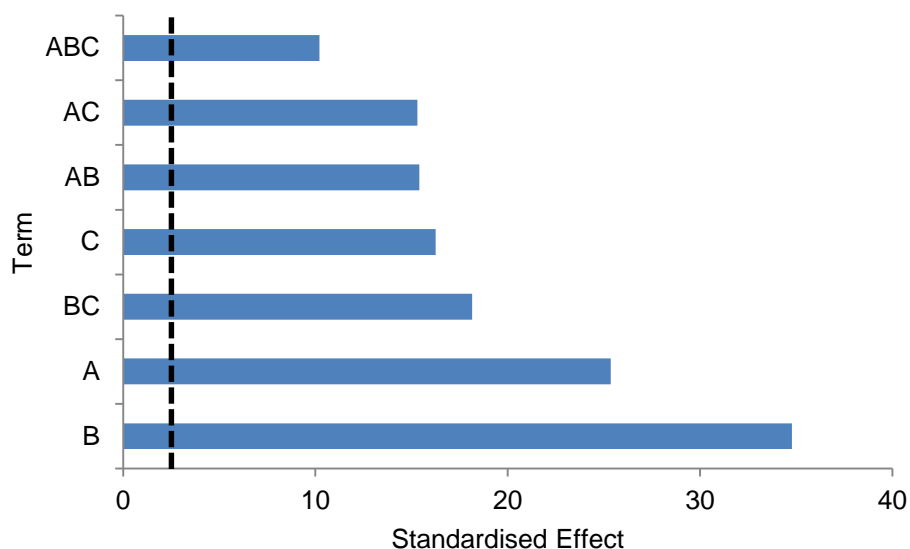


**Figure 5.59** Pareto chart displaying the importance of chitosan (A), PVP (B) and genipin (C) with respect to the swelling ratio of hydrogels in Figure 5.58.

To further investigate the effect of composition of swelling behaviour, the pKa values for the varying compositions were determined via potentiometric titration where the swelling ratio of hydrogels were assessed over a small pH range (5.4-7.2) close to the start of the phase transition (Figure 5.60). Each gel sample was left to equilibrate for 3 h prior to determining the mass. As an approximation, at the apparent pKa of a gel, ionisation is initiated and accompanied by swelling of the network (Richter et al., 2008). From Figure 5.60 it is clear that some gels begin to swell at a low pH (such as HHH and HHL at approximately 6.2 for instance) compared to others where swelling is initiated at a higher pH (such as LLL and LLH at approximately 6.8). Values of pKa for the various gel compositions are shown in Table 5.12. These values were generated following interpretation of Figure 5.60 based on the approximation that the gel pKa is the pH at which swelling is initiated. From these results, it seems that the pKa decreases with increasing chitosan content. Furthermore, the gradient of the swelling curves in Figure 5.60 between pH 5.4 and 6.2 was recorded to assess the speed of swelling. These results align well with the equilibrium swelling data (Figure 5.58) with the steepest gradient (and hence fastest rate of swelling) being -71% and corresponding to LHL composition To corroborate this, from Figure 5.58, it is the LHL composition that shows the fastest rate of swelling together with the highest swelling ratio (170%). Similarly, gels found to swell comparatively slowly between pH 5.4 and 6.2 (HLH and HLL

with gradients of -32% and -36% respectively also exhibit the lowest equilibrium swelling ratios (between 25-30%) as shown in Figure 5.58.

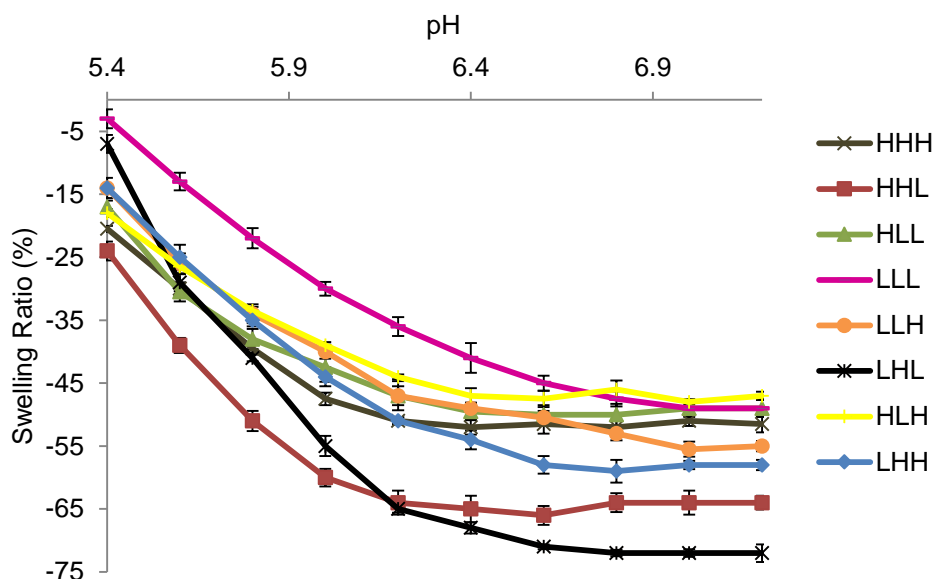


**Figure 5.60** Gravimetric swelling of G-Ch-PVP hydrogels prepared according to Table 5.9 during a potentiometric titration of sodium hydroxide and phosphoric acid. The ionic strength of all solutions was adjusted to  $0.1 \text{ mol kg}^{-1}$  using sodium chloride. Samples were left for 3 h to equilibrate.

**Table 5.12** Values of pKa of G-Ch-PVP hydrogels synthesised according to Table 5.9 as determined from Figure 5.60.

Gel Code	Approximate pKa	Gradient of the line in Figure 5.59 between pH 5.4 and 6.2 (%)
HHH	6.0	-39
HHL	6.0	-51
HLL	6.2	-36
LLL	6.8	-42
LLH	6.8	-40
LHL	6.4	-71
HLH	6.2	-32
LHH	6.4	-47

In agreement with and building on from previous work (Nwosu, 2013), it was found that gels with an “LHL” composition had the comparatively highest swelling ratio (approximately 170% after 3 h (Figure 5.58)), the fastest swelling rate (-71% gradient (Table 5.12)) and was the most lightly crosslinked (Tables 5.10 and 5.11 displaying an absorbance of 0.4 at 610 nm and a pixel intensity of 43 over a  $0.25 \text{ mm}^2$  gel sample respectively). Due to the low absorbance value

obtained, indicating a low level of crosslinking, it is desirable for the stability of the gel composition to be enhanced and because of this; the specimen was a good candidate to study the effects of freezing/freeze-thawing. This was investigated by further exploring previous work conducted (Nwosu, 2013) and gels were synthesised according to Table 5.13.

**Table 5.13** Process parameters used to study the effects of varying gelation temperature and various post-synthetic treatments on the responsiveness of G-Ch-PVP hydrogels synthesised according to the LHL composition (Nwosu, 2013).

<b>Gel Code</b>	<b>Gelation Temperature (°C)</b>	<b>Freezing Time at -10 °C (h)</b>
LHL1	30	72
LHL2	30	3 freeze-thaw cycles: 24 h freezing and 3 h thawing each
LHL3	40	72
LHL4	40	3 freeze-thaw cycles: 24 h freezing and 3 h thawing each
LHL5	50	72
LHL6	50	3 freeze-thaw cycles: 24 h freezing and 3 h thawing each

The absorption at 610 nm together with the fluorescence intensity of hydrogel specimens made according to Table 5.13 was determined (Table 5.14). As the gelation temperature was increased, both the absorbance and fluorescence intensity also increased. This is due to a faster rate of crosslinking at higher temperature, leading to more crosslinks being formed within the gel network and hence a deeper shade of blue observed. There is no measurable difference according to the results in Table 5.14 when comparing as to whether samples were continuously frozen or subjected to freeze-thawing.

**Table 5.14** Absorbance at 610 nm and fluorescence intensity of G-Ch-PVP hydrogels synthesised according to Table 5.13 as determined by UV-Vis spectroscopy and CLSM in fluorescence mode respectively.

<b>Gel Code</b>	<b>Colour</b>	<b>Absorbance at 610 nm</b>	<b>Average pixel intensity of a 0.25 mm<sup>2</sup> area of gel sample</b>
LHL1	Light blue	0.4	38
LHL2	Light blue	0.5	41
LHL3	Light blue	0.6	56
LHL4	Light blue	0.6	54
LHL5	Deep blue	1.0	123
LHL6	Deep blue	1.1	145

The swelling of the gels in Table 5.13 was monitored gravimetrically in a pH 2 glycine buffered solution according to the method in Section 3.10.5 (Figure 5.61). Similar conclusions to when G-Ch-PVP hydrogels were evaluated optically can be constructed (Nwosu, 2013). All LHL samples that were either continuously frozen or freeze-thawed exhibited a lower speed (Table 5.15) and degree of swelling than untreated specimens. Furthermore, all continuously frozen samples displayed a faster speed and a larger degree of swelling than those that were freeze-thawed suggesting that these treatments induce different alterations in the native pore structure of the network, which directly affects swelling behaviour. Finally, for both sets of treatment, unlike the previously reported work (Nwosu, 2013), there was a strong dependence of gelation temperature and degree/speed of swelling. This is corroborated by the absorbance and fluorescence intensity data shown in Table 5.14.

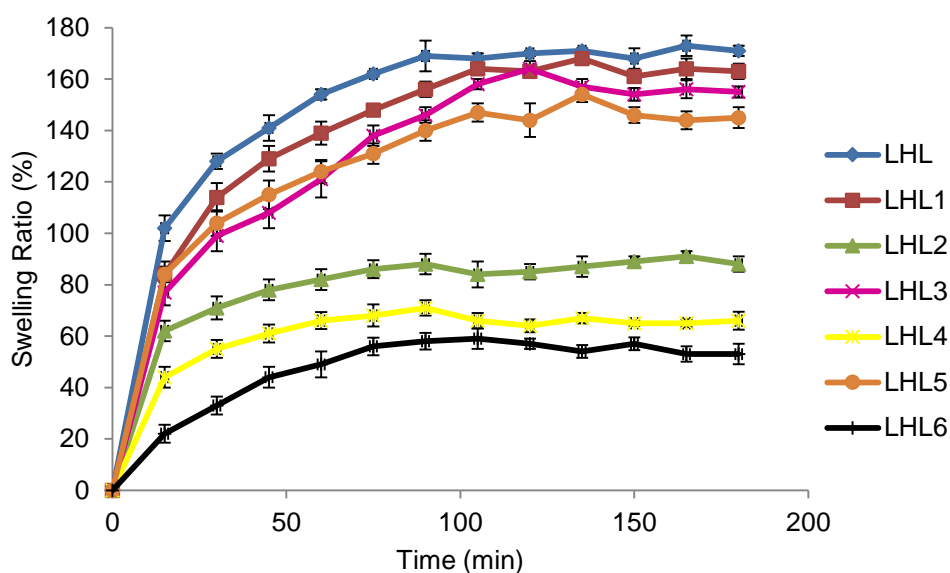


**Figure 5.61** Gravimetric swelling of G-Ch-PVP hydrogels prepared according to Table 5.13 in a pH 2 glycine buffered solution.

**Table 5.15** Initial gradient during the first 30 min of swelling in Figure 5.60 where G-Ch-PVP hydrogels prepared according to Table 5.13 were swollen in a pH 2 glycine buffered solution.

Gel Code	Initial gradient during the first 30 min of swelling (% min <sup>-1</sup> )
LHL	4.3
LHL1	3.8
LHL2	2.4
LHL3	3.3
LHL4	1.8
LHL5	3.5
LHL6	1.1

In order to further understand the effects of continuous freezing and freeze-thawing at various gelation temperatures on the properties of G-Ch-PVP hydrogels, all LHL 1-6 specimens were evaluated morphologically via SEM. The surface porosity of the samples was determined using ImageJ according to the method in Section 3.6.3 (Table 5.16). The untreated sample placed in an oven at 30 °C has a significantly lower surface porosity (6.9 %) than other samples with no post-synthetic treatment (LHLa and LHLb), which formed a gel at a higher temperature and indeed, all other samples tested (LHL1-6). There does not seem to be a discernible trend between gelation temperature and the resulting surface porosity whichever post-synthetic treatment was employed.

**Table 5.16** Surface porosities of freeze-dried G-Ch-PVP hydrogels synthesised according to the LHL composition determined via the analysis of SEM images using ImageJ software.

Gel Code	Gelation Temperature (°C)	Post-Synthetic Treatment	Surface Porosity (%)
LHLa	30	None	6.9
LHL1	30	72 h at -10 °C	22.4
LHL2	30	3 freeze-thaw cycles: 24 h freezing and 3 h thawing each	20.9
LHLb	40	None	28.7
LHL3	40	72 h at -10 °C	20.3
LHL4	40	3 freeze-thaw cycles: 24 h freezing and 3 h thawing each	23.4
LHLc	50	None	23.3
LHL5	50	72 h at -10 °C	24.3
LHL6	50	3 freeze-thaw cycles: 24 h freezing and 3 h thawing each	19.6

The hydrogel sample placed in an oven at 30 °C without any freezing/thawing (Figure 5.62 (a)) has a very compact structure with an average pore diameter of approximately 10-20  $\mu\text{m}$  (and surface porosity of 6.9%). As the gelation temperature is increased to 40 °C (Figure 5.62 (b)), the specimen becomes more porous with an average pore diameter of 40-100  $\mu\text{m}$  (and a surface porosity of 28.7%). Furthermore, when placed in an oven at 50 °C (Figure 5.62 (c)), the bulk structure shows an increase in the number of pores together with both order and uniformity. However the overall surface porosity seems to decrease (23.3%). Overall, at higher gelation temperatures, the extent to which pores are ordered within the network seems to increase.

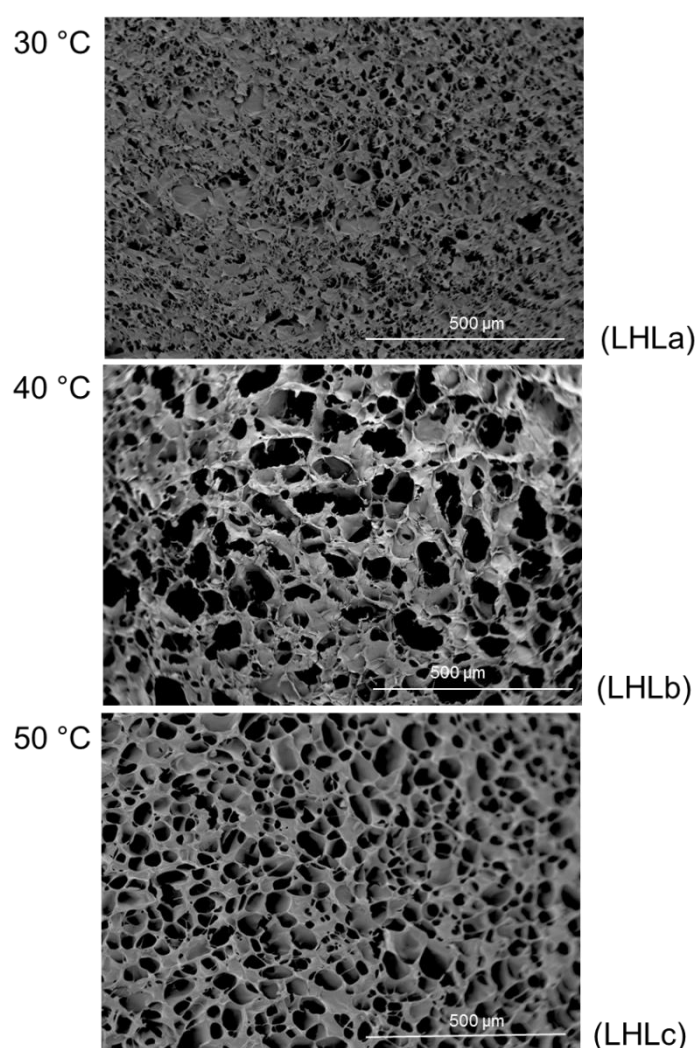


**Figure 5.62** SEM images of G-Ch-PVP hydrogels synthesised according to the LHL gel code composition and placed in an oven at 30 (LHLa), 40 (LHLb) and 50 °C (LHLc) with no post-synthetic treatment.

In contrast, specimens that were continually frozen (Figure 5.63) exhibit a strikingly different morphology to those without post-synthetic treatment (Figure 5.62). This is exemplified at 30 °C in Figure 5.63 where samples have far larger pores within the bulk structure (with an approximate diameter of 100  $\mu\text{m}$  and surface porosity of 22.4%) than an analogous specimen without freezing/thawing (Figure 5.62) where the pore diameter is 10-20  $\mu\text{m}$  and the surface porosity is 6.9%. Such an increase in the diameter of the voids may be due to the freezing of absorbed liquids within the porous network, resulting in crystallisation within the pores, creating an ordered 3-D morphology (Holloway et al., 2013). In the same way as following no post-synthetic treatment, there is no apparent variation in the number, size or order of the pores when increasing the gelation temperature (Figure 5.63).

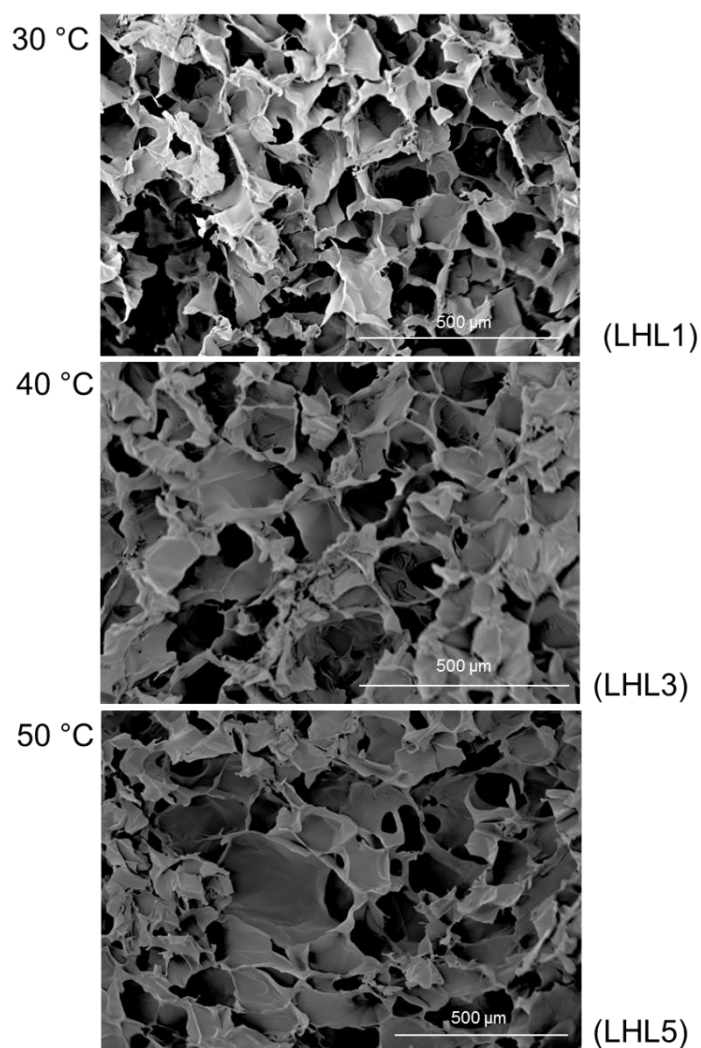


**Figure 5.63** SEM images of G-Ch-PVP hydrogels synthesised according to the LHL gel code composition and placed in an oven at 30 (LHL1), 40 (LHL3) and 50 °C (LHL5) continuously frozen for 72 h.

Freeze-thawed gels (Figure 5.64) exhibit similar morphological structures to specimens that were continually frozen (Figure 5.63). However, compared to other samples tested, freeze-thawed specimens possess pores with a higher average diameter (approximately 150  $\mu\text{m}$ ). Such an enhancement may be attributed to liquid expansion within the hydrogel matrix during each freezing cycle, forcing the polymer chains within close proximity to one another, facilitating hydrogen bonding, leading to a greater degree of crystallite formation (Holloway et al., 2013).

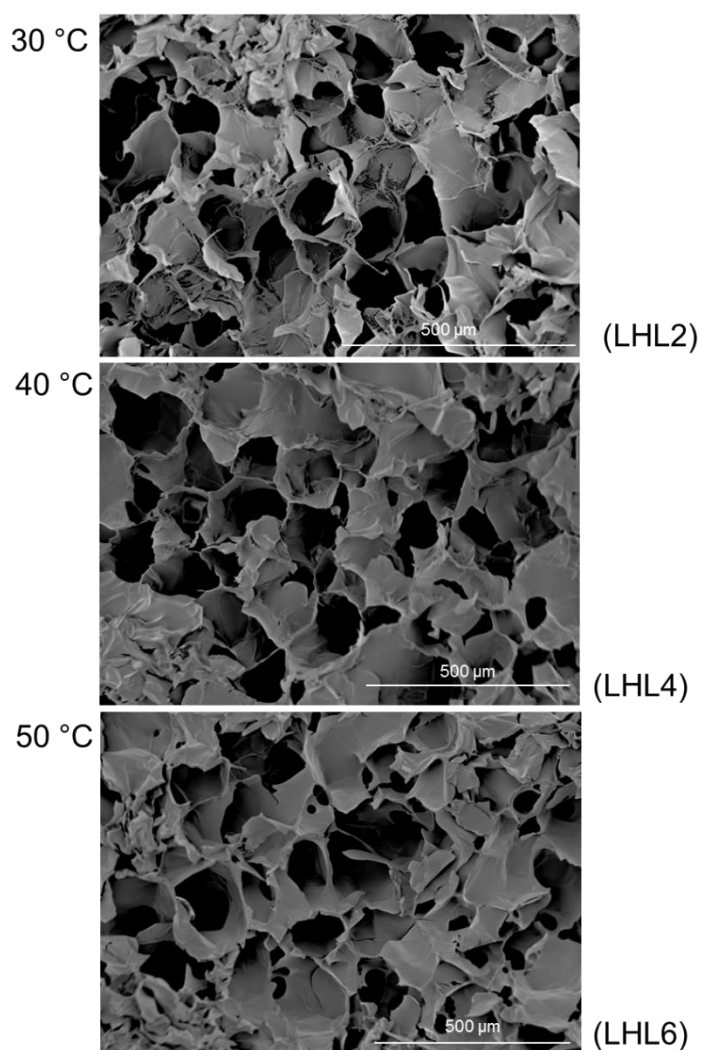


**Figure 5.64** SEM images of G-Ch-PVP hydrogels synthesised according to the LHL gel code composition and placed in an oven at 30 (LHL2), 40 (LHL4) and 50 °C (LHL6) subjected to 3 freeze-thaw cycles of 24 h freezing and 3 h thawing.

However it is noteworthy that the overall surface porosity for freeze-thawed gels is not greater than samples that were continuously frozen (an average of 21.3% compared to 22.3% over the three gelation temperatures studied (Table 5.16)).

In a similar fashion to the continuously frozen samples (Figure 5.63), increasing the gelation temperature has a negligible effect upon the porous architecture (Figure 5.64).

Samples prepared according to the LHL gel code that were either continually frozen or freeze-thawed were investigated via uniaxial compression tests. Samples with no post-synthetic manipulation were too unstable to perform such measurements due to a complete lack of shape retention (Figure 5.65). Once again, it is clear from the photograph in Figure 5.65 that as the gelation temperature is increased, so does the rate of crosslinking, producing an increasingly blue pigmentation that is more gel-like (as evidenced by the inversion test) However, even the sample placed in an oven at 50 °C suffers from low stability without subsequent freezing/thawing.

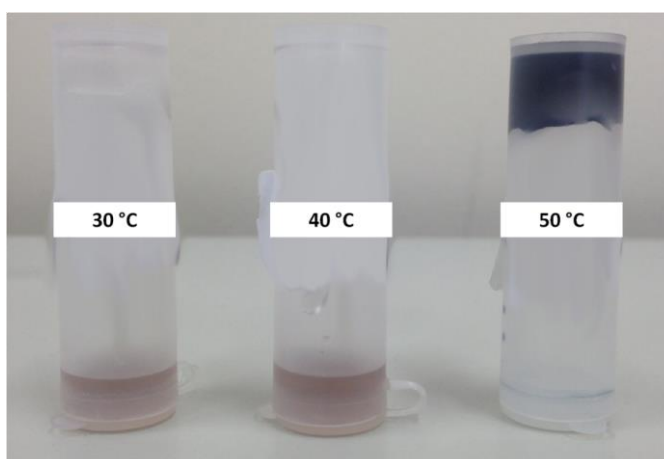


**Figure 5.65** Photograph of LHL hydrogels placed in an oven at 30, 40 and 50 °C and stored in a fridge (5 °C) without subsequent manipulation.

Continuously frozen and freeze-thawed specimens were evaluated following compression testing (Figures 5.66 and 5.67). There appears to be no correlation with the mechanical properties recorded for continually frozen samples in terms of their gelation temperature. This is in agreement with their being no apparent correlation with the gelation temperature and the degree of swelling in a pH 2 glycine buffered solution (Figure 5.61). LHL1 (30 °C) and LHL5 (50 °C) have enhanced mechanical stability compared to LHL3 (40 °C) despite their being no apparent differences in the porous architectures with the average pore diameter being approximately 100  $\mu\text{m}$  as illustrated in Figure 5.63. However, samples that were freeze-thawed exhibited more predictable mechanical behaviour. Upon increasing gelation temperature, the degree of

crosslinking is enhanced, leading to a lower degree of swelling/speed of swelling (Figure 5.61 and Table 5.15 respectively) and enhanced mechanical stability (Figure 5.67).

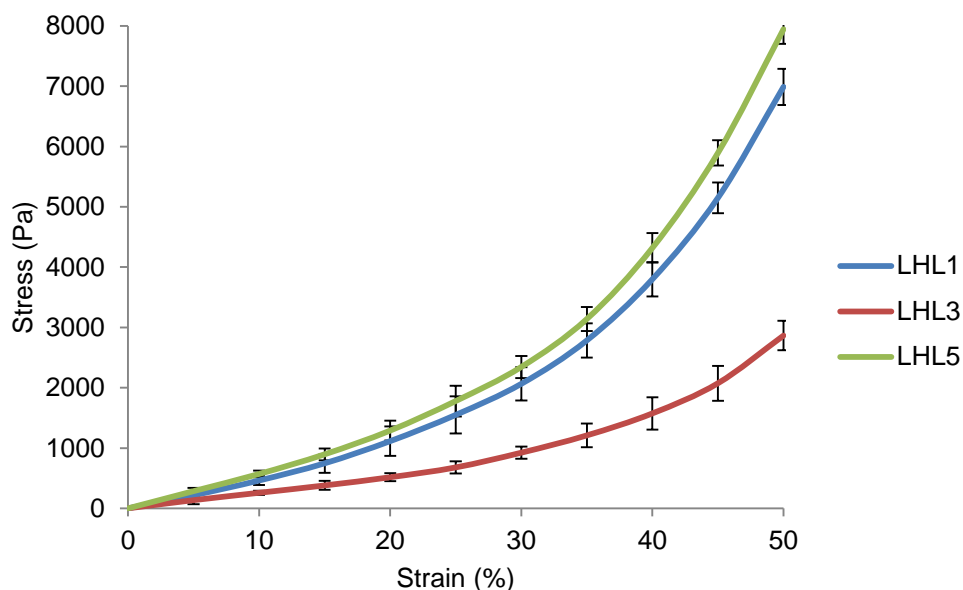


**Figure 5.66** Uniaxial compression tests of LHL G-Ch-PVP hydrogels that were subject to post-synthesis continuous freezing.

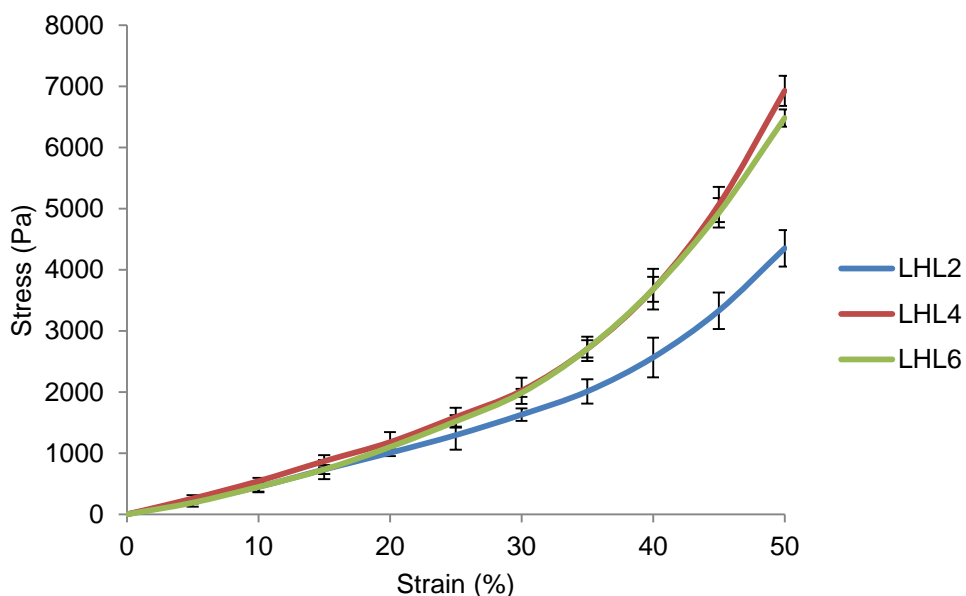


**Figure 5.67** Uniaxial compression tests of LHL G-Ch-PVP hydrogels that were subject to post-synthesis freeze-thaw treatment.

To further investigate the structure-property relationships between LHL hydrogels that have been subjected to various post-synthetic treatments the elastic modulus between 0-20% strain of all specimens was determined (Table

5.17). Samples that were freeze-thawed (LHL2, LHL4 and LHL6) exhibited a higher mean elastic modulus between 0-20% strain (55 Pa) compared to those subjected to continuous freezing (LHL1, LHL3 and LHL5) with a mean elastic modulus of 48 Pa (Figure 5.68). Furthermore, the range in the elastic modulus of freeze-thawed samples is just 8 Pa indicating a narrow distribution compared to specimens that were continuously frozen exhibiting a range of 38 Pa. The superior rigidity of freeze-thawed samples is corroborated by a higher mean fluorescence intensity (80 compared to 72 for continuously frozen samples) and absorbance at 610 nm (0.73 compared to 0.66 for continuously frozen samples). This indicated that a higher degree of crosslinking is correlated with an enhancement in the rigidity of G-Ch-PVP hydrogels. Additionally, the higher mean elastic modulus of freeze-thawed samples (and hence more heavily cross-linked) is also in agreement with the average surface porosity whereby it is lower for freeze-thawed specimens (21.3%) compared to their continuously frozen counterparts (22.3%). From this, we can also expect the swelling of freeze-thawed hydrogels to be less than those continuously frozen. This is what is observed; note the large difference in swelling ratio between gels with the two different post-synthetic treatments in Figure 5.61. Finally, as well as the evidence of the swelling ratio at 180 min being greater for continuously frozen samples, the mean speed of swelling during the first 30 min is far greater for these specimens ( $3.5\% \text{ min}^{-1}$ ) compared to samples prepared via freeze-thawing ( $1.7\% \text{ min}^{-1}$ ). Consequently, there is a link between elastic modulus and gel swelling.

**Table 5.17** Elastic modulus between 0-20% strain of LHL G-Ch-PVP hydrogels that were subject to continuous freezing or freeze-thaw treatment.

<b>Gel Code</b>	<b>Elastic Modulus (Pa)</b>
LHL1	55
LHL2	51
LHL3	26
LHL4	59
LHL5	64
LHL6	55

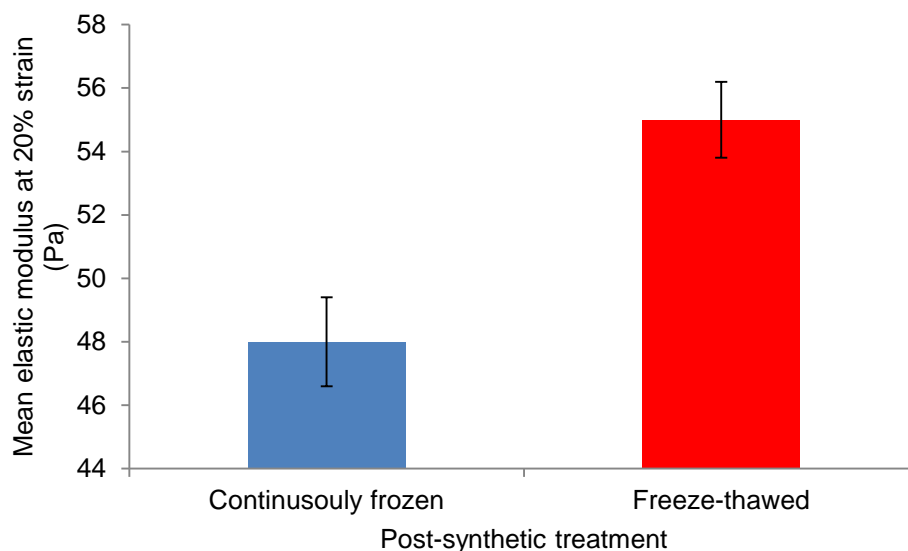


**Figure 5.68** Comparison between the elastic modulus of LHL G-Ch-PVP hydrogels that were subject to continuous freezing or freeze-thaw treatment.

## 5.8 Conclusions

In summary, it has been shown that by freezing and thawing G-Ch-PVP hydrogels a significant improvement in terms of sample stability was observed. Such networks were investigated via numerous visualisation techniques to include optical microscopy, SEM, ESEM and CLSM in fluorescence and reflectance mode enabling the reconstruction of the 3-D architecture of the matrix together with providing information on the sample topography. While SEM imaging after FD preserves the native hydrogel structure to a greater extent than specimens subjected to CPD, both techniques alter the network morphology. Furthermore, it is difficult to elucidate structural detail from optical microscopy and ESEM modes of analysis. However, CLSM has shown to be a valuable alternative structural characterisation technique owing to the in situ nature during image. It was subsequently shown that CLSM is beneficial for studying how the porous structure changes upon network swelling. These findings were related to macroscale gravimetric measurements, which are representative of the whole sample and were found to correlate well. Samples could be analysed in reflectance mode, negating the requirement for addition of a fluorescence probe, which may alter network morphology. Owing to the autofluorescent nature of G-Ch-PVP hydrogels, fluorescence can also be used to visualise gel morphology, although during swelling a lower degree of structural detail was observed compared to using reflectance.

Freeze-thawed G-Ch-PVP hydrogel samples were successfully washed in distilled water and UV-Vis spectroscopy was used to confirm successful removal of unwanted chemical moieties. Mechanical properties of hydrogels freeze-thawed for various times and cycles were evaluated via uniaxial compression testing in both wet and dry immersion environments. By increasing both the freezing time and the number of cycles, an increase in the mechanical stability of the specimens was observed up to a point. Similar trends were observed when the samples were tested when immersed in a pH 2 glycine buffered solution, although sample stability was reduced owing to a higher level of hydration within the network. All samples exhibited a marked improvement in stability compared to those with no post-synthetic freeze-thawing. This data was then subsequently correlated to how the freeze-thawed samples were able to respond when swollen in a pH 2 glycine-buffered environment and the swelling ratio was monitored gravimetrically. Excellent agreement with the data collected during compression testing was observed. Mechanical behaviour (in the form of the elastic modulus) was also correlated with pH of the surrounding solution, network swelling and the structure of the hydrogel (surface porosity measurements).

Finally, the effect of changing the composition of G-Ch-PVP hydrogels on the swelling properties was investigated. This was further extended by conducting a full experimental design where the swelling ratio of eight compositions was evaluated. Specimens with the gel code LHL were found to be the most responsive, although lacked suitable stability in order to be taken further. Subsequently, LHL samples were either continually frozen or freeze-thawed after being placed in an oven at various temperatures in order to enhance the mechanical properties whilst retaining the smart characteristics of the network. Whilst continuously freezing/ freeze-thawing enhance the stability of specimens, it is important to note that these manipulations hamper the responsiveness of samples to some degree. SEM studies were conducted comparing samples without post-synthetic manipulation and those that had been continuously frozen or freeze-thawed. Large differences were observed showing that in particular the size of pores increases quite dramatically following such changes to the network. This is most likely due to freezing of contained liquids, facilitating the formation of ice crystals and crystallisation within the pores, resulting in

expansion. Gelation temperature was shown to make a difference in the morphology of samples receiving no treatment, although no apparent variation in the porous architecture was observed as a result of varying the temperature for specimens that were continuously frozen, or freeze-thawed, suggesting that these post-synthetic manipulations are more dominant in determining the final microstructure. Upon evaluating the mechanical properties of LHL hydrogels, those without any manipulation were too unstable to perform compression tests owing to poor shape retention, although of the samples that could be tested, those subjected to freezing and thawing, exhibited mechanical stability that correlated well with prior responsiveness studies. It was also shown that together with gel swelling, the elastic modulus data could also be correlated with the mode of processing, extent of crosslinking (UV-Vis and fluorescence studies), speed of swelling and surface porosity.

The ability to synthesise such smart networks with an adjustable response whilst retaining good stability is important in their development towards future applications.

## **Chapter 6 – Results and Discussion: Potential Applications of Genipin-Crosslinked Chitosan-Poly(vinyl pyrrolidone) Hydrogels**

Chapters 4 and 5 have considered the synthesis and characterisation of G-Ch-PVP hydrogels in terms of their swelling response, morphology and mechanical properties. Both the swelling response and the stability of these networks have been studied and enhanced via experimental design and freeze-thawing. This chapter will focus on determining how suitable G-Ch-PVP hydrogels can be applied in various environments. Emphasis will be placed on exploring using the gel with an oscillatory reaction and the potential for the network to be used to release absorbed constituents.

### **6.1 Genipin-crosslinked chitosan-poly (vinyl pyrrolidone) hydrogels responding to oscillations in pH**

After demonstrating the ability of G-Ch-PVP hydrogels to respond to an oscillatory regime upon periodically varying the buffers in Chapter 4, and enhancing the stability of the networks as detailed in Chapter 5, freeze-thawed G-Ch-PVP hydrogels were also studied with regard to oscillations (Figure 6.1). Hydrogels were freeze-thawed for 30 min and contained 1 mL chitosan (1.5% w/v), 200  $\mu$ L PVP (5% w/v) and 100  $\mu$ L genipin (0.5% w/v). Following washing in distilled water, they were equilibrated for 24 h in a pH 2 glycine buffered solution before being subjected to a pre-load of 0.050 N. The solution the gels were immersed in was then periodically oscillated between pH 4 and pH 2 every 15 min. The force produced was noted. A stainless steel compression plate was used to make contact with specimens and apply the pre-load (as opposed to a porous glass frit for instance) to ensure that 100% of the top of the sample was covered and hence the most representative force-response from gel samples was recorded. Force-response tests were conducted as this allows in-situ monitoring of the response of the hydrogel to an oscillatory environment as opposed to measuring gravimetrically, where extensive sample handling is required. As previously encountered during gravimetric swelling experiments, the gel responds in an oscillatory manner due to the periodic fluctuations in pH as solvent is exchanged between the hydrogel matrix and the surrounding

solution. This simulation once again demonstrates that G-Ch-PVP hydrogels are good potential candidates as responsive materials in oscillatory reactions.

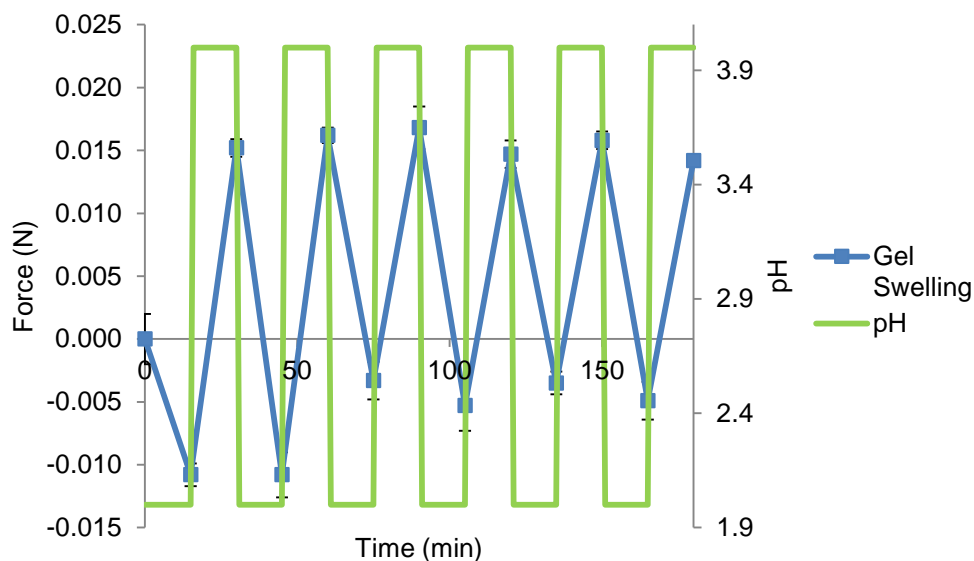


**Figure 6.1** Oscillatory swelling of freeze-thawed G-Ch-PVP hydrogels (30 min, 1 cycle) determined by measuring the change in force exerted on a compression plate during immersion in pH 2 glycine and pH 4 phthalate buffered solutions.

## 6.2 Bromate-sulfite-ferrocyanide oscillatory chemical reaction

Following detailed examination of the literature, the BSF oscillatory chemical reaction shows excellent promise to be coupled to pH-responsive polymers owing to the large variations in pH, the fact that the reaction stays at the extreme pH values for an approximately equivalent time and that the system operates at room temperature (Crook et al., 2002, Crook et al., 2004, Howse et al., 2006, Ryan et al., 2005b, Bilici et al., 2010). This oscillatory system was successfully assembled (Figure 6.2) exhibiting large oscillations approximately between pH 3 and 7. The ionic strength of the oscillatory reaction was calculated using Equation 2.20 to be  $0.42 \text{ mol kg}^{-1}$ . As the pH 2 glycine and pH 4 phthalate buffered solutions used in oscillatory force measurements in Figure 6.1 have an ionic strength of  $0.36 \text{ mol kg}^{-1}$ , a similar degree of swelling (difference of approximately  $0.015 \text{ N}$ ) is to be expected. This force response when coupled to the reaction may be slightly less than  $0.015 \text{ N}$  as the ionic strength of the BSF reaction fluid is slightly more than that of the buffers (difference of  $0.06 \text{ mol kg}^{-1}$ ). It is known that the decrease in pH is due to oxidation of sulfite by bromate producing protons as a positive feedback

mechanism whilst the increase in pH is due to the negative feedback mechanism whereby ferrocyanide is oxidised by bromate (Edblom et al., 1989).

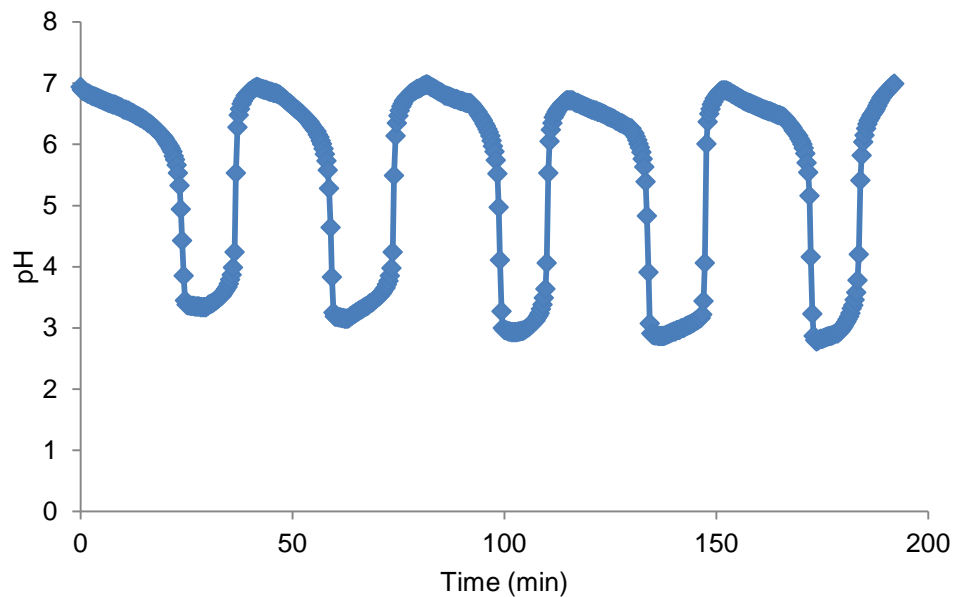


**Figure 6.2** Variation in pH as a function of time during the BSF oscillatory reaction.

Following this, force response tests were conducted as in Figure 6.1, although the pH was varied between pH 4 and pH 7 in line with the oscillations produced by the BSF reaction (Figure 6.3). Oscillatory behaviour was once again demonstrated, indicating that this hydrogel was a good candidate for coupling to the BSF reaction.

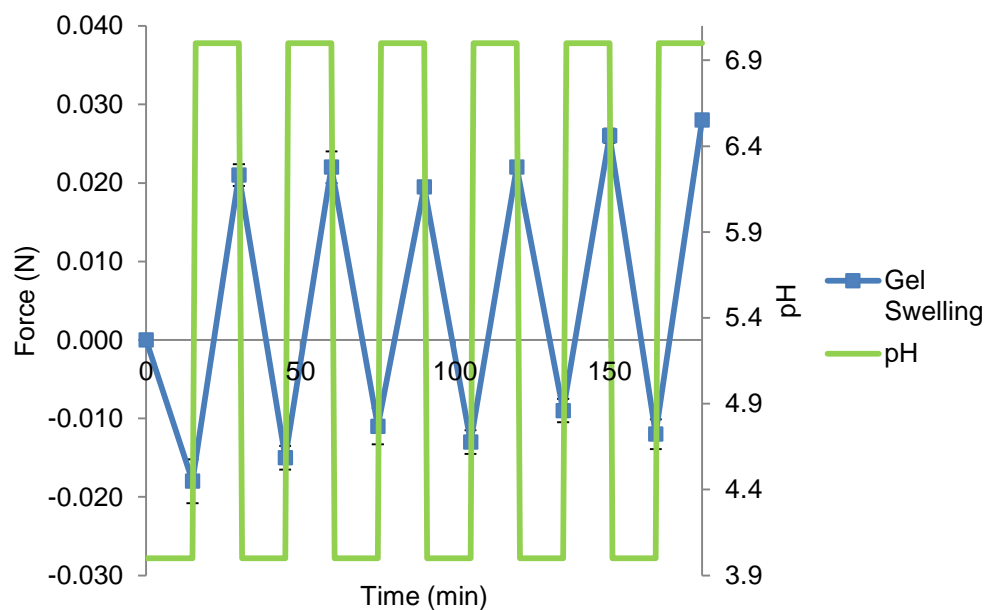


**Figure 6.3** Oscillatory swelling of freeze-thawed G-Ch-PVP hydrogels (30 min, 1 cycle) determined by measuring the change in force exerted on a compression plate during immersion in pH 4 phthalate and pH 7 phosphate buffered solutions.

### **6.3 Combining freeze-thawed genipin-crosslinked chitosan-poly (vinyl pyrrolidone) hydrogels with the bromate-sulfite-ferrocyanide reaction**

Following the successful reproduction of oscillations exhibited by the BSF reaction (Figure 6.2), G-Ch-PVP hydrogels freeze-thawed for 30 min that had shown to be responsive when the pH was varied by manually changing the buffers (Figures 6.1 and 6.3) were combined with the reaction. Swelling and collapse were monitored as a function of force where the gel was subjected to a pre-load of 0.15 N to ensure a uniform contact with the plate (Figure 6.4). The gel had been immersed in a non-oscillatory BSF reaction solution at a pH of 3.4 overnight so that it would adopt a similar size as when combined with the actual oscillatory reaction. An increasingly positive force value indicates that the gel is swelling over time. This could be because expansion is at a faster rate in acidic conditions, hence collapse is slower, and as the oscillations from the BSF reaction are approximately square and uniform, it is expected that overall, the gel will swell. Previous experiments when the buffer was periodically alternated also suggest this (Figures 6.1 and 6.3). The force recorded at 77 min is likely to be an anomalous result (owing to the “0.000 N” force value recorded), although based on the slight trend shown by the rest of the data, it is likely that this part of the red curve would form a slight trough. It is promising that the gel does respond to changes in a real oscillatory environment, although such variations in the force exerted as depicted in Figure 6.4 are very slight. As the ionic strengths of the pH 2 glycine, pH 4 phthalate, pH 7 phosphate and BSF reaction solutions are similar (approximately  $0.4 \text{ mol kg}^{-1}$ ), a potential explanation for the markedly reduced force variation could be potential chelation between metals present in the BSF reaction (such as those forming the potassium hexacyanoferrate (II) trihydrate) and the chitosan/PVP gel constituents. Such a non-reversible interaction could severely inhibit the swelling response of the gel network.

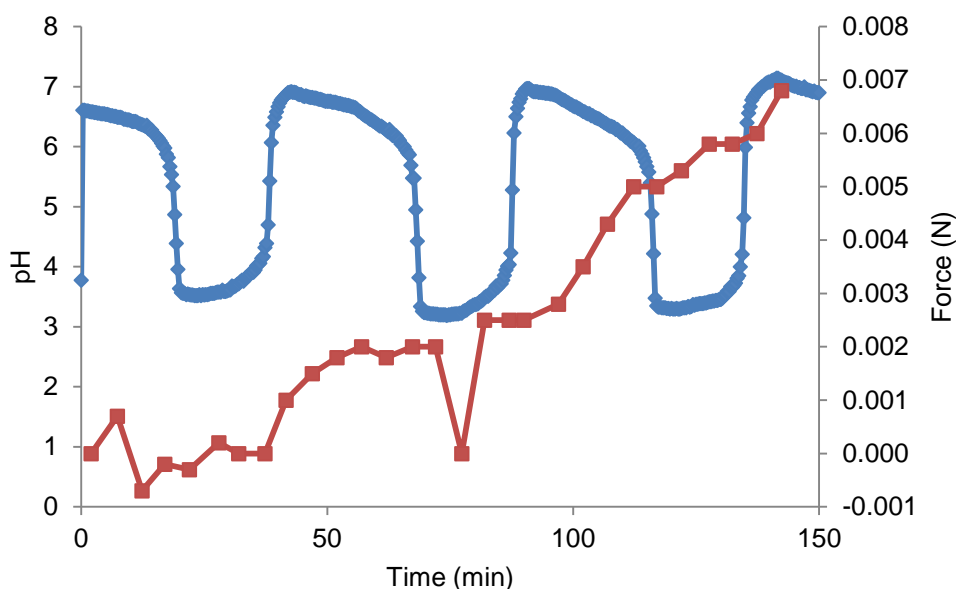


**Figure 6.4** Variation in pH as a function of time during the BSF reaction (blue curve) and the force response of a G-Ch-PVP hydrogel freeze-thawed for 30 min (red curve). Hydrogel is composed of 1 mL chitosan (1.5% w/v), 200  $\mu$ L PVP (5% w/v) and 100  $\mu$ L genipin (0.5% w/v).

In an attempt to increase the responsiveness of the hydrogel, considering that in an oscillatory regime, it is the variation in the number of protonated amine groups, which gives rise to the differences in the amount of electrostatic repulsion within the network that control whether the gel swells or collapses. Consequently a gel containing more amine groups may produce a more responsive network to periodic changes in pH (based on the swelling behaviour shown in Table 5.12) whilst exhibiting good mechanical properties. A G-Ch-PVP hydrogel was synthesised and freeze-thawed for 30 min to enhance stability comprising of 1.5 mL chitosan (1.5% w/v), 50  $\mu$ L PVP (5% w/v) and 100  $\mu$ L genipin (0.5% w/v). The pH response of this gel in citric acid/phosphoric acid combined with sodium hydroxide based buffers that had an ionic strength according to “0% NaCl added” column in Tables 3.5 and 3.6 (which at low pH is similar to that of the BSF reaction) was evaluated (Figure 6.5). In all cases, a large degree of swelling is initiated below pH 6, making this gel composition a strong candidate for combining with the BSF reaction. Furthermore, as shown in Figure 6.5, particularly for gels immersed in phosphoric acid, there is a large difference in swelling ratio between pH 7 and pH 4 (approximately 80%). This further supports that this gel will respond to pH oscillations when coupled to the BSF reaction.

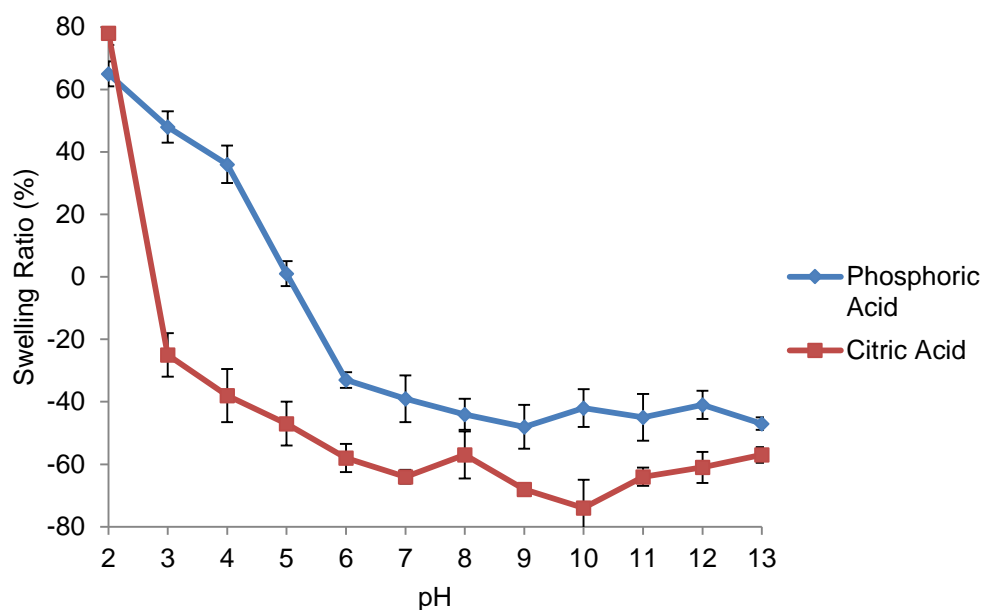


**Figure 6.5** Gravimetric swelling measurements of G-Ch-PVP hydrogels synthesised at 37 °C. Gels were immersed in various mixtures of citric acid/phosphoric acid and sodium hydroxide solutions. The hydrogel is composed of 1.5 mL chitosan (1.5% w/v), 50  $\mu$ L PVP (5% w/v) and 100  $\mu$ L genipin (0.5% w/v).

After being equilibrated overnight in BSF reaction fluid, it was combined with the BSF oscillatory reaction under a 0.15 N pre-load (Figure 6.6). The observed gel behaviour shows a clear decrease in the force value upon a drop in pH, indicating network swelling. There is a slight delay between the pH dropping and the gel responding owing to the diffusion of solvent into/out of the network. It is believed the greater number of amine groups available for protonation is responsible for the enhanced responsiveness of the network. Once again, as shown in Figure 6.6, the force that the gel exerts gradually increases over the course of the experiment due to a faster rate of expansion than collapse in acidic conditions (as in Figure 6.4).

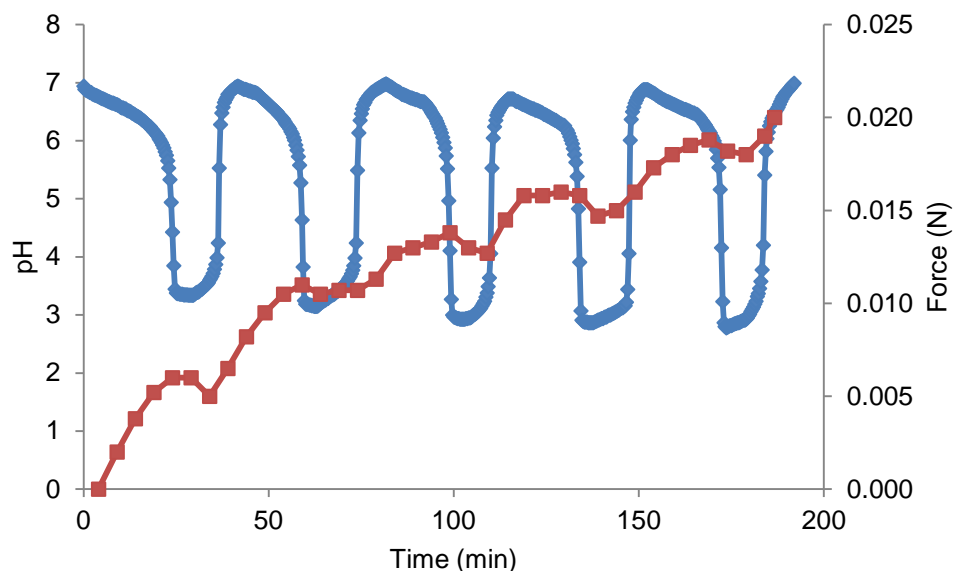


**Figure 6.6** Variation in pH as a function of time during the BSF reaction (blue curve) and the force response of a G-Ch-PVP hydrogel freeze-thawed for 30 min (red curve). The hydrogel is composed of 1.5 mL chitosan (1.5% w/v), 50  $\mu$ L PVP (5% w/v) and 100  $\mu$ L genipin (0.5% w/v).

A plot of pH against force (Figure 6.7) was generated to explore if these parameters are linked. It is clear that as the pH is decreased, this is followed by a decrease in the force response recorded (translating to gel swelling as shown in Figure 6.6). This is exemplified by the crossover of the lines shown in Figure 6.7. It is also apparent that following successive pH oscillations, the force recorded is increasing further, indicating gel collapse. Furthermore, upon repeated pH oscillations, the degree of network collapse is diminished (depicted in Figure 6.7 by smaller increases in the force recorded). This may be because collapse occurs at a faster rate at neutral pH than swelling at an acidic pH (as shown in Figure 6.1). These results therefore demonstrate that after careful optimisation of the hydrogel chemical composition, it is possible to get an oscillating physical response to an oscillatory chemical reaction with this system.

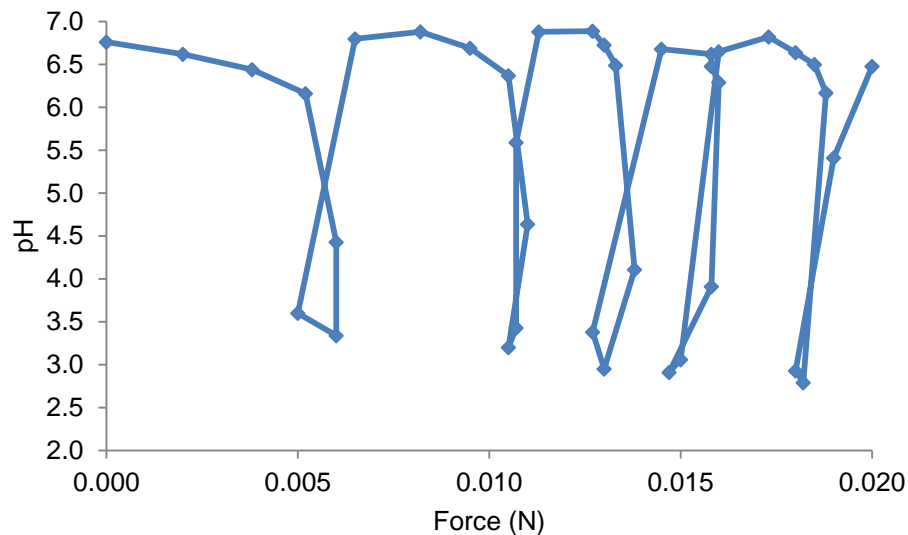


**Figure 6.7** The relationship between variation in pH during the BSF reaction and the force response of a G-Ch-PVP hydrogel freeze-thawed for 30 min. The hydrogel is composed of 1.5 mL chitosan (1.5% w/v), 50  $\mu$ L PVP (5% w/v) and 100  $\mu$ L genipin (0.5% w/v).

#### **6.4 The ability of genipin-crosslinked chitosan-poly (vinyl pyrrolidone) hydrogels to release absorbed constituents**

With the progress made and applications of hydrogels in drug delivery being extensive (Hoare and Kohane, 2008), coupled with the autofluorescent nature of G-Ch-PVP networks for potential use as a biomarker, the ability of these smart systems to release absorbed chemical moieties was considered. A G-Ch-PVP hydrogel (1 mL chitosan (1.5% w/v), 200  $\mu$ L PVP (5% w/v) and 100  $\mu$ L genipin (0.5% w/v)) that was freeze-thawed for 30 min was equilibrated in a pH 7 phosphate buffered solution and transferred to a solution containing FITC-dextran (10 mg mL<sup>-1</sup>). The fluorescence excitation and emission spectra for FITC-dextran is depicted in Figure 6.8. The peak due to excitation is most intense at 495 nm compared to that of approximately 519 nm in the emission spectrum. These results were subsequently used to inform the experimental conditions to be employed when studying the release of FITC-dextran from G-Ch-PVP hydrogels on the macroscale and microscale.

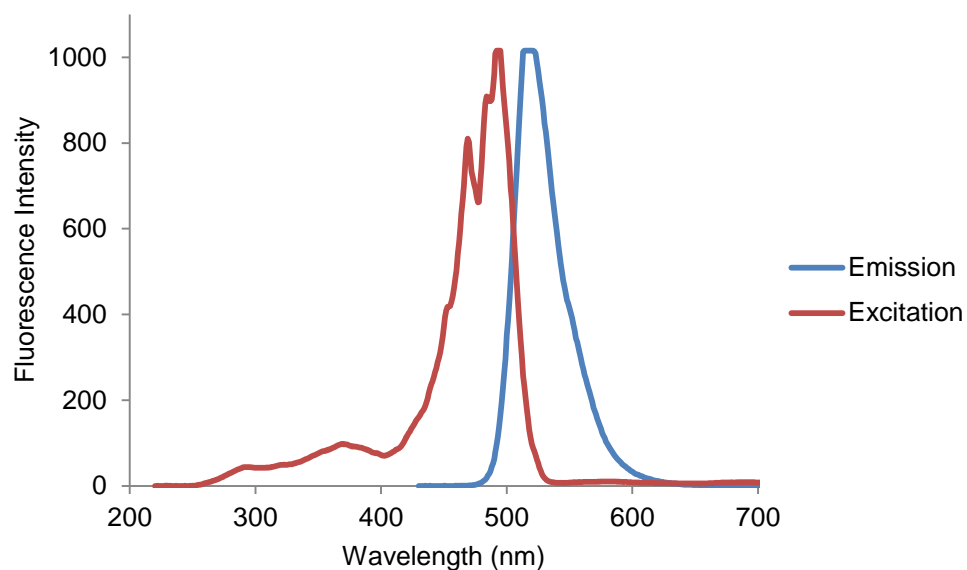


**Figure 6.8** Fluorescence excitation and emission spectra for a FITC-dextran solution ( $10 \text{ mg mL}^{-1}$ ). Parameters utilised to acquire the spectra are detailed in Section 3.14.

The fluorescence from the dextran was visualised on the macroscale when the network was forced to collapse in an alkaline pH 10 borate buffered solution (Figure 6.9). The image at 0 min (a) shows a swollen dextran-loaded hydrogel and over time dextran is expelled from the network (images (b), (c) and (d) show the gel at 1 h, 2h and 3 h respectively). This release is subsequently quantified (Figure 6.10). Furthermore the gel is shrinking as a function of time contributing towards the expulsion of FITC-dextran from the network.

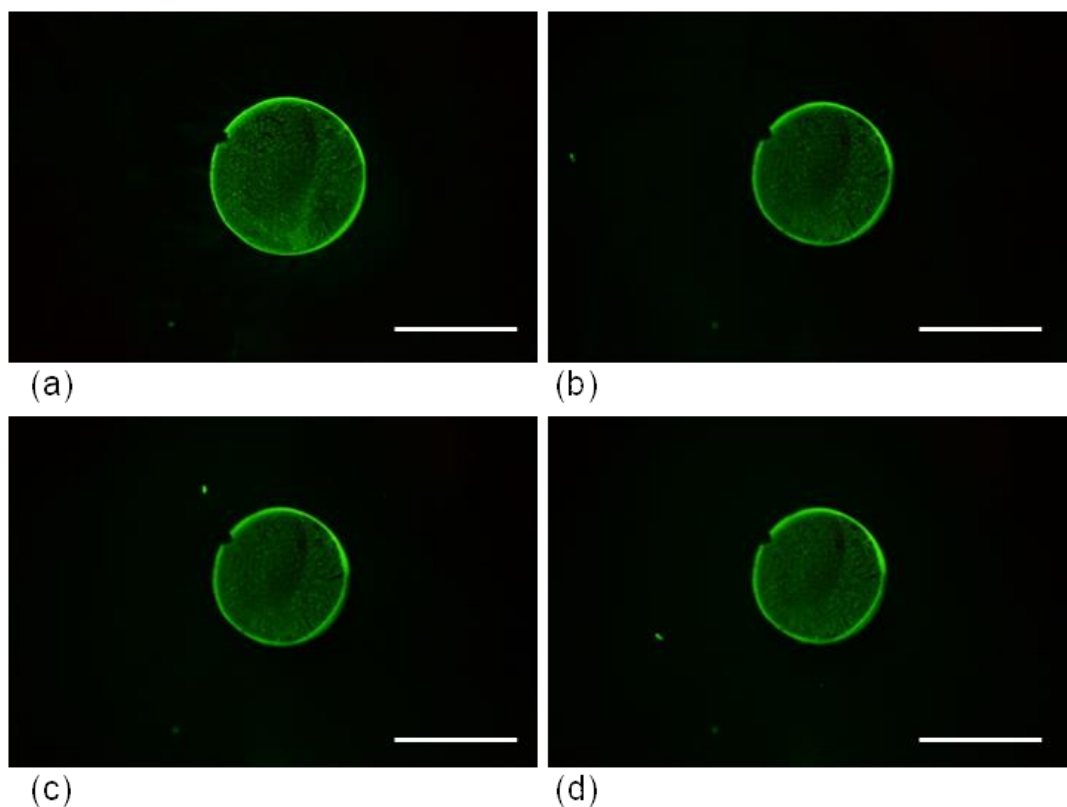


**Figure 6.9** Photographs of a 30 min freeze-thawed G-Ch-PVP hydrogel equilibrated in a pH 7 buffered solution; transferred to a FITC-dextran solution ( $10 \text{ mg mL}^{-1}$ ) and collapsed in a pH 10 borate solution. Images were taken at (a) 0 min, (b) 1 h (c) 2 h and (d) 3 h. All scale bars are 20 mm.

An attempt to quantify the release by examining the variation in fluorescence over time was made (Figure 6.10). As can be seen by the red curve, it is clear the hydrogel collapses quickly initially and then more slowly with time, reaching a plateau after 3 h. As expected, there is a large initial drop in fluorescence intensity of dextran on the gel at the start of the experiment (red curve), although there is a surprising recovery of the fluorescence intensity over time. This may be due to the dextran being attached to the pores within the network, and as it is clear that the bulk gel is collapsing, if this is occurring at a faster rate than dextran release, the density of the crosslinks and hence the density of the fluorescence attributed to the dextran increases during collapse.

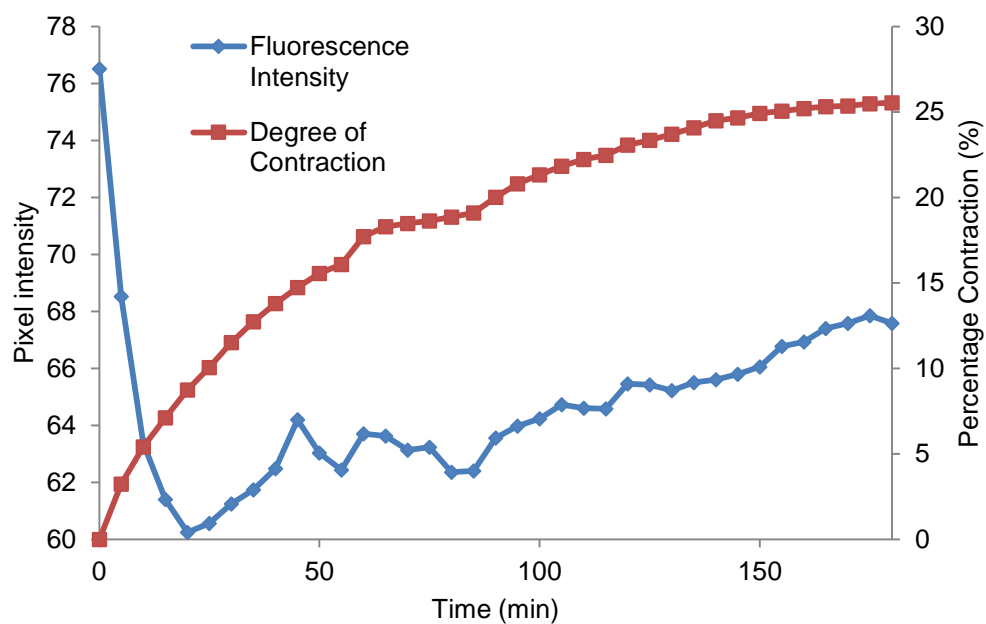


**Figure 6.10** Variation in fluorescence intensity as a function of pixels (blue curve) as a dextran-loaded G-Ch-PVP hydrogel is forced to collapse (red curve).

In order to confirm the location of the dextran within the porous network, CLSM with fluorescence was used to probe the microstructure (Figure 6.11). The autofluorescence due to genipin-crosslinking is depicted in (a) while the location of the dextran within the porous network is shown in (b). The porous architecture in Figure 6.11 (a) compares well with the CLSM image taken of a G-Ch-PVP hydrogel swollen in distilled water (Figure 5.7). An overlay of the fluorescence due to FITC-dextran on top of the autofluorescence attributed to the bulk gel is shown in (c). Clearly, the FITC-dextran is saturated on the surface of the gel framework.

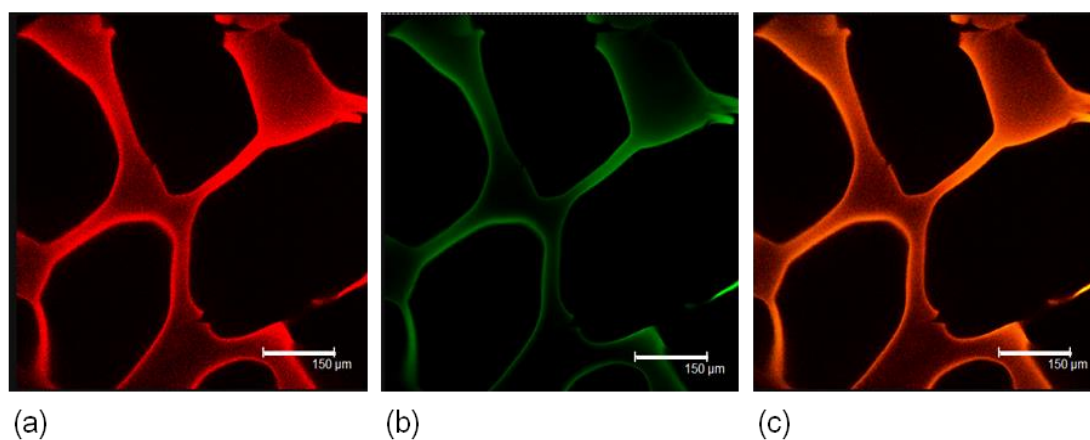


**Figure 6.11** CLSM images of (a) autofluorescence from the hydrogel matrix, (b) fluorescence from FITC-dextran and (c) an overlay of the fluorescence from the FITC-dextran on the autofluorescent gel surface. All scale bars are 150  $\mu\text{m}$ .

Release from the hydrogel matrix on the microscale was monitored using CLSM with identical conditions to that of the macroscale (Figure 6.12) where the variation in fluorescence intensity was studied. As expected, visualising one part of the porous morphology during collapse, the fluorescence specifically due to FITC-dextran at that location decreases as it is forced out of the network. This results in a fast initial burst release and then slowing to a plateau.

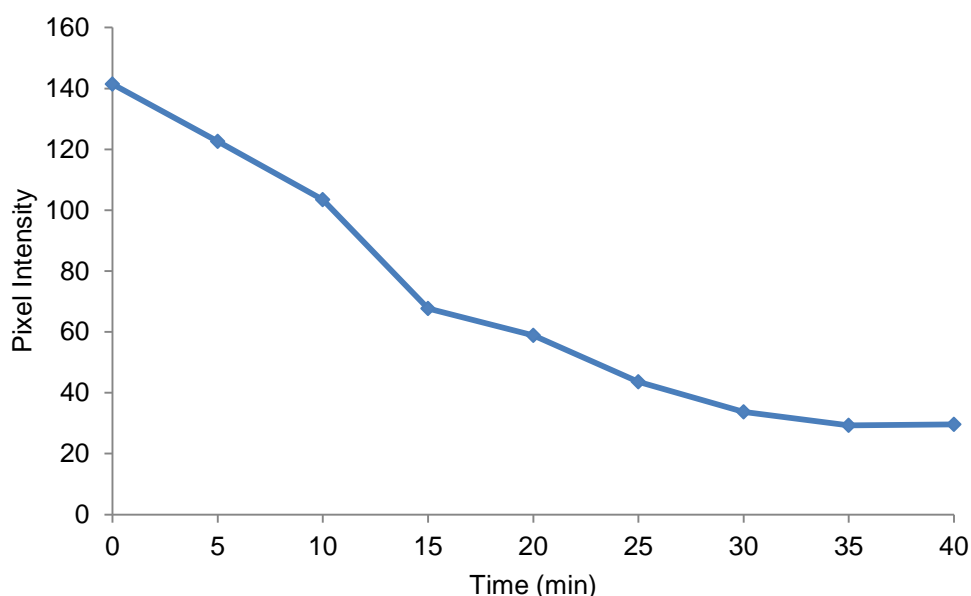


**Figure 6.12** Variation of fluorescence intensity as a function of pixel intensity on the microscale during collapse of G-Ch-PVP hydrogels, resulting in the expulsion of FITC-dextran.

### **6.5 The potential of freeze-dried genipin-crosslinked chitosan-poly (vinyl pyrrolidone) hydrogels to release a therapeutic moiety**

Further to being able to load hydrogels with dextran following gel synthesis with subsequent release being observed, it is also possible to incorporate model compounds prior to gelation. This method has the advantage that the amount of constituents contained in the network is definitively known prior to release, unlike loading once the gel has been synthesised. Amoxicillin is an antibiotic used to treat infections in the GI tract caused by *Helicobacter pylori* bacteria. This was chosen as a model compound owing to the comparatively low cost (£81.30 per 5 g via Sigma Aldrich), good solubility in water and simulated gastric fluid, adequate stability at elevated temperatures (such as 37 °C) and in an acidic environment. Finally, the size of amoxicillin particulates is adequately

small to diffuse through the porous gel network (Patel and Amiji, 1996, Risbud et al., 2000).

Identical G-Ch-PVP hydrogels freeze-thawed for 30 min were prepared as detailed in the studies of dextran release in Section 3.14.1 and 3.14.2 with the exception that 10 mg of amoxicillin was added to the mixture prior to gelation. Amoxicillin-loaded specimens were subsequently freeze-dried. This treatment was based on the superior swelling properties exhibited by such samples as opposed to air-dried counterparts (Risbud et al., 2000). The amount of amoxicillin released was measured via UV-Vis spectroscopy (blue curve) as a function of network swelling in simulated GI fluid determined optically (red curve) is shown in Figure 6.13. This release study was conducted according to the methodology outlined in Section 3.14.3 and was repeated twice where the error bars represent the standard error calculated.

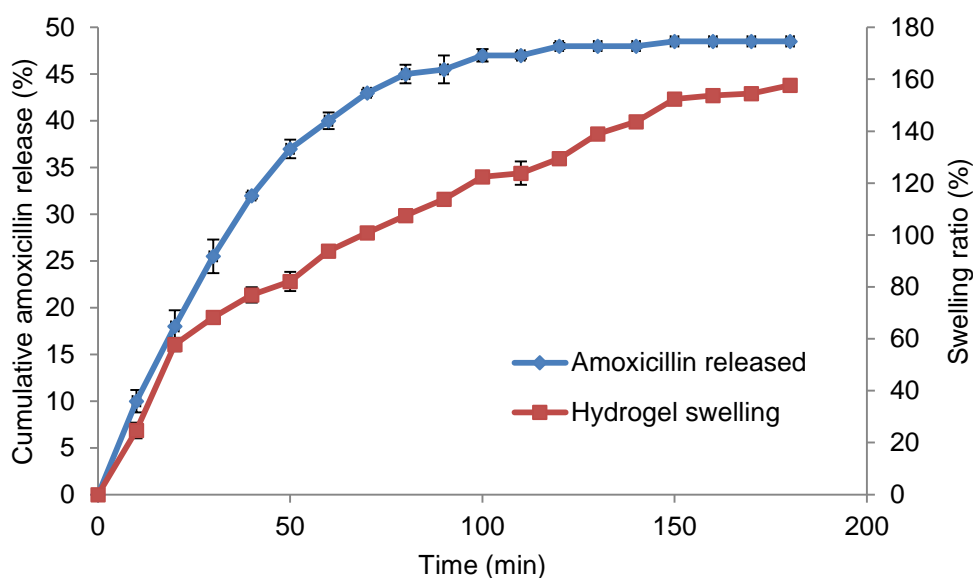


**Figure 6.13** Amoxicillin released from freeze-dried G-Ch-PVP hydrogels in simulated GI fluid (blue curve) and the simultaneous swelling of samples recorded optically (red curve).

Within 30 min 25% of the initial amount of amoxicillin was released followed by a total release of 49% achieved after 3 h. Assuming adequate mixing of the surrounding simulated GI fluid, the remaining 51% of amoxicillin is likely to be within the gel. Hydrogel swelling in the acidic environment of simulated GI fluid enhances the number of amine groups that are protonated within the gel matrix allowing solvent to diffuse through the pores. A comparatively large degree of

swelling is observed (red curve in Figure 6.13). This could be due to the collapsed initial state of the gel network following freeze-drying and the fact that the simulated GI fluid has an ionic strength of just  $0.10 \text{ mol kg}^{-1}$ , meaning that there will be a large difference between the concentrations of the solutions inside and outside of the gel, increasing osmotic pressure and hence enhancing the degree of network swelling. Consequently, hydrogel swelling is in agreement with the cumulative drug release for the initial 100 min of the experiment, although following this, release of the therapeutic equilibrates despite continued swelling. This indicates that after 100 min, amoxicillin release is limited by diffusion and not governed by the degree of network swelling. This is evidenced in Figure 6.14 whereby an approximately linear dependence of the cumulative amount of amoxicillin released on the swelling ratio of freeze-dried G-Ch-PVP hydrogels is observed at low swelling ratios. At higher swelling ratios (above 100%) the graph in Figure 6.14 shows a plateau, indicating that release is now limited via diffusion. Another reason as to why there is residual amoxicillin within the gel network could be due to interactions such as hydrogen bonding between the gel network and amoxicillin moieties (Wu et al., 2014).

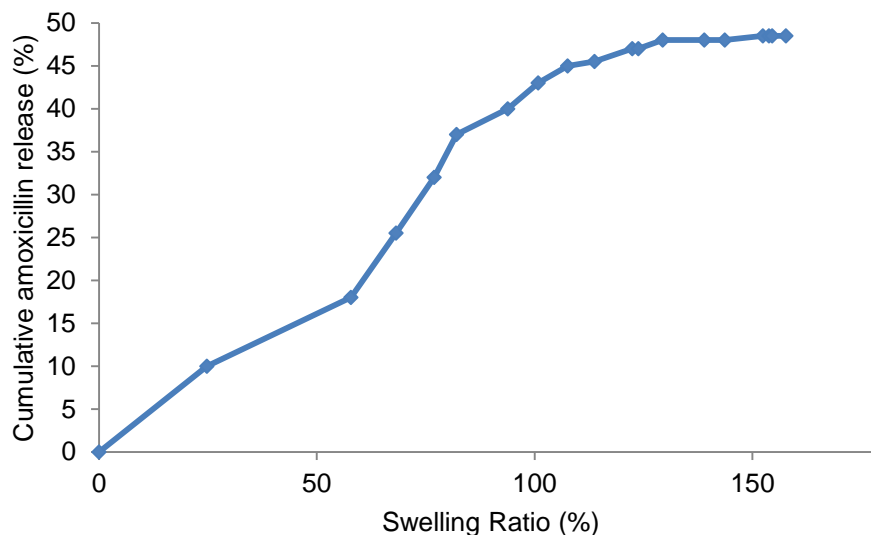


**Figure 6.14** Comparison between cumulative amoxicillin released from freeze-dried G-Ch-PVP hydrogels in simulated GI fluid and the simultaneous swelling of samples recorded optically.

A final release of 49% of amoxicillin over 3 h does not compare well with the literature. For example, the maximal release of amoxicillin from a freeze-dried, glutaraldehyde-crosslinked, chitosan-PVP hydrogel over a period of 3 h was

73% (Risbud et al., 2000). However, no experimental results on the mechanical stability of these networks were provided by the authors. It may be the case that a strong cumulative drug release from the networks has been prioritised over their stability, which is necessary for prospective applications in drug delivery.

## **6.6 Conclusions**

In conclusion, following extensive characterisation of the swelling potential, morphology and mechanical properties of G-Ch-PVP hydrogels, their suitability for application in a range of environments has been determined. Hydrogels that were freeze-thawed for 30 min exhibited excellent potential to be coupled to oscillatory chemical reactions upon manually and periodically varying the pH to simulate such dynamic systems. Large oscillations in force were observed when the gel was subjected to a constant load of 0.050 N due to the diffusion of buffered solutions into and out of the gel network owing to varying degrees of electrostatic charge on the contained amine functionalities.

In the hope that G-Ch-PVP hydrogels could be coupled to a real oscillatory reaction, oscillations in pH during the BSF reaction were successfully recorded. The large pH change (3-7) coupled to the extended duration of time the system spends at extreme pH values makes this reaction ideal for coupling to cationic hydrogels. A G-Ch-PVP hydrogel was combined with the BSF reaction and the variation in the force exerted on a static plate was monitored. Overall, as the reaction progressed the gel collapsed. This could be due to a pre-load of 0.050 N being exerted on the surface of the specimens for the duration of the experiment. During oscillations, there is a very slight variation in the force exerted by the network on the plate suggesting that the change in pH provided by the oscillatory system is stimulating the gel to respond with a concomitant variation in the bulk volume. As this variation is due to a change in the number of protonated amine groups within the network, the amount of chitosan in the samples was increased in the hope of eliciting a more pronounced response. This was found to be the case that the gel can exhibit oscillations in volume at the appropriate time points pending a short delay due to solvent diffusion, upon variation in pH induced by an oscillatory reaction. A link between the pH of the oscillatory reaction and the force generated was found such that as the pH is decreased, this is followed by a diminished response recorded (represented by

gel swelling). Such findings may aid towards the development of an autonomous system able to respond to changes in the local environment.

The potential of G-Ch-PVP hydrogels to release absorbed constituents was subsequently determined using FITC-dextran as a model compound. Release was investigated on the macro and micro-scales. Following synthesis, gels were loaded with dextran and forced to collapse. This was followed optically with appropriate excitation and emission filters, a camera and a light source. During the experiment, the gel collapses and releases the absorbed FITC-dextran. The fluorescence intensity decreases sharply indicating FITC-dextran is diffusing out of the gel matrix, although as the gel is quickly collapsing, the fluorescence intensity subsequently increases, representing an increase in the overall density of FITC-dextran within the network. This was also studied on the microscale where initial observations that FITC-dextran quickly diffuses out of the network following network collapse shown by a decrease in the fluorescence intensity, corroborating initial macroscale measurements. A plateau seems to be reached at approximately 40 min signifying most of the dextran has been released from this part of the network.

In order to specifically quantify release, UV-Vis spectroscopy was used to measure the amount of amoxicillin diffusing from the gel network into simulated GI fluid. Gels were synthesised in a similar manner, although amoxicillin was incorporated into the sample prior to gelation allowing the experimenter to know the exact amount in each specimen. After examining the literature, it was shown that freeze-dried hydrogels with a larger surface area led to an improved release rate. Amoxicillin-loaded gels were subsequently freeze-dried and swollen in simulated GI fluid. Over time, as the network swelled due to an increasing number of protonated amine groups, amoxicillin was able to be released through the voids where an ultimate release of 49% was achieved. G-Ch-PVP hydrogels show good promise to be used as therapeutic release agents, although the ultimate release must be more efficient whilst retaining good sample stability.

## Chapter 7 – Conclusions and Recommendations for Future Work

This work was performed to investigate G-Ch-PVP hydrogels as smart pH responsive materials. Such intelligent systems have been shown to exhibit many favourable properties, allowing multiple applications to be developed. However in order for such networks to be useful, they must demonstrate a sufficiently high swelling response whilst retaining good stability.

Chapters 1 and 2 introduced the topic of the thesis whilst providing an overview of smart polymer gels and their applications. Chapter 3 detailed the methods employed throughout the investigation. In the fourth chapter G-Ch-PVP hydrogels were synthesised in the shape of a disc and the optimal conditions for gelation were explored by varying parameters such as temperature and duration. As these factors increase, the rate of crosslinking is accelerated, leading to gels with an increasingly dark blue pigmentation with enhanced stability. Gels were also shown to be autofluorescent, which opens up potential applications of the networks as biomarkers. Specimens were characterised morphologically via SEM using two drying regimes; CPD and FD. It was shown that both techniques are complementary to one another, although CPD induced extensive network collapse compared to FD. For example, following gelation for 72 h, the porosity measured for freeze-dried samples was 14.4% compared to that of critically point dried samples with 0.4% (Table 4.3). Such a large collapse may be primarily attributed to the ethanol dehydration procedure associated with CPD. The swelling potential of G-Ch-PVP hydrogels was evaluated optically and also gravimetrically in multiple buffered solutions. These studies demonstrated the cationic nature of the network whereby swelling occurred in acidic media due to protonation of the amine functionalities within the matrix, inducing electrostatic repulsion between such moieties, resulting in swelling. For example, it was demonstrated in Figure 4.40 that hydrogels swollen in a pH 2 buffered solution reached a 35% increase in the degree of swelling compared to just 20% when immersed in a pH 7 buffered solution. As well as swelling behaviour being linked to the protonation of amine functional groups, the change in porosity of the network also correlated well with the pH of the solution in which the gel was immersed in. The effect of ionic strength of the surrounding

buffer solution was also investigated. It was found that as the ionic strength increases, gel swelling decreases. This is most likely due to the enhancement in the degree of charge screening within the network, lowering the Donnan potential, resulting in a reduction in the osmotic pressure exerted and hence a lower swelling degree.

G-Ch-PVP hydrogels were also shown to have good potential in responding to an environment exhibiting oscillations in the appropriate stimulus to initiate a concomitant volume change. Following washing in methanol, gels were shown to respond in multiple pH buffered solutions and the dependence on gelation time was investigated. Generally, samples that had undergone gelation for a longer period of time showed a lower degree of swelling than those placed in the oven for shorter periods. This is most likely due to an increased amount of crosslinking, leading to smaller and fewer pores during longer gelation time periods. However uniaxial compression testing confirmed that these particular hydrogels exhibited low stability (6000 Pa at 50% strain (Figure 4.65)) and regularly suffered from fragmentation, making any potential applications of these materials severely limited.

In an attempt to improve the mechanical stability of G-Ch-PVP hydrogels whilst retaining the desirable smart characteristics, samples were freeze-thawed. Gels were far more stable, allowing morphological analysis via a multitude of techniques such as optical microscopy, SEM via CPD and FD, ESEM and CLSM in reflectance and fluorescence modes. The enhanced stability allows gels to be analysed whilst immersed in a solution using a dipping lens via CLSM where a 3-D morphology can be generated. The swelling of such freeze-thawed gels was evaluated on the macro- and micro- length scales and found to correlate well with one another with the variation in porosity aligned with gravimetric data collected. Furthermore, good stability enabled the gels to be easily washed in distilled water in order to reduce the number of residuals, allowing the material to be applied in aqueous systems. Successful removal of unwanted constituents was confirmed via analysing wash solutions with UV-Vis spectroscopy. The effects of freezing and thawing for multiple time periods and cycling on the mechanical properties of G-Ch-PVP hydrogels were evaluated in both dry and wet environments via uniaxial compression testing. It was found that up to a point, increasing the freeze-thawing durations and the number of

freeze-thaw cycles enhanced the mechanical stability of the samples. For example, whilst setting the duration of freeze-thawing at 5 min, by increasing the number of cycles from 1 to 4, an increase of approximately 15,000 Pa at 50% strain was observed (Figure 5.25). Furthermore, comparing samples freeze-thawed for 1 cycle and altering the time between 5 min and 1 h, an increase of 25,000 Pa at 50% strain was measured (Figures 5.25 and 5.28). It is likely that the increase in elastic modulus with freeze-thawing is due to initial phase separation of a polymer-rich and water-rich phase, leading to crystallisation and enhancement of the hydrogen bonding between chitosan and PVP moieties (Figures 5.50-5.52). These results were then related to the swelling potential of the networks in order to further understand the behaviour of these smart materials and correlations were found between elastic modulus, pH, morphology, swelling, protonation, crosslinking and gel processing. Further investigations were conducted to determine the effects of varying the volume of chitosan, PVP and genipin within the specimens and measuring how the swelling response varied. This led to a design of experiments being conducted to understand how these constituents affected the degree of swelling, morphology and mechanical properties.

Following on from this, Chapter 6 explored potential applications of freeze-thawed G-Ch-PVP hydrogels. Swelling and collapse were studied as a function of force following a successful simulation where the buffered solutions the gel was immersed in were periodically changed. Variations in force of approximately 0.030 N were observed (Figure 6.3). This led to combining the gel with a real oscillatory chemical reaction (the BSF reaction). The gel demonstrated an oscillatory response over the period of the reaction, although this was not very recognisable (Figure 6.4). A higher amount of chitosan was incorporated into the network, in order to increase the number of nitrogen moieties available for protonation in order to generate more electrostatic interactions to result in more pronounced swelling changes during the reaction. This was shown to be an effective method to produce a more recognisable oscillatory response (Figure 6.6).

The potential of freeze-thawed G-Ch-PVP hydrogels for the release of absorbed constituents with FITC-dextran used as a model compound was studied on the macro-and micro-scales. This demonstrated that synthesised hydrogels could

be loaded with a compound dissolved in an aqueous solution and upon collapse; absorbed constituents could be forced out of the polymeric network. Release was demonstrated quantitatively via UV-Vis spectroscopy whereby amoxicillin, a therapeutic moiety for the treatment of bacterial infections in the GI tract was incorporated into the chitosan, PVP and genipin mixture prior to gelation, and following FD, the loaded specimens were swollen in simulated GI fluid, resulting in amoxicillin release. A final amoxicillin release of 49% over a period of 3 h was recorded (Figure 6.13).

In conclusion, stable and responsive G-Ch-PVP hydrogels have been synthesised and their swelling potential, morphological and mechanical properties were determined and subsequently optimised. A range of applications have been explored to include implementation in an oscillatory environment and as release agents. As such the main aims and objectives have been met together with providing a more in-depth understanding as to how swelling, crosslinking, pH, morphology, gel processing and elastic modulus are all linked.

Future work could involve using rheology in order to further understand the gel properties to tailor use for application in multiple environments. Such studies could generate more information about the mechanical properties of the hydrogel specimens and is preferable to conducting tensile tests were the samples commonly fracture when gripped. The response achieved when applied in an oscillatory environment could be optimised by systematically varying multiple parameters such as amount of the gel constituents, gelation time and the method of freeze-thawing for instance. In doing so, a greater change in force during oscillations may be generated. This may be useful in developing applications in actuation. Similarly the release of amoxicillin may be improved by varying some of the above parameters in order to increase the ultimate release from 49% after 3 h.

Finally, owing to the good innate bio-related properties of the gel constituents, it may be possible to apply G-Ch-PVP hydrogels in tissue engineering. As the gel can be easily sterilised, and proteins to enhance cell growth can be easily incorporated into the network owing to the abundance of amine groups, various cell lines could be tested whereby CLSM with fluorescence could be used to

determine the extent of cell proliferation. If the network was found to support cell growth, this smart material may go some way to potentially help meet the needs of patients requiring an organ/tissue repair/replacement.

## References

- ABDEEN, Z. 2011. Swelling and reswelling characteristics of cross-linked poly(vinyl alcohol)/chitosan hydrogel film. *Journal of Dispersion Science and Technology*, 32, 1337-1344.
- ALTINISIK, A. & YURDAKOC, K. 2014. Chitosan/poly(vinyl alcohol) hydrogels for amoxicillin release. *Polymer Bulletin*, 71, 759-774.
- ANDRASI, M., BUGLYO, P., ZEKANY, L. & GASPAR, A. 2007. A comparative study of capillary zone electrophoresis and pH-potentiometry for determination of dissociation constants. *Journal of Pharmaceutical and Biomedical Analysis*, 44, 1040-1047.
- ANNAKA, M. & TANAKA, T. 1992. Multiple phases of polymer gels. *Nature*, 355, 430-432.
- ANNAKA, M., TOKITA, M., TANAKA, T., TANAKA, S. & NAKAHIRA, T. 2000. The gel that memorizes phases. *Journal of Chemical Physics*, 112, 471-477.
- ANSETH, K. S., BOWMAN, C. N. & BRANNONPEPPAS, L. 1996. Mechanical properties of hydrogels and their experimental determination. *Biomaterials*, 17, 1647-1657.
- ANTONIETTI, M., CARUSO, R. A., GÖLTNER, C. G. & WEISSENBERGER, M. C. 1999. Morphology Variation of Porous Polymer Gels by Polymerization in Lyotropic Surfactant Phases. *Macromolecules*, 32, 1383-1389.
- ARMSTRONG, R. W., ELBAN, W. L. & WALLEY, S. M. 2013. Elastic, plastic, cracking aspects of the hardness of materials. *International Journal of Modern Physics B*, 27.
- ASHBY, M. F. 2006. The properties of foams and lattices. *Philosophical Transactions of the Royal Society A: Mathematical, Physical and Engineering Sciences*, 364, 15-30.
- ASHBY, M. F., SHERCLIFF, H. R. & CEBON, D. 2009. *Materials: Engineering, Science, Processing and Design*, Butterworth-Heinemann.
- ATKINS, P. & DE PAULA, J. 2006. *Atkins' Physical Chemistry*, Oxford University Press.
- ATKINS, P., OVERTON, T., ROURKE, J., WELLER, M. & ARMSTRONG, F. 2006. *Shriver & Atkins Inorganic Chemistry*, Oxford University Press.

- BABIĆ, S., HORVAT, A. J. M., MUTAVDŽIĆ PAVLOVIĆ, D. & KAŠTELAN-MACAN, M. 2007. Determination of pKa values of active pharmaceutical ingredients. *TrAC - Trends in Analytical Chemistry*, 26, 1043-1061.
- BAI, T., HAN, Y., ZHANG, P., WANG, W. & LIU, W. 2012. Zinc ion-triggered two-way macro-/microscopic shape changing and memory effects in high strength hydrogels with pre-programmed unilateral patterned surfaces. *Soft Matter*, 8, 6846-6852.
- BAJPAI, A. K., SHUKLA, S. K., BHANU, S. & KANKANE, S. 2008. Responsive polymers in controlled drug delivery. *Progress in Polymer Science (Oxford)*, 33, 1088-1118.
- BASHIR, R., HILT, J. Z., ELIBOL, O., GUPTA, A. & PEPPAS, N. A. 2002. Micromechanical cantilever as an ultrasensitive pH microsensor. *Applied Physics Letters*, 81, 3091-3093.
- BATES, R. G. 1948. Definitions of pH scales. *Chemical Reviews*, 42, 1-61.
- BAWA, P., PILLAY, V., CHOONARA, Y. E. & DU TOIT, L. C. 2009. Stimuli-responsive polymers and their applications in drug delivery. *Biomedical Materials*, 4.
- BEEBE, D. J., MOORE, J. S., BAUER, J. M., YU, Q., LIU, R. H., DEVADOSS, C. & JO, B. H. 2000. Functional hydrogel structures for autonomous flow control inside microfluidic channels. *Nature*, 404, 588-590.
- BEER, F., RUSSEL JOHNSTON JUNIOR, E., DEWOLF, J. & MAZUREK, D. 2014. *Mechanics of Materials*, McGraw-Hill.
- BEHRAVESH, E., TIMMER, M. D., LEMOINE, J. L., LIEBSCHNER, M. A. K. & MIKOS, A. G. 2002. Evaluation of the in vitro degradation of macroporous hydrogels using gravimetry, confined compression testing, and microcomputed tomography. *Biomacromolecules*, 3, 1263-1270.
- BELL, C. L. & PEPPAS, N. A. 1996. Water, solute and protein diffusion in physiologically responsive hydrogels of poly(methacrylic acid-g-ethylene glycol). *Biomaterials*, 17, 1203-1218.
- BERGSTRAND, M., SÖDERLIND, E., ERIKSSON, U. G., WEITSCHIES, W. & KARLSSON, M. O. 2012. A semi-mechanistic modeling strategy to link in vitro and in vivo drug release for modified release formulations. *Pharmaceutical Research*, 29, 695-706.

- BHATTARAI, N., GUNN, J. & ZHANG, M. 2010. Chitosan-based hydrogels for controlled, localized drug delivery. *Advanced Drug Delivery Reviews*, 62, 83-99.
- BHATTARAI, N., RAMAY, H. R., GUNN, J., MATSEN, F. A. & ZHANG, M. 2005. PEG-grafted chitosan as an injectable thermosensitive hydrogel for sustained protein release. *Journal of Controlled Release*, 103, 609-624.
- BI, C., TANG, G. H. & HU, Z. J. 2014. Heat conduction modeling in 3-D ordered structures for prediction of aerogel thermal conductivity. *International Journal of Heat and Mass Transfer*, 73, 103-109.
- BILICI, C., KARAYEL, S., DEMIR, T. T. & OKAY, O. 2010. Self-oscillating ph-responsive cryogels as possible candidates of soft materials for generating mechanical energy. *Journal of Applied Polymer Science*, 118, 2981-2988.
- BODUGOZ-SENTURK, H., MACIAS, C. E., KUNG, J. H. & MURATOGLU, O. K. 2009. Poly(vinyl alcohol)-acrylamide hydrogels as load-bearing cartilage substitute. *Biomaterials*, 30, 589-596.
- BOISSONADE, J. 2003. Simple chemomechanical process for self-generation of rhythms and forms. *Physical Review Letters*, 90, 188302/1-188302/4.
- BOISSONADE, J. 2005. Self-oscillations in chemoresponsive gels: A theoretical approach. *Chaos*, 15, 23703-23707.
- BOUKALOUCHE, M., ELEZGARAY, J., ARNEODO, A., BOISSONADE, J. & DE KEPPER, P. 1987. Oscillatory instability induced by mass interchange between two coupled steady-state reactors. *Journal of Physical Chemistry*, 91, 5843-5845.
- BRANNON-PEPPAS, L. & PEPPAS, N. A. 1991. Equilibrium swelling behavior of pH-sensitive hydrogels. *Chemical Engineering Science*, 46, 715-722.
- BRAY, W. C. 1921. A periodic reaction in homogeneous solution and its relation to catalysis. *Journal of the American Chemical Society*, 43, 1262-1267.
- BRAY, W. C. & LIEBHAFSKY, H. A. 1931. Reactions involving hydrogen peroxide, iodine and iodate ion. I. Introduction. *Journal of the American Chemical Society*, 53, 38-44.
- BRIGGS, T. S. & RAUSCHER, W. C. 1973. An oscillating iodine clock. *Journal of Chemical Education*, 50, 496-500.
- BROWN, H. C., BAUDE, E. A. & NACHOD, F. C. 1955. *Determination of Organic Structures by Physical Methods*, Academic Press.

- BROWN, H. R. 2007. A model of the fracture of double network gels. *Macromolecules*, 40, 3815-3818.
- BROWN, L. R., EDELMAN, E. R., FISCHER-GHODSIAN, F. & LANGER, R. 1996. Characterization of glucose-mediated insulin release from implantable polymers. *Journal of Pharmaceutical Sciences*, 85, 1341-1345.
- BUHRMAN, J. S., COOK, L. C., RAYAHIN, J. E., FEDERLE, M. J. & GEMEINHART, R. A. 2013. Proteolytically activated anti-bacterial hydrogel microspheres. *Journal of Controlled Release*, 171, 288-295.
- BURROWS, A., HOLMAN, J., PARSONS, A., PILLING, G. & PRICE, G. 2013. *Chemistry*<sup>3</sup>, Oxford University Press.
- BUTLER, M. F., NG, Y. F. & PUDNEY, P. D. A. 2003. Mechanism and kinetics of the crosslinking reaction between biopolymers containing primary amine groups and genipin. *Journal of Polymer Science, Part A: Polymer Chemistry*, 41, 3941-3953.
- CALDORERA-MOORE, M., KANG, M. K., MOORE, Z., SINGH, V., SREENIVASAN, S. V., SHI, L., HUANG, R. & ROY, K. 2011. Swelling behavior of nanoscale, shape- and size-specific, hydrogel particles fabricated using imprint lithography. *Soft Matter*, 7, 2879-2887.
- CAUICH-RODRÍGUEZ, J. V., DEB, S. & SMITH, R. 2001. Physicochemical characterization of hydrogels based on polyvinyl alcohol-vinyl acetate blends. *Journal of Applied Polymer Science*, 82, 3578-3590.
- CHATERJI, S., KWON, I. K. & PARK, K. 2007. Smart polymeric gels: Redefining the limits of biomedical devices. *Progress in Polymer Science (Oxford)*, 32, 1083-1122.
- CHEN, H., OUYANG, W., LAWUYI, B., MARTONI, C. & PRAKASH, S. 2005. Reaction of chitosan with genipin and its fluorogenic attributes for potential microcapsule membrane characterization. *Journal of Biomedical Materials Research - Part A*, 75, 917-927.
- CHEN, J., PARK, H. & PARK, K. 1999. Synthesis of superporous hydrogels: Hydrogels with fast swelling and superabsorbent properties. *Journal of Biomedical Materials Research*, 44, 53-62.
- CHEN, S. C., WU, Y. C., MI, F. L., LIN, Y. H., YU, L. C. & SUNG, H. W. 2004. A novel pH-sensitive hydrogel composed of N,O-carboxymethyl chitosan

- and alginate cross-linked by genipin for protein drug delivery. *Journal of Controlled Release*, 96, 285-300.
- CLAESSON, P. M. & NINHAM, B. W. 1992. pH-dependent interactions between adsorbed chitosan layers. *Langmuir*, 8, 1406-1412.
- COOKE, D. O. 1979. Iodine concentration behaviour of the hydrogen peroxide-iodic acid- manganese(II)-malonic acid oscillating system. *Inorganica Chimica Acta*, 37, 259-265.
- CREMER, C. & CREMER, T. 1978. Considerations on a laser-scanning-microscope with high resolution and depth of field. *Microscopica Acta*, 81, 31-44.
- CROOK, C. J., CADBY, A., SMITH, A., JONES, R. A. L. & RYAN, A. J. 2004. Measurement of force produced by a pH-responsive hydrogel in a pH oscillator. In: POJMAN, J. A. & TRANCONGMIYATA, Q. (eds.) *Nonlinear Dynamics in Polymeric Systems*. Washington: Amer Chemical Soc.
- CROOK, C. J., SMITH, A., JONES, R. A. L. & RYAN, A. J. 2002. Chemically induced oscillations in a pH-responsive hydrogel. *Physical Chemistry Chemical Physics*, 4, 1367-1369.
- CROWLEY, M. F. & EPSTEIN, I. R. 1989. Experimental and theoretical studies of a coupled chemical oscillator: Phase death, multistability, and in-phase and out-of-phase entrainment. *Journal of Physical Chemistry*, 93, 2496-2502.
- CUMPER, C. W. N., GINMAN, R. F. A. & VOGEL, A. I. 1962. 226. Physical properties and chemical constitution. Part XXXV. The electric dipole moments of some phenanthrolines and bipyridyls. *Journal of the Chemical Society (Resumed)*, 1188-1192.
- DAWSON, R. M. C. 1959. *Data for Biochemical Research*, Clarendon Press.
- DE KEPPEL, P., BOISSONADE, J. & SZALAI, I. 2009. From sustained oscillations to stationary reaction-diffusion patterns. *NATO Science for Peace and Security Series A: Chemistry and Biology*.
- DE KEPPEL, P. & EPSTEIN, I. R. 1982. A mechanistic study of oscillations and bistability in the Briggs-Rauscher reaction. *Journal of the American Chemical Society*, 104, 49-55.
- DE, K. S., ALURU, N. R., JOHNSON, B., CRONE, W. C., BEEBE, D. J. & MOORE, J. 2002. Equilibrium swelling and kinetics of pH-responsive

- hydrogels: Models, experiments, and simulations. *Journal of Microelectromechanical Systems*, 11, 544-555.
- DEGNER, B. M., CHUNG, C., SCHLEGEL, V., HUTKINS, R. & MCCLEMENTS, D. J. 2014. Factors influencing the freeze-thaw stability of emulsion-based foods. *Comprehensive Reviews in Food Science and Food Safety*, 13, 98-113.
- DEGNER, B. M., OLSON, K. M., ROSE, D., SCHLEGEL, V., HUTKINS, R. & MCCLEMENTS, D. J. 2013. Influence of freezing rate variation on the microstructure and physicochemical properties of food emulsions. *Journal of Food Engineering*, 119, 244-253.
- DEMIRCI, S., ALASLAN, A. & CAYKARA, T. 2009. Preparation, characterization and surface pKa values of poly(N-vinyl-2-pyrrolidone)/chitosan blend films. *Applied Surface Science*, 255, 5979-5983.
- DIMONTE, G., NELSON, D., WEAVER, S., SCHNEIDER, M., FLOWER-MAUDLIN, E., GORE, R., BAUMGARDNER, J. R. & SAHOTA, M. S. 1998. Comparative study of viscoelastic properties using virgin yogurt. *Journal of Rheology*, 42, 727-742.
- DOMB, C. 1974. Phase transition in a polymer chain in dilute solution. *Polymer*, 15, 259-262.
- DONLON, L., PARKER, J. & NOVAKOVIC, K. 2014. Oscillatory carbonylation of phenylacetylene in the absence of externally supplied oxidant. *Reaction Kinetics, Mechanisms and Catalysis*, 1-13.
- DRIRA, Z. & YADAVALLI, V. K. 2013. Nanomechanical measurements of polyethylene glycol hydrogels using atomic force microscopy. *Journal of the Mechanical Behavior of Biomedical Materials*, 18, 20-28.
- DRURY, J. L. & MOONEY, D. J. 2003. Hydrogels for tissue engineering: Scaffold design variables and applications. *Biomaterials*, 24, 4337-4351.
- EDBLON, E. C., LUO, Y., ORBÁN, M., KUSTIN, K. & EPSTEIN, I. R. 1989. Kinetics and mechanism of the oscillatory bromate-sulfite-ferrocyanide reaction. *Journal of Physical Chemistry*, 93, 2722-2727.
- EDBLON, E. C., ORBÁN, M. & EPSTEIN, I. R. 1986. A new iodate oscillator: The Landolt reaction with ferrocyanide in a CSTR. *Journal of the American Chemical Society*, 108, 2826-2830.

- EGGENSTEIN, C., BORCHARDT, M., DIEKMANN, C., GRÜNDIG, B., DUMSCHAT, C., CAMMANN, K., KNOLL, M. & SPENER, F. 1999. A disposable biosensor for urea determination in blood based on an ammonium-sensitive transducer. *Biosensors and Bioelectronics*, 14, 33-41.
- ELINGS, V. B., GURLEY, J. A. 1994. *Atomic Force Microscope*. United States Patent patent application.
- EPSTEIN, I. R., POJMAN, J. A. & TRAN-CONG-MIYATA, Q. What is nonlinear dynamics and how does it relate to polymers? , 2010. Wiley-VCH Verlag GmbH & Co. KGaA, 5-19.
- EPSTEIN, I. R. & SHOWALTER, K. 1996. Nonlinear chemical dynamics: Oscillations, patterns, and chaos. *Journal of Physical Chemistry*, 100, 13132-13147.
- FANG, L. & GOH, S. H. 2000. Miscible chitosan/tertiary amide polymer blends. *Journal of Applied Polymer Science*, 76, 1785-1790.
- FERGG, F., KEIL, F. J. & QUADER, H. 2001. Investigations of the microscopic structure of poly(vinyl alcohol) hydrogels by confocal laser scanning microscopy. *Colloid and Polymer Science*, 279, 61-67.
- FIELD, R. J. & FÖRSTERLING, H. D. 1986. On the oxybromine chemistry rate constants with cerium ions in the field-körös-noyes mechanism of the belousov-zhabotinskii reaction: The equilibrium  $\text{HBrO}_2 + \text{BrO}_3^- + \text{H}^+ \rightleftharpoons 2\text{BrO}_2 \cdot + \text{H}_2\text{O}$ . *Journal of Physical Chemistry*, 90, 5400-5407.
- FIELD, R. J. & NOYES, R. M. 1974. Oscillations in chemical systems. IV. Limit cycle behavior in a model of a real chemical reaction. *The Journal of Chemical Physics*, 60, 1877-1884.
- FLORY, P. J. 1941. Molecular size distribution in three dimensional polymers. I. Gelation. *Journal of the American Chemical Society*, 63, 3083-3090.
- FREE, E. E. 1917. Note on the swelling of gelatine and agar gels in solutions of sucrose and dextrose. *Science*, 46, 142-143.
- FU, Y. & KAO, W. J. 2010. Drug release kinetics and transport mechanisms of non-degradable and degradable polymeric delivery systems. *Expert Opinion on Drug Delivery*, 7, 429-444.
- FURROW, S. D. & NOYES, R. M. 1982a. The oscillatory Briggs-Rauscher reaction. 1. Examination of subsystems. *Journal of the American Chemical Society*, 104, 38-42.

- FURROW, S. D. & NOYES, R. M. 1982b. The oscillatory Briggs-Rauscher reaction. 2. Effects of substitutions and additions. *Journal of the American Chemical Society*, 104, 42-45.
- GABAI, R., SALLACAN, N., CHEGEL, V., BOURENKO, T., KATZ, E. & WILLNER, I. 2001. Characterization of the swelling of acrylamidophenylboronic acid-acrylamide hydrogels upon interaction with glucose by faradaic impedance spectroscopy, chronopotentiometry, quartz-crystal microbalance (QCM), and surface plasmon resonance (SPR) experiments. *Journal of Physical Chemistry B*, 105, 8196-8202.
- GARDEL, M. L., SHIN, J. H., MACKINTOSH, F. C., MAHADEVAN, L., MATSUDAIRA, P. & WEITZ, D. A. 2004. Elastic behavior of cross-linked and bundled actin networks. *Science*, 304, 1301-1305.
- GÁSPÁR, V. & SHOWALTER, K. 1987. The oscillatory Landolt reaction. Empirical rate law model and detailed mechanism. *Journal of the American Chemical Society*, 109, 4869-4876.
- GATTÁS-ASFURA, K. M., WEISMAN, E., ANDREOPOULOS, F. M., MICIC, M., MULLER, B., SIRPAL, S., PHAM, S. M. & LEBLANC, R. M. 2005. Nitrocinnamate-functionalized gelatin: Synthesis and "smart" hydrogel formation via photo-cross-linking. *Biomacromolecules*, 6, 1503-1509.
- GONG, J. P. 2010. Why are double network hydrogels so tough? *Soft Matter*, 6, 2583-2590.
- GUPTA, P., VERMANI, K. & GARG, S. 2002. Hydrogels: From controlled release to pH-responsive drug delivery. *Drug Discovery Today*, 7, 569-579.
- GUPTA, S., GOSWAMI, S. & SINHA, A. 2012. A combined effect of freeze-thaw cycles and polymer concentration on the structure and mechanical properties of transparent PVA gels. *Biomedical Materials*, 7, 15-21.
- GURYČA, V., PACÁKOVÁ, V., TLUST'ÁKOVÁ, M., ŠTULÍK, K. & MICHÁLEK, J. 2004. Topographical properties of polymer films deposited in capillaries for electrophoretic separations of large organic molecules. *Journal of Separation Science*, 27, 1121-1129.
- GUTOWSKA, A., BAE, Y. H., FEIJEN, J. & KIM, S. W. 1992. Heparin release from thermosensitive hydrogels. *Journal of Controlled Release*, 22, 95-104.

- HARA, Y. & YOSHIDA, R. 2008. Self-oscillating polymer fueled by organic acid. *Journal of Physical Chemistry B*, 112, 8427-8429.
- HASSAN, C. M. & PEPPAS, N. A. 2000. Structure and morphology of freeze/thawed PVA hydrogels. *Macromolecules*, 33, 2472-2479.
- HENNINK, W. E. & VAN NOSTRUM, C. F. 2002. Novel crosslinking methods to design hydrogels. *Advanced Drug Delivery Reviews*, 54, 13-36.
- HIDAKA, M. & YOSHIDA, R. 2011. Self-oscillating gel composed of thermosensitive polymer exhibiting higher LCST. *Journal of Controlled Release*, 150, 171-176.
- HIROKAWA, Y. & TANAKA, T. 1984. Volume phase transition in a nonionic gel. *The Journal of Chemical Physics*, 81, 6379-6380.
- HOARE, T. R. & KOHANE, D. S. 2008. Hydrogels in drug delivery: Progress and challenges. *Polymer*, 49, 1993-2007.
- HOFFMAN, A. S. 2000. Bioconjugates of intelligent polymers and recognition proteins for use in diagnostics and affinity separations. *Clinical Chemistry*, 46, 1478-1486.
- HOLLOWAY, J. L., LOWMAN, A. M. & PALMESE, G. R. 2013. The role of crystallization and phase separation in the formation of physically cross-linked PVA hydrogels. *Soft Matter*, 9, 826-833.
- HOLME, H. K., DAVIDSEN, L., KRISTIANSEN, A. & SMIDSRØD, O. 2008. Kinetics and mechanisms of depolymerization of alginate and chitosan in aqueous solution. *Carbohydrate Polymers*, 73, 656-664.
- HORVÁTH, J., SZALAI, I. & DE KEPPEL, P. 2009. An experimental design method leading to chemical turing patterns. *Science*, 324, 772-775.
- HOUSECROFT, C. E. & CONSTABLE, E. C. 2006. *Chemistry*, Pearson Education Limited.
- HOWSE, J. R., TOPHAM, P., CROOK, C. J., GLEESON, A. J., BRAS, W., JONES, R. A. L. & RYAN, A. J. 2006. Reciprocating power generation in a chemically driven synthetic muscle. *Nano Letters*, 6, 73-77.
- HSIEH, D. S. T., LANGER, R. & FOLKMAN, J. 1981. Magnetic modulation of release of macromolecules from polymers. *Proceedings of the National Academy of Sciences of the United States of America*, 78, 1863-1867.
- HUANG, M., FURUKAWA, H., TANAKA, Y., NAKAJIMA, T., OSADA, Y. & GONG, J. P. 2007a. Importance of entanglement between first and

- second components in high-strength double network gels. *Macromolecules*, 40, 6658-6664.
- HUANG, T., XU, H. G., JIAO, K. X., ZHU, L. P., BROWN, H. R. & WANG, H. L. 2007b. A novel hydrogel with high mechanical strength: A macromolecular microsphere composite hydrogel. *Advanced Materials*, 19, 1622-1626.
- HUNTER, C. J., IMLER, S. M., MALAVIYA, P., NEREM, R. M. & LEVENSTON, M. E. 2002. Mechanical compression alters gene expression and extracellular matrix synthesis by chondrocytes cultured in collagen I gels. *Biomaterials*, 23, 1249-1259.
- HURST, G. A. & NOVAKOVIC, K. 2013. A facile in situ morphological characterization of smart genipin-crosslinked chitosan-poly(vinyl pyrrolidone) hydrogels. *Journal of Materials Research*, 28, 2401-2408.
- HÜSING, N. & SCHUBERT, U. 1998. Aerogels - Airy Materials: Chemistry, Structure, and Properties. *Angewandte Chemie - International Edition*, 37, 22-45.
- HWANG, Y. J., LARSEN, J., KRASIEVA, T. B. & LYUBOVITSKY, J. G. 2011. Effect of genipin crosslinking on the optical spectral properties and structures of collagen hydrogels. *ACS Applied Materials and Interfaces*, 3, 2579-2584.
- ILMAIN, F., TANAKA, T. & KOKUFUTA, E. 1991. Volume transition in a gel driven by hydrogen bonding. *Nature*, 349, 400-401.
- IMRAN, A. B., SEKI, T. & TAKEOKA, Y. 2010. Recent advances in hydrogels in terms of fast stimuli responsiveness and superior mechanical performance. *Polymer Journal*, 42, 839-851.
- INOMATA, H., GOTO, S. & SAITO, S. 1990. Phase transition of N-substituted acrylamide gels. *Macromolecules*, 23, 4887-4888.
- INOUE, H., NAKAMURA, O., DUAN, Y., HIRAKI, Y. & SAKUDA, M. 1993. Effect of centrifugal force on growth of mouse osteoblastic MC3T3-E1 cells in vitro. *Journal of Dental Research*, 72, 1351-1355.
- IRIE, M. 1986. Photoresponsive polymers. Reversible bending of rod-shaped acrylamide gels in an electric field. *Macromolecules*, 19, 2890-2892.
- ISRAELACHVILI, J. 1991. *Intermolecular & Surface Forces*, Academic Press Limited.

- ITO, Y., NOGAWA, M. & YOSHIDA, R. 2003. Temperature control of the Belousov-Zhabotinsky reaction using a thermoresponsive polymer. *Langmuir*, 19, 9577-9579.
- JAYAKUMAR, R., MENON, D., MANZOOR, K., NAIR, S. V. & TAMURA, H. 2010. Biomedical applications of chitin and chitosan based nanomaterials - A short review. *Carbohydrate Polymers*, 82, 227-232.
- JEON, C. & HÖLL, W. H. 2003. Chemical modification of chitosan and equilibrium study for mercury ion removal. *Water Research*, 37, 4770-4780.
- JEONG, B., BAE, Y. H. & KIM, S. W. 2000. Drug release from biodegradable injectable thermosensitive hydrogel of PEG-PLGA-PEG triblock copolymers. *Journal of Controlled Release*, 63, 155-163.
- JEONG, B. & GUTOWSKA, A. 2002. Lessons from nature: Stimuli-responsive polymers and their biomedical applications. *Trends in Biotechnology*, 20, 305-311.
- JOHNSON, B., BAUER, J. M., NIEDERMAIER, D. J., CRONE, W. C. & BEEBE, D. J. 2004. Experimental techniques for mechanical characterization of hydrogels at the microscale. *Experimental Mechanics*, 44, 21-28.
- KABIRI, K., OMIDIAN, H., HASHEMI, S. A. & ZOHURIAAN-MEHR, M. J. 2003. Synthesis of fast-swelling superabsorbent hydrogels: Effect of crosslinker type and concentration on porosity and absorption rate. *European Polymer Journal*, 39, 1341-1348.
- KATO, N., SAKAI, Y. & SHIBATA, S. 2003. Wide-range control of deswelling time for thermosensitive poly(n-isopropylacrylamide) gel treated by freeze-drying. *Macromolecules*, 36, 961-963.
- KEAN, T. & THANOU, M. 2010. Biodegradation, biodistribution and toxicity of chitosan. *Advanced Drug Delivery Reviews*, 62, 3-11.
- KHAN, S., TØNDERVIK, A., SLETTA, H., KLINKENBERG, G., EMANUEL, C., ONSØYEN, E., MYRVOLD, R., HOWE, R. A., WALSH, T. R., HILL, K. E. & THOMAS, D. W. 2012. Overcoming drug resistance with alginate oligosaccharides able to potentiate the action of selected antibiotics. *Antimicrobial Agents and Chemotherapy*, 56, 5134-5141.
- KHURMA, J. R. & NAND, A. V. 2008. Temperature and pH sensitive hydrogels composed of chitosan and poly(ethylene glycol). *Polymer Bulletin*, 59, 805-812.

- KHURMA, J. R., ROHINDRA, D. R. & NAND, A. V. 2005. Swelling and thermal characteristics of genipin crosslinked chitosan and poly(vinyl pyrrolidone) hydrogels. *Polymer Bulletin*, 54, 195-204.
- KIM, J., YASZEMSKI, M. J. & LU, L. 2009. Three-dimensional porous biodegradable polymeric scaffolds fabricated with biodegradable hydrogel porogens. *Tissue Engineering - Part C: Methods*, 15, 583-594.
- KIM, J. J. & PARK, K. 1998. Smart hydrogels for bioseparation. *Bioseparation*, 7, 177-184.
- KIM, S. H. & CHU, C. C. 2000. Pore structure analysis of swollen dextran-methacrylate hydrogels by SEM and mercury intrusion porosimetry. *Journal of Biomedical Materials Research*, 53, 258-266.
- KIM, S. K. 2010. *Chitin, Chitosan, Oligosaccharides and Their Derivatives: Biological Activities and Applications*, CRC Press.
- KISHI, R., KIHARA, H. & MIURA, T. 2004. Structural observation of heterogeneous poly(N-isopropyl acrylamide-co-acrylic acid) hydrogels in highly hydrated states. *Colloid and Polymer Science*, 283, 133-138.
- KISHI, R., MATSUDA, A., MIURA, T., MATSUMURA, K. & IIO, K. 2009. Fast responsive poly(N, N-diethylacrylamide) hydrogels with interconnected microspheres and bi-continuous structures. *Colloid and Polymer Science*, 287, 505-512.
- KLOUDA, L. & MIKOS, A. G. 2008. Thermoresponsive hydrogels in biomedical applications. *European Journal of Pharmaceutics and Biopharmaceutics*, 68, 34-45.
- KLOXIN, A. M., KLOXIN, C. J., BOWMAN, C. N. & ANSETH, K. S. 2010. Mechanical properties of cellularly responsive hydrogels and their experimental determination. *Advanced Materials*, 22, 3484-3494.
- KOKUFATA, E., ZHANG, Y. Q. & TANAKA, T. 1991. Saccharide-sensitive phase transition of a lectin-loaded gel. *Nature*, 351, 302-304.
- KONDO, S., IWASHITA, M. & YAMAGUCHI, M. 2009. How animals get their skin patterns: Fish pigment pattern as a live Turing wave. *International Journal of Developmental Biology*, 53, 851-856.
- KOOB, T. J. & HERNANDEZ, D. J. 2003. Mechanical and thermal properties of novel polymerized NDGA-gelatin hydrogels. *Biomaterials*, 24, 1285-1292.

- KOST, J., NOECKER, R., KUNICA, E. & LANGER, R. 1985. Magnetically controlled release systems: Effect of polymer composition. *Journal of Biomedical Materials Research*, 19, 935-940.
- KOVACS, K., MCILWAINE, R. E., SCOTT, S. K. & TAYLOR, A. F. 2007. An organic-based pH oscillator. *Journal of Physical Chemistry A*, 111, 549-551.
- KRAEHENBUEHL, T. P., FERREIRA, L. S., ZAMMARETTI, P., HUBBELL, J. A. & LANGER, R. 2009. Cell-responsive hydrogel for encapsulation of vascular cells. *Biomaterials*, 30, 4318-4324.
- KUHN, W., HARGITAY, B., KATCHALSKY, A. & EISENBERG, H. 1950. Reversible dilation and contraction by changing the state of ionization of high-polymer acid networks. *Nature*, 165, 514-516.
- KUKSENOK, O., YASHIN, V. V. & BALAZS, A. C. 2008. Three-dimensional model for chemoresponsive polymer gels undergoing the Belousov-Zhabotinsky reaction. *Physical Review E - Statistical, Nonlinear, and Soft Matter Physics*, 78, 1406-1412.
- KUKSENOK, O., YASHIN, V. V., KINOSHITA, M., SAKAI, T., YOSHIDA, R. & BALAZS, A. C. 2011. Exploiting gradients in cross-link density to control the bending and self-propelled motion of active gels. *Journal of Materials Chemistry*, 21, 8360-8371.
- KUMLER, W. D. 1943. The acid strength of mono and diesters of phosphoric acid. the n-alkyl esters from methyl to butyl, the esters of biological importance, and the natural guanidine phosphoric acids. *Journal of the American Chemical Society*, 2355-2361.
- LABROT, V., DE KEPPEL, P., BOISSONADE, J., SZALAI, I. & GAUFFRE, F. 2005. Wave patterns driven by chemomechanical instabilities in responsive gels. *Journal of Physical Chemistry B*, 109, 21476-21480.
- LAMPRECHT, A., SCHÄFER, U. F. & LEHR, C. M. 2000. Characterization of microcapsules by confocal laser scanning microscopy: Structure, capsule wall composition and encapsulation rate. *European Journal of Pharmaceutics and Biopharmaceutics*, 49, 1-9.
- LEE, E. S., KIM, D., YOUN, Y. S., OH, K. T. & BAE, Y. H. 2008. A virus-mimetic nanogel vehicle. *Angewandte Chemie - International Edition*, 47, 2418-2421.

- LEE, K. Y. & MOONEY, D. J. 2001. Hydrogels for tissue engineering. *Chemical Reviews*, 101, 1869-1879.
- LEVENGOD, S. K. L. & ZHANG, M. 2014. Chitosan-based scaffolds for bone tissue engineering. *Journal of Materials Chemistry B*, 2, 3161-3184.
- LI, L., SHAN, H., YUE, C. Y., LAM, Y. C., TAM, K. C. & HU, X. 2002. Thermally induced association and dissociation of methylcellulose in aqueous solutions. *Langmuir*, 18, 7291-7298.
- LI, P., POON, Y. F., LI, W., ZHU, H. Y., YEAP, S. H., CAO, Y., QI, X., ZHOU, C., LAMRANI, M., BEUERMAN, R. W., KANG, E. T., MU, Y., LI, C. M., CHANG, M. W., JAN LEONG, S. S. & CHAN-PARK, M. B. 2011. A polycationic antimicrobial and biocompatible hydrogel with microbe membrane suctioning ability. *Nature Materials*, 10, 149-156.
- LI, Y. & TANAKA, T. 1990. Kinetics of swelling and shrinking of gels. *The Journal of Chemical Physics*, 92, 1365-1371.
- LI, Y. & TANAKA, T. 1992. Phase transitions of gels. *Annual Review of Materials Science*, 22, 243-277.
- LIECHTY, W. B., KRYSZCIO, D. R., SLAUGHTER, B. V. & PEPPAS, N. A. 2010. Polymers for drug delivery systems. *Annual Review of Chemical and Biomolecular Engineering*, 1, 149-173.
- LIU, Y. Y., SHAO, Y. H. & LÜ, J. 2006. Preparation, properties and controlled release behaviors of pH-induced thermosensitive amphiphilic gels. *Biomaterials*, 27, 4016-4024.
- LU, G., LING, K., ZHAO, P., XU, Z., DENG, C., ZHENG, H., HUANG, J. & CHEN, J. 2010. A novel in situ-formed hydrogel wound dressing by the photocross-linking of a chitosan derivative. *Wound Repair and Regeneration*, 18, 70-79.
- LUO, Y., KIRKER, K. R. & PRESTWICH, G. D. 2000. Cross-linked hyaluronic acid hydrogel films: New biomaterials for drug delivery. *Journal of Controlled Release*, 69, 169-184.
- MABILLEAU, G., BASLÉ, M. F. & CHAPPARD, D. 2006. Evaluation of surface roughness of hydrogels by fractal texture analysis during swelling. *Langmuir*, 22, 4843-4845.
- MAEDA, S., HARA, Y., SAKAI, T., YOSHIDA, R. & HASHIMOTO, S. 2007. Self-walking gel. *Advanced Materials*, 19, 3480-3484.

- MAEDA, S., HARA, Y., YOSHIDA, R. & HASHIMOTO, S. 2008. Peristaltic motion of polymer gels. *Angewandte Chemie - International Edition*, 47, 6690-6693.
- MAITY, G. 2007. Low Molecular Mass Gelators of Organic Liquids. *Journal of Physical Sciences*, 11, 156-171.
- MAITY, I., MUKHERJEE, T. K. & DAS, A. K. 2014. Photophysical study of a  $\pi$ -stacked  $\beta$ -sheet nanofibril forming peptide bolaamphiphile hydrogel. *New Journal of Chemistry*, 38, 376-385.
- MALASHKEVICH, A. V., BRUK, L. G. & TEMKIN, O. N. 1997. New oscillating reaction in catalysis by metal complexes: a mechanism of alkyne oxidative carbonylation. *Journal of Physical Chemistry A*, 101, 9825-9827.
- MALMSTEN, M. 2011. Antimicrobial and antiviral hydrogels. *Soft Matter*, 7, 8725-8736.
- MAMADA, A., TANAKA, T., KUNGWATCHAKUN, D. & IRIE, M. 1990. Photoinduced phase transition of gels. *Macromolecules*, 23, 1517-1519.
- MASUDA, T., HIDAKA, M., MURASE, Y., AKIMOTO, A. M., NAGASE, K., OKANO, T. & YOSHIDA, R. 2013. Self-oscillating polymer brushes. *Angewandte Chemie - International Edition*, 52, 7468-7471.
- MATRICARDI, P., DI MEO, C., COVIELLO, T., HENNINK, W. E. & ALHAIQUE, F. 2013. Interpenetrating polymer networks polysaccharide hydrogels for drug delivery and tissue engineering. *Advanced Drug Delivery Reviews*, 65, 1172-1187.
- MATSUMOTO, A., YAMAMOTO, K., YOSHIDA, R., KATAOKA, K., AOYAGI, T. & MIYAHARA, Y. 2010. A totally synthetic glucose responsive gel operating in physiological aqueous conditions. *Chemical Communications*, 46, 2203-2205.
- MATSUO, E. S. & TANAKA, T. 1988. Kinetics of discontinuous volume-phase transition of gels. *The Journal of Chemical Physics*, 89, 1695-1703.
- MI, F. L. 2005. Synthesis and characterization of a novel chitosan-gelatin bioconjugate with fluorescence emission. *Biomacromolecules*, 6, 975-987.
- MI, F. L., SHYU, S. S. & PENG, C. K. 2005. Characterization of ring-opening polymerization of genipin and pH-dependent cross-linking reactions between chitosan and genipin. *Journal of Polymer Science, Part A: Polymer Chemistry*, 43, 1985-2000.

- MI, F. L., TAN, Y. C., LIANG, H. C., HUANG, R. N. & SUNG, H. W. 2001. In vitro evaluation of a chitosan membrane cross-linked with genipin. *Journal of Biomaterials Science-Polymer Edition*, 12, 835-850.
- MIYATA, T., ASAMI, N. & URAGAMI, T. 1999a. Preparation of an antigen-sensitive hydrogel using antigen-antibody bindings. *Macromolecules*, 32, 2082-2084.
- MIYATA, T., ASAMI, N. & URAGANI, T. 1999b. A reversibly antigen-responsive hydrogel. *Nature*, 399, 766-768.
- MONTEIRO, O. A. C. & AIROLDI, C. 1999. Some studies of crosslinking chitosan-glutaraldehyde interaction in a homogeneous system. *International Journal of Biological Macromolecules*, 26, 119-128.
- MOURA, M. J., FIGUEIREDO, M. M. & GIL, M. H. 2007. Rheological study of genipin cross-linked chitosan hydrogels. *Biomacromolecules*, 8, 3823-3829.
- MUNJERI, O., COLLETT, J. H. & FELL, J. T. 1997. Hydrogel beads based on amidated pectins for colon-specific drug delivery: The role of chitosan in modifying drug release. *Journal of Controlled Release*, 46, 273-278.
- MURASE, Y., MAEDA, S., HASHIMOTO, S. & YOSHIDA, R. 2009. Design of a mass transport surface utilizing peristaltic motion of a self-oscillating gel. *Langmuir*, 25, 483-489.
- MURASE, Y., TAKESHIMA, R. & YOSHIDA, R. 2011. Self-driven gel conveyer: Effect of interactions between loaded cargo and self-oscillating gel surface. *Macromolecular Bioscience*, 11, 1713-1721.
- MUZZARELLI, R. A. A. 2009. Genipin-crosslinked chitosan hydrogels as biomedical and pharmaceutical aids. *Carbohydrate Polymers*, 77, 1-9.
- MÜZZARELLI, R. A. A. 1971. Selective collection of trace metal ions by precipitation of chitosan, and new derivatives of chitosan. *Analytica Chimica Acta*, 54, 133-142.
- MYUNG, D., KOH, W., KO, J., HU, Y., CARRASCO, M., NOOLANDI, J., TA, C. N. & FRANK, C. W. 2007. Biomimetic strain hardening in interpenetrating polymer network hydrogels. *Polymer*, 48, 5376-5387.
- MYUNG, D., WATERS, D., WISEMAN, M., DUHAMEI, P. E., NOOLANDI, J., TA, C. N. & FRANK, C. W. 2008. Progress in the development of interpenetrating polymer network hydrogels. *Polymers for Advanced Technologies*, 19, 647-657.

- NA, Y. H., KUROKAWA, T., KATSUYAMA, Y., TSUKESHIBA, H., GONG, J. P., OSADA, Y., OKABE, S., KARINO, T. & SHIBAYAMA, M. 2004. Structural characteristics of double network gels with extremely high mechanical strength. *Macromolecules*, 37, 5370-5374.
- NA, Y. H., TANAKA, Y., KAWAUCHI, Y., FURUKAWA, H., SUMIYOSHI, T., GONG, J. P. & OSADA, Y. 2006. Necking phenomenon of double-network gels. *Macromolecules*, 39, 4641-4645.
- NAKAJIMA, T., FURUKAWA, H., TANAKA, Y., KUROKAWA, T., OSADA, Y. & GONG, J. P. 2009. True chemical structure of double network hydrogels. *Macromolecules*, 42, 2184-2189.
- NAKAMARU, S., MAEDA, S., HARA, Y. & HASHIMOTO, S. 2009. Control of autonomous swelling-deswelling behavior for a polymer gel. *Journal of Physical Chemistry B*, 113, 4609-4613.
- NAKAMASU, A., TAKAHASHI, G., KANBE, A. & KONDO, S. 2009. Interactions between zebrafish pigment cells responsible for the generation of Turing patterns. *Proceedings of the National Academy of Sciences of the United States of America*, 106, 8429-8434.
- NICHOL, J. W., KOSHY, S. T., BAE, H., HWANG, C. M., YAMANLAR, S. & KHADEMHOSEINI, A. 2010. Cell-laden microengineered gelatin methacrylate hydrogels. *Biomaterials*, 31, 5536-5544.
- NOBUHIKO, Y., TERUO, O. & YASUHISA, S. 1992. Inflammation responsive degradation of crosslinked hyaluronic acid gels. *Journal of Controlled Release*, 22, 105-116.
- NOVAKOVIC, K., GROSJEAN, C., SCOTT, S. K., WHITING, A., WILLIS, M. J. & WRIGHT, A. R. 2007. Achieving pH and Qr oscillations in a palladium-catalysed phenylacetylene oxidative carbonylation reaction using an automated reactor system. *Chemical Physics Letters*, 435, 142-147.
- NOVAKOVIC, K., GROSJEAN, C., SCOTT, S. K., WHITING, A., WILLIS, M. J. & WRIGHT, A. R. 2008. The influence of oscillations on product selectivity during the palladium-catalysed phenylacetylene oxidative carbonylation reaction. *Physical Chemistry Chemical Physics*, 10, 749-753.
- NOVAKOVIC, K., MUKHERJEE, A., WILLIS, M., WRIGHT, A. & SCOTT, S. 2009. The influence of reaction temperature on the oscillatory behaviour

- in the palladium-catalysed phenylacetylene oxidative carbonylation reaction. *Physical Chemistry Chemical Physics*, 11, 9044-9049.
- NOVAKOVIC, K. & PARKER, J. 2011. Catalyst initiation in the oscillatory carbonylation reaction. *International Journal of Chemical Engineering*.
- NOYES, R. M. & FURROW, S. D. 1982. The oscillatory Briggs-Rauscher reaction. 3. A skeleton mechanism for oscillations. *Journal of the American Chemical Society*, 104, 45-48.
- NUGENT, M. J. D. & HIGGINBOTHAM, C. L. 2006. Investigation of the influence of freeze-thaw processing on the properties of polyvinyl alcohol/polyacrylic acid complexes. *Journal of Materials Science*, 41, 2393-2404.
- NWOSU, C. J. 2013. *How smart are intelligent hydrogels?* , Newcastle University MSc Thesis.
- OHMINE, I. & TANAKA, T. 1982. Salt effects on the phase transition of ionic gels. *The Journal of Chemical Physics*, 77, 5725-5729.
- OKAZAKI, N., RÁBAI, G. & HANAZAKI, I. 1999. Discovery of novel bromate-sulfite pH oscillators with Mn<sup>2+</sup> or MnO<sub>4</sub><sup>-</sup> as a negative-feedback species. *Journal of Physical Chemistry A*, 103, 10915-10920.
- OYAMA, H. T., TANG, W. T. & FRANK, C. W. 1987. Complex formation between poly(acrylic acid) and pyrene-labeled poly(ethylene glycol) in aqueous solution. *Macromolecules*, 20, 474-480.
- OYEN, M. L. 2014. Mechanical characterisation of hydrogel materials. *International Materials Reviews*, 59, 44-59.
- ÖZYÜREK, C., ÇAYKARA, T., KANTOĞLU, O. & GÜVEN, O. 2000. Characterization of network structure of poly(N-vinyl 2-pyrrolidone/acrylic acid) polyelectrolyte hydrogels by swelling measurements. *Journal of Polymer Science, Part B: Polymer Physics*, 38, 3309-3317.
- PADDOCK, S. W. 2000. Principles and practices of laser scanning confocal microscopy. *Applied Biochemistry and Biotechnology - Part B Molecular Biotechnology*, 16, 127-149.
- PADDOCK, S. W. & ELICEIRI, K. W. 2014. Laser scanning confocal microscopy: History, applications, and related optical sectioning techniques. *Methods in Molecular Biology*.
- PARK, J. Y., OH, H. J., KIM, D. J., BAEK, J. Y. & LEE, S. H. 2006. A polymeric microfluidic valve employing a pH-responsive hydrogel microsphere as

- an actuating source. *Journal of Micromechanics and Microengineering*, 16, 656-663.
- PARKER, J. & NOVAKOVIC, K. 2013. Influence of water and the reactant addition sequence on palladium(II) iodide-catalyzed phenylacetylene carbonylation. *Industrial and Engineering Chemistry Research*, 52, 2520-2527.
- PATEL, V. R. & AMIJI, M. M. 1996. Preparation and characterization of freeze-dried chitosan-poly(ethylene oxide) hydrogels for site-specific antibiotic delivery in the stomach. *Pharmaceutical Research*, 13, 588-593.
- PAVLUKHINA, S., LU, Y., PATIMETHA, A., LIBERA, M. & SUKHISHVILI, S. 2010. Polymer multilayers with pH-triggered release of antibacterial agents. *Biomacromolecules*, 11, 3448-3456.
- PAWLEY, J. B. 2006. Points, pixels, and gray levels: Digitizing image data. *Handbook of Biological Confocal Microscopy: Third Edition*.
- PEPPAS, N. A., BURES, P., LEOBANDUNG, W. & ICHIKAWA, H. 2000. Hydrogels in pharmaceutical formulations. *European Journal of Pharmaceutics and Biopharmaceutics*, 50, 27-46.
- PLIEVA, F. M., GALAEV, I. Y., NOPPE, W. & MATTIASSON, B. 2008. Cryogel applications in microbiology. *Trends in Microbiology*, 16, 543-551.
- PRIGOGINE, I. & LEFEVER, R. 1968. Symmetry breaking instabilities in dissipative systems. II. *The Journal of Chemical Physics*, 48, 1695-1700.
- PRIGOGINE, I. & NICOLIS, G. 1967. On symmetry-breaking instabilities in dissipative systems. *The Journal of Chemical Physics*, 46, 3542-3550.
- PROCTER, H. R. & WILSON, J. A. 1916. XXXV. - The acid-gelatin equilibrium. *Journal of the Chemical Society, Transactions*, 109, 307-319.
- QIU, Y. & PARK, K. 2001. Environment-sensitive hydrogels for drug delivery. *Advanced Drug Delivery Reviews*, 53, 321-339.
- QU, X., WIRSÉN, A. & ALBERTSSON, A. C. 1999. Structural change and swelling mechanism of pH-sensitive hydrogels based on chitosan and D,L-lactic acid. *Journal of Applied Polymer Science*, 74, 3186-3192.
- QUINTANAR-GUERRERO, D., GANEM-QUINTANAR, A., NAVA-ARZALUZ, M. G. & PIÑÓN-SEGUNDO, E. 2009. Silica xerogels as pharmaceutical drug carriers. *Expert Opinion on Drug Delivery*, 6, 485-498.

- RABEA, E. I., BADAWEY, M. E. T., STEVENS, C. V., SMAGGHE, G. & STEURBAUT, W. 2003. Chitosan as antimicrobial agent: Applications and mode of action. *Biomacromolecules*, 4, 1457-1465.
- RACCIS, R., ROSKAMP, R., HOPP, I., MENGES, B., KOYNOV, K., JONAS, U., KNOLL, W., BUTT, H. J. & FYTAS, G. 2011. Probing mobility and structural inhomogeneities in grafted hydrogel films by fluorescence correlation spectroscopy. *Soft Matter*, 7, 7042-7053.
- RANJHA, N. M., AYUB, G., NASEEM, S. & ANSARI, M. T. 2010. Preparation and characterization of hybrid pH-sensitive hydrogels of chitosan-co-acrylic acid for controlled release of verapamil. *Journal of Materials Science: Materials in Medicine*, 21, 2805-2816.
- RATNER, B. D. & HOFFMAN, A. S. 1976. Synthetic hydrogels for biomedical applications. *Acs Symposium Series*, 1-36.
- REHFELDT, S. & STICHLMAIR, J. 2007. Measurement and calculation of multicomponent diffusion coefficients in liquids. *Fluid Phase Equilibria*, 256, 99-104.
- RICHTER, A., PASCHEW, G., KLATT, S., LIENIG, J., ARNDT, K. F. & ADLER, H. J. P. 2008. Review on hydrogel-based pH sensors and microsensors. *Sensors*, 8, 561-581.
- RIČKA, J. & TANAKA, T. 1984. Swelling of ionic gels: Quantitative performance of the Donnan theory. *Macromolecules*, 17, 2916-2921.
- RISBUD, M. V., HARDIKAR, A. A., BHAT, S. V. & BHONDE, R. R. 2000. pH-sensitive freeze-dried chitosan-polyvinyl pyrrolidone hydrogels as controlled release system for antibiotic delivery. *Journal of Controlled Release*, 68, 23-30.
- RODRIGUES, F. H. A., PEREIRA, A. G. B., FAJARDO, A. R. & MUNIZ, E. C. 2013. Synthesis and characterization of chitosan-graft-poly(acrylic acid)/nontronite hydrogel composites based on a design of experiments. *Journal of Applied Polymer Science*, 128, 3480-3489.
- ROMN, J., CABÃAS, M. V., PĚA, J. & VALLET-REGÍ, M. 2011. Control of the pore architecture in three-dimensional hydroxyapatite-reinforced hydrogel scaffolds. *Science and Technology of Advanced Materials*, 12.
- ROQUE, A. I., SOLIAKOV, A., BIRCH, M. A., PHILIPS, S. R., SHAH, D. S. H. & LAKEY, J. H. 2014. Reversible non-stick behaviour of a bacterial protein

- polymer provides a tuneable molecular mimic for cell and tissue engineering. *Advanced Materials*, 26, 2704-2709.
- RYAN, A. J., CROOK, C. J., HOWSE, J. R., TOPHAM, P., GEOGHEGAN, M., MARTIN, S. J., PARNELL, A. J., RUIZ-PÉREZ, L. & JONES, R. A. L. 2005a. Mechanical actuation by responsive polyelectrolyte brushes and triblock gels. *Journal of Macromolecular Science - Physics*, 44 B, 1103-1121.
- RYAN, A. J., CROOK, C. J., HOWSE, J. R., TOPHAM, P., JONES, R. A. L., GEOGHEGAN, M., PARNELL, A. J., RUIZ-PÉREZ, L., MARTIN, S. J., CADBY, A., MENELLE, A., WEBSTER, J. R. P., GLEESON, A. J. & BRAS, W. 2005b. Responsive brushes and gels as components of soft nanotechnology. *Faraday Discussions*, 128, 55-74.
- SAKURAI, K., MAEGAWA, T. & TAKAHASHI, T. 2000. Glass transition temperature of chitosan and miscibility of chitosan/poly(N-vinyl pyrrolidone) blends. *Polymer*, 41, 7051-7056.
- SALLACH, R. E., CUI, W., WEN, J., MARTINEZ, A., CONTICELLO, V. P. & CHAIKOF, E. L. 2009. Elastin-mimetic protein polymers capable of physical and chemical crosslinking. *Biomaterials*, 30, 409-422.
- SCHWAEBEL, T., TRAPP, O. & BUNZ, U. H. F. 2013. Digital photography for the analysis of fluorescence responses. *Chemical Science*, 4, 273-281.
- SEHAQUI, H., SALAJKOVÁ, M., ZHOU, Q. & BERGLUND, L. A. 2010. Mechanical performance tailoring of tough ultra-high porosity foams prepared from cellulose i nanofiber suspensions. *Soft Matter*, 6, 1824-1832.
- SEHAQUI, H., ZHOU, Q. & BERGLUND, L. A. 2011. High-porosity aerogels of high specific surface area prepared from nanofibrillated cellulose (NFC). *Composites Science and Technology*, 71, 1593-1599.
- SELBY, A., MALDONADO-CODINA, C. & DERBY, B. 2014. Influence of specimen thickness on the nanoindentation of hydrogels: Measuring the mechanical properties of soft contact lenses. *Journal of the Mechanical Behavior of Biomedical Materials*, 35, 144-156.
- SERSHEN, S. & WEST, J. 2002. Implantable, polymeric systems for modulated drug delivery. *Advanced Drug Delivery Reviews*, 54, 1225-1235.

- SHAWKY, H. A., EL-SAYED, M. H., EL-HAG ALI, A. & ABDEL MOTTALEB, M. S. 2006. Treatment of polluted water resources using reactive polymeric hydrogel. *Journal of Applied Polymer Science*, 100, 3966-3973.
- SHEN, D., WAN, C. & GAO, S. 2010. Molecular weight effects on gelation and rheological properties of konjac glucomannan-xanthan mixtures. *Journal of Polymer Science, Part B: Polymer Physics*, 48, 313-321.
- SHIBAYAMA, M., TANAKA, T. & HAN, C. C. 1992. Small-angle neutron scattering study on weakly charged temperature sensitive polymer gels. *The Journal of Chemical Physics*, 97, 6842-6854.
- SHIGA, T., HIROSE, Y., OKADA, A. & KURAUCHI, T. 1992. Electric field-associated deformation of polyelectrolyte gel near a phase transition point. *Journal of Applied Polymer Science*, 46, 635-640.
- SHINOHARA, S. I., SEKI, T., SAKAI, T., YOSHIDA, R. & TAKEOKA, Y. 2008. Photoregulated wormlike motion of a gel. *Angewandte Chemie - International Edition*, 47, 9039-9043.
- SHIRAKI, Y. & YOSHIDA, R. 2012. Autonomous intestine-like motion of tubular self-oscillating gel. *Angewandte Chemie - International Edition*, 51, 6112-6116.
- SIDORENKO, A., KRUPENKIN, T., TAYLOR, A., FRATZL, P. & AIZENBERG, J. 2007. Reversible switching of hydrogel-actuated nanostructures into complex micropatterns. *Science*, 315, 487-490.
- SILVER, L. L. & BOSTIAN, K. A. 1993. Discovery and development of new antibiotics: The problem of antibiotic resistance. *Antimicrobial Agents and Chemotherapy*, 37, 377-383.
- SINGH, A., NARVI, S. S., DUTTA, P. K. & PANDEY, N. D. 2006. External stimuli response on a novel chitosan hydrogel crosslinked with formaldehyde. *Bulletin of Materials Science*, 29, 233-238.
- SKOURI, R., SCHOSSELER, F., MUNCH, J. P. & CANDAU, S. J. 1995. Swelling and elastic properties of polyelectrolyte gels. *Macromolecules*, 28, 197-210.
- SOGIAS, I. A., WILLIAMS, A. C. & KHUTORYANSKIY, V. V. 2008. Why is chitosan mucoadhesive? *Biomacromolecules*, 9, 1837-1842.
- SONG, J. J. & OTT, H. C. 2011. Organ engineering based on decellularized matrix scaffolds. *Trends in Molecular Medicine*, 17, 424-432.

- STANOJEVIĆ, M., KRUŠIĆ, M. K., FILIPOVIĆ, J., PAROJČIĆ, J. & STUPAR, M. 2006. An investigation into the influence of hydrogel composition on swelling behavior and drug release from poly(acrylamide-co-itaconic acid) hydrogels in various media. *Drug Delivery: Journal of Delivery and Targeting of Therapeutic Agents*, 13, 1-7.
- STRANGE, D. G. T. & OYEN, M. L. 2012. Composite hydrogels for nucleus pulposus tissue engineering. *Journal of the Mechanical Behavior of Biomedical Materials*, 11, 16-26.
- SUKNUNTHA, K., TANTISHAIYAKUL, V., WORAKUL, N. & TAWEEPRED, W. 2011. Characterization of muco- and bioadhesive properties of chitosan, PVP, and chitosan/PVP blends and release of amoxicillin from alginate beads coated with chitosan/PVP. *Drug Development and Industrial Pharmacy*, 37, 408-418.
- SUNG, H. W., HUANG, R. N., HUANG, L. L. H. & TSAI, C. C. 1999. In vitro evaluation of cytotoxicity of a naturally occurring cross-linking reagent for biological tissue fixation. *Journal of Biomaterials Science-Polymer Edition*, 10, 63-78.
- SUZUKI, A. & TANAKA, T. 1990. Phase transition in polymer gels induced by visible light. *Nature*, 346, 345-347.
- SUZUKI, D., TANIGUCHI, H. & YOSHIDA, R. 2009. Autonomously oscillating viscosity in microgel dispersions. *Journal of the American Chemical Society*, 131, 12058-12059.
- SWANN, J. M. G., BRAS, W., HOWSE, J. R., TOPHAM, P. D. & RYAN, A. J. 2010. Quantifying hydrogel response using laser light scattering. *Soft Matter*, 6, 743-749.
- TABATA, O., HIRASAWA, H., AOKI, S., YOSHIDA, R. & KOKUFUTA, E. 2002. Ciliary motion actuator using self-oscillating gel. *Sensors and Actuators, A: Physical*, 95, 234-238.
- TANAKA, T. 1978. Collapse of gels and the critical endpoint. *Physical Review Letters*, 40, 820-823.
- TANAKA, T. 1979. Phase transitions in gels and a single polymer. *Polymer*, 20, 1404-1412.
- TANAKA, T., FILLMORE, D., SUN, S. T., NISHIO, I., SWISLOW, G. & SHAH, A. 1980. Phase Transitions in Ionic Gels. *Physical Review Letters*, 45, 1636-1639.

- TANAKA, T. & FILLMORE, D. J. 1979. Kinetics of swelling of gels. *The Journal of Chemical Physics*, 70, 1214-1218.
- TANAKA, T., NISHIO, I., SUN, S. T. & UENO-NISHIO, S. 1982. Collapse of gels in an electric field. *Science*, 218, 467-469.
- TANAKA, Y., KUWABARA, R., NA, Y. H., KUROKAWA, T., GONG, J. P. & OSADA, Y. 2005. Determination of fracture energy of high strength double network hydrogels. *Journal of Physical Chemistry B*, 109, 11559-11562.
- TOKAREV, I. & MINKO, S. 2009. Stimuli-responsive hydrogel thin films. *Soft Matter*, 5, 511-524.
- TOLAIMATE, A., DESBRIÈRES, J., RHAZI, M., ALAGUI, A., VINCENDON, M. & VOTTERO, P. 2000. On the influence of deacetylation process on the physicochemical characteristics of chitosan from squid chitin. *Polymer*, 41, 2463-2469.
- TOPHAM, P. D., GLIDLE, A., TOOLAN, D. T. W., WEIR, M. P., SKODA, M. W. A., BARKER, R. & HOWSE, J. R. 2013. The relationship between charge density and polyelectrolyte brush profile using simultaneous neutron reflectivity and in situ attenuated total internal reflection FTIR. *Langmuir*, 29, 6068-6076.
- TOPHAM, P. D., HOWSE, J. R., CROOK, C. J., ARMES, S. P., JONES, R. A. L. & RYAN, A. J. 2007a. Antagonistic triblock polymer gels powered by pH oscillations. *Macromolecules*, 40, 4393-4395.
- TOPHAM, P. D., HOWSE, J. R., CROOK, C. J., GLEESON, A. J., BRAS, W., ARMES, S. P., JONES, R. A. L. & RYAN, A. J. 2007b. Autonomous volume transitions of a polybase triblock copolymer gel in a chemically driven pH-oscillator. *Macromolecular Symposia*, 256, 95-104.
- TOPHAM, P. D., HOWSE, J. R., FERNYHOUGH, C. M. & RYAN, A. J. 2007c. The performance of poly(styrene)-block-poly(2-vinyl pyridine)-block-poly(styrene) triblock copolymers as pH-driven actuators. *Soft Matter*, 3, 1506-1512.
- TRAITEL, T., COHEN, Y. & KOST, J. 2000. Characterization of glucose-sensitive insulin release systems in simulated in vivo conditions. *Biomaterials*, 21, 1679-1687.

- TRAITEL, T., GOLDBART, R. & KOST, J. 2008. Smart polymers for responsive drug-delivery systems. *Journal of Biomaterials Science, Polymer Edition*, 19, 755-767.
- TRIEU, H. H. & QUTUBUDDIN, S. 1994. Polyvinyl alcohol hydrogels I. Microscopic structure by freeze-etching and critical point drying techniques. *Colloid & Polymer Science*, 272, 301-309.
- TSUKESHIBA, H., HUANG, M., NA, Y. H., KUROKAWA, T., KUWABARA, R., TANAKA, Y., FURUKAWA, H., OSADA, Y. & GONG, J. P. 2005. Effect of polymer entanglement on the toughening of double network hydrogels. *Journal of Physical Chemistry B*, 109, 16304-16309.
- TURING, A. M. 1952. The chemical basis of morphogenesis. *Philosophical Transactions*, 237B, 37-72.
- UEKI, T., TAKASAKI, Y., BUNDO, K., UENO, T., SAKAI, T., AKAGI, Y. & YOSHIDA, R. 2014. Autonomous viscosity oscillation via metallo-supramolecular terpyridine chemistry of branched poly(ethylene glycol) driven by the Belousov-Zhabotinsky reaction. *Soft Matter*, 10, 1349-1355.
- UENO, T., BUNDO, K., AKAGI, Y., SAKAI, T. & YOSHIDA, R. 2010. Autonomous viscosity oscillation by reversible complex formation of terpyridine-terminated poly(ethylene glycol) in the BZ reaction. *Soft Matter*, 6, 6072-6074.
- VAN DER LINDEN, H. J., HERBER, S., OLTHUIS, W. & BERGVELD, P. 2003. Stimulus-sensitive hydrogels and their applications in chemical (micro)analysis. *Analyst*, 128, 325-331.
- VANBLARCOM, D. S. & PEPPAS, N. A. 2011. Microcantilever sensing arrays from biodegradable, pH-responsive hydrogels. *Biomedical Microdevices*, 13, 829-836.
- VASHIST, A., VASHIST, A., GUPTA, Y. K. & AHMAD, S. 2014. Recent advances in hydrogel based drug delivery systems for the human body. *Journal of Materials Chemistry B*, 2, 147-166.
- VÁZQUEZ, B., SAN ROMAN, J., PENICHE, C. & COHEN, M. E. 1997. Polymeric hydrophilic hydrogels with flexible hydrophobic chains. Control of the hydration and interactions with water molecules. *Macromolecules*, 30, 8440-8446.
- VINTILOIU, A. & LEROUX, J. C. 2008. Organogels and their use in drug delivery - A review. *Journal of Controlled Release*, 125, 179-192.

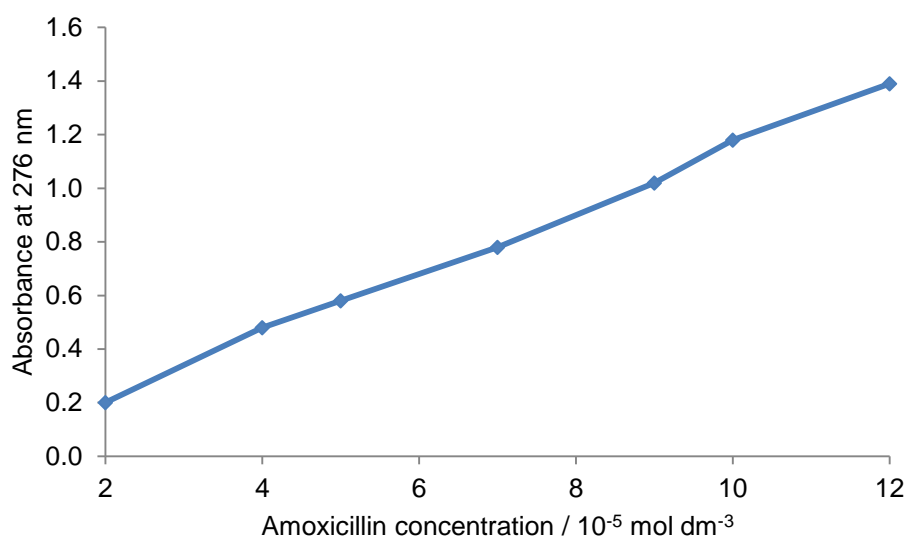
- WAN NGAH, W. S., ENDUD, C. S. & MAYANAR, R. 2002. Removal of copper(II) ions from aqueous solution onto chitosan and cross-linked chitosan beads. *Reactive and Functional Polymers*, 50, 181-190.
- WANG, B. & WASIELEWSKI, M. R. 1997. Design and synthesis of metal ion-recognition-induced conjugated polymers: An approach to metal ion sensory materials. *Journal of the American Chemical Society*, 119, 12-21.
- WANG, K. L., BURBAN, J. H. & CUSSLER, E. L. 1993. Hydrogels as separation agents. *Advances in Polymer Science*, 110, 66-79.
- WANG, Q. & LI, L. 2005. Effects of molecular weight on thermoreversible gelation and gel elasticity of methylcellulose in aqueous solution. *Carbohydrate Polymers*, 62, 232-238.
- WATERS, J. C. 2009. Accuracy and precision in quantitative fluorescence microscopy. *Journal of Cell Biology*, 185, 1135-1148.
- WEBBER, R. E., CRETON, C., BROWN, H. R. & GONG, J. P. 2007. Large strain hysteresis and mullins effect of tough double-network hydrogels. *Macromolecules*, 40, 2919-2927.
- WICHTERLE, O. & LÍM, D. 1960. Hydrophilic Gels for Biological Use. *Nature*, 185, 117-118.
- WILSON, M. K., K.; SMITH, G.; SIMMONS, M.; RAGUSE, B. 2004. *Nanotechnology: Basic Science and Emerging Technologies*, University of New South Wales Press Ltd.
- WINFREE, A. T. 1984. The prehistory of the Belousov-Zhabotinsky oscillator. *Journal of Chemical Education*, 61, 661-663.
- WOERLY, S., FORT, S., PIGNOT-PAINTRAND, I., COTTET, C., CARCENAC, C. & SAVASTA, M. 2008. Development of a sialic acid-containing hydrogel of poly[N-(2-hydroxypropyl) methacrylamide]: Characterization and implantation study. *Biomacromolecules*, 9, 2329-2337.
- WU, Q. X., LIN, D. Q. & YAO, S. J. 2014. Design of chitosan and its water soluble derivatives-based drug carriers with polyelectrolyte complexes. *Marine Drugs*, 12, 6236-6253.
- XUE, W. & HAMLEY, I. W. 2002. Thermoreversible swelling behaviour of hydrogels based on N-isopropylacrylamide with a hydrophobic comonomer. *Polymer*, 43, 3069-3077.

- YAMAMOTO, T. & YOSHIDA, R. 2013. Self-oscillation of polymer and photo-regulation by introducing photochromic site to induce LCST changes. *Reactive and Functional Polymers*, 73, 945-950.
- YAN, C. & POCHAN, D. J. 2010. Rheological properties of peptide-based hydrogels for biomedical and other applications. *Chemical Society Reviews*, 39, 3528-3540.
- YASHIN, V. V., KUKSENOK, O. & BALAZS, A. C. 2010. Modeling autonomously oscillating chemo-responsive gels. *Progress in Polymer Science (Oxford)*, 35, 155-173.
- YEONG, W. Y., CHUA, C. K., LEONG, K. F., CHANDRASEKARAN, M. & LEE, M. W. 2007. Comparison of drying methods in the fabrication of collagen scaffold via indirect rapid prototyping. *Journal of Biomedical Materials Research - Part B Applied Biomaterials*, 82, 260-266.
- YIN, X., HOFFMAN, A. S. & STAYTON, P. S. 2006. Poly(N-isopropylacrylamide-co-propylacrylic acid) copolymers that respond sharply to temperature and pH. *Biomacromolecules*, 7, 1381-1385.
- YOKOYAMA, F., MASADA, I., SHIMAMURA, K., IKAWA, T. & MONOBE, K. 1986. Morphology and structure of highly elastic poly(vinyl alcohol) hydrogel prepared by repeated freezing-and-melting. *Colloid & Polymer Science*, 264, 595-601.
- YOSHIDA, R. 2010. Self-oscillating gels driven by the belousov-zhabotinsky reaction as novel smart materials. *Advanced Materials*, 22, 3463-3483.
- YOSHIDA, R. 2011. Self-oscillating polymer gel as novel biomimetic materials exhibiting spatiotemporal structure. *Colloid and Polymer Science*, 289, 475-487.
- YOSHIDA, R., SAKAI, T., HARA, Y., MAEDA, S., HASHIMOTO, S., SUZUKI, D. & MURASE, Y. 2009. Self-oscillating gel as novel biomimetic materials. *Journal of Controlled Release*, 140, 186-193.
- YOSHIDA, R., SAKAI, T., TAMBATA, O. & YAMAGUCHI, T. 2002. Design of novel biomimetic polymer gels with self-oscillating function. *Science and Technology of Advanced Materials*, 3, 95-102.
- YOSHIDA, R., TAKAHASHI, T., YAMAGUCHI, T. & ICHIJO, H. 1996. Self-oscillating gel. *Journal of the American Chemical Society*, 118, 5134-5135.

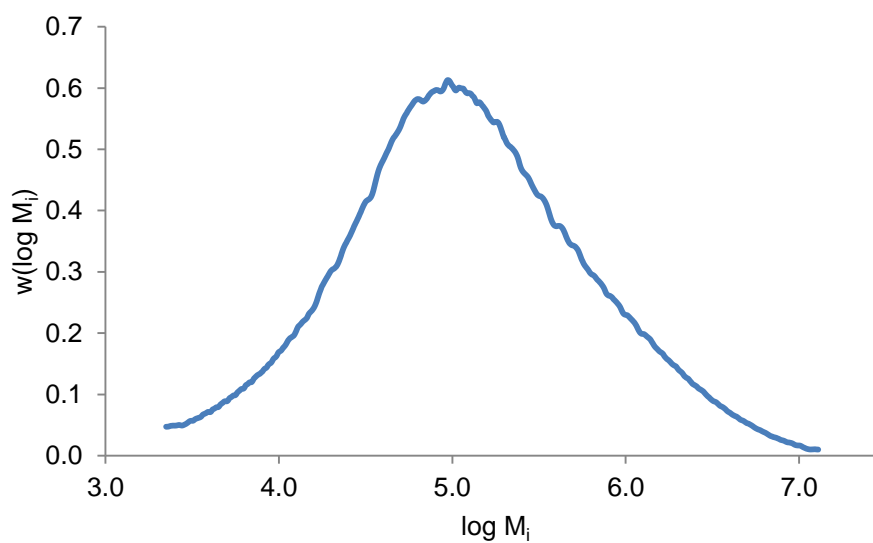
- YOSHIDA, R., TAKEI, K. & YAMAGUCHI, T. 2003. Self-beating motion of gels and modulation of oscillation rhythm synchronized with organic acid. *Macromolecules*, 36, 1759-1761.
- YOSHIDA, R., TANAKA, M., ONODERA, S., YAMAGUCHI, T. & KOKUFUTA, E. 2000. In-phase synchronization of chemical and mechanical oscillations in self-oscillating gels. *Journal of Physical Chemistry A*, 104, 7549-7555.
- YOSHIDA, R., UCHIDA, K., KANEKO, Y., SAKAI, K., KIKUCHI, A., SAKURAI, Y. & OKANO, T. 1995. Comb-type grafted hydrogels with rapid deswelling response to temperature changes. *Nature*, 374, 240-242.
- YUSEN, R. D., CHRISTIE, J. D., EDWARDS, L. B., KUCHERYAVAYA, A. Y., BENDEN, C., DIPCHAND, A. I., DOBBELS, F., KIRK, R., LUND, L. H., RAHMEL, A. O. & STEHLIK, J. 2013. The registry of the international society for heart and lung transplantation: Thirtieth adult lung and heart-lung transplant report - 2013; Focus theme: Age. *Journal of Heart and Lung Transplantation*, 32, 965-978.
- ZAIKIN, A. N. & ZHABOTINSKY, A. M. 1970. Concentration wave propagation in two-dimensional liquid-phase self-oscillating system. *Nature*, 225, 535-537.
- ZENG, M. F., FANG, Z. P. & XU, C. W. 2004. Effect of compatibility on the structure of the microporous membrane prepared by selective dissolution of chitosan/synthetic polymer blend membrane. *Journal of Membrane Science*, 230, 175-181.
- ZHANG, H., MARDYANI, S., CHAN, W. C. W. & KUMACHEVA, E. 2006. Design of biocompatible chitosan microgels for targeted pH-mediated intracellular release of cancer therapeutics. *Biomacromolecules*, 7, 1568-1572.
- ZHANG, R., TANG, M., BOWYER, A., EISENTHAL, R. & HUBBLE, J. 2005. A novel pH- and ionic-strength-sensitive carboxy methyl dextran hydrogel. *Biomaterials*, 26, 4677-4683.
- ZHANG, X., DAVIES, G. A. O. & HITCHINGS, D. 1999. Impact damage with compressive preload and post-impact compression of carbon composite plates. *International Journal of Impact Engineering*, 22, 485-509.
- ZHANG, X. Z., WU, D. Q. & CHU, C. C. 2004. Synthesis, characterization and controlled drug release of thermosensitive IPN-PNIPAAm hydrogels. *Biomaterials*, 25, 3793-3805.

- ZHANG, Y. & CHU, C. C. 2002. Thermal and mechanical properties of biodegradable hydrophilic-hydrophobic hydrogels based on dextran and poly (lactic acid). *Journal of Materials Science: Materials in Medicine*, 13, 773-781.
- ZHANG, Y., LI, N., DELGADO, J., ZHOU, N., YOSHIDA, R., FRADEN, S., EPSTEIN, I. R. & XU, B. 2012. Structural modulation of self-oscillating gels: Changing the proximity of the catalyst to the polymer backbone to tailor chemomechanical oscillation. *Soft Matter*, 8, 7056-7061.
- ZHANG, Y. Q., TANAKA, T. & SHIBAYAMA, M. 1992. Super-absorbency and phase transition of gels in physiological salt solutions. *Nature*, 360, 142-144.
- ZRÍNYI, M. 2000. Intelligent polymer gels controlled by magnetic fields. *Colloid and Polymer Science*, 278, 98-103.
- ZUIDEMA, J. M., RIVET, C. J., GILBERT, R. J. & MORRISON, F. A. 2014. A protocol for rheological characterization of hydrogels for tissue engineering strategies. *Journal of Biomedical Materials Research - Part B Applied Biomaterials*, 102, 1063-1073.

## Appendix



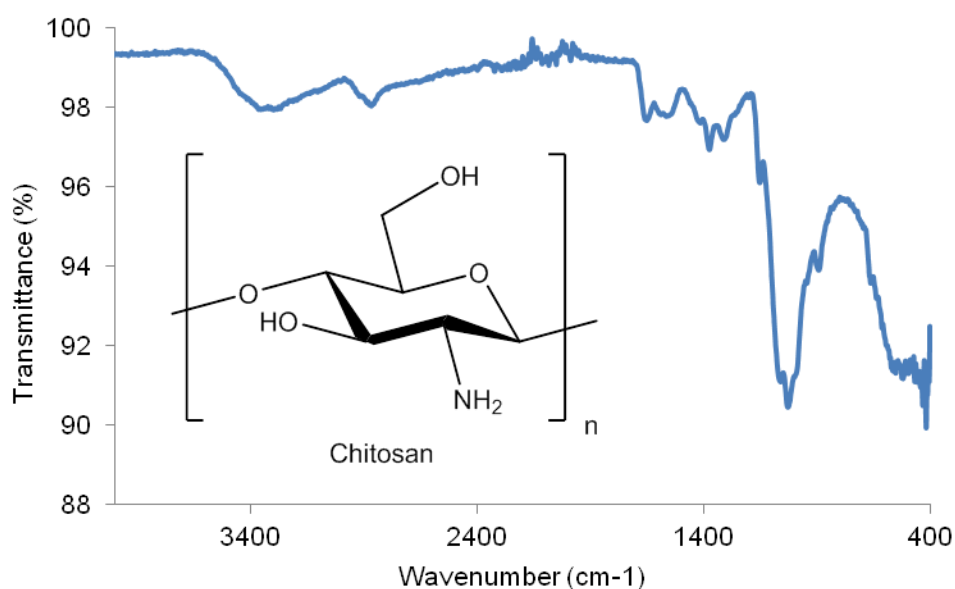
**Figure A1** Calibration of amoxicillin in distilled water measured using UV-Vis spectroscopy



**Figure A2** Molar mass distribution of a sample of chitosan (0.1% (w/v)).

**Table A1** Molecular mass data of a sample of chitosan (0.1% (w/v)).

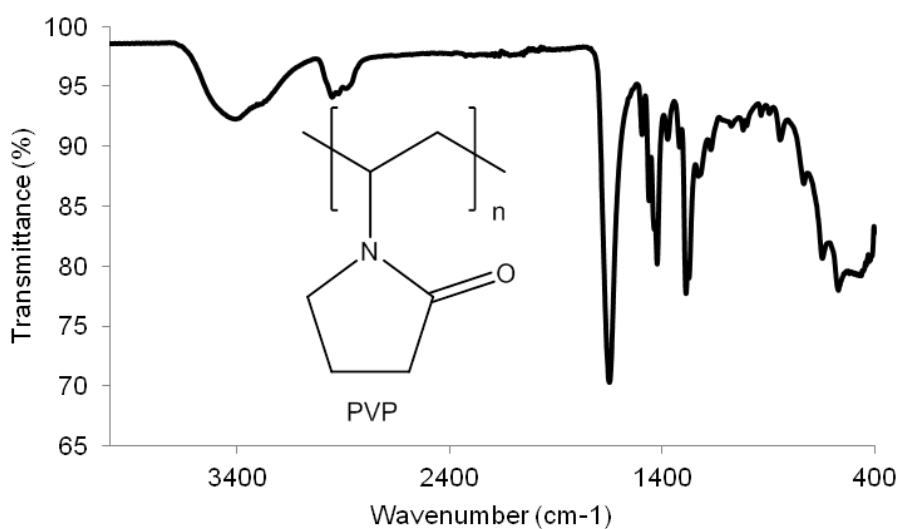
$M_n$ ( $\text{gmol}^{-1}$ )	30755
$M_w$ ( $\text{gmol}^{-1}$ )	428180
$M_z$ ( $\text{gmol}^{-1}$ )	2739568
$M_v$ ( $\text{gmol}^{-1}$ )	428120
$M_w/M_n$	13.922



**Figure A3** Chemical structure and FTIR spectrum of chitosan.

**Table A2** Spectral assignment following FTIR of chitosan.

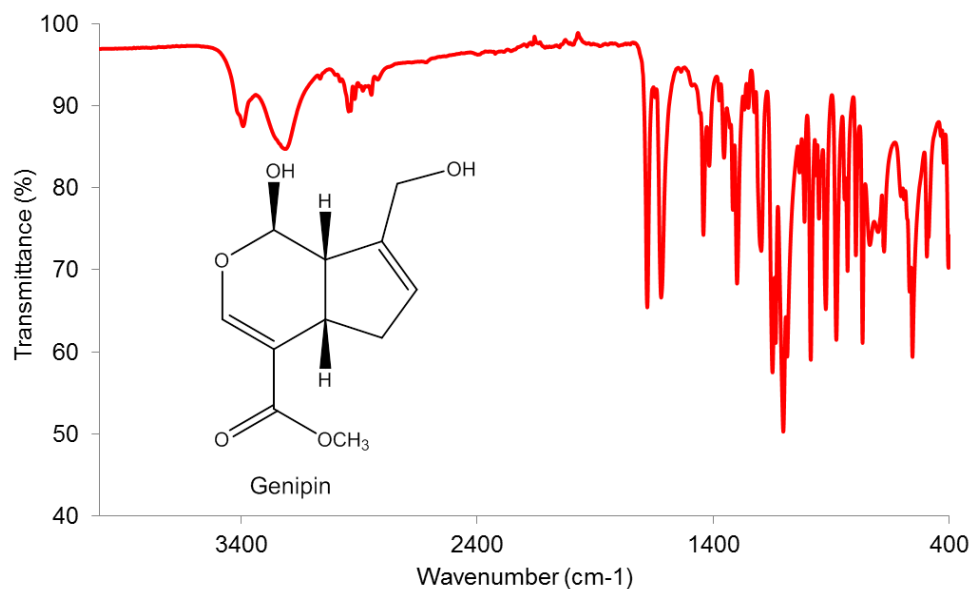
Peak (cm <sup>-1</sup> )	Assignment
3600-3000	O-H stretches overlapped with the symmetric N-H stretches
2920	Antisymmetric C-H stretches
2875	Symmetric C-H stretches
1636	N-H bend
1420/1375	C-H bending
1306	Symmetric C-H stretch of CH <sub>3</sub> group on deacetylated repeat units
1139/1068/1028	C-O-C stretches
877	Wagging of chitosan chain



**Figure A4** Chemical structure and FTIR spectrum of PVP.

**Table A3** Spectral assignment following FTIR of PVP.

Peak (cm <sup>-1</sup> )	Assignment
3600-3000	O-H stretches due to hydrogen bonding
2952	Antisymmetric C-H stretches
2870	Symmetric C-H stretches
1644	C=O of amide
1493/1461/1422/1373	C-H bending of cyclic ring
1287/1267	C-N stretch

**Figure A5** Chemical structure and FTIR spectrum of genipin.**Table A4** Spectral assignment following FTIR of genipin.

Peak (cm <sup>-1</sup> )	Assignment
3400-3000	O-H stretches
2945	Antisymmetric C-H stretches
2880	Symmetric C-H stretches
1680	-C=C- stretch
1621	C-C stretch from cycloolefin
1441	C-H bend
1356	C-H rock
1300/1151/1104	C-O stretch from ester/alcohol

The FTIR spectrum of citric acid is depicted in Figure A6. Notable peaks include a broad O-H stretch at 3400-3000  $\text{cm}^{-1}$  accompanied by a sharp C=O stretch at 1760-1690  $\text{cm}^{-1}$  due to the presence of a carboxyl group.

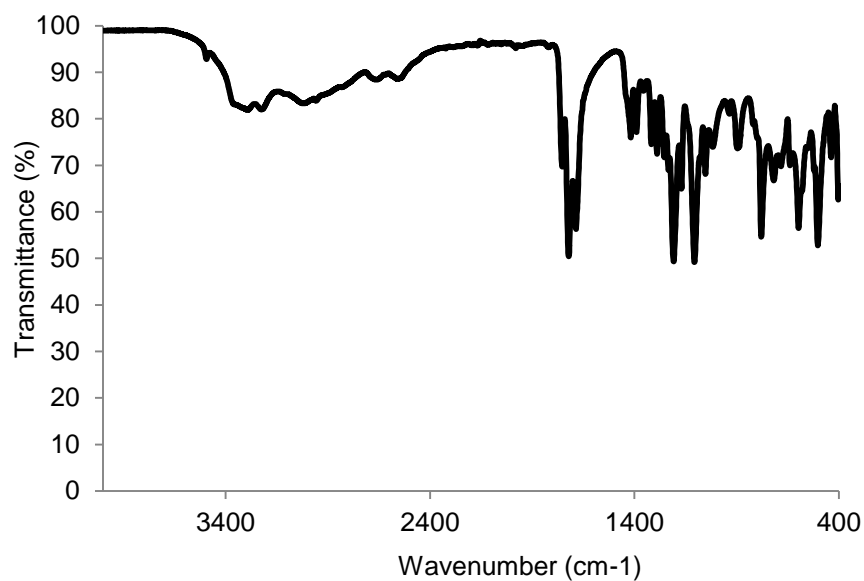


**Figure A6** FTIR spectrum of citric acid.

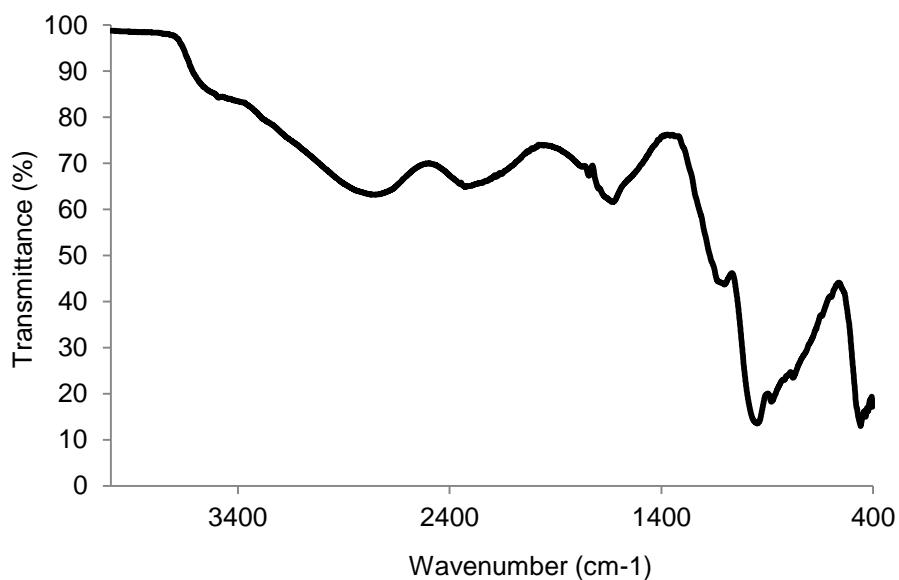


**Figure A7** FTIR spectrum of phosphoric acid.

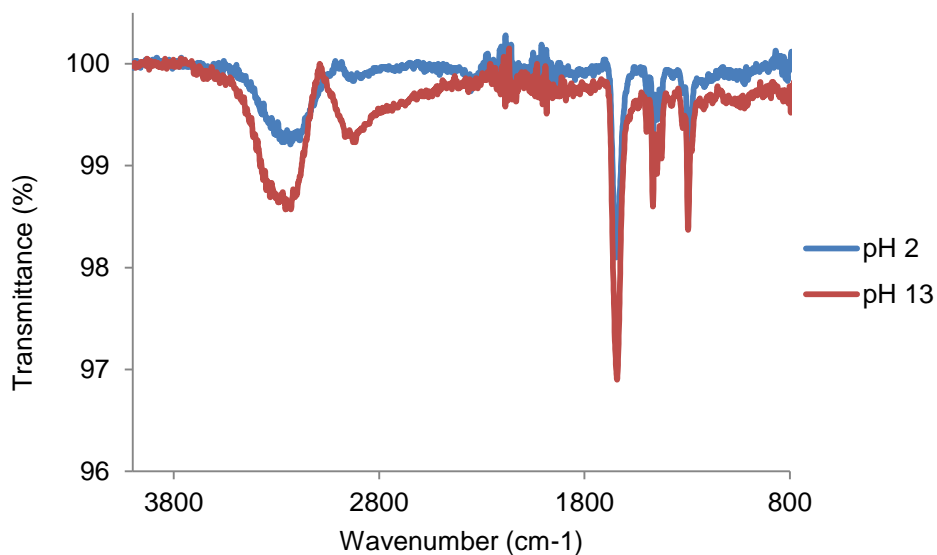


**Figure A8** FTIR spectra of PVP immersed in a pH 2 and a pH 13 solution of mixtures of hydrochloric acid and sodium hydroxide.

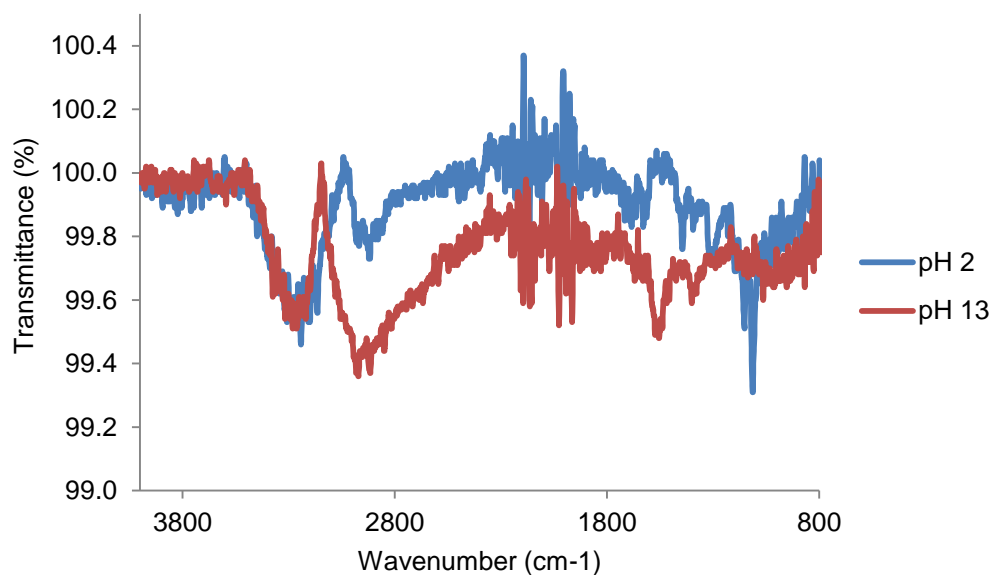


**Figure A9** FTIR spectra of genipin immersed in a pH 2 and a pH 13 solution of mixtures of hydrochloric acid and sodium hydroxide.

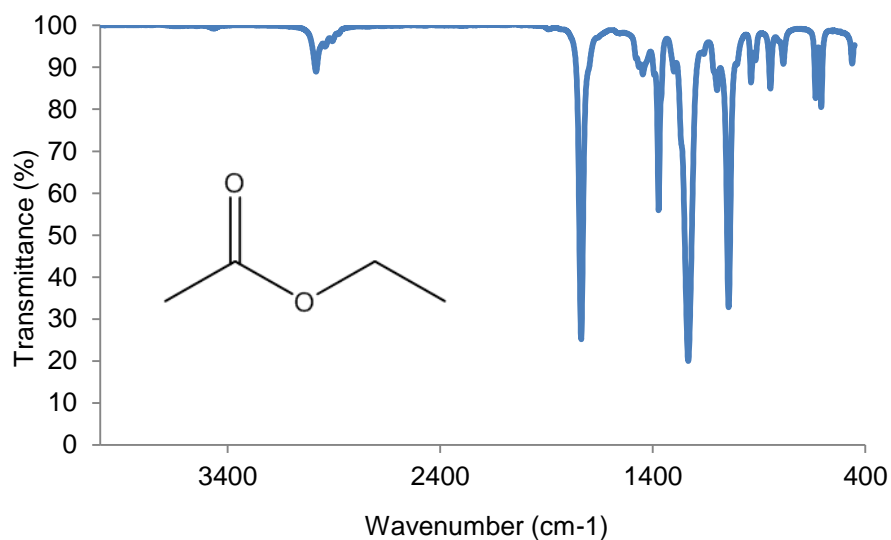


**Figure A10** FTIR spectra of ethyl acetate.

**Table A5** Spectral assignment following FTIR of ethyl acetate.

Peak (cm <sup>-1</sup> )	Assignment
2987	C-H stretch (alkyl)
1738	Saturated ester C=O stretch
1236, 1045	C-O stretches

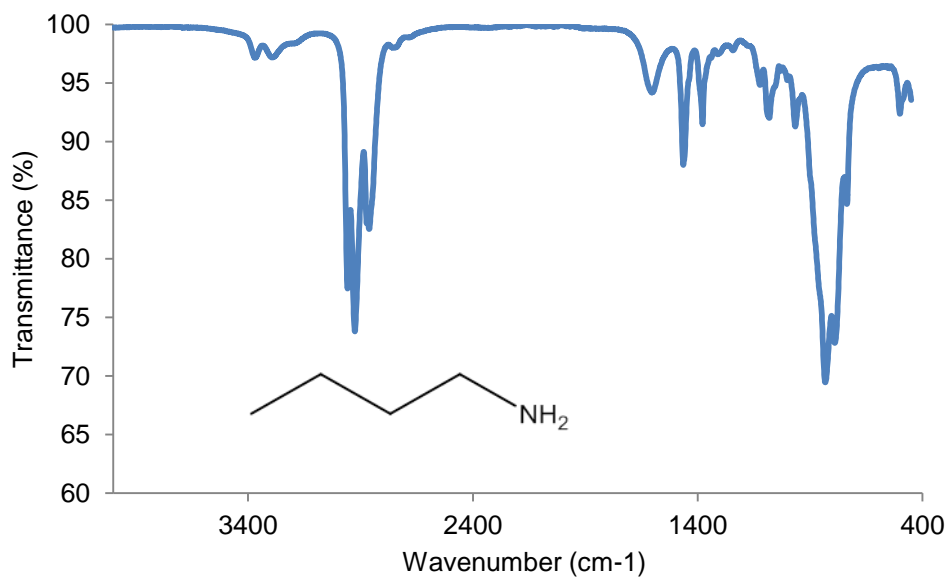


**Figure A11** FTIR spectra of n-butylamine.

**Table A6** Spectral assignment following FTIR of n-butylamine.

Peak (cm <sup>-1</sup> )	Assignment
3388, 3318	N-H stretch
2873	C-H stretch
1618	N-H bend
1466	C-H bend
1380	C-H rock

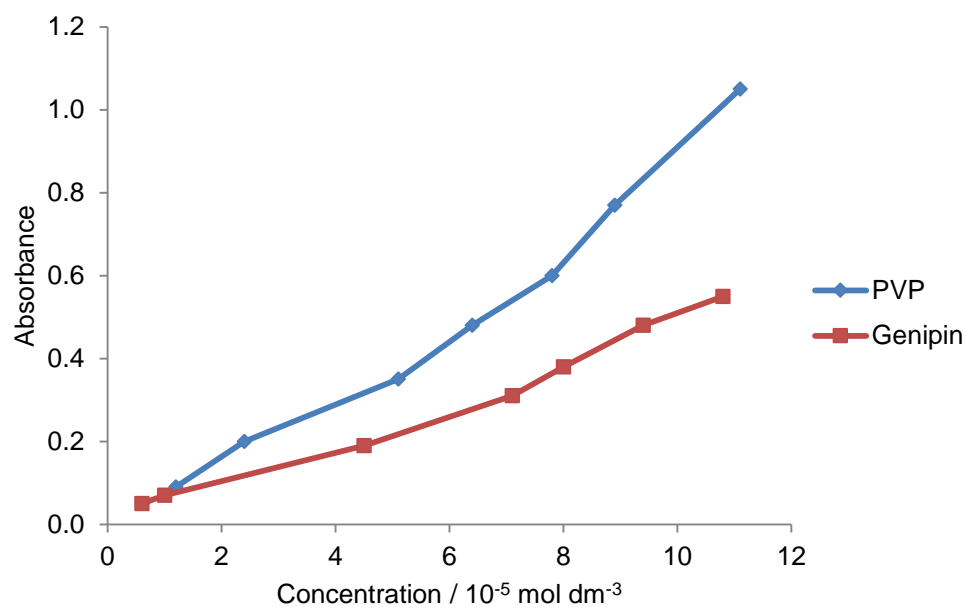


**Figure A12** Calibration of PVP in distilled water at an absorbance of 213 nm and genipin in distilled water at an absorbance of 240 nm using UV-Vis spectroscopy.